PERFORMANCE BASED STRUCTURAL FIRE SAFETY CONCEPT FOR INDUSTRIAL BUILDINGS: STRENGTH AND STABILITY

by

Taygun Fırat Yolaçan

B.S., Civil Engineering, Middle East Technical University, 2014

Submitted to the Institute for Graduate Studies in
Science and Engineering in partial fulfillment of
the requirements for the degree of
Master of Science

Graduate Program in Civil Engineering

Boğaziçi University

2017

ACKNOWLEDGEMENTS

I would like to express my sincere gratitude to my thesis supervisor Assistant Prof. Serdar Selamet for his guidance and help during the preparation of this thesis.

I would like to express my special thanks to my colleague Hasan Börke Birgin for his helps on preparation of graphical outputs.

Most of all, I would like to express my special thanks to my friends Hande Asena Yumuk and Gözde Tayyip for the endless support and encouragement they have given me throughout my studies.

ABSTRACT

PERFORMANCE BASED STRUCTURAL FIRE SAFETY CONCEPT FOR INDUSTRIAL BUILDINGS: STRENGTH AND STABILITY

The aim of this thesis is to investigate fire characteristics and fire induced structural performance of large scale industrial buildings to draw conclusions for a better and more robust sustainable structural design for fire. According to National Fire Protection Association, an estimated average of 37.000 fires at industrial buildings is reported in the U.S. during 2015. The structural fire performance of five different steel framed industrial buildings are investigated by conducting thermo-mechanical analysis in finite element software. The three-dimensional models of the buildings consist of structural members (column, beams, purlins, cross diagonals and tie-beams) and rigid connections between these members. To simulate the collapse of the buildings, an implicit dynamic analysis technique is employed. In addition, a simplified methodology is developed in order to investigate the thermo-mechanical behavior of composite floor systems. This methodology is implemented into Matlab. Realistic fire scenarios are used for the thermo-mechanical analyses of the buildings. From strength and stability point of view, it is observed that fire performance of isolated structural members is significantly different than the fire performance of the members within a structural system. According to the analyses, the most severe conditions are observed in the regions where pre-flashover localized fire is subjected and only two of the five buildings satisfy the required structural fire performance assessment. Adding a reinforced concrete slab to steel framed floor systems significantly reduces the span deflections during fire due to catenary action in the slab. It is anticipated that the data collected in this thesis will lead to better understanding the fire induced collapse mechanisms of industrial buildings.

ÖZET

ENDÜSTRİ YAPILARININ PERFORMANSA DAYALI YAPISAL YANGIN GÜVENLİK KONSEPTİ: DAYANIM VE STABİLİTE

Bu tezin amacı, büyük ölçekli endüstri yapılarında gerçekleşebilecek olan yangınların niteliklerini ve bu yangınların endüstri yapıları üzerinde oluşturdukları yapısal etkileri anlayarak, yangın etkileri için daha dayanıklı ve sürdürülebilir yapı dizaynlarının gerçekleştirilmesine olanak sunmaktır. Amerikan Ulusal Yangın Önleme Dernegi'nin verilerine göre Amerika Birleşik Devletlerin'de 2015 yılı içerisinde endüstri yapılarında gerçekleşen 37.000 yangın rapor edilmiştir. Beş farklı çelik çerçeveli endüstri yapısının termo-mekanik analizleri bir sonlu eleman yazılımı ile gerçekleştirilmiştir. Endüstri yapılarının üç boyutlu modelleri kiriş, kolon, aşık, çapraz ve kuşak yapı elemanlarından oluşmaktadır ve bu yapı elemanları arasında tam bağlantı bulunmaktadır. Endüstri yapılarının çökme simülasyonu için implicit dinamik analiz tekniği kullanılmıştır. Bununla birlikte, kompozit döşeme sistemlerinin termo-mekanik davranışlarını araştırmak için basitleştirilmiş bir metodoloji geliştirilmiş ve bu metodoloji Matlab ortamında kodlanmıştır. Yapıların termo-mekanik analizlerinde gerçekci yangın senaryoları kullanılmıştır. Yapı elemanlarının dayanım ve stabilite incelemeleri ile izole halde bulununan yapı elemanlarının yangın performanslarının bir yapı içerisindeki yangın performanslarında oldukça farklı olduğu görülmüştür. Analizler sonucunda, yapısal olarak en kritik sonuçların parlama öncesi lokal yangınların etkili olduğu bölgelerde olduğu ve incelenen beş yapıdan sadece iki tanesinin yangın dayanım kriterlerini sağladığı görülmüştür. Betonarme döşemenin çelik çerçeve kat sistemlerine eklenmesi sonucunda oluşan çekme etkileri, yangın esnasında çelik çerçevede oluşan açıklık eğilmelerini büyük ölçüde azaltmıştır. Bu çalışmadan elde edilen veriler ile endüstri yapılarının yangın kaynaklı çökme mekanizmalarının daha iyi anlaşılması amaçlanmaktadır.

TABLE OF CONTENTS

ACKNOWLEDGEMENTS iii
ABSTRACT iv
ÖZET v
LIST OF FIGURES ix
LIST OF TABLES xix
LIST OF SYMBOLS xxii
LIST OF ABBREVIATIONS/ABBREVIATIONS xxvii
1. INTRODUCTION 1
1.1. General 1
1.2. Thesis Outline 3
2. LITERATURE REVIEW 4
2.1. Performance Based Structural Fire Safety Concept 4
2.1.1. Prescribed Building Code Approach to Fire Performance of Buildings 4
2.1.2. Realistic Structural Performance of Buildings under Fire 8
2.1.3. Performance-Based Structural Fire Safety Concept Framework . 13
2.1.4. Numerical Modelling Methods for Structural Analysis 16
2.1.5. Simulation Methods for Performance-Based Structural Safety Concept 20
2.1.6. Heat Transfer Analysis Methods 37
2.1.7. Assessment Criteria for Performance Based Structural Fire Safety Concept 43
2.2. Research Significance 45
2.3. Objective and Scope of the Study 46
3. METHODOLOGY (FRAMEWORK) 48
3.1. General 48
3.2. Design Load Combination 48
3.3. Material Model 50
3.4. Finite Element Modelling 52

3.4.1. Determination of Column Initial Bow Imperfection 55
3.5. Fire Simulation Method 59
3.5.1. Zone Model Fire Simulation 59
3.5.2. Pre-flashover Localized Fire Simulation 61
3.5.3. Entire Time-Temperature History 65
3.6. Heat Transfer Analysis 67
3.7. Assessment Criteria 71
4. CASE STUDIES 73
4.1. General 73
4.2. Building - 1 76
4.2.1. Building Description 76
4.2.2. Fire Simulation and Heat Transfer Analysis 82
4.2.3. Structural Analysis 84
4.3. Building - 2 90
4.3.1. Building Description 90
4.3.2. Fire Simulation and Heat Transfer Analysis 94
4.3.3. Structural Analysis 97
4.4. Building - 3 102
4.4.1. Building Description 102
4.4.2. Fire Simulation and Heat Transfer Analysis 114
4.4.3. Structural Analysis 116
4.5. Building - 4 126
4.5.1. Building Description 126
4.5.2. Fire Simulation and Heat Transfer Analysis 130
4.5.3. Structural Analysis 132
4.6. Building - 5 137
4.6.1. Building Description 137
4.6.2. Fire Simulation and Heat Transfer Analysis 142
4.6.3. Structural Analysis 143
5. THERMO-MECHANICAL BEHAVIOR OF STEEL FRAMED CONCRETE SLAB COMPOSITE FLOOR SYSTEMS 148
5.1. General 148

5.2. Thermo-Mechanical Behaviors of Beams and Plates 149
5.2.1. Deflections of a Beam Subjected to Membrane Force, Thermal Gradient and Transvers Loading 149
5.2.2. Deflections of a Simply Supported Beam Subjected to Uniform Transverse Loading and Thermal Gradient 151
5.2.3. Deflections of a Plate Subjected to Membrane Forces, Transverse Loading and Temperature Gradient 153
5.2.4. Deflections of a Simply Supported Plate Subjected to Uniform Transverse Loading and Thermal Gradient 156
5.3. Validation of the Governing Beam and Plate Deflection Equations . . . 158
5.4. Simplified Method to Calculate Interior Steel Beam Reinforced Concrete Slab Composite Floor System Deflections under Fire Conditions 160
5.5. Validation of the Simplified Method 163
5.5.1. Summary of the Assumptions Adopted in the Simplified Method and Capabilities of the Matlab Code 164
5.5.2. Description of the Finite Element Model 165
5.5.3. Comparison of the FE Analysis and Simplified Method 168
5.6. Thermo-Mechanical Behavior of the Composite Floor Systems Located in Building - 4 170
6. SUMMARY AND CONCLUSIONS 175
6.1. Summary 175
6.2. Conclusions 176
6.3. Recommended Future Studies 178
REFERENCES 179
APPENDIX A: FIRE SIMULATION PARAMETERS OF THE BUILDINGS 189

LIST OF FIGURES

Figure 2.1. Standard Fire Test Curves for Various Countries (Boring *et al.*, 1981). 5

Figure 2.2. Ingber's Fire Load Concept (Canadian Wood Council, 1996). . . . 6

Figure 2.3. Comparison of Critical Temperature Value to Axial Restraint Ratio. 9

Figure 2.4. Displaced Geometry of Composite Floor System Tested in Cardington Fire Test-7. 12

Figure 2.5. Comparison of Steel Beam-Reinforced Concrete Slab Composite Floor Systems Mid-Point Deflections with Respect to Their Rebar Ratio. 13

Figure 2.6. Framework for Simulating the Fire Induced Progressive Collapse of Super-Tall RC Buildings. 14

Figure 2.7. Performance Based Structural Fire Safety. 15

Figure 2.8. Representation of Prototype Building. 17

Figure 2.9. Details of Parametric Study for Performance Based Structural Fire Safety Concept. 18

Figure 2.10. 3D View and Dimensions of the Finite Element Model of the Case Study. 19

Figure 2.11. Phases of Natural Fire Mechanism. 21

Figure 2.12. Comparison of ISO834, Hydrocarbon and External Fire Curves for 120 Minutes Fire Duration. 22

Figure 2.13. Comparison of Cardington Test-2 and Test-3 Results with Eurocode Parametric Fire and BS476 (Also known ISO834) Fire Curves. 27

Figure 2.14. Comparison of BFD, Eurocode and ISO 834 Fire Curves. 29

Figure 2.15. Comparison of iBMB Curve and Different Fire Design Software Results with Compartment Fire Test Results for Ordinarily Furnished Office Building. 30

Figure 2.16. Schematic Diagram of One Zone Models. 32

Figure 2.17. Schematic Diagram of Two Zone Models. 34

Figure 2.18. Comparison of Maximum Temperatures Obtained from Furnace Tests with Ozone Results. 35

Figure 2.19. Comparison of BFD, Eurocode, ISO 834 and Zone Model Fire Curves for the Large Scale Warehouse Building. 37

Figure 2.20. Temperature-time History of Steel Beam Mid-Span for Three Dimensional Heat Transfer Analysis and Cardington Fire Test. . . . 40

Figure 3.1. Plastic Stress - Strain Model of Structural Steel. 51

Figure 3.2. General Layout of Out-of-plane Braced Portal Frame Structural System. 53

Figure 3.3. Braced Column Illustration. 56

Figure 3.4. Possible First Elastic Buckling Modes of the Highlighted Column. 57

Figure 3.5. Flowchart for the Transition of Two-zone Fire Model to One-zone Fire Model. 61

Figure 3.6. Representation of Flame Dimensions for a Ceiling Not Impacted Localized Fire. 63

Figure 3.7. Representation of Flame Dimensions for a Ceiling Impacted Localized Fire. 64

Figure 3.8. Illustration of Fire Curves: Localized, Hot-zone and Combined Fire Curves. 66

Figure 3.9. Flame Temperatures for Varying Flame Heights and Hot-zone Temperatures. 67

Figure 3.10. Specific Compartment Fire. 69

Figure 3.11. Illustration of the Steel Portal Framed Industrial Building. 70

Figure 4.1. General Layout of Building - 1. 77

Figure 4.2. Steel Sections. 77

Figure 4.3. Steel Sections along Axes 1 and 3. 78

Figure 4.4. Steel Sections at the Roof Level. 78

Figure 4.5. General Layout of the Crane Level with Steel Sections. 79

Figure 4.6. Architectural Drawings of the Building with the Highlighted Ventilation Openings. 79

Figure 4.7. Crane Platforms (Grey Surfaces) and Points of Application of Crane Self-Weights (Hollow Circles). 80

Figure 4.8. Structurally Critical Region. 81

Figure 4.9. Hot and Cold Zones Temperatures. 83

Figure 4.10. Hot-zone Temperatures, Local Fire Flame Temperatures and ISO 834 Standard Fire Temperatures for 120 minutes. 83

Figure 4.11. Column Located at D-3 Axis Coordinate. 86

Figure 4.12. Fire Induced Behavior of the Rafter Located along E Axis. 87

Figure 4.13. Fire Induced Behavior of the Rafter Located along Axis F. 89

Figure 4.14. General Layout of Building - 2. 90

Figure 4.15. Steel Sections. 91

Figure 4.16. Steel Sections of the Out-of-plane Diagonals and Tie-beams. . . . 91

Figure 4.17. Steel Sections at the Roof Level. 92

Figure 4.18. Architectural Drawings of the Building with the Highlighted Ventilation Openings. 93

Figure 4.19. Structurally Critical Region. 94

Figure 4.20. Hot and Cold Zones Temperatures. 95

Figure 4.21. Hot-zone Gas Temperatures, Local Fire Flame Temperatures and ISO 834 Standard Fire Temperatures for 120 minutes. 96

Figure 4.22. Column Located at F-1 Axis Coordinate. 99

Figure 4.23. Rafter Located between F-1 and F-5 Axis Coordinates. 100

Figure 4.24. Column Located at B-5 Axis Coordinate. 101

Figure 4.25. Fire Induced Behavior of the Rafter Located Between B-1 and B-5 Axis Coordinates. 103

Figure 4.26. General Layout of Building - 3. 104

Figure 4.27. Moment Resistance Alignment of the Two Different Type Portal Frames. 105

Figure 4.28. General Layout, Adjacent Building and Out-building Platform. . . 105

Figure 4.29. Steel Sections. 106

Figure 4.30. Steel Sections. 107

Figure 4.31. Dimensions of the Built - up Section. 107

Figure 4.32. Steel Sections of the Tie-beams, Diagonals and Crane Support Columns. 108

Figure 4.33. General Layout and Steel Sections at Roof of the Building. 108

Figure 4.34. General Layout and the Steel Section Profiles at Crane Level. . . . 109

Figure 4.35. Architectural Drawings of the Building with the Highlighted Ventilation Openings. 110

Figure 4.36. Live Load Application Areas. 111

Figure 4.37. The Point of Application, Magnitude and Direction of Thermal Friction Forces along Axis 5. 112

Figure 4.38. The Point of Application of Indoor Platform and Equipment Self weights and Live Loads. 112

Figure 4.39. Structurally Critical Region. 113

Figure 4.40. (a) Hot and Cold Zone Temperatures. 115

Figure 4.41. Hot-zone Gas Temperatures, Local Fire Flame Temperatures and ISO 834 Standard Fire Temperatures for 120 minutes. 116

Figure 4.42. Column Located at D - 5 Axis Coordinate. 119

Figure 4.43. Located at E - 5 Axis Coordinate. 120

Figure 4.44. Fire Induced Behavior of the Rafter Located Between A - 7 and E - 7 Axis Coordinates. 122

Figure 4.45. Fire Induced Behavior of the Rafter Located Between E-1 and E-5 Axis Coordinates. 123

Figure 4.46. Fire Induced Behavior of the Rafter Located Between B - 1 and B - 5 Axis Coordinates. 124

Figure 4.47. Entire Model Kinetic Energy. 125

Figure 4.48. General Layout of Building - 4. 127

Figure 4.49. Steel Sections. 127

Figure 4.50. Steel Sections. 128

Figure 4.51. Fire Compartment of Building - 4. 129

Figure 4.52. Architectural Drawings of the Building with Highlighted Ventilation Openings. 129

Figure 4.53. Hot and Cold Zones Temperatures. 131

Figure 4.54. Column Located at E-1 Axis Coordinate. 134

Figure 4.55. Perimeter Beam Located along E Axis. 135

Figure 4.56. Secondary Beam Located between E and F Axes. 136

Figure 4.57. General Layout of Building - 5. 138

Figure 4.58. Steel Sections. 139

Figure 4.59. Steel Sections. 139

Figure 4.60. Fire Compartment of Building - 5. 140

Figure 4.61. Architectural Drawings of the Building with the Highlighted Ventilation Openings. 141

Figure 4.62. Hot and Cold Zones Temperatures. 143

Figure 4.63. Located at the B-3 Axis Coordinate. 145

Figure 4.64. Rafter Located between B-2 and B-3 Axis Coordinates. 146

Figure 5.1. Beam Element Subjected to Transverse Loading. 149

Figure 5.2. Stress resultants on a plate subjected to transverse loading and in-plane normal forces. 153

Figure 5.3. The Beam Mid-length Deflections under $T_z = 1\ ^o$C/mm. 159

Figure 5.4. The Plate Mid-point Deflections under $T_z = 1\ ^o$C/mm. 160

Figure 5.5. Finite Strips Demonstration of Rectangular Plate. 162

Figure 5.6. Iterative Solution Method to Calculate Composite Floor Deflections with Closed form Plate Deflection Equations. 163

Figure 5.7. Entire Algorithm that for the Developed Simplified Methodology. . 164

Figure 5.8. Composite Floor Assembly. 166

Figure 5.9. Flat Concrete Slab Model. 166

Figure 5.10. 120 minutes ISO834 Fire with the Temperature Distributions. . . 167

Figure 5.11. Composite Floor Mid-point Deflections for FE Analysis and Simplified Algorithms. 169

Figure 5.12. Deflections of the Composite Floor at the end of the analysis. . . . 170

Figure 5.13. Hot-Zone Temperatures of Building - 4 with the Temperature Distribution Across. 173

Figure 5.14. Composite Floor Mid-point Deflections. 174

Figure 5.15. Deflections of the Composite Floor at the end of the Analysis. . . 174

Figure A.1. General Fire Parameters of Building. 189

Figure A.2. Compartment Details of Building. 190

Figure A.3. Detailed Fire Parameters of Building. 191

Figure A.4. General Fire Parameters of Building. 192

Figure A.5. Compartment Details of Building. 193

Figure A.6. Detailed Fire Parameters of Building. 194

Figure A.7. General Fire Parameters of Building. 195

Figure A.8. Compartment Details of Building. 196

Figure A.9. Detailed Fire Parameters of Building. 197

Figure A.10. General Fire Parameters of Building. 198

Figure A.11. Compartment Details of Building. 199

Figure A.12. Detailed Fire Parameters of Building. 200

Figure A.13. General Fire Parameters of Building. 201

Figure A.14. Compartment Details of Building. 202

Figure A.15. Detailed Fire Parameters of Building. 203

LIST OF TABLES

Table 2.1. Comparison of Ingberg's FRR vs NBCC FRR (Parkinson, 2002). . 7

Table 2.2. General Properties of the Warehouse Building. 38

Table 2.3. Emissivity Values for Different Construction Types and Fire Exposure Scenarios. 42

Table 2.4. Limit States of Failure Assessment Criteria for Different Structural Members. 46

Table 3.1. Recommended Values of Load Factors. 49

Table 3.2. Temperature Dependent Mechanical Material Properties of Structural Steel and Steel Reinforcement. 52

Table 3.3. Temperature Dependent Mechanical and Thermal Material Properties of Calcareous Aggregated Normal Weight C20 Concrete. . . 52

Table 3.4. General Properties of the Large Scale Compartment. 68

Table 4.1. General Geometric Properties of the Investigated Buildings. 73

Table 4.2. Characteristic Value of the Snow Load Applied on Roof of the Buildings. 74

Table 4.3. General Parameters for the Fire Simulations of the Buildings. . . . 75

Table 4.4. Opening factor of the Buildings. 75

Table 4.5. Thermal Properties of Lining Materials. 76

Table 4.6. Amount, Density and Characteristic Calorific Value of the Fire Loads Exist in Building - 1. 82

Table 4.7. The Fire Curves Used for the Heating of the Structural Members of Building - 1. 84

Table 4.8. Fire Induced Performances of the Investigated Structural Members of Building - 1. 89

Table 4.9. The Fire Curves Used for the Heating of the Structural Members of Building - 2. 96

Table 4.10. Fire Induced Performances of the Investigated Structural Members of Building - 2. 103

Table 4.11. The Equipment and Piping Systems Self-Weights, Live Loads and the Equipment Loads Applied to the Columns that Align on the Axes 5 and 10. 113

Table 4.12. Type and Amount of the Combustible Materials that exist in Building - 3. 113

Table 4.13. The Fire Curves Used for the Heating of the Structural Members of Building - 3. 116

Table 4.14. Fire Induced Performances of the Investigated Structural Members of Building - 3. 126

Table 4.15. Fire Induced Performances of the Investigated Structural Members of Building - 4. 137

Table 4.16. Fire Induced Performances of the Investigated Structural Members of Building - 5. 147

Table 5.1. S275 Structural Steel Plasticity. 167

Table 5.2. C20 Concrete Damaged Plasticity Coefficients Behavior. 168

Table 6.1. Summary of the Fire Simulations and Finite Element Analyses. . . 176

LIST OF SYMBOLS

A	Area
a	Dimension of Rectangular Plate (x direction)
A_d	Accidental Actions
A_f	Floor Area
A_m	Surface Area per Unit Length
A_t	Total Surface Area of Enclosure
A_v	Total Area of Vertical Openings
b	Dimension of Rectangular Plate (y direction)
b_i	Thermal Inertia of Lining Materials
c_a	Specific Heat of Steel
c_b	Specific Heat of Boundary of Enclosure
c_c	Specific Heat of Concrete
c_i	Thermal Insulation Coefficient of Compartments
d	Depth of Beam
D	Flexural Rigidity
D_f	Diameter of Fire
E	Modulus of Elasticity
E_g	Internal Gas Energy
f_t	Concrete Peak Tensile Strength
$f_{b,o}$	Initial Equibiaxial Compressive Yield Stress
$f_{c,o}$	Initial Uniaxial Compressive Yield Stress
$G_{k,j}$	Gravitational Actions
H	Distance between Fire Source and Ceiling
$\dot{h}$	Heat Flux to Unit Surface Area
$\dot{h}_{net,d}$	Design Value of the Net Heat Flux per Unit Surface Area
h_v	Mean Height of Vertical Openings
k	Fire Growth Constant
K	The ratio of the Second Stress Invariant on the Tensile Meridian to that on the Compressive Meridian at initial Yield

K_c	Axial Stiffness of Column
k_p	Pyrolysis Coefficient
k_{sh}	Shadow Effect Correction Factor
K_{sr}	Axial Stiffness Provided by Surrounding Structure to Column
L	Beam Length
L_f	Flame Length
L_h	Horizontal Flame Length
L_L	Lower Layer
m	Mass
$M*$	Thermal Moment Resultant per Unit Distance
M_{RK}	Characteristic Moment Resistance of Structural Members
M_x	Bending Moment per Unit Distance on x Plane
M_y	Bending Moment per Unit Distance on y Plane
$N*$	Thermal Force Resultant per Unit Distance
N_{RK}	Characteristic Normal Force Resistance of Structural Members
N_x	Normal Force per Unit Distance on x Plane
N_{xm}	Tensile Membrane Force per Unit Distance on x Plane
N_{xy}	Shearing Force per Unit Distance on x Plane and Parallel to y Axis
N_y	Normal Force per Unit Distance on y Plane
N_{ym}	Tensile Membrane Force per Unit Distance on y Plane
N_{yx}	Shearing Force per Unit Distance on y Plane and Parallel to x Axis
O	Opening Factor
p	Intensity of Distributed Transverse Force
p_{ax}	Axial Restraint Ratio
P_{int}	Internal Pressure
Q	Rate of Heat Release
Q_c	Convective Part of Rate of Heat Release
$q_{f,d}$	Design Value of Fuel Load Density Related to Floor Area
Q_H	Non-dimensional Rate of Heat Release

$Q_{k,l}$	Leading Variable Action
$Q_{k,i}$	Secondary Variable Actions
$q_{t,d}$	Design Value of Fuel Load Density Related to Total Surface Area of Enclosure
Q_x	Shear Force per Unit Distance on x Plane
Q_y	Shear Force per Unit Distance on y Plane
r	Horizontal Distance between Vertical Axis of Fire and Point along Ceiling where Thermal Flux is Calculated
R	Universal Gas Constant
s_c	Shape Constant
T	Temperature
t	Time
$t*$	Fictitious Time
T_o	Initial Temperature
T_g	Gas Temperature
t_{lim}	Fire Growth Duration Limitation
t_m	Peak Temperature Time of BFD Parametric Fire
T_{max}	Maximum Gas Temperature
u	Displacement in x Direction
U_L	Upper Layer
V	Volume
v	Displacement in y Direction
w	Displacement in z Direction
w_T	Beam Mid-length Displacement in Vertical Direction
z_o	Virtual Origin of Flame Axis
α	Coefficient of Thermal Expansion
α_a	Thermal Expansion Coefficient of Steel
α_c	Thermal Expansion Coefficient of Concrete
α_{ch}	Coefficient of Heat Transfer by Convection
α_{cr}	Minimum Force Amplifier for Structural Member to Reach Elastic Critical Buckling

α_{imp}	Imperfection Factor
$\alpha_{ult,k}$	Minimum Force Amplifier for Structural Member to Reach Characteristic Resistance without Buckling
Δt	Time Interval
$\Delta\theta_{\alpha,t}$	Temperature Increase in an Unprotected Steel Member
ε	Flow Potential Eccentricity
ε_{cr}	Concrete Tensile Cracking Strain
ε_{cu}	Concrete Strain Corresponding to Characteristic Value of the Compressive Cylinder Strength
ε_f	Emissivity of Fire
ε_m	Surface Emissivity of Member
ε_x	Normal Strain in x Direction
ε_y	Normal Strain in y Direction
ε_z	Normal Strain in z Direction
η_{cr}	Critical Elastic Buckling Shape
η_{inil}	Initial Column Imperfection
μ	Viscocity Parameter
θ_g	Gas Temperature
θ_m	Surface Temperature of Member
θ_r	Effective Radiation Temperature of Fire Environment
θ_z	Flame Temperature along the Vertical Flame Axis
λ	Thermal Conductivity
$\bar{\lambda}$	Relative Slenderness
λ_a	Thermal Conductivity of Steel
λ_b	Thermal Conductivity of Boundary Enclosure
λ_c	Thermal Conductivity of Concrete
ρ_a	Steel Density
ρ_b	Density of Boundary of Enclosure
ρ_c	Concrete Density
ρ_g	Gas Density
σ	Stephan Boltzmann Constant

σ_u	Characteristic Value of the Compressive Cylinder Strength of Concrete
σ_y	Yield Strength of Steel
ϕ	Configuration or View Factor
φ	Dilation Angle
χ	Reduction Factor
ψ	Load factors for Design Load Combination
ν	Poisson Ratio
Γ	Modification Factor

LIST OF ABBREVIATIONS/ABBREVIATIONS

2D	Two Dimensional
3D	Three Dimensional
ASCE	American Society of Civil Engineers
ASTM	American Society of Testing and Materials
CFD	Computational Fluid Dynamics
FE	Finite Element
FEM	Finite Element Method
FRR	Fire Resistance Rating
NFPA	National Fire Protection Association
NRCC	National Building Code of Canada
PBSFSC	Performance-based Structural Fire Safety Concept
PEEQ	Equivalent Plastic Strain
RC	Reinforced Concrete

1. INTRODUCTION

1.1. General

Steel is generally used as a construction material for industrial buildings. High material strength, uniformity, elasticity, ductility, weldability, lightness and easy of erection are some of the main reasons for the usage of steel in construction of industrial buildings. However, as a construction material, the fire resistance of steel is weak. In addition, non- compartmentalization of large storage and production areas and high flammable fire load density existence in industrial buildings cause these buildings to be highly risky for fire. Fire induced collapse of these buildings not only causes loss of the structures but also loss of human life, production equipment and stored goods. In addition, fire induced collapse of industrial buildings that are used for production or storage of chemical substances might harm the environment irrevocably. To prevent these results, natural fire mechanism and fire induced structural behavior of steel framed industrial buildings should be analyzed during the design phase of the structure and necessary precautions should be taken.

Strength, stability and serviceability are three main criteria that define structural performance of the buildings at elevated temperatures. Prescribed structural fire design codes describe structural fire safety requirements of the buildings according to strength and stability of the individual structural elements under the effect of standard fires. However, fire induced behavior of the structural system cannot be treated as isolated; the structural elements affect each other during fire. There have been numerous analytical and experimental studies to investigate fire induced behavior of steel framed structures. Most of these studies showed that there are significant differences between individual element behavior and structural system behavior under elevated temperature. Because standard fire does not properly reflect the natural fire curve under realistic fire load and ventilation, and isolated elements fire tests do not include the effects of connecting structural elements, the differences arise between the prescribed and performance based approach.

Modern design codes implement performance-based analysis approach to observe more realistic fire induced behavior of structures during the design phase. Fire simulation and structural analysis under elevated temperature are the two main steps of the performance-based structural fire safety concept. On the other hand, the complexity of the structural mechanism causes considerable need for reliable analytical modelling approaches for performance-based structural fire safety concept.

In this study, relatively simple yet robust framework is followed for fire simulations and structural analyses of industrial buildings together with the performance-based fire safety concept. In addition, thermo-mechanical behavior of steel-framed reinforced-concrete slab composite floor systems are investigated with a simplified method which is developed with differential beam and plate deflection equations. The proposed closed form formulations for thermo-mechanical behavior of composite floor systems are implemented in Matlab together with nonlinear analysis solution strategy and verified against finite element (FE) model results. Five different steel framed industrial buildings are investigated with the methodologies that are proposed for fire simulation, strength, stability and serviceability limit states. On the light of this research, 3D structural models of industrial buildings are modelled and analyzed with ABAQUS (DS-Simulia, 2012), widely used FE computer software. For fire simulations of these buildings zone modelling technique is used with Ozone (Cadiron *et al.*, 2001), commercial fire modeling software, and heat transfer analyses of structural members is completed with Elefir-EN (Real and Franssen, 2015), commercial fire design software.

To evaluate the industrial buildings fire performances, vertical displacement of the beams, in-plane and out-of-plane displacements of the columns, mid-length displacement rates of the columns and beams, equivalent plastic strains (PEEQ) developed along the columns and beams are investigated and compared with the prescribed limit states. Results of this study include fire induced collapse initiation time and collapse time estimations, and the underlying mechanisms behind for the collapse of the industrial buildings.

1.2. Thesis Outline

This thesis focus on performance based structural fire safety concept for industrial buildings and consist of 6 chapters. In Chapter 1, an introduction is presented for performance based structural fire safety concept. Detailed literature review, as well as the significance of the study, the objective and the scope of the study are provided in Chapter 2. Adopted methodologies to determine design load combination, constitute material models, create finite element models, simulate building fires, conduct heat transfer analysis, and fire induced performance assessment criteria of the buildings are detailed in Chapter 3. Detailed description of 5 different industrial buildings with respect to their architectural layout, structural system, state of static loading, structurally critical region, characteristic fire load density, fire compartment, boundary conditions, and results of the fire simulations and structural analyses are presented in Chapter 4. Description of developed simplified methodology to determine thermo-mechanical behavior of the composite floor systems, verification of results of the developed methodology against finite element model, and thermo-mechanical behavior of the composite floor system located in one of the investigated industrial building are presented in Chapter 5. Finally, concluding remarks and recommendations for future studies are presented in Chapter 6.

2. LITERATURE REVIEW

2.1. Performance Based Structural Fire Safety Concept

Understanding fire induced behavior of structures is an area of growing interest and structural engineers have been adopting performance-based structural fire safety concept for fire safety designs rather than simply applying prescribed design codes provisions.

During last two decades performance-based structural fire safety concept has gained importance and performance-based provisions have been introduced by International Code Council (ICC, 2002) and the National Fire Protection Association (NFPA, 2002) to be alternative to the prescribed fire design codes. In addition, Society of Fire Protection Engineering (SFPE, 2000), the European Convention for Constructional Steelwork (ECCS, 2001), the American Institute of Steel Construction (AISC, 2005) have conducted studies to improve performance-based engineering concepts for structural fire safety engineering and design process.

Fire science, structural engineering and fire safety design tools are be interdisciplinary research fields and they must be used for performance-based structural fire safety concept (PBSFSC)

2.1.1. Prescribed Building Code Approach to Fire Performance of Buildings

Prescribed design codes define structural performance requirements of fire subjected structural members with fire resistance ratings (FRR). Fire resistance rating of a structural member is described in units of hours and it is related with fire severity, and fire severity of a compartment is determined according to the fire load density in the compartment and the level of fire initiation risk.

Ingberg (1928) developed a methodology, known as "Fire Load Concept", to determine required FRR of a structural member for different fire load densities. According to this concept, total heat release at the time that all the combustible materials are consumed in the compartment by natural fire mechanism of this compartment is thought as fire severity, and fire severity of a compartment equals to the area under the natural fire curve of the compartment. As a result, the equivalent area under the standard fire test's temperature-time curve defines the required FRR of the structural members in the compartment. Figure 2.1 represents several standard fire test curves and Figure 2.2 represents required FRR of structural members by Ingberg's method for specific fire load densities. According to Figure 2.2, a floor assembly of the tested compartment is expected to sustain the effects of an actual fire for a longer time than 45 minutes. In addition, American Society of Testing and Materials (ASTM 119, 2016) and National Fire Protection Association (NFPA 251, 2015) also define fundamental basis for determining required FRR of structural elements and assemblies.

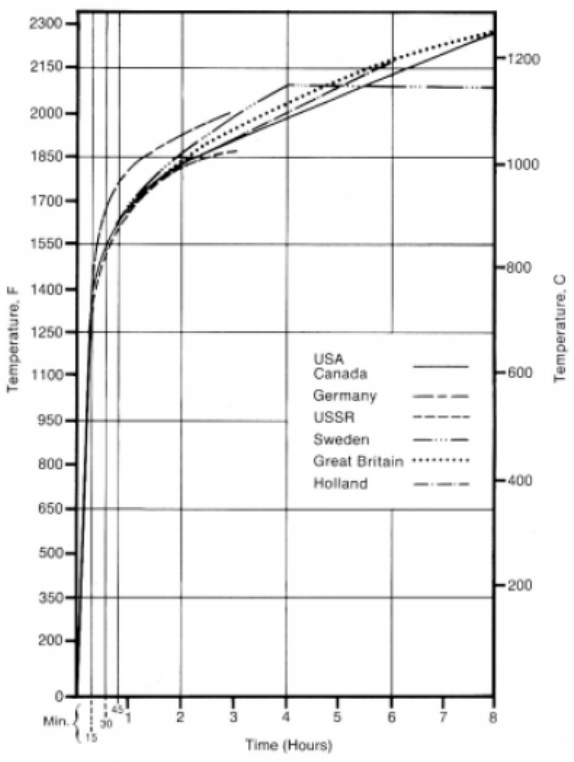

Figure 2.1. Standard Fire Test Curves for Various Countries (Boring *et al.*, 1981).

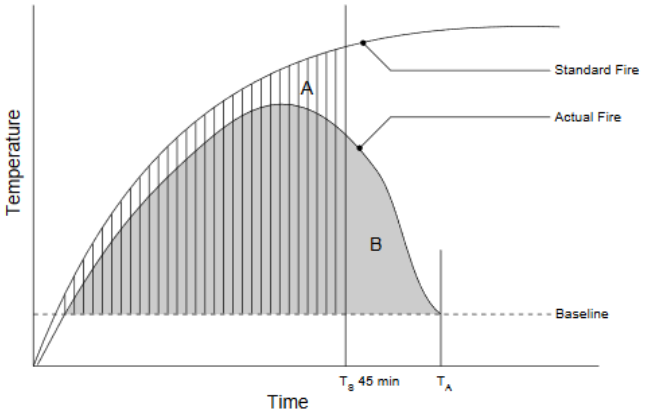

Figure 2.2. Ingber's Fire Load Concept (Canadian Wood Council, 1996).

Prescribed FRR for structural elements provided reasonable level of safety and frequent building failure has not been observed for structural fires. On the other hand, uncertainties in temperature-time curves that are used for standard fire tests might cause required FRR of structural members to be wrongly estimated, and these structural members might show undesirable behavior under a real fire conditions. (Parkinson and Kodur, 2006).

Fire curves that are used in standard fire tests were developed in 1917-1920 at the underwriters laboratory in Chicago with empirical data obtained from full scale fire tests and observation of building fire (Babrauskas and Williamson 1978a, b). However, fire loads in modern buildings are differentiated over last 100 years and wood based products which were used for the development of standard fire curves are no longer used as high as in modern buildings. Plastic materials that have higher heat release rate when burned than wood based products are more commonly used in modern buildings (Babrauskas and Williamson 1978a, b). Moreover properties of test furnaces that are used to determine required FRR of structural members also affect prescribed FRR values. Pettersson (1978) showed that real gas temperature in the furnace can be 100 ^{o}C higher than the measured temperature from the thermocouples placed in the furnace depending upon construction of furnace walls. Sultan (1996), Thomson and Preston (1996) determined that furnace test results also depend on furnace construction and operation type and stated that difference between real gas temperature

and temperature measured with thermocouples may result significant consequences with respect to determination of required FRR of structural members. Thomson and Preston (1996) reported 30% difference for the prescribed FRR of identical structural members due to characteristics of two different furnaces in the UK. Gilvery and Dexter (1997) have performed studies on the available furnace temperature-time test data that were produced according to American Society of Testing and Materials (ASTM E119, 2016) and equivalent test procedures in different furnaces. Their studies showed that identical steel and concrete columns' structural performances differ up to 27% and 39% respectively due to variations in the test data that were collected from different furnaces.

Parkinson (2002), compared required FRR of structural members determined by Ingberg (Ingberg, 1928) and National Building Code of Canada (NRCC, 1995) for different hazard levels and building usage types. Table 2.1 represents this comparison and it is seen that FRR of structural members determined by Ingberg and NRCC differ in a range from 30 minutes to 120 minutes due to different test procedure usage of Ingberg and NRCC.

Table 2.1. Comparison of Ingberg's FRR vs NBCC FRR (Parkinson, 2002).

Fire Hazard	Building Type	Fuel Load (Thomas, 1986) MJ/m^2	FRR from Ingberg (Drysdale, 1985) minutes	FRR from NBCC (NRCC, 1995) minutes
Light	Office	600-800	60	45-60
	School	300	30	45-60
	Hospital	300	30	60-120
	Bank	800	60	45-60
Medium	Packaging Plant	1600-1800	120	60-90
	Wax Plant	1300	90	60-90
	Storage Room	1200-1400	90	60-90
High	Wood Preserving	3000	180	90-120
	Synthetics Plant	3400	240	90-120
	Paint Plant	4200	>240	90-120

Having discussed the importance of fire characteristics on the performance of structural members, Section 2.1.5 of this thesis describes the different methodologies and their weaknesses and strengths to determine appropriate design fire for performance

based structural fire safety concept.

2.1.2. Realistic Structural Performance of Buildings under Fire

Structural performance of structural members against fire depends on boundary conditions, continuity, and interaction with the surrounding elements, connections, alternative load paths, and restraints. Due to furnace limitations it is not possible to test structural assemblies and determine required fire resistance rating. Moreover, due to cost and safety concerns, it is not a common practice to conduct full-scale fire tests. Only few full-scale fire test have been conducted for office and residential buildings, such as Cardington Fire Tests (Vassart and Zhao, 2011) and far fewer full-scale fire tests have been conducted for industrial buildings. Although, Guo *et al.* (2011) investigated results of a large scale factory fire experiment conducted in Huang Shan Industrial Park, they only conducted studies to investigate differences between standard fire curves and natural fire mechanism of industrial buildings. Therefore, performance based fire safety concept is an alternative to costly furnace tests to investigate fire performance of entire structure.

Franssen (2000) conducted studies to identify structural fire behavior of an isolated column and a column as a part of a frame. According to his studies, the column failure was accelerated due to axial restraint effect of the surrounding structure. Wang and Moore (1994) and Shepherd (1999) explained simplified mathematical model to calculate level of axial restraint experienced by a column by the surrounding structure. Shepherd and Burgess (2011) investigated the behavior of steel column that is axially restrained by surrounding structure under elevated temperature with mathematical model of axial restraint of Wang and Moore (1994). According to their study, the induced load due to axial restraint caused heated steel column to become unstable and they stated that as the axial restraint ratio increases the critical temperature that causes column to be unstable decreases. The relation between axial restraint ratio and the critical temperature for an identical column found by Shepherd and Burgess is

shown with Figure 2.3 and Equation 2.1 represents formulation of axial restraint ratio.

$$p_{ax} = \frac{K_{sr}}{K_c} \tag{2.1}$$

where K_{sr} represents axial stiffness provided by surrounding structure to the heated column and K_c represents axial stiffness of the column.

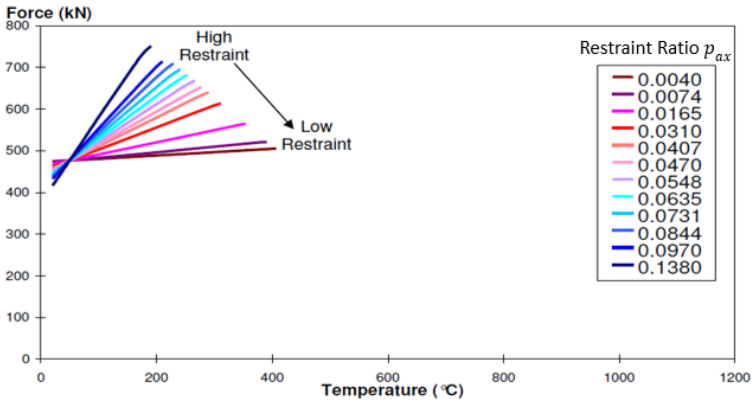

Figure 2.3. Comparison of Critical Temperature Value to Axial Restraint Ratio (Shepherd and Burgess, 2001).

In addition, Shepherd and Burgess (2011) also investigated behavior of surrounding cooler structure after heated column becomes unstable and concluded that the buckled column transfers load on it to the adjacent structure and hang from its beam and surrounding structure. They emphasized that if the surrounding structure is also under the effect of fire, progressive collapse of entire structure is possible due to load transfer from the buckled column to surrounding structure. Neither prescribed fire safety design codes which only focus on behavior of isolated structural elements, nor standard fire tests that are conducted to determine structural performance of isolated structural elements or assemblies consider force redistribution that takes place when single structural element or assemblies fail. This might cause unexpected structural behavior of entire structure if it is designed according to prescribed fire codes.

Jiang *et al.* (2014) studied the effects of bracings to the structural performance of the entire structure in case of fire. They simulated multi-story steel framed build-

ing on OpenSees, open-source object-oriented software framework developed at UC Berkeley, and result of their study showed that fire resistance of steel frames against progressive collapse is directly related with existence of lateral and vertical bracings. They concluded that application of lateral and vertical restraints together increases the fire resistance of structure. On the other hand, application of lateral and vertical restraints separately causes local collapse of the heated compartment to expand the global collapse of the entire structure. Moreover, the role of force redistribution on the progressive collapse was investigated in their study and they resulted that progressive collapse is triggered by the buckling of the heated columns and followed by the sequent buckling of the columns at same story due to force re-distribution along the adjacent beams to down these columns.

Rini *et al.* (2011) studied the effects of fire to bracings in a structure for different fire scenarios. They performed whole frame thermo-mechanical analysis and concluded that local buckling on the bracing elements does not cause global instabilities due to alternative load path (force re-distribution) and reserved capacity that is provided by cooler structure.

Moss *et al.* (2009) conducted performance based analysis on steel portal frame building with concrete tilt-up panels at elevated temperatures. Their studies investigated the effects of column base support conditions and axially restrained purlins to fire-induced collapse mechanisms of steel portal frame building. Moss *et al.* demonstrated that presence of the axial restraint on purlins reduced the roof deflection under fire exposure by providing catenary action over the full length of the building. According to their studies, portal frames with fixed column base condition is more resistant to fire action than portal frames with pinned column base condition and catenary action that is governed by axially restraint purlins might avoid progressive collapse of a structure with pinned base condition.

Selamet and Garlock (2011) investigated the structural performance of single plate, single angle and double angle shear connections under fire action. These shear connections were modelled as a subassembly of concrete slab, steel girder beam and steel

secondary beam to consider realistic thermally induced forces on shear connections. Their study showed that angle shear connections are more resistant than single plate shear connection for fire action due to high bolt bearing capacity. The results of their study proved that identical fire compartments can show different fire performance depending on their connection type.

Parkinson (2002) emphasized fire performance of structural members depends on real loading conditions of structural members. On the other hand, standard fire test procedures require structural elements and assemblies to be tested under maximum allowable stress conditions. Parkinson stated that the differences between real loading conditions and fire test loading conditions of structural members may result unexpected structural performance of the building.

Stability of the floor system under fire action has crucial importance for the stability of the columns, thus stability and serviceability of the entire structure. Structural performance of fire subjected steel framed reinforced concrete composite floor systems that were tested with standard fire test procedure showed differences than ones that were tested in full scale fire tests (Vassart and Zhao, 2011). Many studies have been conducted to investigate reasons of these differences. The studies resulted that development of the tensile membrane action in the reinforced concrete slab and the catenary action in the steel beams increase the structural fire performance of composite floor systems (Vassart and Zhao, 2011). Development of the tensile membrane action of floor assembly proved that alternative load carrying mechanisms are possible and the failure of single structural element does not reflect the structural performance of the entire structure.

Rini and Lamont (2008) conducted a case study to analyze the structural performance of a multi-story building that consists of steel framed reinforced concrete floors. Results of their study showed that the analyzed can maintain 1.3 m deflection at the mid-span without losing its stability, if it was reinforced sufficiently. Similar behavior of steel framed composite floor systems was observed in full-scale Cardington Fire Tests (Vassart and Zhao, 2011). Results of central compartment full-scale fire test

(Test-7) conducted in Cardington showed that composite floor systems can undergo 1.2 m vertical deflection by surpassing the predicted collapse of the floor. Figure 2.4 shows the displaced geometry of the composite floor system that was tested in Cardington Full Scale Fire Test Program within Test-7 (Vassart and Zhao, 2011).

Figure 2.4. Displaced Geometry of Composite Floor System Tested in Cardington Fire Test-7 (Vassart and Zhao, 2011).

Displacement capacity of a composite floor system for fire action is related with reinforcement ratio, because tensile forces that result from large deflections are carried by the reinforcements in the concrete slab. Selamet (2013) conducted several parametric studies to investigate effects of reinforcement size and location to structural performance of fire subjected steel framed reinforced concrete composite floor systems. His studies showed that it is possible to decrease the deflection of the floor system by increasing the rebar area (ratio) due to increasing tensile capacity of the concrete slab. Figure 2.5 represents the effect of reinforcement ratio on the deflection performance of the composite floor system (Selamet, 2013).

Series of steel framed two-way reinforced concrete slabs were tested under fire condition by Lin and Wade (2002). Two of these tests were carried out with identical slab size and loads, the only difference between test specimens (DH12 and D147) was the reinforcement ratio. They concluded that higher reinforcement ratio decreases vertical deflections of the floor assembly and prevents forming of full scale cracks along the reinforced concrete slab.

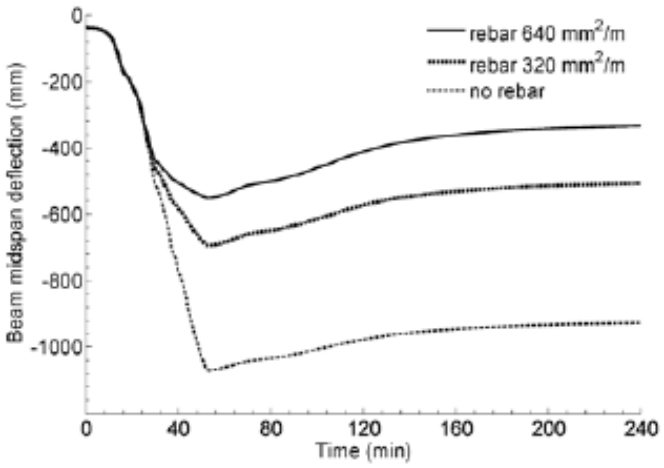

Figure 2.5. Comparison of Steel Beam-Reinforced Concrete Slab Composite Floor Systems Mid-Point Deflections with Respect to Their Rebar Ratio (Selamet, 2013).

This chapter has described effects of boundary conditions, continuity, surrounding elements, connections, alternative load paths, and restraints to the overall structural performance of buildings under fire. It is clear that the fire performance structures cannot satisfactorily be determined by standard fire tests which only focus on the performance of isolated members. Moreover, modern building construction materials are not tested yet with standard fire test procedures. Therefore, prescribed code approach cannot be applied for modern building construction materials.

2.1.3. Performance-Based Structural Fire Safety Concept Framework

There have been many studies to define robust framework for performance based structural fire safety concept. The framework is separated to four-step process which are fire modelling, structural modelling, exposure of the developed fire model to the structural model and assessment of elements, assemblies and entire structure according to predefined assessment criteria with thermo mechanical response of the structure. Lue *et al.* (2016) conducted performance based case study for super tall reinforced concrete (RC) building and followed the frame work that is shown with Figure 2.6.

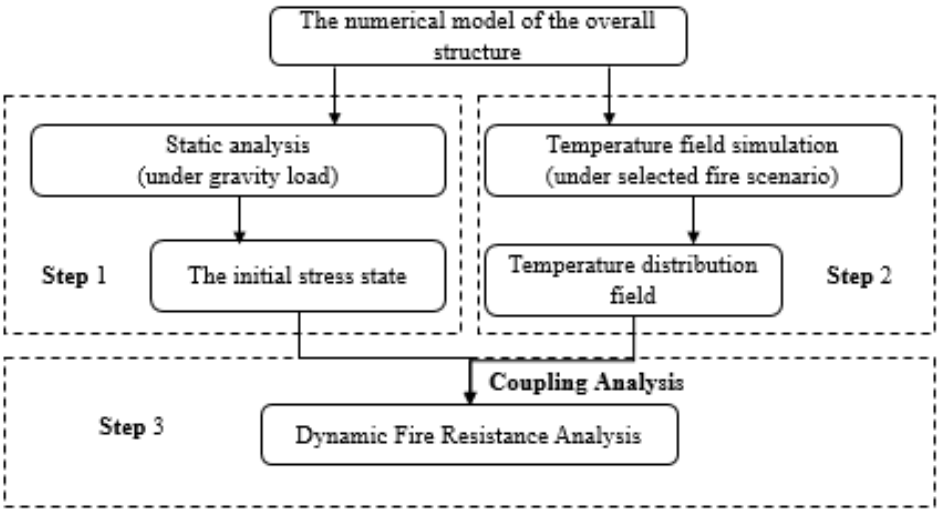

Figure 2.6. Framework for Simulating the Fire Induced Progressive Collapse of Super-Tall RC Buildings (Lu and Ying, 2016).

Rini and Lamont (2008) analyzed structural performance of Ropemaker Place, London under fire action and followed the framework described as below;

- Determination of credible design fire,
- Heat Transfer analyses for the structural members with the design fire,
- Quantification of thermo-mechanical response of the structure for the duration of fire,
- Strength and weakness analysis for the global response of the structure.

Johann (2002) developed a framework to integrate performance-based fire safety concept to structural design process. Johann divided his framework into five steps which are structural design for gravity and lateral loads, consideration of member protection and events that change the structural configuration and details, definition of design fire conditions for the building, analysis of structural response with the design fire conditions and evaluation of the acceptability of the predicted performance. Johann's framework is shown as a flowchart in Figure 2.7. Johann *et al.* (2006) also divided each step shown in Figure 2.7 to the detailed flowcharts to clarify the process.

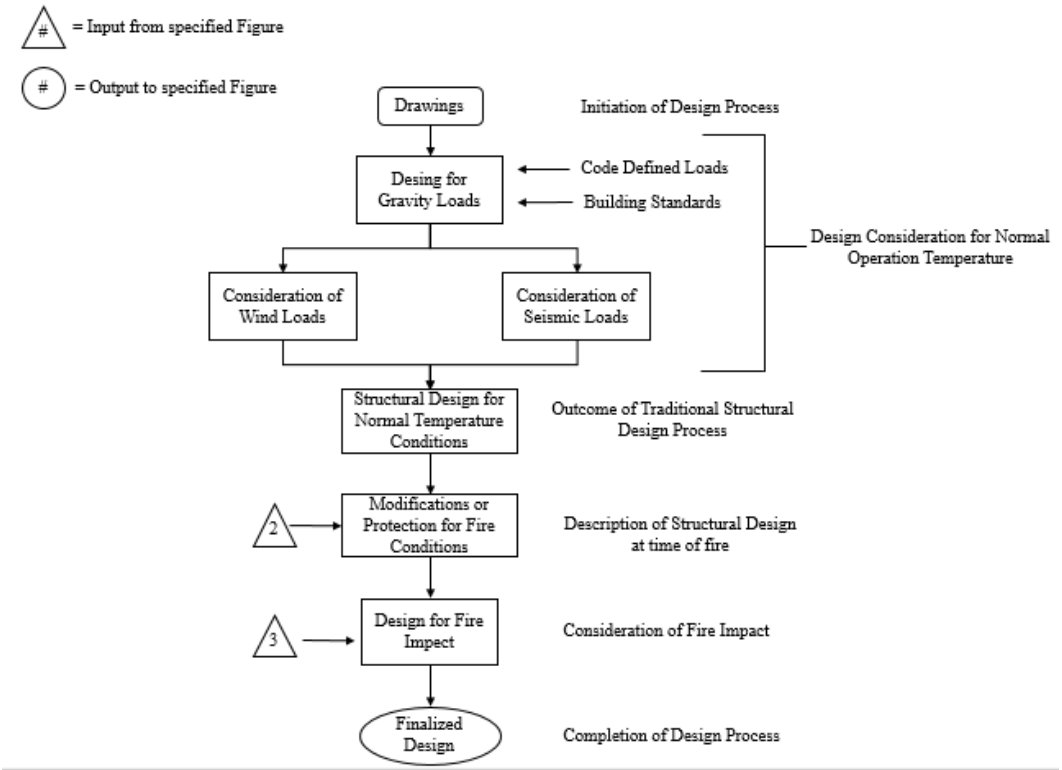

Figure 2.7. Performance Based Structural Fire Safety (Johann, 2002).

In the sections that follows, detailed literature review for each steps of performance based structural fire safety concept will be discussed.

Design of modern buildings are becoming more complex by the development of technology and increased demand to larger application area of buildings. Prescribed fire resistance codes focus on the performance of single structural elements and assemblies with respect to required FRR of these elements and assemblies. Uncertainties on the determination of FRR and effect of overall structure to performance might result overly estimated fire protection level or unexpected failure of the buildings. Therefore, it is important to develop robust framework for performance based structural fire safety concept to satisfy life safety intent, achieve architectural objectives and economical designs.

2.1.4. Numerical Modelling Methods for Structural Analysis

The modulus of elasticity and yield strength of materials decrease with increasing temperature. This situation causes highly nonlinear material behavior and large displacements during fire. Therefore, plastic hinge formation, brittle failure of connections, partial failure of structural members and progressive collapse of structure might occur due to fire action. It is not possible to capture these structural behaviors with static analysis, thus nonlinear implicit or explicit dynamic analysis must be conducted for performance-based structural fire safety concept. Finite element (FE) analysis method is a strong tool to conduct nonlinear dynamic analysis, thus structural performance of elements, assemblies and buildings subjected to fire can be obtained from the results of FE analysis. However, it is important to determine level of complexity of the finite element models. Although, detailed finite element modeling allows engineers to obtain detailed information about mechanics, interaction and capacity of structural members under elevated temperature, it might be inefficient and computationally expensive.

Quiel and Garlock (2008) investigated importance of several finite element modelling parameters for prediction of behavior and capacity of high-rise steel moment framed building under elevated temperature. The parameters that were investigated are shown below;

- Performance of 3D frame model versus that of a 2D plane-frame model, both of which include the steel frame and the floor slab.
- The representation of the slab in the 2D plane frame model.

In their study, girders, columns and the slab in 2D plane frame models were modelled with three-node 2D non-torsional beam elements. Three-node 3D beam elements (capable of torsion) were used to represent the steel frame members and four-node shell elements were used to represent concrete slab in 3D models. The representation of the 2D FE model of plane frame and 3D FE model of wire frame used by Quiel and Garlock are shown with Figure 2.8.

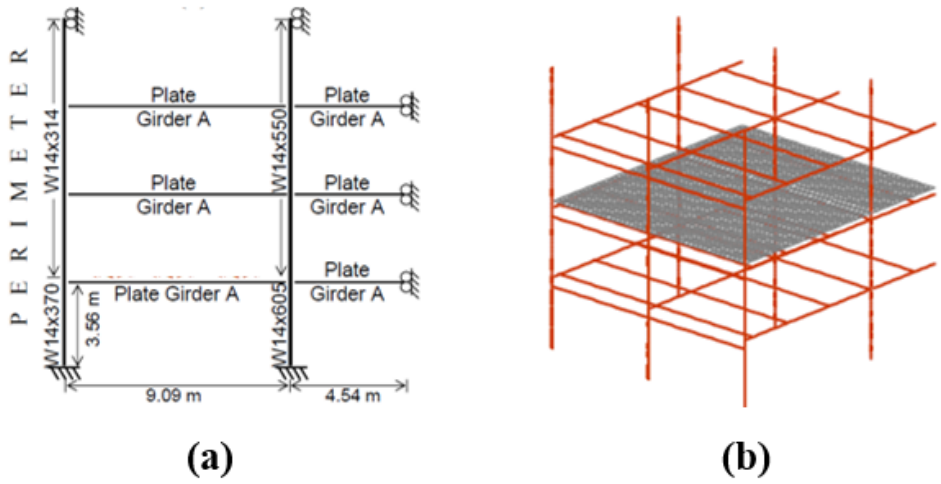

Figure 2.8. Representation of Prototype Building as (a) 2D Frame (b) 3D Wireframe (Quiell and Garlock, 2008).

2D and 3D analyses of Quiell and Garlock showed similar structural behavior with respect to lateral displacement of columns, vertical displacement of girder beams and moment along the perimeter columns. Moreover, both 2D and 3D analysis terminated at same limit states and 2D analysis was 250 times computationally less expensive than 3D analysis.

Analyses conducted to test the second parameter by Quiel and Garlock showed that concrete slab should be included in the thermal analysis of the structural parts but there is no need to present concrete slab for 2D performance based structural analysis of steel frames under elevated temperature.

Vassart *et al.* (2004) compared 2D and 3D FE modelling methods for performance based structural analysis of an industrial hall under elevated temperature with different FE computer software. Figure 2.9 represents the detail of the studies that were conducted by Vassart *et al.* The main differences between 2D and 3D analyses were the allowance of out of plane displacement of columns and beams, and existence of secondary structural elements, purlins and tie-beams, in 3D models.

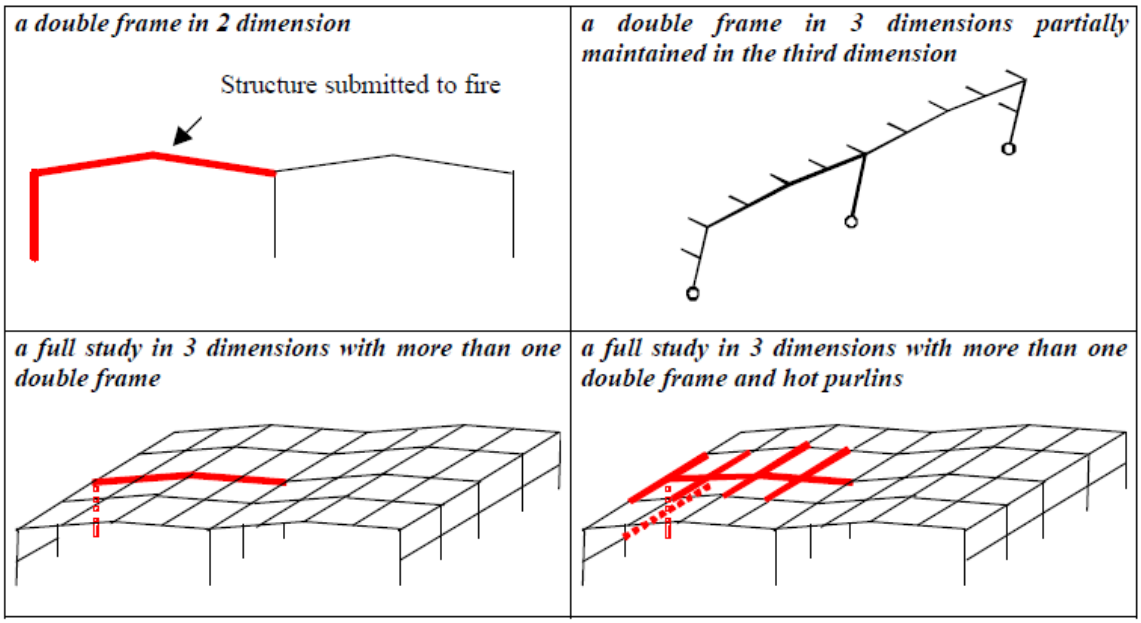

Figure 2.9. Details of Parametric Study for Performance Based Structural Fire Safety Concept (Vassart *et al.*, 2004).

The following paragraph briefly explains the results of the studies shown with Figure 2.9.

Although, collapse mechanism was not observed for 2D frame analysis in 2D space, collapse mechanism was observed as out-of-plane buckling of heated column and beam for 2D frame analysis in 3D space. A visible collapse mechanism has not been observed for 3D frame analysis for fire scenario when only mid-frame heated. On the other hand, for 3D frame analysis in which mid-frame and adjacent purlins are heated, local collapse of the mid-frame region was observed. Parametric study of Vassart *et al.*, showed that thermo-mechanical behavior of the steel framed industrial halls mainly depends on the out-of-plane buckling behavior of the columns and beams, and the state of the purlins. Final remark of the their study states that 3D analyses are required to obtain true thermo mechanical behavior of steel portal framed long span structures.

Moss *et al.*, (2009) conducted several parametric studies to determine structural fire behavior of a steel portal frames with concrete tilt-up panels. A 3D finite element

model of the structure is used. To decrease the computational capacity and demand, they did not include tilt-up wall panels into the structural models and these panels were represented by providing restraints to the columns at the two points where they are connected to the wall panels in the actual structure. Moreover, the steel roof sheet also was not included in the finite element model due to capacity concerns. It is logical not to include steel roof sheet in the FE model, because the steel roof sheet loses its' stiffness at high temperature, thus providing beneficial diagraph effect for the structure. Figure 2.10 represents 3D view of the finite element model of the structure studied by Moss *et al.* (2009).

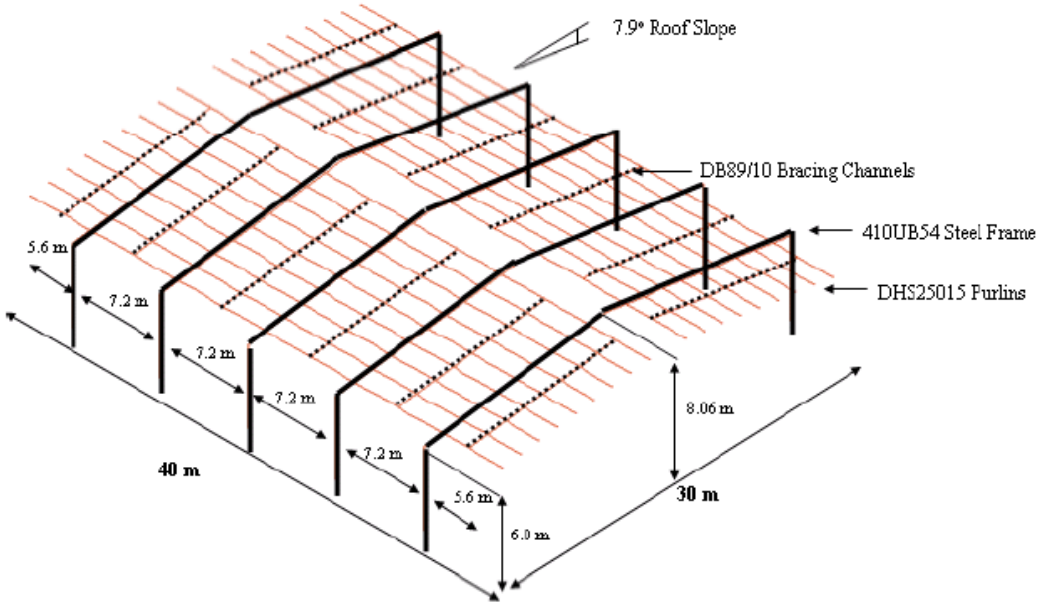

Figure 2.10. 3D View and Dimensions of the Finite Element Model of the Case Study (Moss *et al.*, 2009).

The portal frames of the structure seen in Figure 2.10 were discretized to two-node 40 finite beam elements by Moss *et al.* The nodes of beam elements of portal frames had seven degrees of freedom: three translation, three rotation and one warping. The apex points of the portal frames were defined with two different nodes that represent left and right rafters and it was assumed that there is a perfect bond between these two nodes, thus translational, rotational and warping behavior of these nodes are identical. Although, the knee points of the portal frames were also defined with two

different nodes to represent rafter and column, it was assumed that the bond type of these two nodes does not transmit warping behavior and each nodes behave individually with respect to warping. Moss *et al.* (2009) obtained realistic structural behavior of steel portal framed long span building for different fire scenarios and support conditions with this study, and results of the study showed that it is possible to obtain realistic structural behavior for performance based fire safety concept if the details of the structure are logically simplified for computational efficiency.

In this thesis, the details of the actual structures are simplified in finite element models and detailed explanation of these simplifications are given in Chapter-4.

2.1.5. Simulation Methods for Performance-Based Structural Safety Concept

Temperature-time curves of compartment fires are defined with growth, fully developed and decay periods (phases). These phases are related with total fire load density and configuration of fire load, heat release rate of fire load, ventilation openings and compartment walls lining materials' thermal properties. Growth and fully developed phases of a fire are also described as pre-flashover fire and post-flashover fire, respectively. Transition from pre-flashover fire to post-flashover fire occurs when several conditions related with gas temperature, smoke layer height and fire flame area are satisfied. Once these conditions are satisfied, all fire load inside the compartment ignite and gas temperature increases rapidly, this rapid increase in the gas temperature is defined as flashover. Figure 2.11 illustrates temperature-time relation of real fire with the phases mentioned above.

Standard fire curves and nominal fire curves are developed to express temperature-time relation of compartment fires. These curves do not separate the fire mechanism into different phases and they rise monotonically as function of time. Temperature-time relation of standard fire curve is defined with Equation 2.2 by ISO (ISO, 1999), BSI (BSI, 1987) and DIN (DIN, 1998). Standard fire curve is the most commonly used fire curve to determine fire resistance of building materials and structural elements

with furnace tests. Temperature-time relation of standard fire curve has been developed in the 1930s with data collected from fires that occurred in residential, office and commercial buildings (Zehfuss and Hosser, 2007).

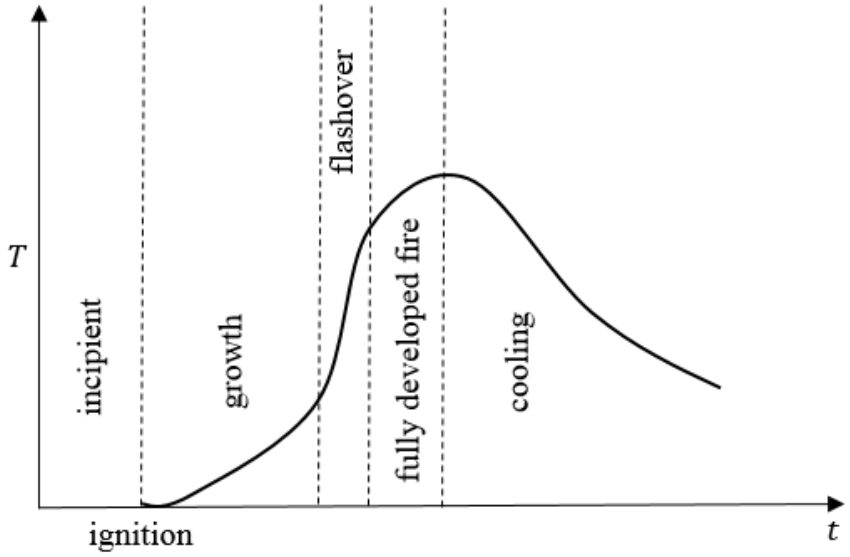

Figure 2.11. Phases of Natural Fire Mechanism.

$$T = 345\log_{10}(8t + 1) + T_0 \tag{2.2}$$

External and hydrocarbon fire curves are examples of nominal fire curves defined in Eurocode 1991.1.2 (CEN, 2002). Hydrocarbon fire curve is applicable for fire scenarios where petrochemical materials are considered as fire load and external fire curve is developed for performance tests of structural members located outside of the burning compartment. Equation 2.3 and Equation 2.4 formulate hydrocarbon and external fire curves, respectively. Figure 2.12 shows temperature-time relations of ISO834 standard fire, Eurocode external and hydrocarbon nominal fire curves.

$$T = 1080\left(1 - 0.325e^{-0.167t} - 0.657e^{-2.5t}\right) + 20 \tag{2.3}$$

$$T = 660\left(1 - 0.687e^{-0.32t} - 0.313e^{-3.8t}\right) + 20 \tag{2.4}$$

ISO834 and nominal fire curves are independent from ventilation and boundary conditions of real buildings. That's why they do not represent the natural fire in a building. Heating rate, fire intensity and duration of a real fire might be different than standard fire and the decay (cooling) phase of a real fire is not included in standard fire curve. Moreover, although standard fire curves are designed for severe fire scenario, they do not always represent the most severe fire conditions. For example, "a short duration high temperature fire can result in spalling of concrete exposing steel reinforcement due to thermal shock" (Bailey, 2004). Industrial buildings tend to contain large quantities of highly flammable materials such as stacked wooden pallets, lube oil, gear oil, solvent, paint, diesel gasoline, cables etc. These materials are high in calorific value, thus fire severity of these buildings will be higher with respect to standard fire and a short duration high temperature fire can be observed in such structures. As a result of these, developing natural fire curve of a compartment for performance based structural fire safety concept (PBSFSC) has gained importance and three well known methodology were developed to define the approximate temperature-time relation of compartments. These methodologies are known as parametric fire curve method, field model method and zone model method.

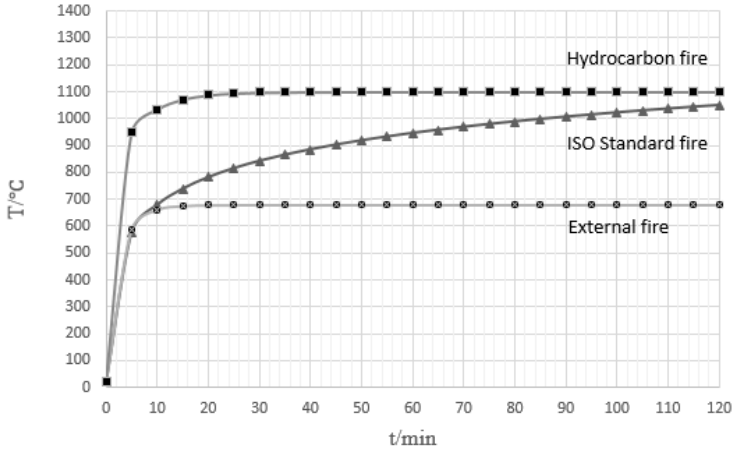

Figure 2.12. Comparison of ISO834, Hydrocarbon and External Fire Curves for 120 Minutes Fire Duration.

Numerous studies have been conducted to define the most reliable parametric fire curve with empirical equations that include heat release rate and compartment boundaries. Magnusson and Thelandersson (1970) have conducted several studies to describe natural fire mechanism of a compartment by solving heat balance and mass balance equations. They introduced effects of gas flow and heat flow through openings to balance equations for enclosed spaces and proposed temperature-time curves for different boundary conditions (fire load, ventilation size, compartment size). These curves have been incorporated with Swedish standard (Pettersson *et al.*, 1976). Wickstrom (1981) showed that the gas temperature in a compartment depends on the ventilation conditions and the thermal properties of the compartment walls. Methodologies described by Wickstrom and Pettersson were used as basis of parametric fire curve defined in Eurocode 1991-1-2 (CEN and BIS, 1996).

Temperature-time relation of heating phase of a compartment fire is formulated with Equation 2.5 in Eurocode 1991-2-2 (CEN, 1996):

$$\theta_g = 1325\left(1 - 0.324e^{-0.2t^*} - 0.204e^{-1.7t^*} - 0.427e^{-19t^*}\right) \tag{2.5}$$

where t^* represents fictitious time and formulated with Equation 2.6;

$$t^* = tx\Gamma\,(hr) \tag{2.6}$$

where Γ "gamma" is the modification factor and formulated with Equation 2.7. O and b_i are the opening factor and thermal inertia of boundary of enclosure, respectively and these parameters are also formulated with Equations 2.8 and Equation 2.9;

$$\Gamma = \left[O/b_i\right]^2 \Big/ \left(0.04/1160\right)^2 \tag{2.7}$$

$$O = A_v\sqrt{h_{eq}}/A_t\left(m^{1/2}\right) \tag{2.8}$$

$$b_i = \sqrt{\rho_b c_b \lambda_b} (J/m^2 s^{1/2} K) \tag{2.9}$$

where ρ_b is the density of boundary of enclosure, c_b is the specific heat of boundary of enclosure, λ_b is the thermal conductivity of boundary of enclosure, A_v is the total area of vertical openings on all walls, h_{eq} is the weighted average of opening heights on all walls and A_t is the total area of enclosure.

By retaining Equation 2.5, improvements have been done for Eurocode parametric fire with respect to the influence of the compartment boundaries, maximum temperature and scope of applications in the most recent version of Eurocode (CEN, 2002). Modifications on the scope of application of Equation 2.5 are listed as below.

- Compartment floor area limitation is increased from up to 100 m^2 to 500 m^2.
- Range of thermal inertia values of compartment linings are increased from $1000 \leq b_i \leq 2000 J/m^2 s^{1/2} K$ to $100 \leq b_i \leq 2200 J/m^2 s^{1/2} K$
- Calculation method has been revised to consider compartment boundaries formed with different materials.
- Fire growth rate duration limitation separated for slow fire growth rate, medium fire growth rate and fast fire growth rate, respectively $t_{lim} = 15\ min, t_{lim} = 20\ min$ and $t_{lim} = 25\ min$

Eurocode parametric fire curve heating phase that is formulated with Equation 2.5 does not represent growth (pre-flashover) phase of a fire and considers fully developed fire (post-flashover) only. On the other hand, for structures with large compartments such as industrial buildings, fully developed fire occurs after several minutes from the ignition of the fire. Therefore, growth phase of a fire has importance on the structural performance of buildings with large compartment area. Growth phase of a fire has been studied by many researches and widely known method to determine growth phase heat release rate *Q (MW)* at time *t(s)* is developed. This method is

known as t-squared method and formulated with Equation 2.10:

$$Q = (\frac{t}{k})^2 \tag{2.10}$$

where k is growth constant.

Temperature-time relation of decay (cooling) phase of a fire is formulated with three linear equations in Eurocode (CEN, 2002). These equations are shown with Equation 2.11 to Equation 2.13;

$$T = T_{max} - 625\,(t^* - t^*_{\max}) \quad for \quad t^*_{max} \quad < \quad 0.5 \tag{2.11}$$

$$T = T_{max} - 250\,(3 - t^*_{\max})\,x\,(t^* - t^*_{\max}) \quad for \quad 0.5 \quad < \quad t^*_{max} \quad < \quad 2 \tag{2.12}$$

$$T = T_{max} - 250\,(t^* - t^*_{\max}) \quad for \quad t^*_{max} \quad \geq \quad 2 \tag{2.13}$$

where t^*_{max} is fictitious time that the maximum temperature (T_{max}) occurs. Similar to Equation 2.6, t^*_{max} can be determined with Equation 2.14.

$$t^*_{max} = t_{max} \quad x \quad \Gamma \tag{2.14}$$

Equation 2.15 formulates t_{max} in which $q_{t,d}$ is the design value of the fuel load density that is related to the total surface area (A_t) of the enclosure;

$$t_{max} = \max\left[(0.2x10^{-3}q_{t,d}/O); t_{lim}\right] \tag{2.15}$$

The value of t_{lim} that is seen in Equation 2.15 is related to fire growth rate and equals to; 25 min for slow fire growth rate, 20 min for medium fire growth rate and 15

min for fast fire growth rate. Design value of the fuel load density, $q_{t,d}$, is formulated with Equation 2.16 and limiting values of $q_{t,d}$ are shown with Equation 2.17;

$$q_{t,d} = q_{f,d} A_f / A_t \tag{2.16}$$

$$50 \leq q_{t,d} \leq 1000 \tag{2.17}$$

where $q_{f,d}$ is design value of the fuel load density related to the surface area A_f of the floor.

Lennon and Moore (2003) investigated Cardington Fire Tests results (Vassart and Zhao, 2011) to validate modifications on the application area of Eurocode parametric temperature-time equation (CEN, 2002) and resulted that while Eurocode parametric equation approximately estimates maximum compartment temperatures with respect to Cardington Fire Tests, it underestimates duration of entire fire and wrongly estimates peak temperature time. The reason of wrong estimation for duration of entire fire and peak temperature time is related with non-consideration of rate of heat release in Eurocode parametric temperature-time equation (Zehruss and Hosser, 2004). In addition, representation of decay (cooling) phase of a fire by Eurocode that is formulated with Equations 2.11 to Equations 2.13 does not reflect real fire decay phase and it cannot be justified.

Lennon and Moore (2003) also compared temperature-time curves of Cardington Fire Tests with ISO834 standard fire curve and showed that maximum temperature values obtained in Cardington Fire Tests were higher than the maximum temperature value of ISO834 standard fire for the entire duration of the tests. This result proved that usage of ISO834 fire curve for structural fire safety designs might cause unexpected structural behavior due to underestimation of fire severity. Comparison of ISO834 standard fire curve (also known as BS476 standard fire curve), Eurocode parametric fire curve and temperature-time history of two of the Cardington Fire Tests is shown with Figure 2.13. Cardington Fire Test-2 and Test-3 shown in Figure 2.13 were conducted

with identical insulation characteristics and opening factors, but polypropylene was used as part of fire load in Test-3. Due to usage of same opening factor, insulation characteristic and fire load density for Test-2 and Test-3, Eurocode parametric fire curve for both of these tests is same, because, as explained before, effect of rate of heat release of polypropylene cannot be modelled in Eurocode parametric equation.

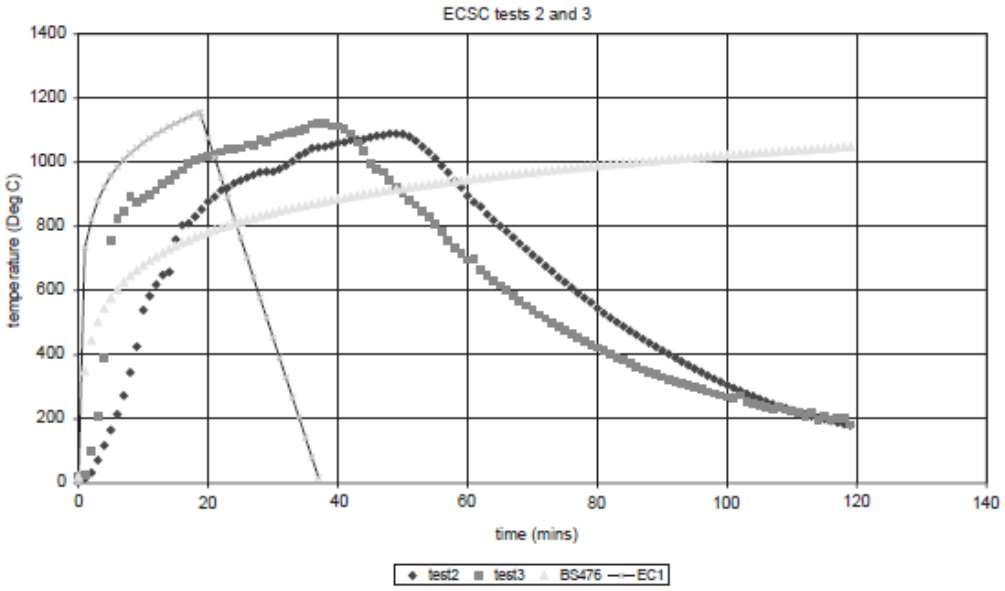

Figure 2.13. Comparison of Cardington Test-2 and Test-3 Results with Eurocode Parametric Fire and BS476 (Also known ISO834) Fire Curves (Lennon and Moore, 2003).

There have been several attempts to develop simplified equation to formulate temperature-time relation of natural compartment fires. Lie's parametric curves (Lie, 1974), Law's maximum temperature equations (Law, 1983) and Barnett's BFD curves (Barnett, 2002, 2007) are widely known of these studies.

Barnett (2002) has developed single log normal equation to describe both growth and decay phase of a compartment fire and fire curves developed with this log normal equation are also known as "BFD Curves". Decay (cooling) phase of BFD curves fits with decay phase of natural compartment fires and BFD curves are validated with several compartment fire tests. Therefore, Barnett's BFD curves are good alternative to Eurocode parametric curves to determine temperature-time relation of compartment

fires. Equation 2.18 shows the lognormal formula used for the derivation of BFD curves. Temperature-time history of 142 natural compartment fires that were conducted with different fire load densities and ventilation openings were used to derive Equation 2.18.

$$T = T_{max}e^{-z} + T_0(^oC) \tag{2.18}$$

where,

$$z = (\log_e t - \log_e t_m)^2/s_c \tag{2.19}$$

Barnett and Clifton (2004) suggested that the value of maximum temperature (T_{max}) in Equation 2.18 can be found with Law's maximum temperature equations (Law, 1983) and peak temperature time of a fire (t_m) used in Equation 2.19 can be found from parametric temperature-time equation of Eurocode 1 Part 1.2 Annex-A (CEN, 1996) and using Equation 2.20.

$$t_m = 60t_{max} \tag{2.20}$$

The formula of shape constant (s_c) used in Equation 2.19 is shown with Equation 2.21 and it is related with thermal insulation of compartments (c_i) and pyrolysis coefficient (k_p).

$$s_c = c_i k_p, \tag{2.21}$$

$$k_p = 1/(148F_{o2} + 3.8), \tag{2.22}$$

$$F_{o2} = A_v h_v / A_{t2}, \tag{2.23}$$

$$A_{t2} = A_t - A_v \tag{2.24}$$

where, c_i is 38 for compartments with minimum insulation, steel sheet roof and walls and 16 for compartments with maximum typical insulations, timber floors, plasterboard lined walls and ceiling, A_t is the total internal surface area of compartment including openings, A_v and h_v are the sum of opening areas and mean height of vertical openings respectively.

Figure 2.14 represents comparison of BFD parametric fire curve with Eurocode Parametric fire curve and ISO834 standard fire curve for fire load density ($q_{f,d}$) equals to 400 MJ/m^2, opening factor (O) equals to 0.066 m$^{0.5}$ and thermal inertia of the compartment (b_i) equals to 1558 J/m^2 s$^{1/2}$ K

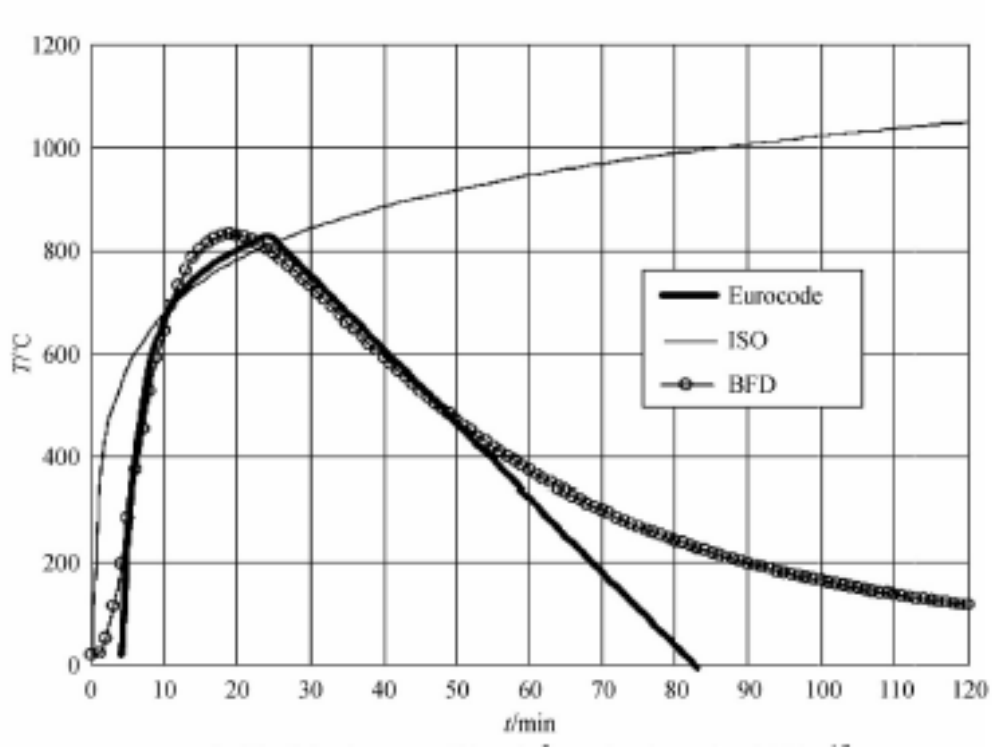

Figure 2.14. Comparison of BFD, Eurocode and ISO 834 Fire Curves (Barnett, 2007).

Zehruss and Hosser (2004) developed parametric equations (iBMB parametric equations) to simulate each phase of compartment fires of residential and office buildings. The effects of heat release rate of burning materials and compartment boundary

conditions on a compartment fire were included in iBMB parametric equations. The upper bound of usage of iBMB parametric equations was determined with maximum possible fire load density (1300 MJ/m^2) for office and residential building compartments. It is possible to use iBMB parametric equations to simulate temperature-time curve of compartments that contain smaller value of fire load than upper bound by calibrating formulas for each phase of a fire. Zehruss and Hosser compared temperature-time curves of fire test and fire design software results with iBMB curve for ordinarily furnished office building fire. Figure 2.15 represents this comparison and it is obvious that iBMB fire curve approximately estimates temperature-time history of the fire test.

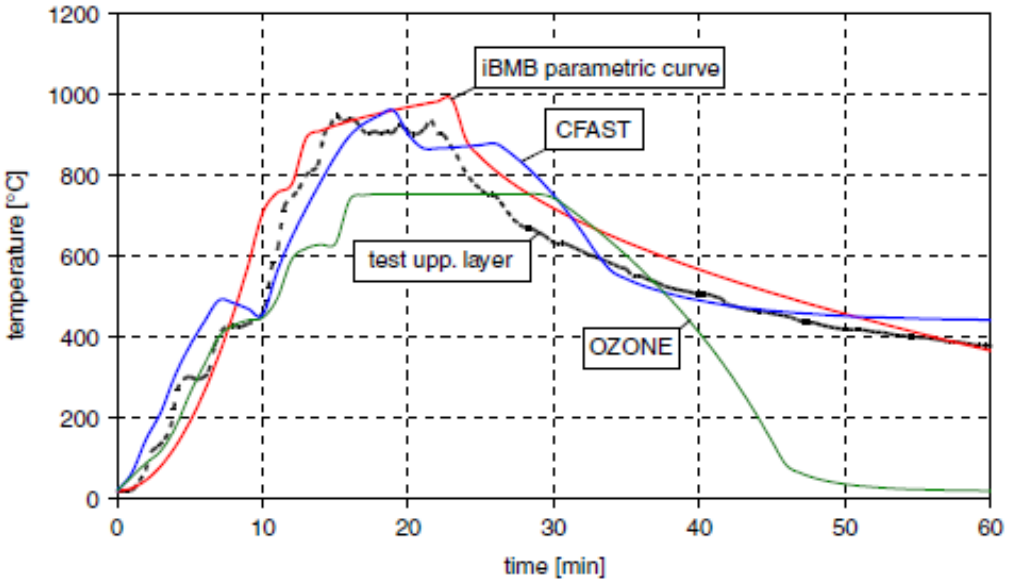

Figure 2.15. Comparison of iBMB Curve and Different Fire Design Software Results with Compartment Fire Test Results for Ordinarily Furnished Office Building (Zehruss and Hosser, 2004).

Although maximum temperature of a compartment fire and temperature-time history of a residential and office building compartment fires were approximately estimated with parametric fire curve equations, application area of these parametric equations are limited with respect to fuel load density, ventilation location and orientation, compartment wall insulation materials and compartment dimensions. Moreover, scope of application of parametric fire curves does not allow designers to model active

firefighting devices (sprinkler systems, smoke dampers etc.). Therefore, advanced fire modelling techniques have been developed to determine temperature-time curves of compartment fires.

Two different modelling techniques are available for advanced fire modelling. These are field modelling technique and zone modelling technique. Computational Fluid Dynamics (CFD) method represents field modelling technique. Compartment is divided to finite number of controlling volumes in CFD modelling method and, heat and mass balance in these controlling volumes are determined by solving transient differential equations, wildly known as Navier-Stokes equations, to determine temperature-time history, rate of heat release, height of flame, temperature of flame, height of smoke layer, velocity of smoke layer, effect of active firefighting devices to smoke movement and fire mechanism for entire compartment or different sub-areas of the compartment. Although, wide range of data can be collected with CFD modelling method, it requires advanced experience to proper modelling and CFD models must be validated before being used for performance based structural fire safety concept. Field modeling is out of scope of this thesis and will not be detailed in the subsequent sections of this thesis.

Zone modelling technique is similar to field modelling technique in means of dividing compartment to controlling volumes. However, in zone modelling technique number of controlling volumes are assumed as one or two. Temperature-time history of the buildings that are analyzed in this thesis are developed by the zone modelling technique.

First numerical studies on zone models were conducted by Pettersson (1976), these studies conducted on one zone model. Magnussun *et al.* (1976) also conducted numerical studies for zone modeling approach. Theoretical basis of zone models depends on conservation of energy and mass in fire compartments. Zone models take into account of rate of heat release of combustible materials, fire plume, mass flow, smoke movement and gas temperature. They rely on some assumptions concerning physic of fire behavior and smoke movement suggested by experimental observation of real

fires in compartments. The fundamental mass and energy balance equations that are required to be solved for one zone models are listed as below;

- The energy balance between the heat released by the fire, the gas in the compartment, the compartment boundaries, and the external atmosphere through openings.
- The mass balance between the pyrolysis released by the fire, and the incoming and outgoing air through the openings.

One zone models are used for the prediction of temperature-time history of fully developed compartment fires, they do not give information about pre-flashover behavior of a fire. In one zone models gas temperature, gas density, internal energy and pressure are assumed uniformly distributed in the compartment. Figure 2.16 represents schematic diagram for development of one zone models.

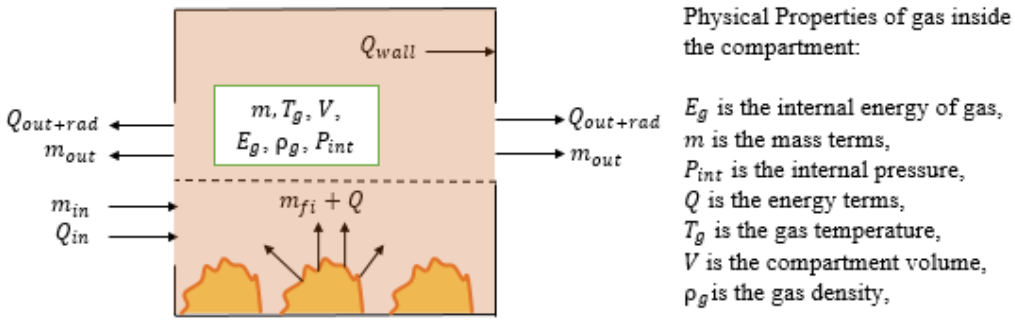

Figure 2.16. Schematic Diagram of One Zone Models.

Basic equations of conservation of mass and energy for one-zone models are available in Eurocode 1991-1-2, 2002 Annex-D (CEN, 1996) and shown with Equation 2.25 to Equation 2.27.

$$P_{int} = \rho_g R T_g \tag{2.25}$$

Equation 2.25 defines ideal gas law where P_{int} is the internal gas pressure of the compartment is, ρ_g is the gas density, R is the universal gas constant and T_g is the gas

temperature.

$$\frac{dm}{dt} = \dot{m}_{in} - \dot{m}_{out} + \dot{m}_{fi} \tag{2.26}$$

The mass balance of a compartment is shown with Equation 2.26 in which $\frac{dm}{dt}$ is rate of change of gas mass in the compartment, $\dot{m}_{fi}$ is the rate of pyrolysis products generated, $\dot{m}_{in}$ is the rate of gas mass coming in through the openings and $\dot{m}_{out}$ is the rate of gas mass going out through the openings.

Finally, Equation 2.27 defines the energy balance of the gases in the compartment where E_g is the internal energy of gas, Q is the rate of heat release of the fire, Q_{in} is the increase of energy due to gas mass coming in through the openings, Q_{out} is the loss of energy due to gas mass going out through the openings, Q_{rad} is the loss of energy due by radiation through the openings and Q_{wall} is the loss of energy to the enclosure surfaces.

$$\frac{dE_g}{dt} = Q + Q_{out} + Q_{in} - Q_{wall} - Q_{rad} \tag{2.27}$$

It is assumed that gas temperature in one zone models is uniformly distributed along the compartment as stated before. On the other hand, in most cases fire ignition is localized and therefore a fire remains localized during a certain amount of the time. Therefore, there were need to define initial phase of fire, and two-zone modelling technique was developed.

The compartment is divided into two different zones that are upper layer and lower layer in two-zone compartment fire models. Figure 2.17 represents schematic diagram of fire simulation with two zone models. Two-zone models are also based on the solving the ordinary differential equations for the conservation of mass and energy in the compartment, equations used in two-zone models are more complex comparing with the equations of one-zone models. Numerical two-zone models are normally based

on 11 physical variables and these variables are linked by 7 constraints to 4 differential equations that describes the mass and the energy balances in each zone (Cadiron *et al.*, 2001). However, the number of variables are 7 and the number of constraints are 4 for one-zone models.

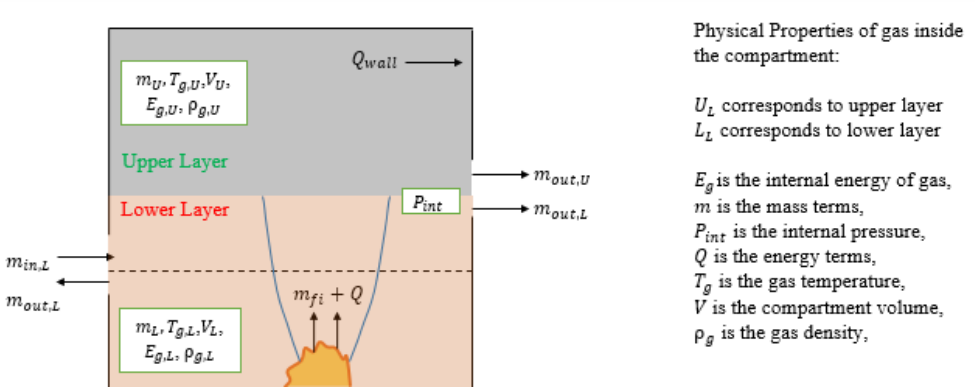

Figure 2.17. Schematic Diagram of Two Zone Models.

Following the ignition of fire in compartment, if gas temperatures along the compartment is sufficiently high to provoke spontaneous ignition of all the combustible materials in the compartment, a flashover occurs and if some conditions with respect to fire area and smoke layer thickness encountered, two-zone model switches to one-zone model. Thus, it is possible to observe all phases of fire by incorporating two-zone models and one-zone models. The conditions that are required two-zone model to switch one-zone model are shown as below (CEN, 2002);

- If the gas temperature of the upper layer is higher that 500 ^{o}C,
- If the upper layer is growing to cover 80% of the compartment height.

There have been several attempts to develop computer programs to conduct parametric studies with zone modelling techniques. Compartment boundary conditions, rate of heat release of burning materials, ventilation openings, fire load density and effect of active firefighting devices are some of the parameters that are considered for the development of computer programs. Jarmai (2010) has conducted a study to determine publicly available software for fire design. According to his studies there are 48 publicly available zone modeling software. Ozone (Cadiron *et al.*, 2001) and CFAST

(Portier *et al.*, 1992) are widely known zone modelling software which are capable to simulate compartment fires with two-zone modelling technique and switching two-zone model to one-zone model.

Results obtained from these software were compared with fire test data to analyze degree of reliability of zone modelling technique for performance based structural fire safety concept. Cadiron *et al.* (2001) validated results of Ozone with 67 different test data. The tests that were used for validation of Ozone were conducted with fire load density that were varying between 37 to 151 MJ/m^2 and opening factor that were varying between 0.0015 to 0.157 m$^{0.5}$. Comparison of the test data and the Ozone results is shown with Figure 2.18. The each point represented with red dot on Figure 2.18 shows maximum gas temperature measured in fire tests and the oblique line represents location of perfect fit according to Ozone results. The dotted line on Figure 2.18 represents linear regression of test data and Ozone results among all points.

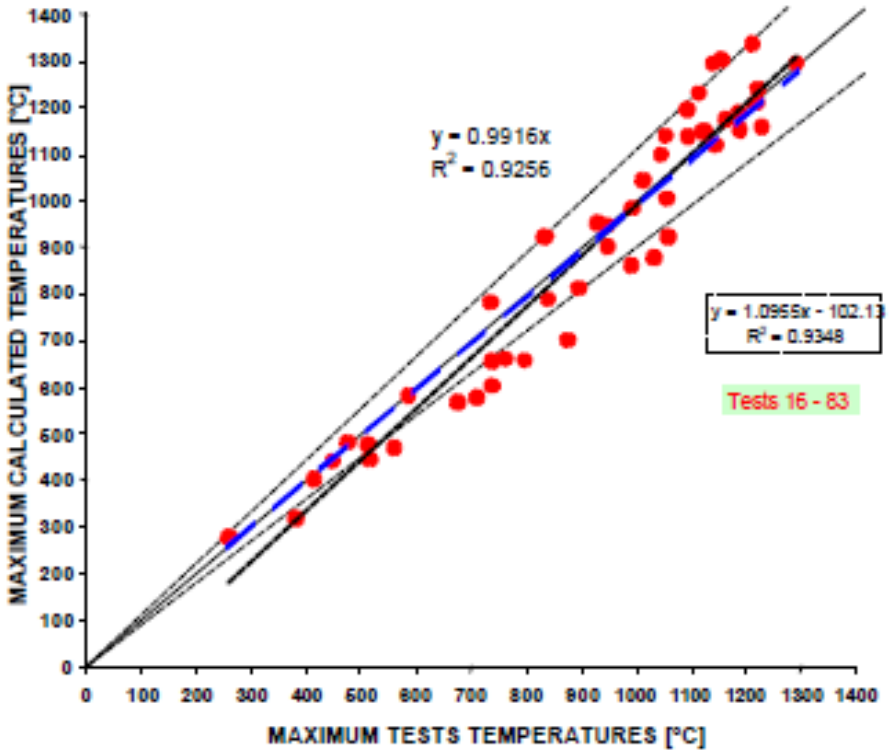

Figure 2.18. Comparison of Maximum Temperatures Obtained from Furnace Tests with Ozone Results (Cadiron *et al.*, 2001).

A considerable amount of literature have been published to analyze structural fire behavior of buildings with performance-based structural fire safety design concept. Different fire simulation methods that were explained in this chapter were adopted in the studies. The following paragraph is a brief review of usage of different fire simulation methods for performance-based structural fire safety concept in the literature.

Paya-Zaforteze and Garlock (2002) used two different nominal fire curves to analyze fire subjected structural performance of simply supported typical steel girder bridge. Hydrocarbon fire (CEN, 2002) and temperature-time history of a real fire event were used in their analyses and results of their study showed that different structural behavior of steel girder bridge might be obtained according to selection of the fire simulation method. Quiel and Marjanishvilli (2012) conducted a study to analyze structural performance of a building that has exposed the explosion and fire that arise from the explosion. They used ISO834 standard fire curve (ISO, 1999), but they emphasized that decay (cooling) phase of a real fire event might result unexpected failure of the structure. Moss *et al.* (2009) analyzed behavior of steel portal framed industrial building under fire action. They used ISO834 standard fire curve and external fire curve (CEN, 2002) in their analyses. The result of their studies showed that steel portal frames subjected to external fire resist longer duration than the steel portal frames subjected to ISO834 standard fire. Lue and Ying (2016) investigated fire induced-progressive collapse mechanism of super-tall reinforced concrete structure by using ISO834 standard fire with 10 hours heating process to model simplified extreme fire scenario. Rini and Lamont (2008) conducted a case study for 21-story office building and used Eurocode parametric fire equations (CEN, 2002) to simulate fire scenarios for the building. Zhou *et al.* (2015) used field modelling technique to simulate realistic fire scenario for the performance-based analysis of air-supported membrane structure. Behnam and Rezvani (2014) used traveling fire phenomena to analyze performance of multi-story building subjected to post-earthquake fire. Result of their study showed that considerable difference on structural behavior might be observed if traveling fire is selected as a design fire instead of uniform fire (One-Zone model fire, Standard Fire, Nominal Fires, Parametric Fires).

Figure 2.19 shows temperature-time curves that are generated with the different methods explained in this section for large scale warehouse building fire. The building's ventilation openings characteristics, fire parameters, wall lining thermal properties and geometry are given in Table 2.2. Eurocode parametric fire curve, BFD fire curve, ISO834 standard fire curve and hot-zone fire curve obtained from zone model fire simulation of the building are represented in Figure 2.19. According to the figure, the zone model fire curve best fit with the real fire curve shown in Figure 2.11.

Zone model fire simulations are used in this thesis to simulate industrial building fires because zone model fire simulations accurately represent real fire behavior of large industrial buildings with including pre-flashover fire phase, and there are prescribed limitations of BFD and Eurocode parametric fire equations that do not allow to simulate large industrial building fires.

2.1.6. Heat Transfer Analysis Methods

To conduct performance-based structural analysis under elevated temperature, time-temperature history of each structural member and assembly must be determined. Heat transfer analysis between design fire and structural members must be conducted to determine time-temperature history of the structural parts.

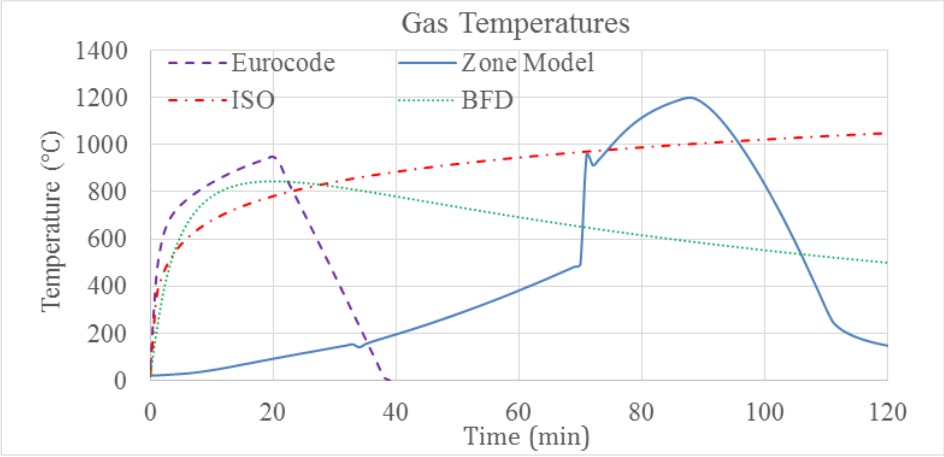

Figure 2.19. Comparison of BFD, Eurocode, ISO 834 and Zone Model Fire Curves for the Large Scale Warehouse Building.

Table 2.2. General Properties of the Warehouse Building.

Building Geometry			
Width (m)	Length (m)	Height (m)	Floor Area (m^2)
40	70	11.5 - 15.5 (5.7^o Roof Inclination)	2800
Characteristics of Ventilation Openings			
Dimensions and Vertical Alignment	Type 1	Type 2	Type 3
Height (m)	2.1	5	2
Width (m)	2	5	12
Vertical Alignment (m)	0 - 2.1	0 - 5	9-Nov
Number of Openings on the Perimeter Walls			
Wall - 1	2	-	-
Wall - 2	2	1	1
Wall - 3	1	-	1
Wall - 4	2	1	-
General Fire Parameters			
Characteristic Fire Load Density (MJ/m^2)	Design Fire Load Density (MJ/m^2)	Fire Growth Rate	Fire Duration (min)
511	416	Medium	120
Thermal Properties of Wall Lining			
Thickness (cm)	Unit mass (kg/m^3)	Conductivity (W/mK)	Specific Heat (J/kgK)
15	30	0.026	1470

Time-Temperature history of structural members can be obtained with one, two and three dimensional heat transfer analysis or with lumped mass method. While three dimensional heat transfer analysis is generally used for details of structures, such as connections, time-temperature history of columns and beams are sufficiently determined with two dimensional thermal analysis. One dimensional heat transfer analysis generally used to determine time-temperature history of slab assemblies through the slab's thickness.

A computer software SAFIR (Franssen, 2005) that has been developed at the University of Liege is capable to conduct two dimensional heat transfer analysis for various type of structural members and construction materials. Numerous studies have been conducted with SAFIR to determine time-temperature history of structural members exposed to fire. Quiel and Marjanishvilli (2011) investigated structural performance

of a building that was subjected to multi-hazard, explosion and subsequent fire. They used two dimensional solid elements (fibers) within the SAFIR to conduct heat transfer analysis. Neal *et al.* (2012) analyzed structural performance of high rise building subjected to extreme event and subsequent fire. They have used two dimensional heat transfer analysis to determine temperature distribution along the steel beam and columns with SAFIR. Quiel and Garlock (2008) conducted parametric studies to determine effect of finite element (FE) modelling parameters on the fire induced behavior and capacity of high-rise steel moment frame (MF) building. They have conducted two dimensional heat transfer analysis for columns and beams of MF and one dimensional heat transfer analysis for reinforced concrete slab to determine temperature-time history of these members with SAFIR. Although, three dimensional heat transfer analysis is out of scope of SAFIR, there are several commercial computer software to conduct three dimensional heat transfer analysis.

Selamet and Garlock (2014) investigated fire resistance performance of shear connections for a subassembly used in Cardington Fire Test (Lennon and Moore, 2013). They modeled subassembly that includes shear connection region of the real compartment with three dimensional elements with ABAQUS (DS-Similua, 2012), commercial finite element analysis software that is capable to conduct three dimensional heat transfer analysis. Selamet and Garlock compared steel beam mid-span thermo-couple readings of Cardington Fire Test with time-temperature history of same region obtained from three dimensional heat transfer analysis. This comparison is represented with Figure 2.20 and it is obvious that three dimensional heat transfer analysis reliably estimates temperature distribution along the beam depth.

Although dimensional heat transfer analyses properly estimate temperature distribution of fire subjected structural members, these analyses require advanced knowledge of finite element modelling techniques and computationally expensive. In addition, if fire is fully engulfed in the compartment, all structural members will be heated by surrounded hot gases and due to high conductivity of the steel, temperature distribution along the steel members will be close to uniform (ASCE, 1992).

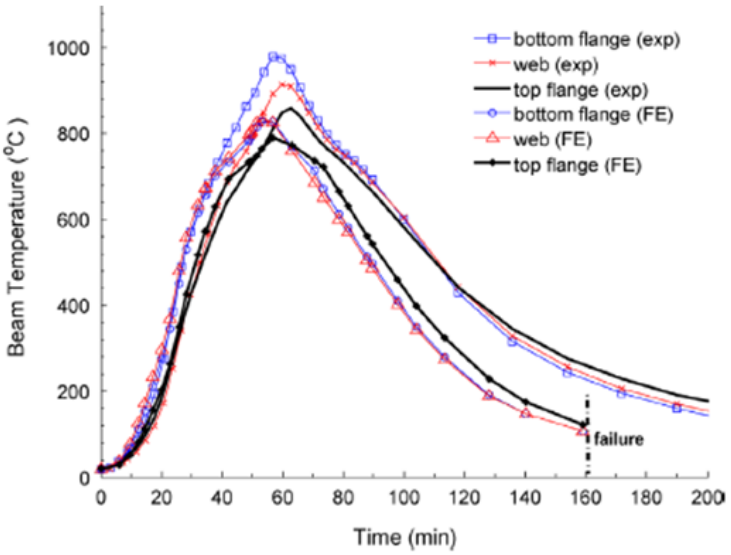

Figure 2.20. Temperature-time History of Steel Beam Mid-Span for Three Dimensional Heat Transfer Analysis and Cardington Fire Test (Selamet and Garlock 2014).

Uniform heating of steel cross section, thus uniform temperature distribution can also be considered for members subjected to flame of localized fire (e.g. pre-flashover fire). Lumped mass method can be used to find time-temperature history of structural members that have uniform temperature distribution. Lumped mass method considers the entire section of a structural material as "lumped" and this method approximate but simplifies the transient heat transfer problem greatly. In the transient problem net energy transfer to the "lumped" section is nonzero and it causes the internal energy of the section to increase at each time step.

The increase of temperature in an unprotected steel member during specified time interval is formulized with Equation 2.28 in Eurocode-3 Part 1-2 (CEN, 2005) according to Lumped mass method.

$$\Delta\theta_{a,t} = \mathrm{k}_{sh}\frac{A_m/V}{c_a\rho_a}\dot{h}_{net,d}\Delta t \tag{2.28}$$

where $\Delta\theta_{a,t}$ is the increase of temperature in an unprotected steel member, k_{sh} is the correction factor for shadow effect, A_m/V is the section factor for unprotected steel

members $(1/m)$, A_m surface area of the member per unit length ($m^2/(m)$), V is the volume of the member per unit length ($m^3/(m)$), c_a is the specific heat of steel (J/kgK), $\dot{h}_{net,d}$ is the design value of the net heat flux per unit area (W/m^2), Δt is the time interval (seconds), ρ_a is the unit mass of steel ($kg/(m^3)$).

For I sections under nominal fire action, the correction factor for the shadow effect may be determined with Equation 2.29.

$$k_{sh} = 0.9[A_m/V]_b / [A_m/V] \tag{2.29}$$

where $[A_m/V]_b$ represents box value of the section factor. For all other cases than I sections, k_{sh} should be determined with Equation 2.30.

$$k_{sh} = [A_m/V]_b / [A_m/V] \tag{2.30}$$

Shadow effect does not have importance for cross sections that has a convex shape and fully embedded in fire, thus it should be taken as unity. The value of Δt in Equation 2.28 should not be less than 5 seconds. The value of section factor A_m/V should not be taken less than 10 m^{-1} in Equation 2.28.

The design value of the net heat flux $\dot{h}_{net,d}$ might be obtained from Equation 2.31 according to Eurocode 1991-1-2 (CEN, 2002).

$$\dot{h}_{net,d} = \alpha_{hc}\,(\theta_g - \theta_m) + \Phi.\varepsilon_m.\varepsilon_f.\sigma.[(\theta_r + 273)^4 - (\theta_m + 273)^4] \tag{2.31}$$

where, α_{hc} is the coefficient of heat transfer by convection (W/m^2 K), θ_g is the gas temperature in the vicinity of the fire exposed member (^{o}C), θ_m is the surface temperature of the member (^{o}C), Φ is the configuration or view factor, ε_m is the surface emissivity of the member, ε_f is the emissivity of the fire, σ is the Stephan Boltzmann constant (=5,67.10^{-8} W/m^2K^4), θ_r is the effective radiation temperature of the fire environment (^{o}C).

The coefficient of heat transfer by convection (α_{hc}) can be obtained from relevant temperature-time curve of the design fire. For standard fire curves (ISO834, BS-476, DIN4102) recommended value for α_{hc} is (25 W)/(m^2 K). The emissivity of fire (ε_f) is generally taken as 1. The configuration factor (Φ) should be taken as 1 and lower value may be chosen to take account of so called position and shadow effect. In the case of fully engulfment of members by fire, the radiation temperature (θ_r) may be represented by the gas temperature (θ_g) around the member (CEN, 2002). The gas temperature of a compartment might be found with the methodologies that have been explained in the section 2.1.5 of this thesis. The value of surface emissivity of the structural member (ε_m) depends position of the structural member, flame and emissivity of the material and flame. Petterson *et al.* (1976) represented acceptable values for surface emissivity of steel members as shown in Table 2.3.

Table 2.3. Emissivity Values for Different Construction Types and Fire Exposure Scenarios (Petterson *et al.*, 1976).

Position of Steel Members and Fire Exposure	Suggested Emissivity
Column exposed to fire in all sides	0.7
Column outside to building facade	0.3
Floor girder with floor slab of concrete, only the underside of the bottom flange being exposed to fire	0.5
Floor girder with floor slab on the top flange	0.5
Box girder and lattice girder	0.7

Several computer software are available to calculate time-temperature history of fire subjected steel members according to Eurocode provisions. Elefir-EN (Real and Franssen, 2015) and Ozone (Cadiron *et al.*, 2001) are widely used software. Vassart *et al.* (2004) simulated fire induced structural behavior of industrial hall with different finite element computer software to determine differences between two dimensional finite element models and three dimensional finite element models. They used lumped mass method for thermal analysis of structural members with Eurocode provisions. Kilic and Selamet (2013) investigated fire induced symmetric and asymmetric collapse mechanisms of a multi-story steel structure. They also used lumped mass method to

calculate time-temperature history of steel members with 25 W/(m^2 K) for coefficient of heat transfer by convection (α_{hc}) and 0.5 for surface emissivity of the members (ε_m).

In this thesis, time-temperature history of steel members are calculated with lumped mass method with Eurocode provisions for strength analysis of the case studies. Moreover, 2D heat transfer analysis is conducted to determine thermo-mechanical behavior of steel framed reinforced-concrete slab composite floor systems.

2.1.7. Assessment Criteria for Performance Based Structural Fire Safety Concept

Performance-based structural fire safety concept (PBSFSC) is used to understand behavior of the structures under real fire conditions. The results gathered from PBSFSC analysis must provide level of agreement with the prescribed design criteria to achieve life-safety of building occupants and fire fighters during fire action, and serviceability of the building after fire action. Stability of the structural elements, assemblies and whole structure, and integrity of the structural members are two main criteria for the assessment of PBSFSC analysis results.

To achieve stability of the columns, beams and floor systems during the entire fire duration, load bearing capacity of these structural members should be maintained without any observation of sudden increase in the displacement within the structural members. Integrity of the structural members are defined as the capacity of the members to restrict fire separation. Crack formation within the floor systems and walls, collapse of these structural members and brittle behavior of connection should be avoided to achieve integrity. Considerable amount of study have been conducted to determine limit states for the achievement of stability and integrity during the entire fire duration. The limit states for stability and integrity are mainly determined with respect to state of the demand-capacity ratio, displacement, rate of displacement, temperature distribution and equivalent plastic strain along the structural members for the entire duration of fire.

British Standards (BSI, 1987) defines fire resistance limit states of the fire subjected beams with respect to deflection and rate of deflection as below:

- The maximum deflection of beams should not exceed L/20 for entire fire duration,
- The rate of deflection should not exceed the value that is determined with Equation 2.32,

$$\frac{L^2}{9000d}\,(mm/min) \tag{2.32}$$

where L is the span length of beam (mm) and d is the depth of the beam (mm).

American Society of Civil Engineers divides resistance limit states of structural members to two categories, force controlled limit states and deformation controlled limit states (ASCE, 2007). Resistance limit state of structural member whose axial load demand-capacity ratio is less than 0.5 under the ambient temperature conditions is defined with deformation control by ASCE. Generally, beams, girders, purlins and tie-beams are defined as low axially loaded members. These structural members can show plastic deformation without significant decrease in their stiffness and deformation limit states of these structural members are determined with the plastic rotation capacity of the members. Plastic rotation limits of these members are listed in ASCE SEI 41-06 Chapter-5 Table 5.4. (ASCE, 2007), these limits can also be used for PBSFSC of steel framed structures.

American Society of Testing and Materials defines fire resistance limit state of the columns according to their strength decrease ration under elevated temperature (ASTM, 2016). According to ASTM, when the axial load carrying capacity of a steel column decreases 50% of that at ambient temperature, the column can be assumed as failed (ASTM, 2016).

Material model for structural steel defined by the Eurocode (CEN, 2005) states that plasticized steel fibers will begin to unload at 15% strain and they will not be able

to carry load when they reach 20% strain.

Gernay *et al.* (2016) defines limit state criteria of steel beams and columns according to rate of displacements for the entire duration of fire. They states that when the vertical rate of displacement of mid-span of the beams and transverse rate of displacement of mid-height of the columns reach to 50 mm/min, these structural members might be defined as failed members.

The failure criteria of reinforced concrete slab defined with thermal limit state by American Society of Testing and Materials (ASTM, 2016). Accordingly, the thermal failure of reinforced concrete slab occurs when the temperature of steel rebars that carry tensile forces reaches to 593 ^{o}C (ASTM, 2016). On the other hand, due to low conductivity of concrete slab it is low likelihood scenario for rebars to reach 593 ^{o}C before the excessive displacement of the floor system (Vassart and Zhao, 2011). Floor systems can maintain excessive displacement for the entire duration of fire if they are properly reinforced (Rini and Lamont, 2008). Thus, rate of displacement of floor system and steel rebar strain are far acceptable criteria for the limit state of the reinforced concrete floor systems subjected to fire.

Table 2.4 represents limit states for the failure assessment of several structural members for fire action according to the literature review explained in this section.

2.2. Research Significance

Performance-based structural fire safety concept (PBSFSC) has gained importance in recent years after the fire-induced collapse of several iconic buildings, the World Trade Center and the Windsor Tower. Considerable amount of study have been conducted to understand fire and collapse mechanisms of high-rise steel and reinforced concrete buildings. These studies have shown that reliable prediction of structural behavior under elevated temperature can be obtained with PBSFSC. On the other hand, only few study have been conducted to determine structural behavior of industrial buildings under fire action. Industrial buildings tend to contain larger quantities

of highly flammable materials than office and residential buildings, and due to large compartment area of industrial buildings, fire characteristic and collapse mechanism of industrial buildings differ from office and residential buildings. Therefore, a commonly used PBSFSC frameworks are not proper for the analysis of industrial buildings and there is a need for simple yet reliable framework to simulate fire and response characteristics of industrial buildings.

Table 2.4. Limit States of Failure Assessment Criteria for Different Structural Members.

References	Type of Member	Assessment Criteria	Limit State
British Standard Institute British Standard Institute	Steel Beam	Deflection	L/20
British Standard Institute (BS-476, 1987)	Steel Beam	Rate of Displacement	$L^2/(9000d)$
American Society of Civil Engineers (ASCE SEI-41/06, 2007)	Low Axially Loaded Steel Members	Plastic Rotation Plastic Rotation	Table 5.4 Table 5.4
American Society of Material and Test (ASTM, 2016)	Steel Column	Strength Decrease	50%
American Society of Material and Test (ASTM, 2016)	Steel Rebar	Thermal	593 ^oC
Eurocode (CEN, 2005)	Steel Column, Beam, Rebar	Strain (Yielding)	2%
Eurocode (CEN, 2005)	Steel Column, Beam, Rebar	Strain (Failure)	15% - 20%
Gernay (Gernay *et al.*, 2016)	Steel Column, Beam	Rate of Displacement	50 mm/min

2.3. Objective and Scope of the Study

The aim of this thesis is to develop relatively simple yet robust framework to forecast fire mechanism and its impact for industrial buildings. The proposed framework within this thesis allows designers to use PBSFSC for industrial building with large compartment area and increase application area of PBSFSC.

Within the scope of this study, natural fire mechanism, strength and serviceability limit states of 5 industrial buildings that are different with respect to their structural system, fire load density, fire load location and compartment boundary con-

ditions are investigated with developed PBSFSC framework. In addition to this, a simplified methodology is developed to simulate thermo-mechanical behavior of composite floor systems with close form differential beam and plate deflection equations and implemented in to Matlab together with nonlinear analysis solution strategy. The developed simplified methodology is verified against finite element model results and used to estimate serviceability limit state of composite floor systems that are located in one of the investigated industrial building.

3. METHODOLOGY (FRAMEWORK)

3.1. General

The fire induced structural performance of 5 different industrial buildings are investigated as case studies in this thesis. Each building has a minimum fire resistance rate according to Turkish Fire Code (Republic of Turkey Ministry of Environment and Urbanization, 2009). Each building is unique with respect to their fire load type and density, ventilation openings, architectural layout, structural system and gravitational loads. Therefore, a slightly different scenario is considered for performance-based structural analysis of each of the buildings. General methodologies that are utilized to determine design load combination, material models and assessment criteria of the case studies are described in Sections 3.2, 3.3 and 3.7, respectively. Finite element modelling technique, fire simulation and heat transfer analysis methods that are utilized for the performance-based structural fire safety concept of the case studies are described in Sections 3.4, 3.5 and 3.7, respectively.

3.2. Design Load Combination

Fire action on buildings is considered as an accidental action and it is not combined with earthquake loads according to the provisions of the Eurocode - 1 (CEN, 2002) as explained with the following clause.

- Clause 4.2.2.: "*Simultaneous occurrence with other independent accidental actions needs not to be considered*". (CEN, 2002).

Equation 3.1 represents general equation for structural design load combinations of buildings according to Eurocode - 1 (CEN, 2002).

$$\sum_{j\geq 1} G_{k,j} + A_d + (\Psi_{1,1} or \Psi_{2,1}) \quad x \quad Q_{k,1} + \sum_{i>1} \Psi_{2,1} \quad x \quad Q_{k,i} \tag{3.1}$$

where $G_{k,j}$ represents gravitational actions, A_d represents accidental action, $Q_{k,1}$ represents leading variable action, $Q_{k,i}$ represents secondary variable actions, ψ represents load factors for the design load combination.

Snow loads, live loads and self-weights of structural members, walls, ceiling, equipment and cranes are taken into account for performance-based structural fire analyses of the case studies. Snow loads are considered as the leading variable action assuming that all of the buildings are located 1000 m above the sea level and live loads are considered as secondary variable action. Wind loads are not taken into account. Table 3.1 represents load factors that are recommended by Eurocode - 1 (CEN, 2002) for variable actions.

Combination value factor of loads (ψ_0) is used for the verification of ultimate limit and irreversible limit states, frequent value factor of loads (ψ_1) is used for verification of ultimate limit states involving accidental actions and verification of reversible serviceability limit states, and quasi-permanent value factor of loads (ψ_2) is used for verification of ultimate limit states involving accidental actions and also long term effects.

Table 3.1. Recommended Values of Load Factors (CEN, 2002).

Action	ψ_0	ψ_1	ψ_2
Imposed Loads in buildings, category (see EN 1991-1-1)			
Category A: domestic, residential areas	0.7	0.5	0.3
Category B: office areas	0.7	0.5	0.3
Category C: congregation areas	0.7	0.7	0.6
Category D: shopping areas	0.7	0.7	0.6
Category E: starage areas	1.0	0.9	0.8
Category F: traffic areas, vhicle weight 30 kN	0.7	0.7	0.6
Category G: traffic areas, 30 kN vhicle weight 160 kN	0.7	0.5	0.3
Category H: roofs	0	0	0
Show loads on buildings (see EN 1991-1-3)*			
Finland, Iceland, Norway, Sweden	0.70	0.50	0.20
Remainder of CEN Member States, for sites			
located at altitude H¿ 1000 m a.s.l.	0.70	0.50	0.20
Remainder of CEN Member States, for sites			
located altitude H< 1000 m.a.s.l.	0.50	0.20	0
Wind loads on buildings (see EM 1991-1-4)	0.6	0.2	0
Temperature (non-fire) in buildings (see EN 1991-1-5)	0.6	0.5	0
NOTE ψ The values may be set by the National annex.			
*For countries not mentioned below, see relevant local conditions.			

As stated before, fire and fire induced forces on building are accidental actions. Therefore, to determine design load combination of performance-based structural fire analysis the frequent or quasi-permanent values of load factors must be used for leading variable actions, and quasi-permanent values of load factors must be used for secondary variable actions. Selecting the frequent or quasi-permanent values for leading variable action is generally determined with national annex. On the other hand, usage of the quasi-permanent load factors for leading variable actions is developed to create load combinations that include earthquake action. Therefore, selecting frequent values of load factor for leading variable actions is the most proper solution to create performance-based structural fire analysis design load combination (Franssen *et al.*, 2009).

Following values of the load factors are used for the leading variable action (snow load) and the secondary variable action (live loads) in the design load combination of the case studies:

- ψ_1=0.5 (Assuming that all the buildings are above 1000 m of sea level),
- ψ_2=0.8 (Categorizing industrial buildings as Category-E).

3.3. Material Model

Structural steel, hot-rolled steel reinforcement and calcareous aggregated normal weight concrete are used as the construction materials of the structures of the case studies. Stress-strain relationship, stiffness (Elastic Modulus), specific heat, conductivity and thermal expansion coefficient of these construction materials vary with elevated temperatures. Therefore, fire induced behaviors of the structures are closely related to the temperature dependent material properties of these construction materials.

Temperature dependent elastic stress-strain relationship and thermal properties of structural steel, steel reinforcement and concrete are taken from Eurocode - 3 Part 1-2 and Eurocode - 4 Part 1-2 (CEN 2005, 2004) for performance-based structural fire analyses. Moreover, “Von Mises” yield criterion is used to model plasticity of the struc-

tural steel with isotropic strain hardening. Figure 3.1 shows plasticity model of the structural steel under elevated temperatures. Stress-strain relationship of steel reinforcement and concrete are assumed to show linear elastic behavior for entire duration of the heating and due to convergence concerns, no material softening is included in the material models of the construction materials. Moreover, it is assumed that material models of the structural steel, steel reinforcement and concrete return to their original states during cooling phase of structural members.

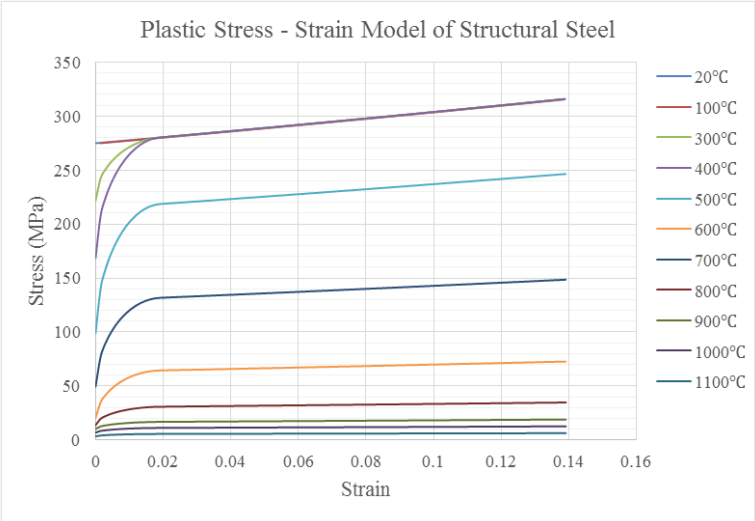

Figure 3.1. Plastic Stress - Strain Model of Structural Steel.

Temperature dependent mechanical and thermal material properties of structural steel and hot-rolled steel reinforcement can be assumed as identical according to the following clause of Eurocude 4 - Part 1-2 (CEN, 2005). Therefore, elastic stress - strain relationship of structural steel is used as the stress - strain relationship of steel reinforcement for performance-based structural fire analyses. Temperature dependent mechanical and thermal properties of structural steel and steel reinforcement are shown in Table 3.2.

- Clause 3.2.3.4.: "*In case of thermal actions according to natural fire models, the stress-strain relationships of structural steel, may be used as a sufficiently precise approximation for hot rolled reinforcing steel*". (CEN, 2005).

Table 3.2. Temperature Dependent Mechanical Material Properties of Structural Steel and Steel Reinforcement.

Temperature Dependent Mechanical and Thermal Material Properties of Structural Steel and Steel Reinforcement												
T (^{o}C)	20	100	200	300	400	500	600	700	800	900	1000	1100
ρ_a (kg/m^3)	7850	7850	7850	7850	7850	7850	7850	7850	7850	7850	7850	7850
E (GPa)	210	210	189	168	147	126	65.1	27.3	18.9	14.2	9.5	4.7
ν	0.3	0.3	0.3	0.3	0.3	0.3	0.3	0.3	0.3	0.3	0.3	0.3
σ_y (MPa)	275	275	275	275	275	214	129	118	30.3	16.5	11	5.5
α_a ($1/^o$C)	1.41 E-21	1.25 E-5	1.29 E-5	1.33 E-5	1.37 E-5	1.41 E-5	1.45 E-5	1.49 E-5	1.41 E-5	1.34 E-5	1.31 E-5	1.51 E-5
λ_a (W/mK)	53.3	50.7	47.3	44	40.7	37.5	34	30.7	27.3	27.3	27.3	27.3
c_a (J/kgK)	440	487	533	564	606	666	760	1008	803	650	650	650

Stress-strain relationship of C20 calcareous aggregated normal weight concrete that is presented in Eurocode 4 - Part 1-2 (CEN, 2005) is used to estimate compressive strength and stiffness of concrete under elevated temperatures for performance-based structural fire analyses. Table 3.3 represents temperature dependent mechanical and thermal material properties of calcareous aggregated normal weight concrete.

Table 3.3. Temperature Dependent Mechanical and Thermal Material Properties of Calcareous Aggregated Normal Weight C20 Concrete.

Temperature Dependent Mechanical and Thermal Material Properties of C20 Calcareous Aggregated Normal Weight Concrete												
T(^{o}C)	20	100	200	300	400	500	600	700	800	900	1000	1100
ρ_a (kg/m^3)	2349	2331	2307	2284	2260	2237	2213	2190	2166	2143	2119	2096
E (GPa)	8	5	3.46	2.43	1.5	0.8	0.36	0.24	0.12	0.06	0.03	0.008
ν	0.2	0.2	0.2	0.2	0.2	0.2	0.2	0.2	0.2	0.2	0.2	0.2
ε_{cu}	0.0025	0.004	0.0055	0.007	0.01	0.015	0.025	0.025	0.025	0.025	0.025	0.025
σ_c (MPa)	20	20	19	17	15	12	9	6	3	1.6	0.8	0.2
α_c ($1/^o$C)	5.61 E-9	6.18 E-6	6.62 E-6	7.35 E-6	8.36 E-6	9.65 E-6	1.21 E-5	1.31 E-5	1.52 E-5	1.76 E-5	1.22 E-5	1.11 E-5
λ_c (W/mK)	1.95	1.77	1.55	1.36	1.19	1.04	0.91	0.81	0.72	0.66	0.62	0.6
c_c (J/kgK)	900	900	1000	1050	1100	1100	1100	1100	1100	1100	1100	1100

3.4. Finite Element Modelling

Moment resistant steel portal frames and cross diagonals are used as in-plane and out-of-plane load carrying mechanisms for structures of the case studies. Parallel portal frames are connected with each other by roof purlins and tie-beams in all the buildings. Figure 3.2 represents example general layout of a building that is designed with moment resistant parallel portal frames and cross bracings. Moreover, two of the buildings consist of a steel-framed reinforced-concrete-slab composite floor systems as

secondary load carrying mechanism.

In this section, the details of the modelling technique to define portal frames, secondary structural members (purlins, tie-beams, cross diagonals, stability braces, wind columns etc.), composite floor systems, boundary conditions, and column initial bow imperfection are described.

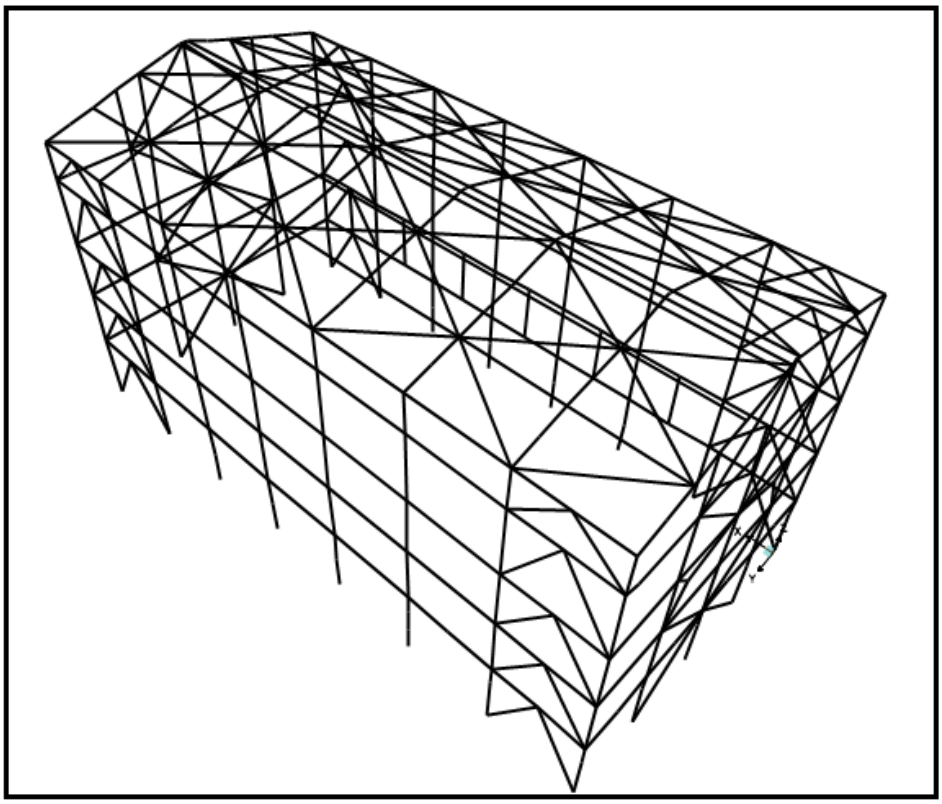

Figure 3.2. General Layout of Out-of-plane Braced Portal Frame Structural System.

ABAQUS, finite element analysis software, (DS-Simulia) is utilized to simulate 3D finite element models of the buildings.

3D two-node shear flexible B31 linear beam element is used to model columns and rafters of the portal frames, secondary structural members (purlins, tie-beams, cross diagonals, stability braces, wind columns etc.) and composite floor beams. B31 linear beam element has six degrees of freedom at each node. Three of them represent translations and the other three of them represent rotations in 3D space. B31 beam

element have no warping degrees of freedom at its nodes, and warping is considered as unconstrained at its nodes, thus any axial stress due to warping is neglected. Moreover, B31 beam element have no temperature degrees of freedom at its nodes. Therefore, structural analyses are uncoupled from heat transfer analyses and steel temperatures that are obtained from heat transfer analyses are applied as a predefined field into the structural analyses.

It is assumed that there are fully compatibility at knee points of the portal frames where columns and rafter are connected and at apex point of the portal frames where two rafter are connected. Moreover, there is also fully compatibility between composite floor perimeter beams and columns.

Translational degrees of freedom at purlin ends where they connect with rafters are identical with translational degrees of freedom of rafters, but their rotational degrees of freedom are independent from each other in all models. This connection type generally known as pin connection and it is also used between tie beams and columns, cross diagonals and columns, roof diagonals and rafters, composite floor secondary beams and perimeter beams in finite element models of the buildings.

In all models, it is assumed that twisting of the purlins, tie-beams, and cross diagonals are restrained along their entire length by the screws between cladding and these secondary structural members.

Level of base fixity of all structures is modelled with the same boundary conditions in the following:

- Translational degrees of freedom of column base are fully restrained.
- Rotational degrees of freedom of column base are restrained along the longitudinal axis and along the moment resistance direction of the portal frames.
- Rotational degree of freedom of column base is free to rotate along the orthogonal direction to the moment resistance direction of the portal frames.

Steel sheeting of roofs and perimeter walls are not simulated in finite element models of the buildings, and the beneficial diaphragm effect of the roof sheeting is also ignored due to the fact that thin steel sheeting loss its strength and stiffness at high temperature. On the other hand, self-weights of the perimeter wall and roof sheeting is included in the structural analyses.

The steel-framed reinforced-concrete-slab floor assemblies exist in two of the buildings. They are not included in the finite element models due to computational complexity. The thermal effect of the concrete slab is however considered for the heat transfer analyses of the perimeter and secondary beams.

Thermo-mechanical behavior of composite floor assemblies are also investigated with simplified methodologies that are described in Chapter-5 of this.

Once the finite element models are constructed with the methodologies explained in this section, design loads that are calculated according to Section 3.2 are applied to the models and static analyses are conducted. Subsequently, an implicit dynamic analysis is conducted with the effect of fire temperatures.

3.4.1. Determination of Column Initial Bow Imperfection

Column buckling is a sudden failure phenomenon and causes local or global collapse of structures. To capture buckling initial bow imperfection must be defined to the columns of the structure. Real structural members are rarely perfectly straight and have a natural curvature, and load carrying capacity of columns are directly related with this natural curvature (Hailemichael and Liivo, 2014). General assumption about shape of the natural column curvature states that the first elastic buckling shape of a column shall be used as initial imperfect geometry of the column with appropriate displacement coefficient (CEN, 2005). But, the first elastic buckling shape of a column depends on stiffness and position of cross-diagonals and tie-beams in real structures. The stiffness of these bracing members reduces during fire and these members may fail due to thermally induced normal forces. As a result, bracing effects of these mem-

bers may not be achieved and imperfect geometry of the column that is defined at the ambient temperature may fail to represent true geometry under a fire. Therefore, there is a need of new methodology to define initial column imperfection for the thermo-mechanical analysis of entire structure.

The methodology that is adopted to define initial bow imperfection to columns of the structures is explained in following paragraphs with an example.

Figure 3.3 shows columns that are braced at different levels with cross-diagonals and tie-beams along global y axis and not braced along global x axis. The column that is highlighted with green rectangle in Figure 3.3 may have five different possible first elastic buckling shapes for buckling around the global x axis according to state of the bracing members at elevated temperature and have one possible first elastic buckling shape for buckling around the global y axis.

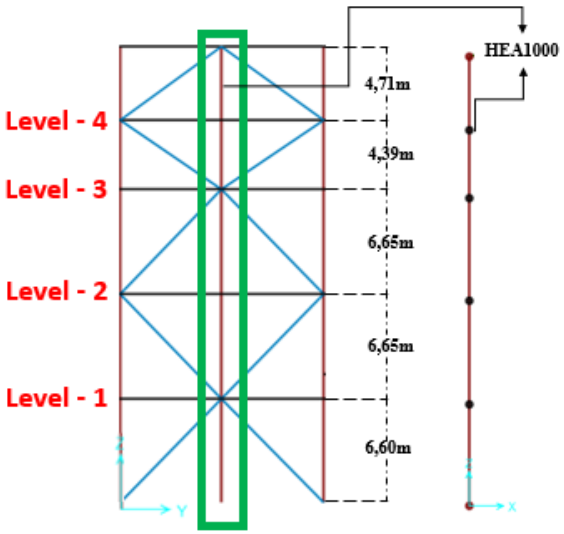

Figure 3.3. Braced Column Illustration.

The highlighted column may have 5 different first elastic buckling shapes depending on the fire performance of the cross-diagonals and the tie-beams. These shapes are shown in Figure 3.4. As explained above, the initial bow imperfection of the column should be defined in a way that it should represent possible first elastic buckling shape.

Since, there are 5 different possible first elastic buckling shapes of the highlighted column, all of these shapes should be considered while defining the initial bow imperfection to the column to get the most realistic structural performance of the column in case of a fire. Therefore, following steps are performed to define the initial imperfection to the highlighted column.

Firstly, 5 different buckling analyses are conducted for the highlighted column by suppressing the bracing members at each level in sequence. Secondly, nodal displacements of the column that are obtained from the buckling analyses are saved for each possible first elastic buckling shape and multiplied by initial bow imperfection coefficient which is unique value for each of the first elastic buckling shapes. The initial bow imperfection coefficient reduces nodal displacements of the buckled column to the nodal displacements of the initial natural curvature of the column and determined with Eurocode-3 Part 1-1 (CEN, 2005) provisions as explained in following paragraphs. Finally, nodal displacements of all the 5 different natural curvatures are averaged to represent all possible initial bow imperfections and applied to the highlighted column before the structural analysis.

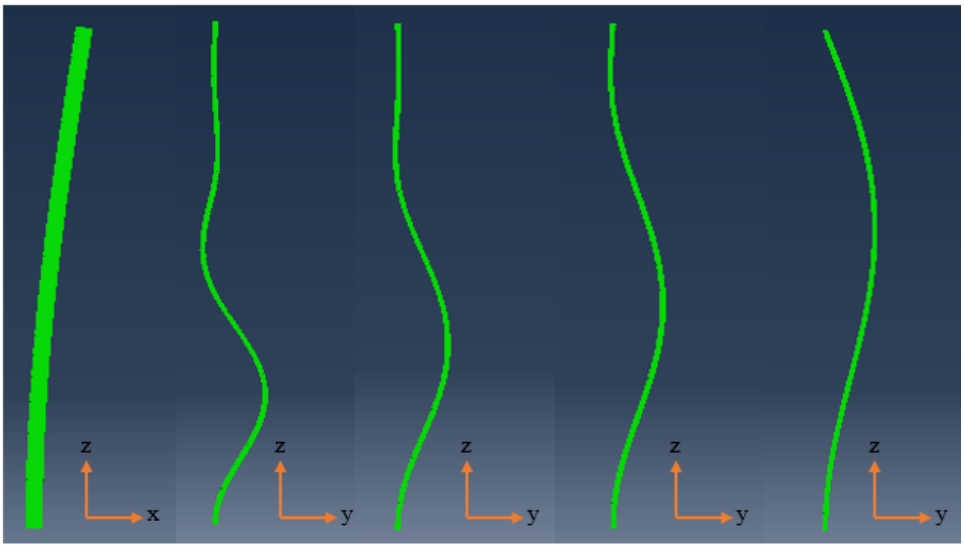

Figure 3.4. Possible First Elastic Buckling Modes of the Highlighted Column.

Equation 3.2 is adopted from Eurocode-3 Part 1-1 (CEN, 2005) to convert first elastic buckling shape of column to initial bow imperfection. The first two terms of

Equation 3.2 represent initial bow imperfection coefficient and the last term represents elastic buckling mode shape.

$$\eta_{inil} = e_0 \frac{N_{cr}}{EI \mid \ddot{\eta}_{cr} \mid_{max}} \eta_{cr} \tag{3.2}$$

where

$$e_0 = \left(\bar{\lambda} - 0.2\right) \frac{M_{rk}}{N_{rk}} \frac{1 - \frac{\chi\bar{\lambda}^2}{\gamma_{M1}}}{\chi\bar{\lambda}^2} \quad for \quad \bar{\lambda} \quad > \quad 0.2 \tag{3.3}$$

and

$$\bar{\lambda} = \sqrt{\frac{\alpha_{ult,k}}{\alpha_{cr}}} \tag{3.4}$$

is the relative slenderness of the structure (e.g. column, beam)

where α_{imp} is the imperfection factor for the relevant buckling curve according to Eurocode-3 Part 1-1 (CEN, 2005), χ is the reduction factor for the relevant buckling curve depending on the relevant cross section Eurocode-3 Part 1-1 (CEN, 2005), $\alpha_{ult,k}$ is the minimum force amplifier for the axial force configuration N_{ed} in members to reach the characteristic resistance N_{rk} of the most axially stressed cross section without taking buckling into account, α_{cr} is the minimum force amplifier for the axial force configurationN_{ed} in members to reach the elastic critical buckling load, M_{Rk} is the characteristic moments resistance of the critical cross section, e.g. $M_{el,Rk}$ or $M_{pl,Rk}$ as relevant, N_{Rk} is the characteristic resistance to normal force of the critical cross section, i.e. $N_{pl,Rk}$, $EI \mid \ddot{\eta}_{cr} \mid_{max}$ is the bending moment due to η_{cr} at the critical cross section, η_{cr} is the shape of elastic critical buckling shape.

Initial bow imperfections for all columns in actual finite element models of the buildings are defined with the Equation 3.2. There are 16 different columns with respect to their cross section dimensions, lengths and bracing systems in the finite element models of the buildings. On the other hand, according to the definition of η_{ult}, k and η_{cr}, columns that are identical with respect to their cross section dimensions, lengths

and bracing systems may have different initial bow imperfection depending on the axial force that they carry. Therefore, to reduce computational effort for the definition of initial bow imperfections in the finite element models of the buildings, the maximum axial force on the identical columns is used for the calculation of η_{ult}, k and η_{cr}. As a summary, initial bow imperfection of identical columns are assumed as identical with largest possible natural curvature. Total 54 different first elastic buckling shapes of the 16 different columns are analyzed in ABAQUS (Ds-Simulia, 2012) and results of these analyses are incorporated with the explained methodology to implement initial bow imperfections to the columns of the finite element models of the buildings.

3.5. Fire Simulation Method

In this thesis, two-zone and one-zone fire models whose mathematical backgrounds are described in Section 2.1.6, and localized fire method that is explained in Section 3.5.1 are combined to simulate natural fire mechanisms of the buildings.

3.5.1. Zone Model Fire Simulation

Zone model fire simulations of the buildings are performed with Ozone, fire simulation software, (Cadiron *et al.*, 2001). Fire load density, rate of heat release, dimensions and alignment of the ventilation openings, thermal properties of the lining materials, and fire compartment geometry are inputs of the Ozone to estimate hot and cold zone temperatures, heat release rate, fire area, and smoke elevation level.

As explained in Section 2.1.6, if several conditions are fulfilled during zone model fire simulations, two-zone fire model switches to one-zone fire model. Ozone has ability to perform this switching process automatically with fulfillment of predefined conditions. These predefined conditions are listed as below for zone model fire simulations of the investigated buildings, and fulfillment of one of these conditions is sufficient for two-zone fire model to be switched one-zone fire model.

- Upper layer temperature $\geq$ 500 ^{o}C,
- Combustible in Upper Layer + Upper Layer Temperature $\geq$ Combustible Ignition Temperature (300 ^{o}C),
- Interface Height (Height of Upper and Lower Layer Interface) $\leq$ 0.2 Compartment Height,
- Fire Area $\geq$ 0.25 Compartment Floor Area.

Two-zone fire models are generally applicable to calculate hot-zone (gas/smoke) temperatures for localized fire scenarios. Localized fires may occur in two different scenarios as explained with the following paragraph.

The first scenario for the occurrence of localized fire is related with localization of the fuel load. If combustible materials are concentrated in small area of the compartment floor surface, the fire will be localized and two-zone fire model will be applicable for the entire duration of the fire simulation. However, although the fulfillment probability of the predefined conditions is quite low for the localized fire load concentration, it is important to consider that if one of the predefined conditions is fulfilled the two-zone fire model should be switched to the one-zone fire model for proper estimation of hot-zone (gas/smoke) temperatures.

The second scenario for the occurrence of localized fire is related with the phases of fire. If fire loads are uniformly distributed on the entire floor surface area of the building, fire ignition will be localized and fire will remain localized during certain amount of time and two-zone fire model will be applicable to estimate hot zone (gas/smoke) temperatures. If gas temperatures are sufficiently high (first condition) to provoke spontaneous ignition of all the combustible present in the compartment a flashover occurs and two-zone fire model switches to one-zone fire model. On the other hand, it is important to note that, although the gas temperatures are not sufficiently high for the flashover, two-zone fire model might also switch to one-zone fire model with fulfillment of the other pre-defined conditions during the pre-flashover phase of the fire. Moreover, if condition-(1) is not fulfilled for during the fire simulation, the fire remains localized for distributed fire load.

Figure 3.5 shows algorithms that are used for the transition of two-zone fire model to one-zone fire model for different fire load concentration types. The algorithm shown in Figure 3.5b is followed to find hot-zone (gas/smoke) temperatures for fire simulations of the buildings due to conservative assumption that total fire loads in the buildings are distributed on the total floor surface area of the buildings.

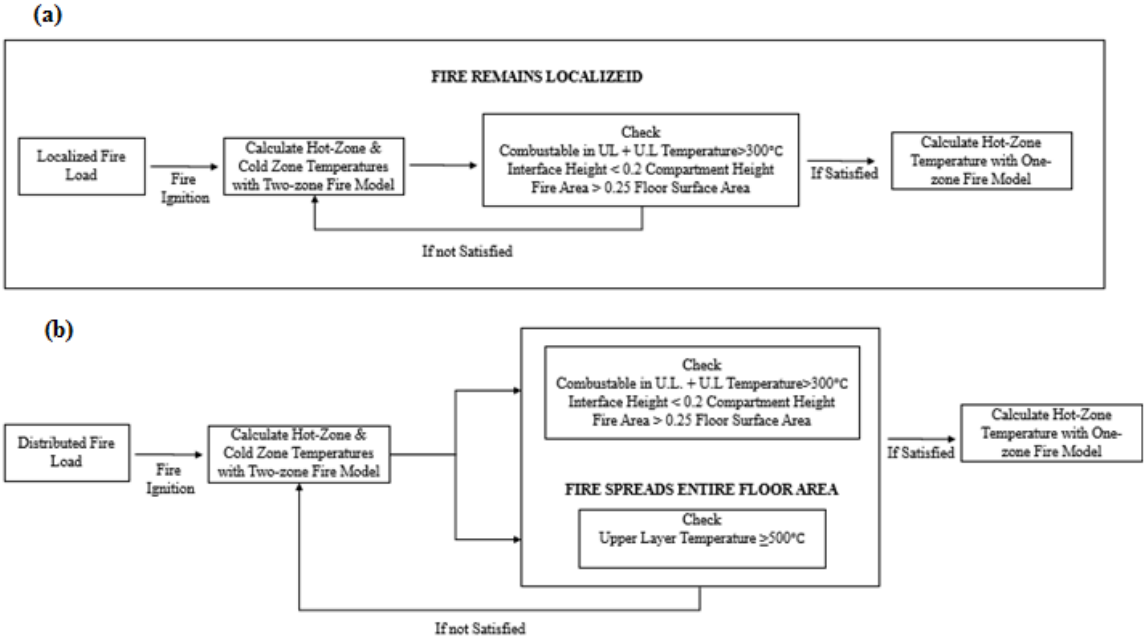

Figure 3.5. Flowchart for the Transition of Two-zone Fire Model to One-zone Fire Model (a) Localized Fire Load, (b) Distributed Fire Load.

3.5.2. Pre-flashover Localized Fire Simulation

Fire induced behaviors of structural members located near fire source are also evaluated by generating local fires for the pre-flashover phase of the fire. In general, structural components near the fire source will be subjected to a much more severe heat than other components located away from the fire source before the flashover. Therefore, structurally critical regions of the investigated buildings are determined, and these regions are subjected to localized fire until the flashover to consider worst case fire scenario. The methodology adopted to determine structurally critical regions of the buildings and the alignment of these regions along the geometry of the buildings are given in Chapter-4.

Localized fire is assumed to have same heat release rate with zone model fire simulation until flashover and it is only considered for the pre-flashover fire duration. The heat release rate collected from zone model fire simulation is used as input to ELEFIR-EN, fire simulation software (Real and Franssen, 2015), to estimate localized fire flame temperatures at varying flame heights. Elefir-EN uses Eurocode-1 Part 1-2 Annex-C (CEN, 2002) provisions that are explained in following paragraphs to calculate varying height flame temperatures and maximum flame height.

Equation 3.5 represents formulation of the flame length calculation of the localized fire according to Figure 3.6.

$$L_f = -1.02D_f + 0.0148Q^{2/5}[m] \tag{3.5}$$

When flame is not impacting ceiling of the compartment ($L_f <$ H according to Figure 3.6), the temperatures (θ_z) of the plume along the symmetrical vertical flame axis is calculated with Equation 3.6,

$$\theta_z = 20 + 0.25Q_c^{2/3}(z - z_0)^{-5/3} \leq 900[^oC] \tag{3.6}$$

where D_f is the diameter of the fire [m], Figure 3.6, Q is the rate of heat release [W] (obtained from zone model - until flashover), Q_c is the convective part of rate of heat release [W], with $Q_c = 0.8\ Q$ by default, z is the height [m] along the flame axis, Figure 3.6, H is the distance [m] between the fire source and the ceiling, Figure 3.6, z_0 is the virtual origin of the flame axis and formulated with Equation 3.7.

$$z_0 = -1.02D + 0.00524Q^{2/5}[m] \tag{3.7}$$

When the flame is impacting ceiling of the compartment ($L_f \geq H$ according to Figure 3.7) the heat flux $\dot{h}[W/m^2]$ received by the fire exposed unit surface area of the

structural members that are located ceiling level is given by Equation 3.8, Equation 3.9 and Equation 3.10,

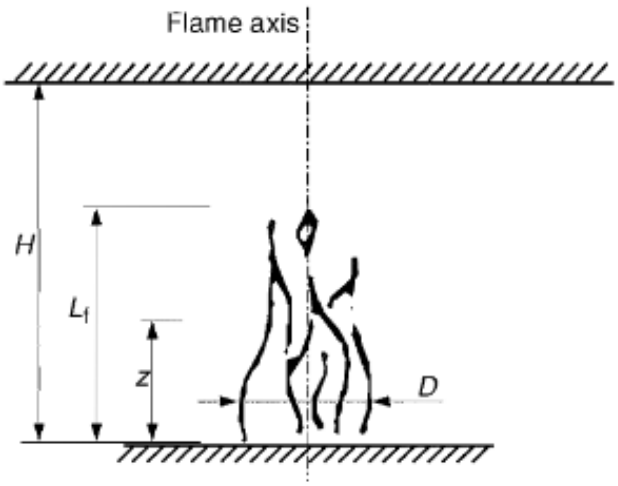

Figure 3.6. Representation of Flame Dimensions for a Ceiling Not Impacted Localized Fire (CEN, 2002).

$$\dot{h} = 100.000 \quad if \quad y \quad \leq \quad 0.3 \tag{3.8}$$

$$\dot{h} = 136.300 to 121.000 y \quad if \quad 0.3 \quad < \quad y \quad < \quad 1.0 \tag{3.9}$$

$$\dot{h} = 15.000 y^{3.7} \quad if \quad y \quad \geq \quad 1.0 \tag{3.10}$$

where y is the parameter [-] given by $y = \frac{r+H+z^{\imath}}{L_h+H+z^{\imath}}$, r is the horizontal distance [m] between the vertical axis of the fire and the point along the ceiling where the thermal flux is calculated, Figure 3.7, H is the distance [m] between fire source and the ceiling, Figure 3.7, $z^{\imath}$ is the vertical position of the virtual heat source [m] and formulated with Equation 3.11 and Equation 3.12, L_h is the horizontal flame length and formulated

with Equation 3.14,

$$z^{\imath} = 2.4D\left(\dot{Q}_D^{2/5} - \dot{Q}_D^{2/3}\right) \quad when \quad \dot{Q}_D < 10 \tag{3.11}$$

$$z^{\imath} = 2.4D\left(1\dot{Q}_D^{2/5}\right) \quad when \quad \dot{Q}_D \geq 10 \tag{3.12}$$

where

$$\dot{Q}_D = Q/1.11x10^6 D^{2/5}[-] \tag{3.13}$$

$$L_{\mathrm{h}} = \left(2.9H(\dot{Q}_H)^{0.33}\right) - \mathrm{H[m]} \tag{3.14}$$

where $\dot{Q}_H$ is the non-dimensional rate of heat release and formulated with Equation 3.15.

$$\dot{Q}_H = Q/(1.11x10^6 H^{2.5}) \tag{3.15}$$

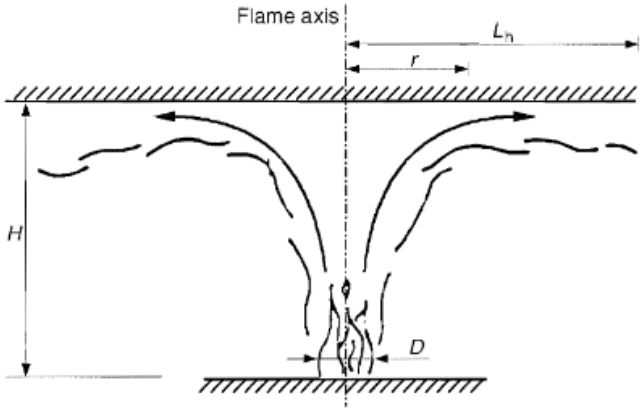

Figure 3.7. Representation of Flame Dimensions for a Ceiling Impacted Localized Fire (CEN, 2002).

Once the heat flux is found with the above equations for a local fire scenario in which flame impact the ceiling the net heat flux ($\dot{h}_{net}$) received by the fire exposed surface area of the structural members located at the ceiling can be found with Equation 3.16:

$$\dot{h}_{net} = \dot{h} - \alpha_c \left(\theta_m - 20\right) - \Phi.\varepsilon_m.\varepsilon_f.\sigma.[(\theta_m + 273)^4 - (293)^4] \tag{3.16}$$

where the various coefficients of the expression are explained in Section 2.1.6 and they are formulated with Equation 3.8, Equation 3.9 and Equation 3.10.

Usage of the equations that are described in this section to simulate localized fire is limited by Eurocode with following criteria:

- The diameter of the fire is limited to $D_f \leq 10$ m;
- The rate of heat release of the fire is limited to Q $\leq$ 50 MW

On the other hand, these equations can also be used for fire simulations with larger fire diameters and heat release rates, but these extreme values are experimentally not validated (Franssen and Real, 2015).

3.5.3. Entire Time-Temperature History

Fire simulations of the investigated buildings assumed to continue until the fire burnout or at most 120 minutes. 120 minutes fire duration is the maximum fire resistance rating according to several standards (CEN, 2005 & ASFP, 2014).

Time-temperature history of the compartment volume that are not in the structurally critical region are obtained with zone model fire simulation that is explained in Section 3.5.1. Therefore, hot-zone (gas/smoke) temperatures are used to simulate fire in structurally non-critical regions of the buildings.

If fire remains localized for certain amount of time, fire simulation of the structurally critical region are performed with combination of localized fire flame temperatures and hot-zone (gas/smoke) temperatures. Figure 3.9 illustrates combination of the localized fire flame temperatures and the hot-zone (gas/smoke) temperature to simulate a fire for structurally critical region.

Although, fire simulation of structurally critical region is simulated with the combined fire curve that is illustrated in Figure 3.8, it is important to state that if flame does not impact the ceiling of the building, flame temperatures decrease with increasing flame height according to Equation 3.5. Therefore, different fire curves that represent varying height flame temperatures should be considered to simulate fire in structurally critical region. Figure 3.9 illustrates local fire flame temperatures for varying flame heights and hot-zone (gas/smoke) temperatures. According to Figure 3.9, heat transfer analyses of structural members that align at different heights of the structurally critical region should be conducted with the respective combination of the flame temperatures and the hot-zone (gas/smoke) temperatures.

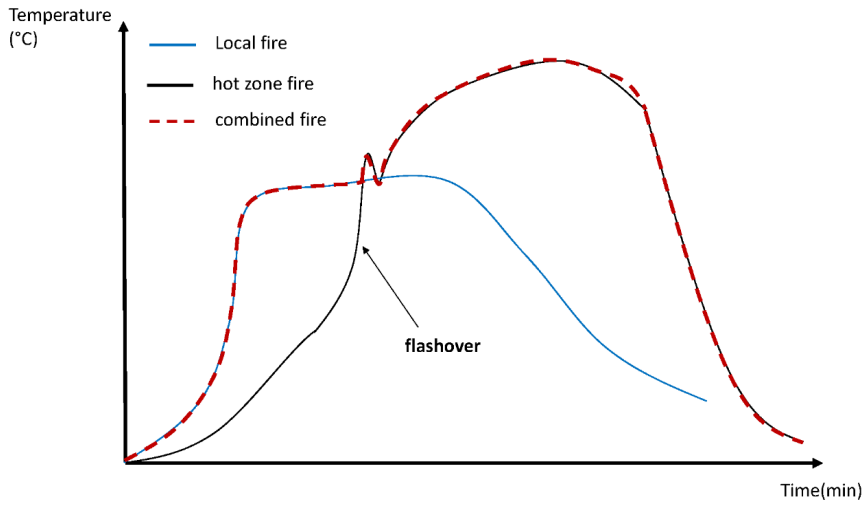

Figure 3.8. Illustration of Fire Curves: Localized, Hot-zone and Combined Fire Curves.

According to fire characteristics of the buildings, if duration of the localized fire (pre-flashover fire) is relatively short with respect to the entire duration of the fire, flame

temperatures of localized fire may be ignored and hot-zone (gas/smoke) temperatures can be used to simulate fire for the buildings.

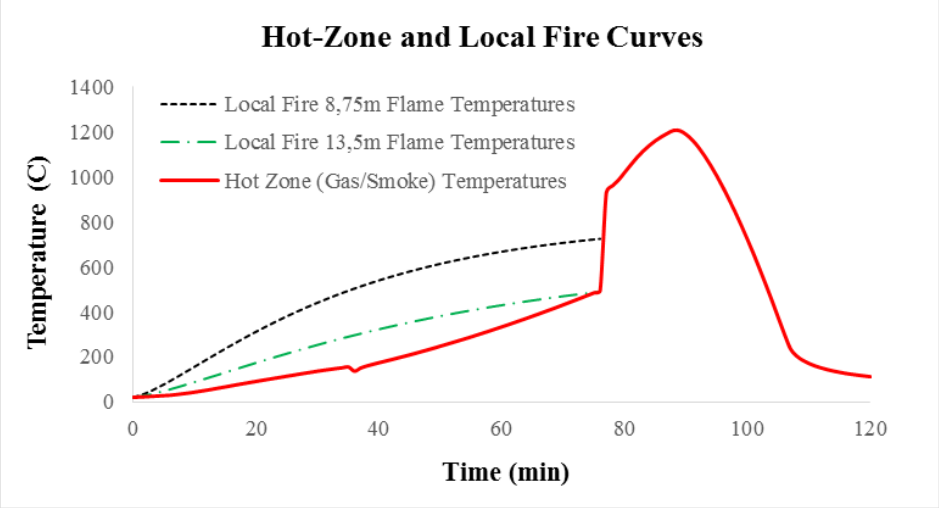

Figure 3.9. Flame Temperatures for Varying Flame Heights and Hot-zone Temperatures.

3.6. Heat Transfer Analysis

Once the fire curves of the structurally critical region and non-critical regions of the building are established, time-temperature histories of the structural members are calculated with Eurocode Lumped Mass Method (CEN, 2005) by considering convective heat transfer coefficient and emissivity as h= 35 W/m^2 ^{o}C and ε_f = 0.7, respectively. Mathematical model of Lumped Mass Method is explained in Section 2.1.6. This method takes account of non-uniform heating in the cross section yet it does not create thermal gradients. The thermal gradients do not play a significant role if the steel sections are unprotected. The unprotected steel profiles are exposed to fire on 3 - sides or 4 - sides depending on their location (perimeter or internal column or beams). Perimeter columns and beams are heated on 3 - sides, internal columns are heated on 4 sides.

As explained in Section 3.4, thermo-mechanical behaviors of the composite floor systems that exist in two of the investigated buildings are performed separately with

the simplified methodologies. Therefore, 2D heat transfer analysis method is adopted to calculate time-temperature histories of the structural components of the composite floor assemblies.

Simulating the fire with two-zone fire model for certain duration results with occurrence of two different time-temperature histories for the buildings. Figure 3.10a represents these two different time-temperature histories for a specific large scale compartment. The specific compartment ventilation openings, fire parameters, wall linings' thermal properties and geometry are given in Table 3.4. According to Figure 3.10a, the cold-zone temperatures are relatively low compared with the hot-zone temperatures. Moreover, according to Figure 3.10b, the hot-zone layer reaches to $< 20.0\%$ of the compartment height at the 14^{th} minute of the fire and two-zone fire model switches to one-zone fire model. Therefore, structural members that align in the structurally non-critical regions and above the local fire maximum flame length are simultaneously exposed to the hot-zone temperatures for heat transfer analyses of the buildings.

Table 3.4. General Properties of the Large Scale Compartment.

Compartment Geometry			
Width (m)	Length (m)	Height (m)	Floor Area (m^2)
27	54	28.2 - 24.6 (15^o Roof Inclination)	1464
Characteristics of Ventilation Openings			
Dimensions and Vertical Alignment	Type 1	Type 2	Type 3
Height (m)	5	2.1	1
Width (m)	5	1	4
Vertical Alignment (m)	0 - 5	0 - 2.1	18 - 19
Number of Openings on the Perimeter Walls			
Wall - 1	1	1	-
Wall - 2	-	3	1
Wall - 3	2	1	-
Wall - 4	-	3	1
General Fire Parameters			
Characteristic Fire Load Density (MJ/m^2)	Design Fire Load Density (MJ/m^2)	Fire Growth Rate	Fire Duration (min)
195	369	Fast	120
Thermal Properties of Wall Lining			
Thickness (cm)	Unit mass (kg/m^3)	Conductivity (W/mK)	Specific Heat (J/kgK)
15	30	0.026	1470

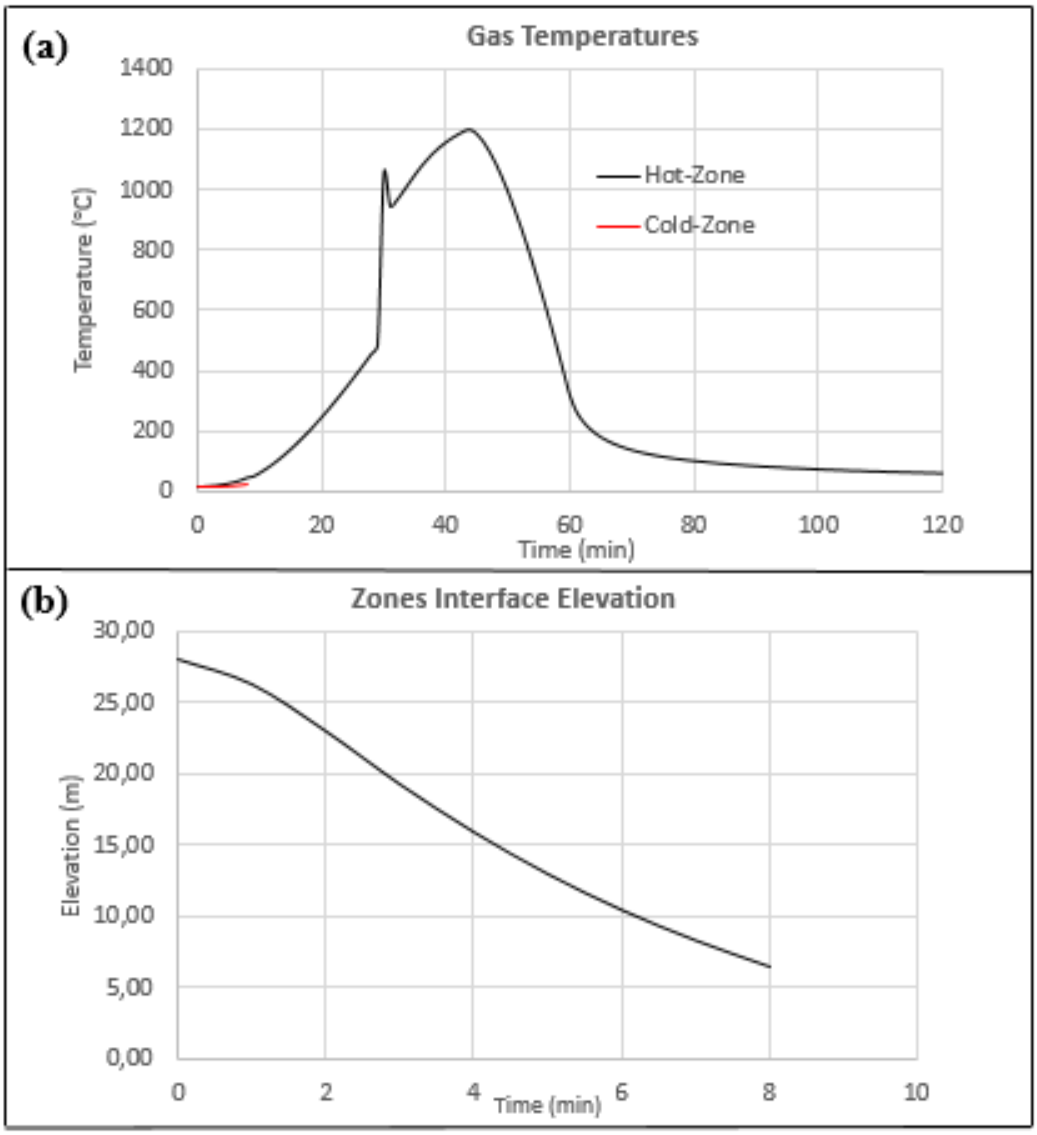

Figure 3.10. Specific Compartment Fire (a) Hot and Cold Zone Temperatures, (b) Zones Interface Elevation.

According to Section 3.5.3, for heat transfer analyses of the structural members that are located at different heights (e.g. tie-beams, crane-beams) and that align vertically (e.g. columns) in the structurally critical region of the buildings, combinations of the different height flame temperatures and hot-zone (gas/smoke) temperatures are used.

The following example explains the methodology adopted for the heat transfer analyses of the structural members that are located in the structurally critical region

of the buildings.

A typical industrial building layout is shown in Figure 3.11. The highlighted portal frames in Figure 3.11a represent structurally critical region of the building. Therefore, until the flashover the structural members that align in this region are exposed to the localized fire flame temperatures for heat transfer analyses.

Assuming that the maximum area of the localized fire equals to the total surface area of the structurally critical region and the maximum flame length equals to 10 m, structural members and part of the structural members that are located in the first 10 m in the structurally critical region are heated with three different flame temperature. The first 7 m of the columns that are highlighted with green lines are heated with 3.5 m local fire flame temperatures, the tie-beams that are highlighted with yellow lines are heated with 7 m flame temperatures and the column parts that are highlighted with blue lines are heated with 8.5 m flame temperatures. Moreover, the other structural members which align above the maximum flame length are simultaneously exposed to the hot-zone temperatures for the entire duration of the fire.

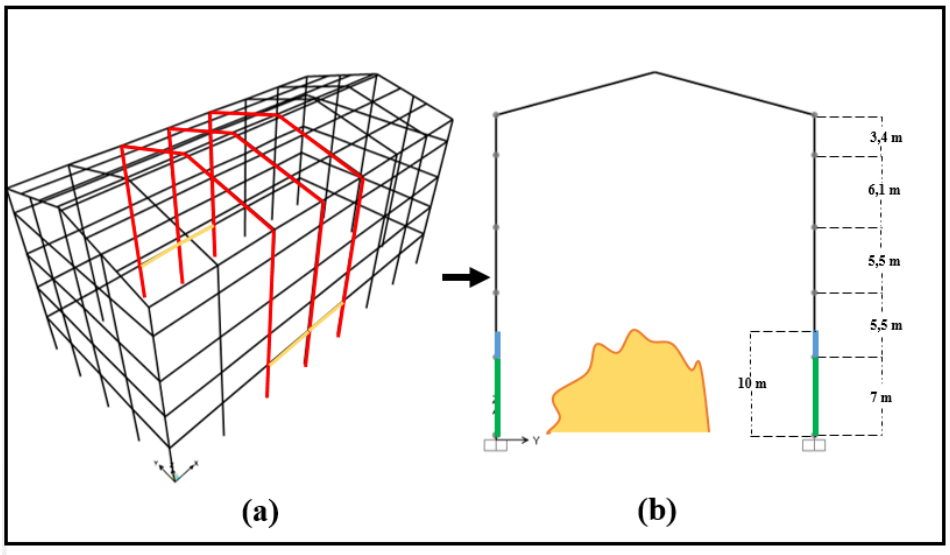

Figure 3.11. Illustration of the Steel Portal Framed Industrial Building.

To summarize, structural members that align vertically in the structurally critical region of the buildings are divided several parts. The length of these parts are

determined with the location of tie-beams and maximum flame length, and these parts are exposed to flame temperatures that corresponds to their mid-length until the flashover. Structural members that align horizontally in the structurally critical region of the buildings are exposed to the flame temperatures that corresponds to the vertical alignment of these parts until the flashover. Once the flashover occurs the hot-zone (gas/smoke) all of the structural members are heated with the hot-zone (gas/smoke) temperatures.

3.7. Assessment Criteria

Fire induced structural performance of the buildings are determined with the detailed investigation of the critical columns, rafters, composite floor beams, reinforced concrete slab deflections and reinforcements tensile forces. These structural members are assessed with four different failure criteria. Maximum allowable limits states for these criteria are presented and formulated in Table 2.4.

Development of the maximum equivalent plastic strains along the beam length, vertical displacement and rate of vertical displacement at beam mid-length are investigated during the fire for assessments of the rafters and the composite floor beams.

To capture column buckling during the fire, development of the maximum in-plane (column's minor axis) and out-of-plane (column's major axis) displacements and rate of these displacements are investigated along column height. However, due to post-buckling strength of the columns and redistribution of the loads on the columns to undamaged columns of the structure, column buckling does not necessarily indicate failure of the columns as explained in Section 2.1.2. Therefore, development of the maximum equivalent plastic strains along the column height and vertical displacement rate at the column mid-height are investigated for assessment of the columns. Equivalent plastic strain is defined in the following paragraph;

For isotropic material any arbitrary three-dimensional infinitesimal element of structural member has six-dimensional stress space. Therefore, for realistic loading

conditions uniaxial stress state is not a valid criteria to determine state of the element, thus the structural member. As a result, for design purposes it is required to represent this six-dimensional stress space as a single positive stress value (also called von Mises Stress). Because six-dimensional stress space is being collapsed into a single number, von Mises stress, there are many stress states that produce same equivalent stress, and they collectively define a surface in the stress space. The particular collection of these stresses in the stress surface define a yield surface and the strain normal to this surface is defined as the equivalent plastic strain.

The mid-point vertical displacement of the composite floor system located in one of the buildings is investigated for the entire duration of the fire to determine fire induced performance of the composite floor system. Moreover, to understand overall thermo-mechanical behavior of composite floor systems vertical displacements along the floor area and tensile forces on the reinforcements are investigated for the entire duration of the fire.

4. CASE STUDIES

4.1. General

Fire induced performances of 5 different industrial buildings are investigated as a case study in this thesis. General geometric properties of the buildings are listed in Table 4.1. Selection of the buildings are made with respect to their specific structural and fire characteristics to reflect suitability of the application of the developed simplified methodologies for performance-based structural fire safety concept of industrial buildings.

Table 4.1. General Geometric Properties of the Investigated Buildings.

Buildings	GEOMETRIC PROPERTIES			
	Width (m)	Length (m)	Floor Area (m^2)	Total Surface Area (m^2)
Building - 1	26	42.5	1105	4235.5
Building - 2	40	70	2800	8710
Building - 3	60.5	52	3146	12187
Building - 4	7	30	210	759.5
Building - 5	13	18	234	390.1

Steel portal frames that are braced with cross diagonals, tie-beams and purlins in out-of-plane direction (orthogonal direction to portal frame alignment) are utilized as main load carrying structural system for all of the buildings. In addition, Building - 4 and Building - 5 consist of a steel-framed reinforced-concrete-slab composite floor systems. Steel sections of the structural members, alignments of the portal frames, angle of roof inclination, application points and magnitudes of the loads, and type of the bracing systems are slightly different for each of the buildings. Definition of the structural systems and state of the loadings are detailed in this chapter for each of the buildings.

Self-weights of steel sections, cranes, floor assemblies, walls and ceiling are main gravitational loads for all of the buildings. Moreover, as explained in Section 3.2, snow load and live loads are applied to the buildings for the performance based structural

fire analyses. Characteristic value of the snow loads that are applied to the buildings are determined according to the provisions of Turkish Standard of Design Loads for Buildings - TS498 (Turkish Standard Institution, 1997) and shown in Table 4.2. Magnitudes of live loads depend on the intended use of the buildings and they are specific for each of the buildings. Therefore, characteristic values and points of application of live loads are detailed in the following sections for each of the buildings. Different types of cranes exist in Building - 1 and Building - 3, application points and magnitudes of crane weights are determined according to respective technical manuals and shown in the following sections.

Table 4.2. Characteristic Value of the Snow Load Applied on Roof of the Buildings.

SNOW LOAD	BUILDINGS				
	Building - 1	Building - 2	Building - 3	Building - 4	Building - 5
(kN/m^2)	1.45	1.45	1.45	1.45	1.45

Non-uniform existence of the live loads, and crane weights in the Building - 1, 2 and 3 result to occurrence of load concentration around the specific regions of these buildings. Therefore, structurally critical region of these buildings are determined and shown in the following sections for each of the buildings.

Total fire loads in the buildings are conservatively assumed to be distributed on the total floor surface area of the buildings. Characteristic values of the distributed fire load densities of Building - 1, 3, 4 and 5 are determined with field surveys carried by the operators of the buildings. Characteristic value of the distributed fire load density of Building - 2 is conservatively assumed as generic fire load for an office building according to Eurocode - 1 Part 1-2 Annex-E (CEN, 2002) due to lack of information. Calculation of design values of the fire load densities are done with the provisions of Eurocode - 1 Part 1-2 Annex-E (CEN, 2002). The parameters that are considered in these calculations are given in Appendix-A and summarized in Table 4.3.

Combustion behavior of the fire loads is determined according to Eurocode - 1 Part 1-2 Annex-E (CEN, 2002) provisions. Fire growth rates used in the fire simulations

of Building - 1 and Building - 3 that contain large amount highly flammable lubricant, solvent and diesel are determined with parameters that reflect fast growth fire. Fire growth rates used in the fire simulations of Building - 2, 4 and 5 that contain wood based combustible materials are determined with parameters that reflect medium growth fire.

Required fire resistance ratings and active fire protection systems of the buildings are also different. Sprinkler and smoke-heat detection systems are the main active fire protection systems used in the buildings. Table 4.3 shows main parameters used in the fire simulations of the buildings and the detailed description of these parameters, and rest of the variable needed to run the fire simulations of the buildings are given in the following sections and Appendix-A.

Table 4.3. General Parameters for the Fire Simulations of the Buildings.

General Fire Simulation Parameters	BUILDINGS				
	Building - 1	Building - 2	Building - 3	Building - 4	Building - 5
Characteristic Fire Load Density (MJ/m^2)	136.35	511	246	622	622
Rate of Heat Release (KW/m^2)	500	250	500	250	250
Fire Growth Rate	150	300	150	300	300
Sprinkler System	NO	YES	NO	YES	NO
Smoke Exhaust System	NO	NO	NO	NO	NO
Fire Detection by Heat	YES	YES	YES	NO	YES
Fire Detection by Smoke	NO	NO	NO	YES	NO
Required Fire Resistance Rate (min)	90	60	120	60	90
Danger of Fire Activation	1	1	1	1	1

Ventilation openings that exist on perimeter walls of the buildings have also unique characteristics for each of the buildings. Detailed drawings and dimensions of the openings are given in the following sections for each of the buildings. Table 4.14 represents openings factors that are calculated with Equation 2.8 to illustrate the unique ventilation opening characteristics of the buildings.

Table 4.4. Opening factor of the Buildings.

OPENING FACTOR	BUILDINGS				
	Building - 1	Building - 2	Building - 3	Building - 4	Building - 5
($m^{0.5}$)	0.0293	0.0187	0.0143	0.0497	0.0316

Two different wall linings are used for the perimeter walls and ceiling of the buildings. Thermal properties of these materials are taken from operators of the buildings

and shown in Table 4.5. The walls that are covered by these lining materials are described in the following sections. Normal weight concrete is used as the floor cover for all of the buildings. Thermal properties of normal weight concrete is taken from Eurocode - 4 Part 1-2 (CEN, 2005) and given in Table 4.5.

Table 4.5. Thermal Properties of Lining Materials.

LINING MATERIALS	Thickness (cm)	Unit Mass (kg/m^3)	Conductivity (W/mK)	Specific Heat (J/kgK)	Emissivity H.S.	Emissivity C.S.
WALLS						
G.C. Bricks	15	550	0.14	840	0.8	0.8
S.S.Metal Panel (PUR Insulation)	15	30	0.026	1470	0.8	0.8
FLOOR						
N.W. Concrete	20	2300	1.6	1000	0.8	0.8
CEILING						
S.S.Metal Panel (PUR Insulation)	15	30	0.026	1470	0.8	0.8
G.C. = Gas Concrete, N.W. =Normal Weight, H.S. = Hot-Surface, C.S.= Cold-Surface, S.S. = Self-supporting, PUR = Rigid Polyurethane						

4.2. Building - 1

4.2.1. Building Description

The building is 42.5 m in length, 26 m in width and 13.5 m to 17 m in height with a single pitch roof. Figure 4.1 shows the general layout of the building with the distances between the portal frames, crane support columns (also utilized as the wind columns on axes A and G), purlins, tie-beams, and the roof inclination angle.

Steel sections of the portal frames that align along A, D and G axes, and in-plane diagonals, tie-beams that connect crane support columns to these portal frames are shown in Figure 4.2a. Steel sections of the portal frames that align along E and F axes are shown in Figure 4.2b.

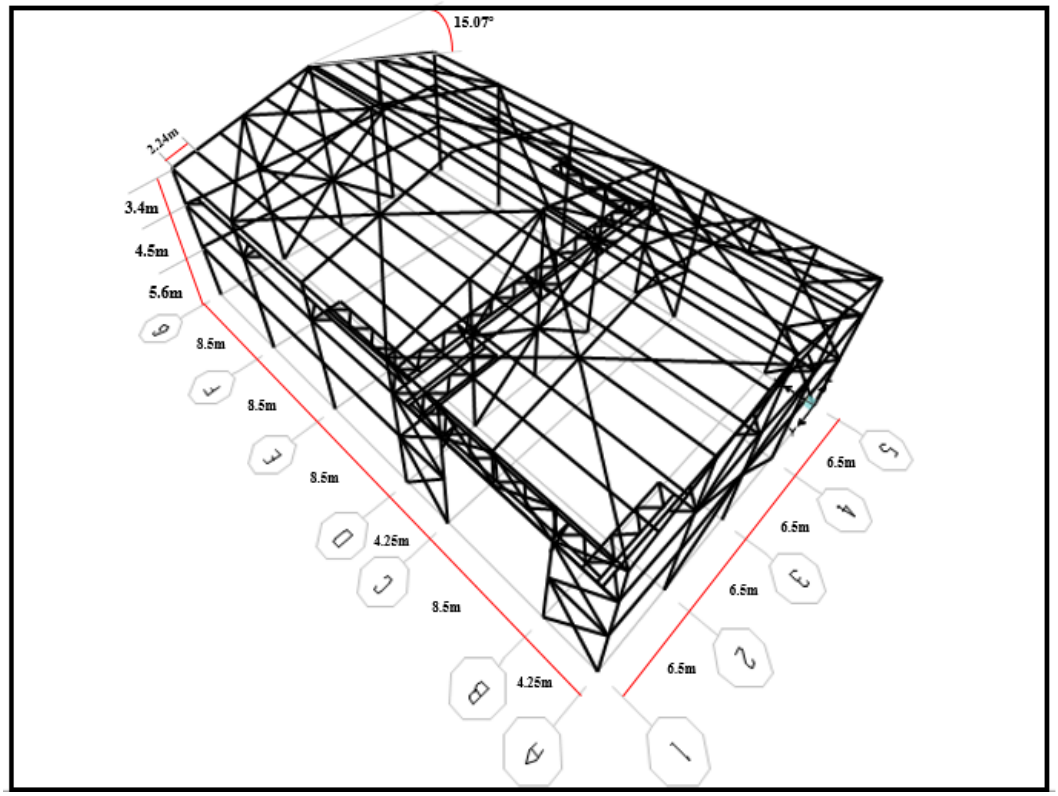

Figure 4.1. General Layout of Building - 1.

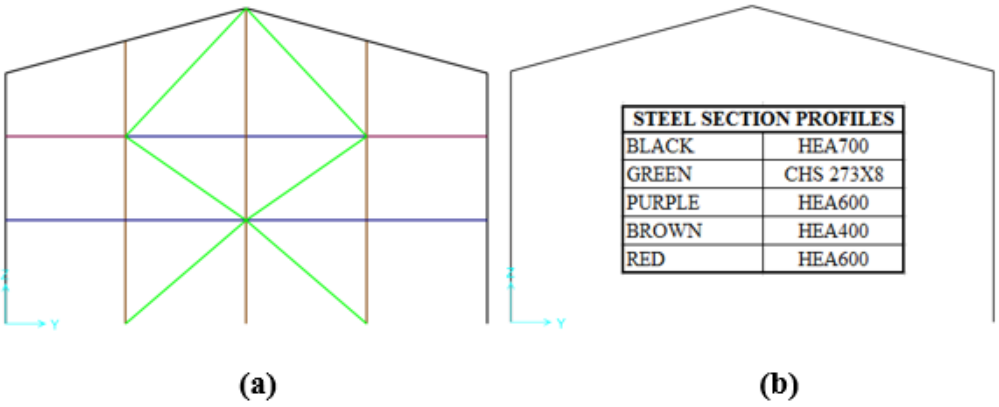

Figure 4.2. Steel Sections of the (a) Portal Frames, Tie-beams and Diagonals along A, D and G Axes, (b) Portal Frames along E and F Axes.

Steel sections of the out-of-plane diagonals and tie-beams that align along axes 1 and 3, and steel sections of the structural members that are located at the roof level of the building are shown in Figure 4.3 and Figure 4.4.

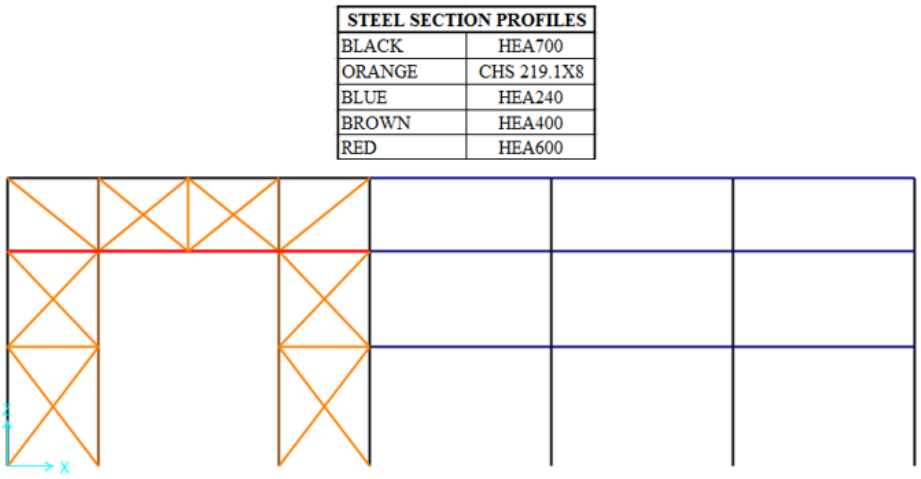

Figure 4.3. Steel Sections along Axes 1 and 3.

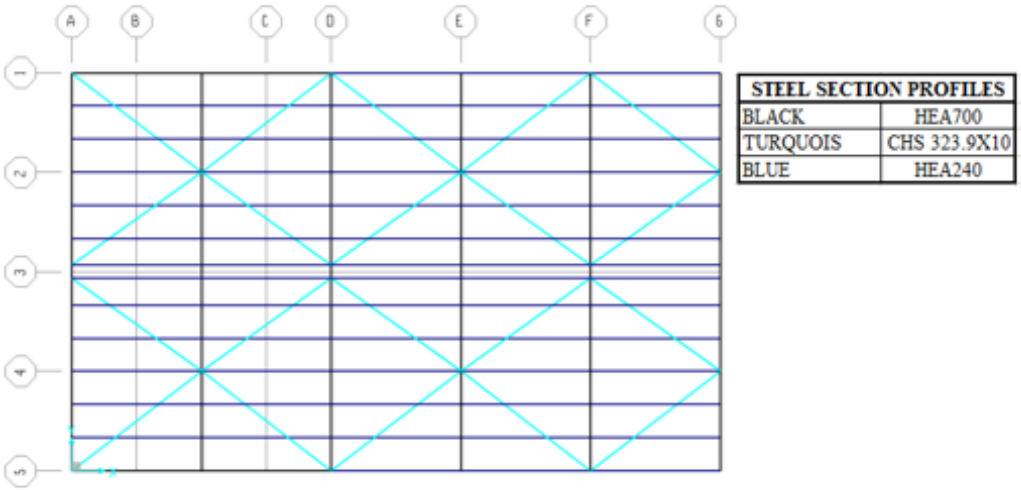

Figure 4.4. Steel Sections at the Roof Level.

There are two different cranes at 10.1 m height of the building. One of the cranes moves between 1 and 5 axes, and span length of this crane equals to the distance between A and D axes. The other crane moves between D and G axes, and span length of this crane equals to the distance between 1 and 5 axes. General layout of the crane level is shown in Figure 4.5 with crane beams and beam-diagonals steel sections.

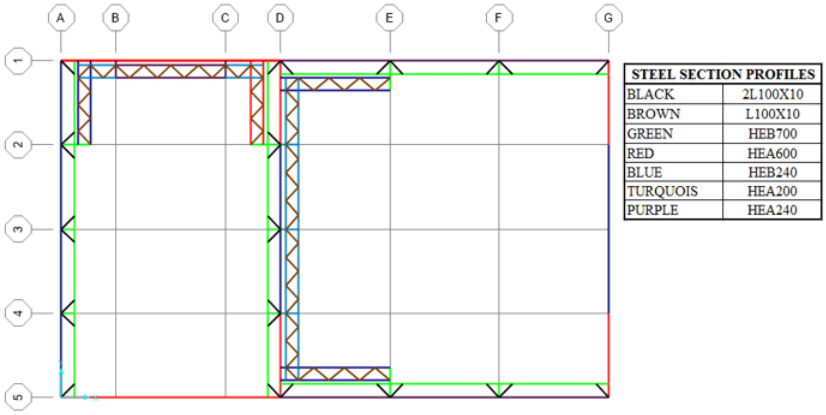

Figure 4.5. General Layout of the Crane Level with Steel Sections.

Three different ventilation opening types exist on perimeter walls of the building. Figure 4.6 shows general layout, dimensions and vertical alignments of these openings. Identical openings are highlighted only once in Figure 4.6 for each side of the building. Roll-up doors which are highlighted with the blue rectangle in Figure 4.6a and Figure 4.6c are assumed to be open for fire simulation of the building. The ventilation openings shown in Figure 4.6d are part of the adjacent building that is located on the rear side of the main building, on the peripheral wall of the main building. Therefore these openings are not included to fire simulation of the building.

VENTILATION OPENINGS			
Color	Height (m)	Width (m)	Vertical Alignment (m)
Blue	5	5	0 - 5
Red	2	2	11 - 13
Green	2.1	2	0 - 2.1

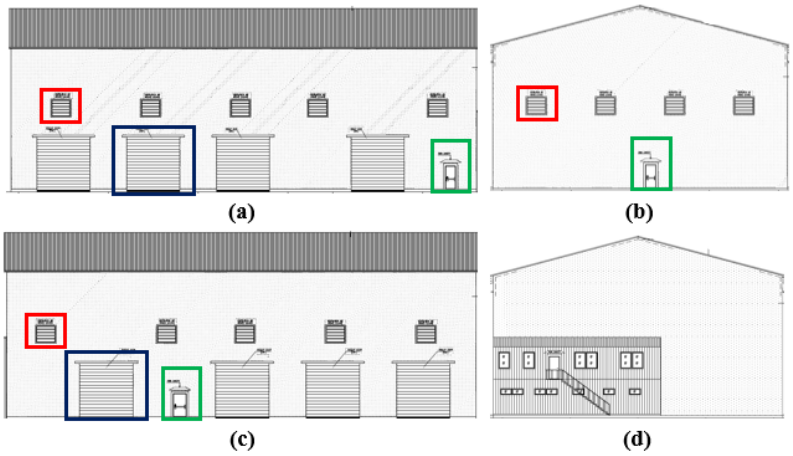

Figure 4.6. Architectural Drawings of the Building with the Highlighted Ventilation Openings (a) 1 Axis View, (b) A Axis View, (c) 5 Axis View, (d) G Axis View.

The building's perimeter walls and ceiling are covered with self-supporting metal panels according to the information given by the operator of the building and the floor of the building is covered with normal weight concrete. The thermal properties and unit weights of these materials are given in Table 4.5.

Characteristic value of the snow load applied to the roof of the building is given in Table 4.2. The live loads on the building are due to the equipment on the crane platforms at the height of 10.1 m. The surfaces highlighted with the grey color in Figure 4.7 represent crane platforms. The live loads on these platforms equal to 5 kN/m^2. The weight of the cranes is determined according to Stahl Crane Systems technical manual (Stahl, 2008) and applied to the highlighted points shown in Figure 4.7.

Snow load and live loads are multiplied by the design load coefficients described in Section 3.2 and applied to the respective structural members according to tributary area method. The weight of the walls and ceiling is also applied to the respective structural members according to the tributary are method, but they are not multiplied by any design load coefficients, similar to the weight of the steel sections and the cranes.

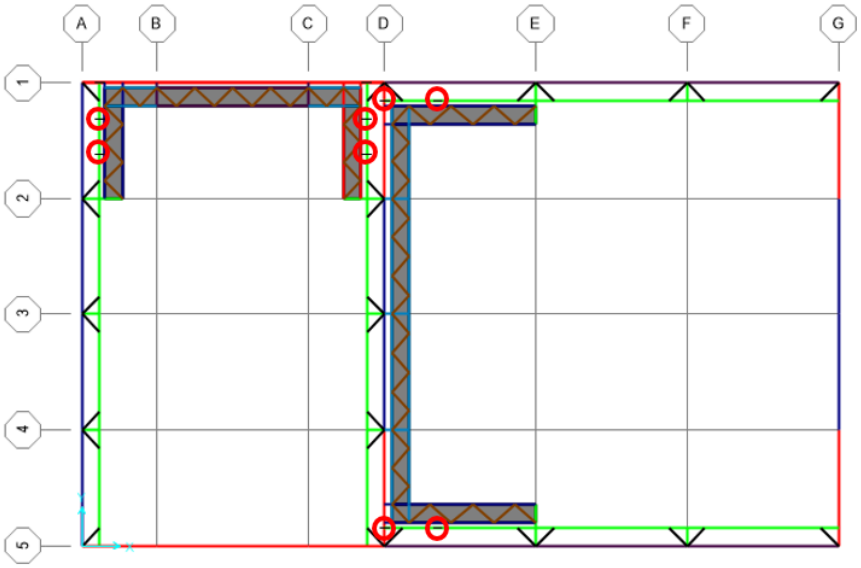

Figure 4.7. Crane Platforms (Grey Surfaces) and Points of Application of Crane Self-Weights (Hollow Circles).

Structurally critical region of the building is determined by a dynamic implicit structural analysis with the application of 10 times increased gravitational loads. Figure 4.8 shows the area of the building that corresponds to the structurally critical region of the building with the highlighted members. Some of the roof purlins and the crane beams are not shown in Figure 4.8 for clarity of the figure.

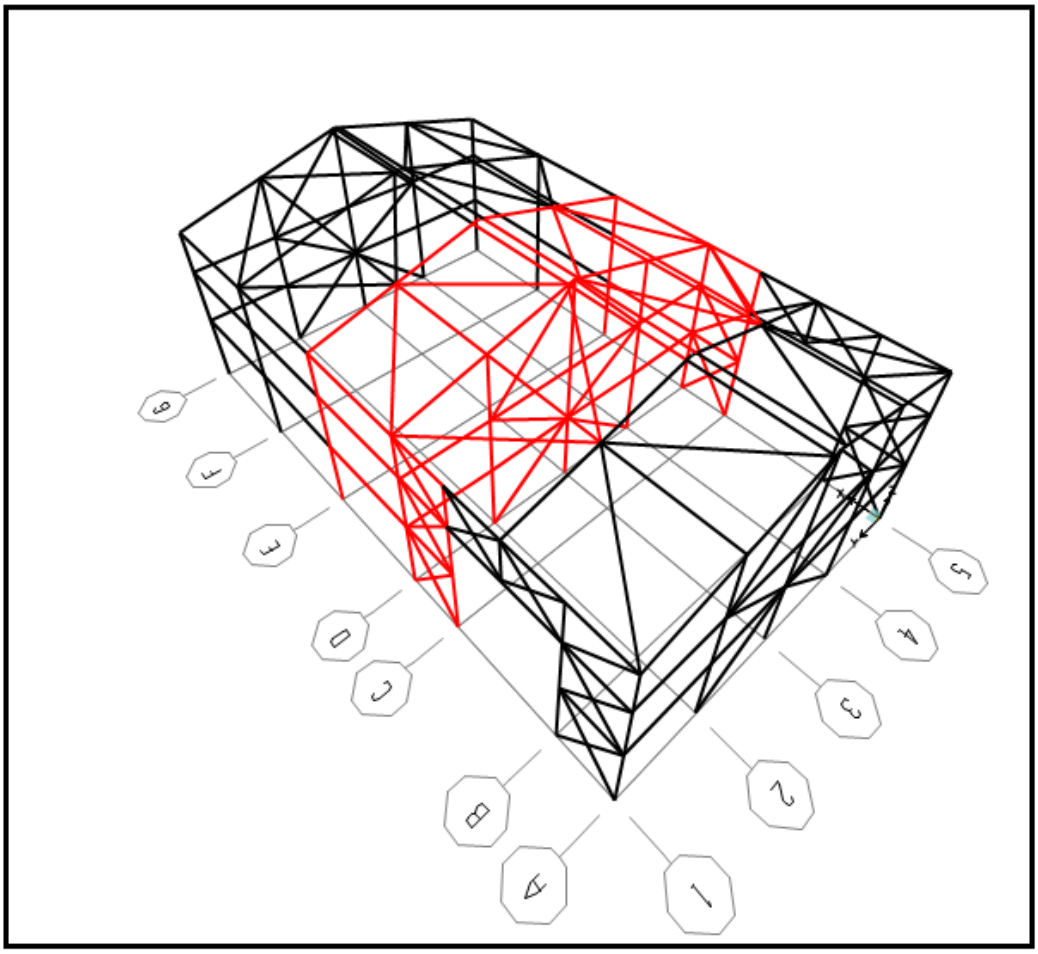

Figure 4.8. Structurally Critical Region.

Fire load survey is carried out by the building operator. The amount, density and characteristic calorific value of the fire loads and the characteristic value of the distributed fire load are given in Table 4.6. The design value of the fire load density for the floor surface of the building is given in Appendix-A.

Table 4.6. Amount, Density and Characteristic Calorific Value of the Fire Loads Exist in Building - 1.

Type of Fire Load	Volume (m^3)	Density (kg/m3)	Calorific Value (MJ/kg)	Building - 1 Floor Area (m^2)
Grease	1	870	45	1105
Engine Oil	1	870	45	
Diff Oil	1	870	45	
Acetlyne	0.6	1.097	50	
Cotton Bale	3.375	472	11	
Cleaning Solvent	0.4	870	45	
Uniformly Distributed Fire Load - 136.35 MJ/m^2				

4.2.2. Fire Simulation and Heat Transfer Analysis

The preliminary parameters to simulate the design fire of the building according to the methodologies explained in Section 3.5 are given in Appendix-A. The hot and cold zone temperatures, the heat release rate, the smoke elevation and the fire area for the entire duration of the fire are shown in Figure 4.9a, Figure 4.9b, Figure 4.9c and Figure 4.9d, respectively.

According to results of the fire simulation of the building, the two-zone fire model switches to the one-zone fire model at the 28^{th} minute of the fire, because the upper layer (hot-zone) reaches to $< 20.0\%$ of the compartment and the maximum fire area reaches to 25% of the total floor area (1105.00 m^2). The fire has flashover (fully engulfed) at the 37^{th} minute of the simulation, because the hot-zone (gas/smoke) temperatures reach 500.0 ^oC. It is obvious from the sudden jump in the heat release rate and the fire area the flashover occurs at the 37^{th} minute of the fire.

Pre-flashover localized fire is simulated with the methodologies explained in Section 3.5.2. The local fire does not impact the ceiling (13.5 m) and the maximum local fire area is 438 m^2, which is larger than the area of the structurally critical region. But effecting the local fire simultaneously to 438 m^2 floor area is very conservative approach that's why local fire is only affected to the structurally critical region (331.5 m^2) of the building. Flame height of the local fire reaches 8 m from the floor surface level. Therefore, according to the alignment of the tie-beams and the maximum

flame height, three different local fire time-temperature histories are used for the heat transfer analysis of the structural members located in the structurally critical region as explained in Section 3.6. Figure 4.10 shows the hot-zone time-temperature history, time-temperature histories of the varying flame heights and ISO834 standard fire curve (ISO, 1999).

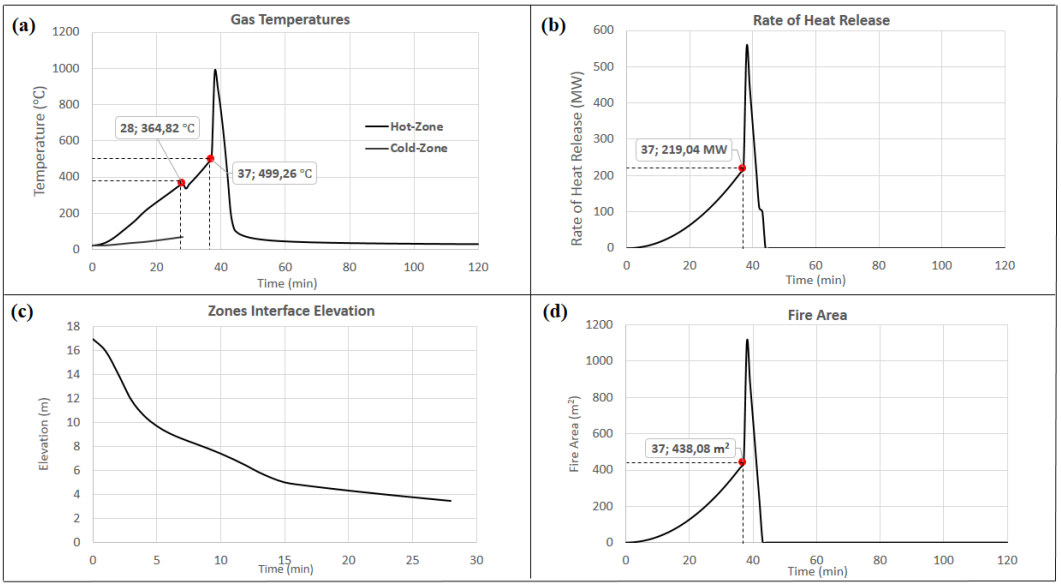

Figure 4.9. (a) Hot and Cold Zones Temperatures (Peak: 979 °C at: 38 min) (b) RHR Computed (Peak: 552.5 MW at: 38 min), (c) Zones Interface Elevation (h = 3.45 m at: 28.00 min), (d) Fire Area (1105 m^2 at 38 min).

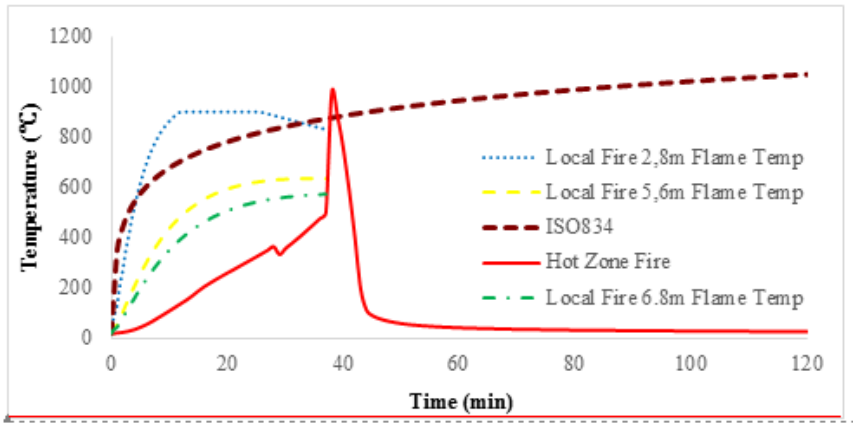

Figure 4.10. Hot-zone Temperatures, Local Fire Flame Temperatures and ISO 834 Standard Fire Temperatures for 120 minutes.

As explained in Section 3.6, the column parts above 8 m height in the structurally critical region, and the structural members that are located in the structurally non-critical regions of the building are simultaneously exposed to the hot-zone gas temperatures for heat transfer analyses. Moreover, heat transfer analyses of the tie-beams, the cross-bracings and the part of the columns that align below the 8 m height in the structurally critical region are conducted by using combination of the hot-zone (gas/smoke) temperatures and the localized fire flame temperatures that are shown in Figure 4.10. The fire curves used for the heating of the structural members of Building - 1 are summarized in Table 4.7.

Table 4.7. The Fire Curves Used for the Heating of the Structural Members of Building - 1.

CRITICAL REGION - (Refer to Figure 4.1 and Figure 4.8)			
Columns			
Axis Coordinate	C1, C5, D1, D2, D3, D4, D5, E1, E5		
Vertical Alignment	0 - 5.6 m	5.6 m - 8 m	8 m - Ceiling
Pre-flashover	2.8 m L.F.T.	6.8 m L.F.T.	H.Z.T.
Post-flashover	H.Z.T	H.Z.T	H.Z.T
Tie-Beams & Crane Beams			
Axis Coordinate	C1 - D1, D1 - E1, C5 - D5, D5 - E5, D1 - D2, D2 - D3, D3 - D4, D4 - D5		
Vertical Alignment	5.6 m	10.1 m, 13.5m	
Pre-flashover	5.6 m L.F.T.	H.Z.T	
Post-flashover	H.Z.T	H.Z.T	
Cross Diagonals			
Axis Coordinate	C1 - D1, D2 - D3, D3 - D4, C5 - D5		
Vertical Alignment	0 - 5.6 m	5.6 m - 8 m	8 m - Ceiling
Pre-flashover	2.8 m L.F.T.	6.8 m L.F.T.	H.Z.T.
Post-flashover	H.Z.T	H.Z.T	H.Z.T
NON-CRITICAL REGIONS - (Refer to Figure 4.8)			
Pre-flashover	H.Z.T		
Post-flashover	H.Z.T		
L.F.T. = Local Fire Flame Temperatures, H.Z.T = Hot-zone Temperatures			

4.2.3. Structural Analysis

Fire induced structural performance of the building is determined with implicit dynamic analysis method. The predefined steel temperatures that are determined according to Section 4.2.2 are used as input for the analysis. Detailed fire induced behaviors of one column and rafter that are located in the structurally critical region of the building are investigated to determine state of the structurally critical region. State of the structurally non-critical regions of the building is determined with the

fire induced performance of one rafter, because the columns that are located in the structurally non-critical regions of the building do not show structural instability and do not lose their total load carrying capacities for the entire duration of the fire.

The column that is located at D - 3 axis coordinate (Figure 4.8) is the structural member which shows first structural instability during the analysis. Therefore, state of the structurally critical region is determined with the detailed investigation of the fire induced behaviors of this column and the rafter that is located along E axis (Figure 4.8). Fire induced performance of the structurally non-critical region of the building is determined with the detailed investigation of the rafter that aligns along F axis.

Assessments of the investigated structural members are conducted with the allowable limits that are presented and formulated in Table 2.4. 50 mm/min mid-height vertical displacement rate (Gernay *et al.*, 2016) and development of 15% equivalent plastic strains (CEN, 2005) along the column height are used as the maximum allowable limits for the assessment of the column. Maximum allowable mid-length vertical displacement and rate of the vertical displacements for the rafters are 1345 mm (BS-476, 1987) and 50 mm/min (Gernay *et al.*, 2016), respectively. Moreover, development of 15% equivalent plastic strains (CEN, 2005) along the rafters is also used for the assessment of the rafters.

The first 5.6 m of the column that is located at D-3 axis coordinate is exposed to 2.8 m flame temperatures until the flashover as shown in Section 4.2.2. Therefore, this part of the column yields at the 30.7^{th} minute of the fire as highlighted in Figure 4.11b which shows the maximum equivalent plastic strains that develop along the column height during the fire. The analysis time that shows the yielding of the column is visualized in Figure 4.11d (I). In-plane displacement rates along the column height reach to 50 mm/min at the 42.3^{rd} minute of the fire and the column buckles. After the buckling, load carrying capacity of the column decreases immediately and the plastic equivalent strains (PEEQ) along the column height reach to 15% at the 44.7^{th} minute of the fire and the column fails. The analysis time that shows the failure of the column is visualized in Figure 4.11d (II). Moreover, the maximum in-pane displacements along

the column height and the mid-height vertical displacements of the column are shown in Figure 4.11a and Figure 4.11c, respectively for the entire duration of the fire. The analysis times that correspond to the buckling of the column and occurrence of the maximum vertical displacement rate at the column mid-height are visualized in Figure 4.11d (III), and Figure 4.11d (IV).

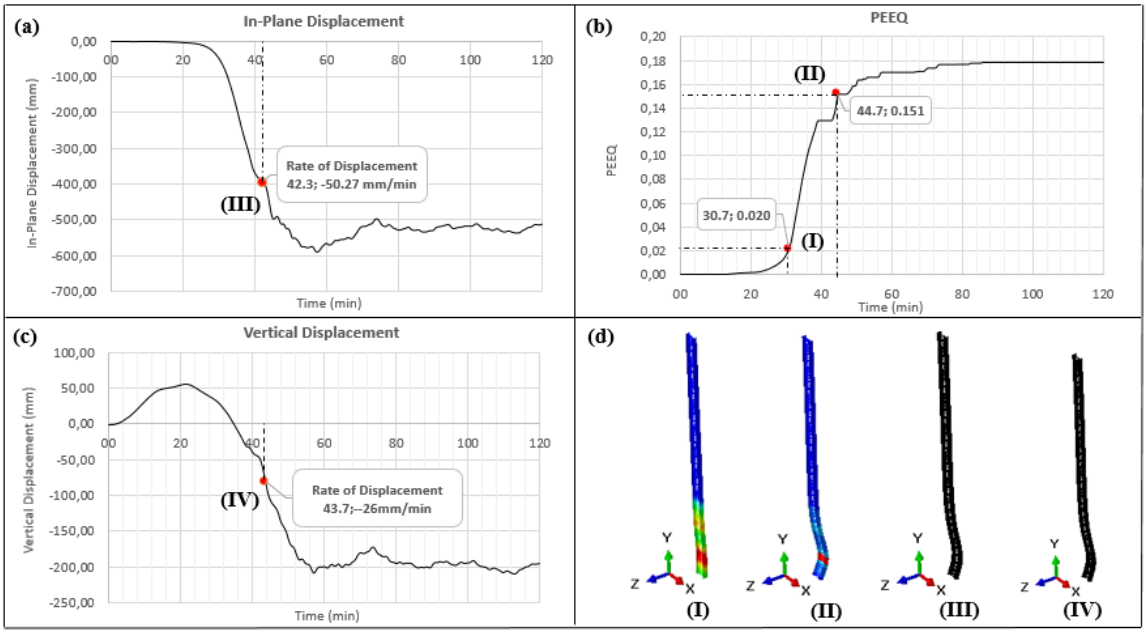

Figure 4.11. Fire Induced Behavior of the Column Located at D-3 Axis Coordinate (a) Maximum In-plane Displacements, (b) Maximum PEEQ, (c) Mid-height Vertical Displacements, (d) Analysis Times (I) Yielding - (II) Strength Loss Initiation - (III) Buckling - (IV) Maximum Vertical Displacement Rate.

To summary, for the entire duration of the fire mid-height vertical displacement rates do not reach to 50 mm/min as shown in Figure 4.11c. However, the column buckles and loses its' load carrying capacity at the 42.3^{rd} and at the 44.7^{th} minutes of the fire, respectively. These results indicate that the column hangs on its' rafter and loads acting on it are redistributed to the perimeter columns that are located along E axis by the rafter. Therefore, post buckling behavior of the structurally critical region is investigated with the fire induced performance of the rafter that is located along E axis.

Mid-length vertical displacements of the rafter that is located along E axis and their rates are shown in Figure 4.12a and Figure 4.12c for the entire duration of the fire. The maximum equivalent plastic strains along the rafter are shown in Figure 4.12b during the fire. According to Figure 4.12a, the maximum vertical displacement at the mid-length of the rafter is 217.2 mm and it is lower than the maximum allowed mid-length displacement. Moreover, maximum vertical displacement rate at the mid-length of the rafter is 34.89 mm/min for the entire duration of the fire and it is also lower than the maximum allowed mid-length vertical displacement rate. Figure 4.12d (I) visualize the analysis time that corresponds to the occurrence of the maximum vertical displacement at the mid-length of the rafter. In addition, equivalent plastic strains along the rafter do not reach yielding limit (2%), and remain constant at 0.8% after the first 43 minutes of the fire. These results indicate non-failure of the rafter during the fire.

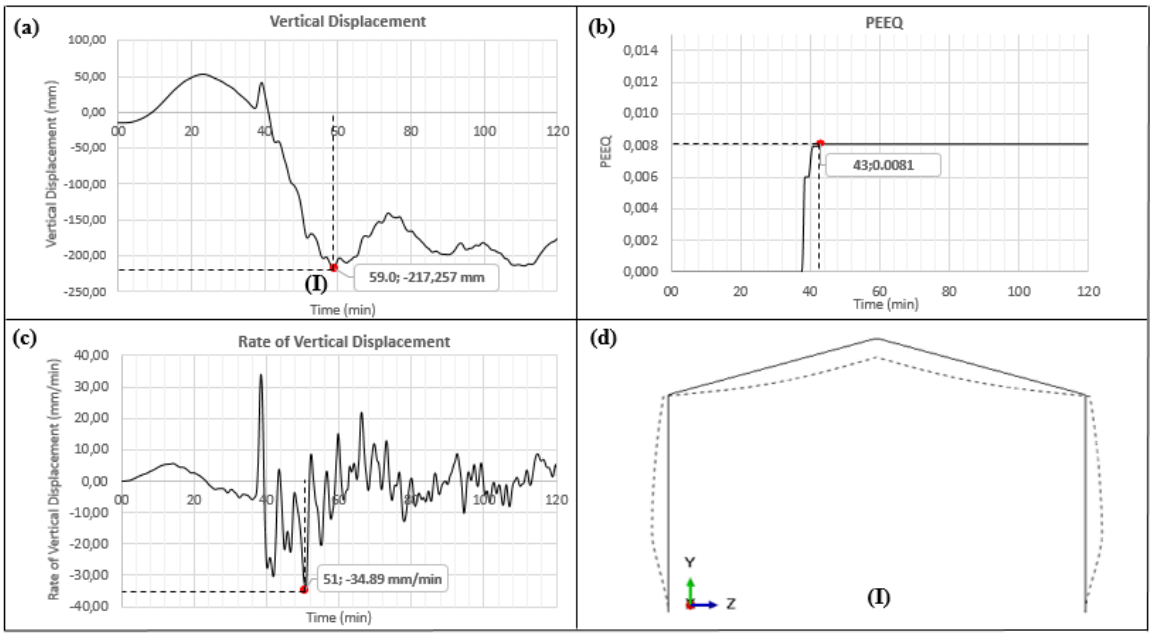

Figure 4.12. Fire Induced Behavior of the Rafter Located along E Axis (a) Mid-length Vertical Displacements, (b) Maximum PEEQ, (c) Mid-Length Vertical Displacement Rates, (d) Analysis Time (I) Maximum Vertical Displacement (x5).

Although the column that is located at D-3 axis coordinate fails due to initiation of the load carrying capacity loss at the 44.7^{th} minute of the fire, the column does not collapse and hangs on its rafter. Moreover, the rafter that is located along E axis does

not fail for the entire duration of the fire. Therefore, structurally critical region of the building does not collapse during the fire.

The state of the structurally non-critical regions of the building is determined with the fire induced performance investigation of the rafter that aligns along F axis (Figure 4.8).

The vertical displacements and their rates at the mid-length of the rafter that is located along F axis are shown in Figure 4.13a, and Figure 4.13c for the entire duration of the fire. The maximum equivalent plastic strains along the rafter are shown in Figure 4.13b for the entire duration of the fire. The maximum rate of the vertical displacement and the maximum vertical displacement at the mid-length of the rafter are 37.61 mm/min and 190.5 mm and they occur at the 43.5^{th} and at the 100.4^{th} minutes of the fire, respectively. Both of the maximum vertical displacement and the maximum rate of vertical displacement of the mid-length are below against the maximum allowable limits. Moreover, maximum equivalent plastic strain along the rafter equals to 0.99% according to Figure 4.13b, thus the rafter does not yield for the entire duration of the fire. According to these results, the investigated rafter, thus the structurally non-critical regions of the building do not collapse during the fire. Figure 4.13d (I) visualize the analysis time that corresponds to the occurrence of the maximum vertical displacement at the mid-length of the rafter.

To conclude, the columns that align in the structurally critical region of the building buckle between the 40^{th} and 50^{th} minutes of the fire, but due to load re-distribution by the rafters to the columns that are located in the structurally non-critical regions, the building does not collapse in that time interval. Moreover, after the flashover all the combustible materials burnout in a very short duration and cooling period of the fire begins at the 39^{th} minute of the fire. During the cooling period, structural members regain their strength as explained in Section 3.5 and post-buckling strength of the columns increases rapidly. Therefore, the building does not locally or globally collapse and pass the 90 minutes fire resistance rate which is given in Table 4.3. Fire induced performances of the investigated structural members of Building - 1

are summarized in Table 4.8.

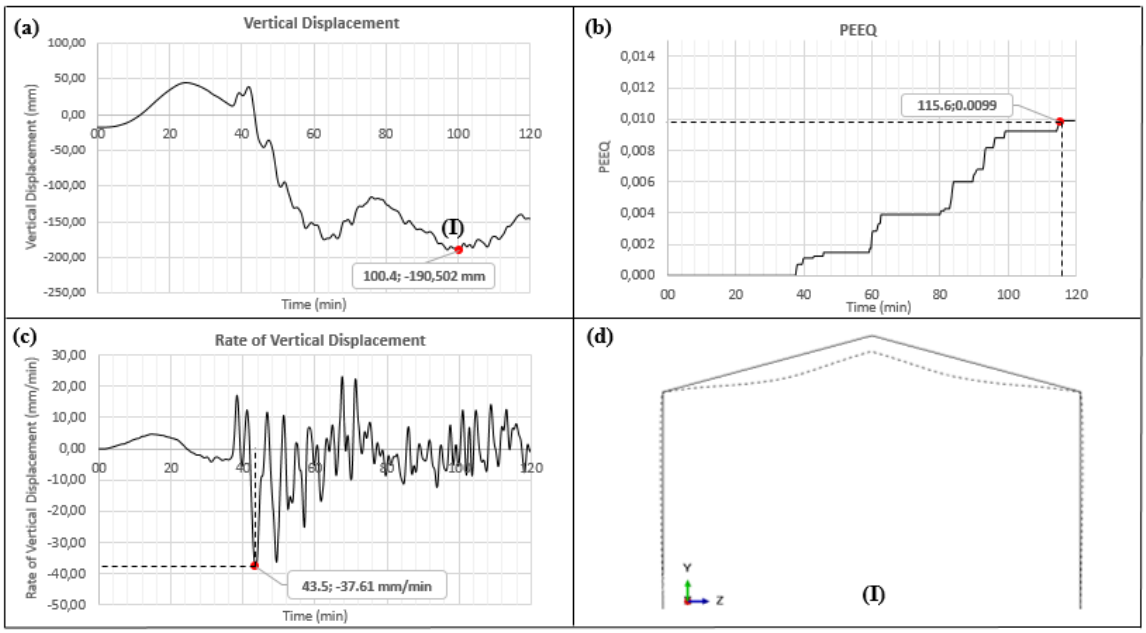

Figure 4.13. Fire Induced Behavior of the Rafter Located along Axis F (a) Mid-length Vertical Displacements, (b) Maximum PEEQ, (c) Mid-Length Vertical Displacement Rates, (d) Analysis Time (I) Maximum Vertical Displacement (x5).

Table 4.8. Fire Induced Performances of the Investigated Structural Members of Building - 1.

CRITICAL REGION (Refer to Figure 4.8)		
Refer to Figures Figure 4.11 and Figure 4.12	Columns	Rafters
Location	D3 Axis Coordinate	E1 - E5 Axis Coordinate
Yielding Time (min)	30.7	N/A
Buckling Time (min)	42.3	N/A
Failure Time (min)	44.7	N/A
Failure Criteria	15% PEEQ	N/A
NON-CRITICAL REGIONS (Refer to Figure 4.8)		
Refer to Figure 4.13	Columns	Rafters
Location	-	F1 - F5 Axis Coordinate
Yielding Time (min)	-	N/A
Buckling Time (min)	-	N/A
Failure Time (min)	-	N/A
Failure Criteria	-	N/A
PEEQ = Plastic Equivalent Strain		

4.3. Building - 2

4.3.1. Building Description

The building is 70 m in length, 40 m in width and 11.5 m to 15.5 m in height with a single pitch roof. Double-bay single pitch steel portal frames with internal column are utilized as the main load carrying mechanism of the building. Total floor area of the building is 2800 m^2 and occupied as storage. Figure 4.14 shows general layout of the building with the distances between the portal frames, wind columns, purlins, tie-beams, and the roof inclination angle. There are two different adjacent building that are located along K axis. These buildings have no connection with the main building and their volumes are separated by non-combustible gas-concrete brick wall that is constructed along K axis. Therefore, these adjacent buildings are not shown in Figure 4.14 and are not modelled in the fire simulation and finite element model of the building.

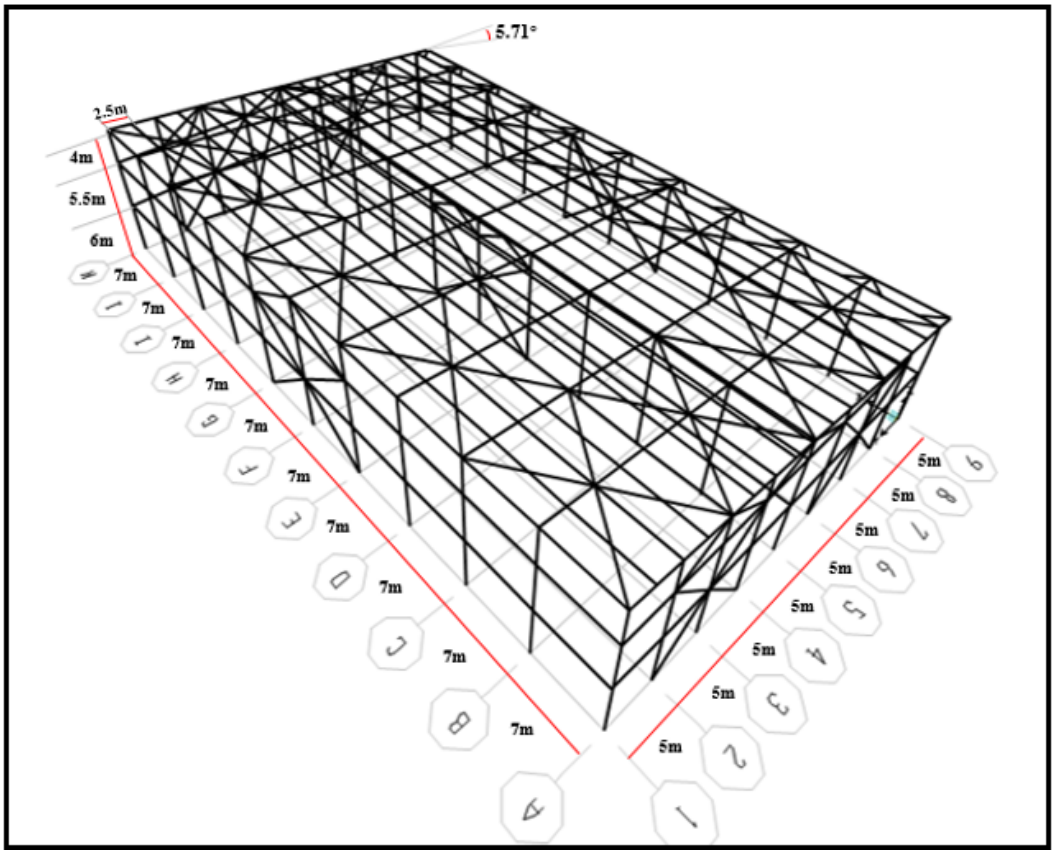

Figure 4.14. General Layout of Building - 2.

Steel sections of the portal frames that align along A and K axes, and in-plane diagonals and tie-beams that connect wind columns to these portal frames are shown in Figure 4.15a. Steel sections of the portal frames that align between B and I axes are shown in Figure 4.15b.

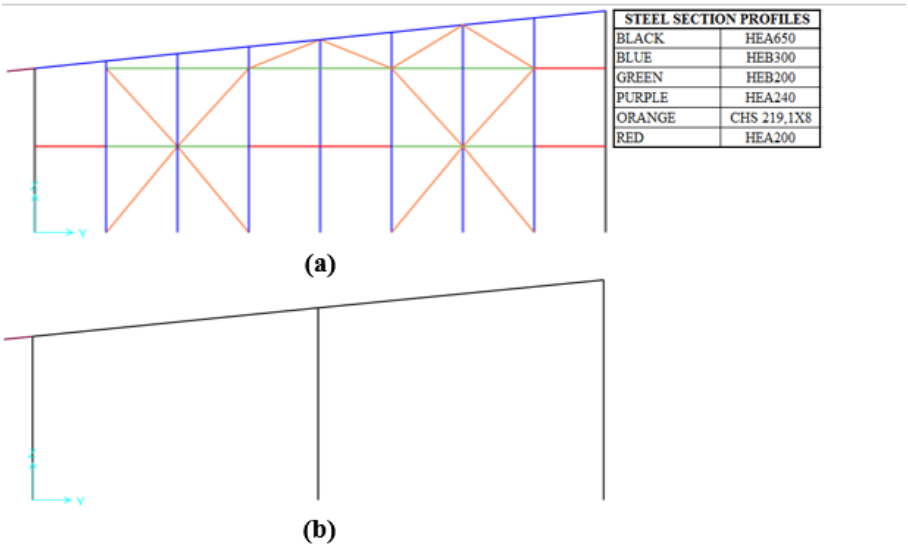

Figure 4.15. Steel Sections of the (a) Portal Frames, Tie-beams and Diagonals along A and K axes, (b) Portal Frames between B and J axes.

Steel sections of out-of-plane diagonals and tie-beams that align along 1, 5 and 9 axes and structural members located at the roof level of the building are shown in Figure 4.16 and Figure 4.17, respectively.

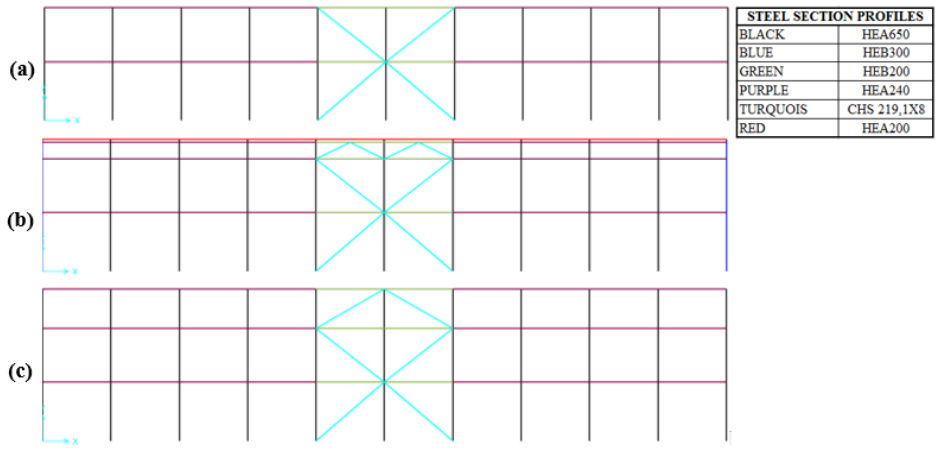

Figure 4.16. Steel Sections of the Out-of-plane Diagonals and Tie-beams (a) Along Axis 9, (b) Along Axis 5, (c) Along Axis 1.

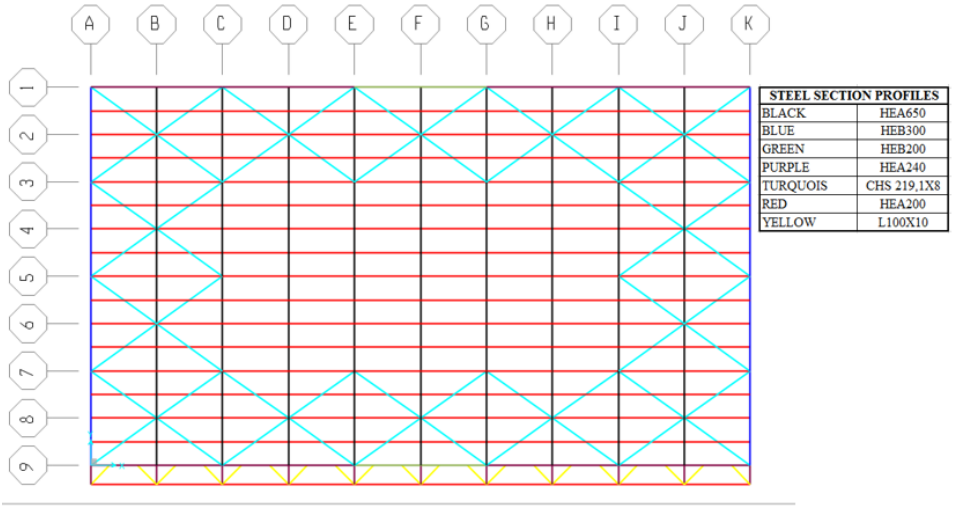

Figure 4.17. Steel Sections at the Roof Level.

Three different ventilation opening types exist on the perimeter walls of the building. Figure 4.18 shows general layout, dimensions and vertical alignments of these openings. Identical openings are highlighted only once for each side of the building in Figure 4.18. The hatched areas shown in Figure 4.18c and Figure 4.18d represent ventilation openings located on the adjacent buildings walls and these buildings have no connection with the main building. Therefore, these openings are not included to fire simulation of the building. The roll-up doors that are highlighted with the blue rectangles on Figure 4.18b and Figure 4.18c are assumed to be open in case of fire. Therefore they are modelled as to be opened in the fire simulation of the building. The openings that are highlighted with the green rectangles on Figure 4.18b and Figure 4.18d operate at the same time as the smoke detectors and they open in case of a fire.

Two different lining materials are used for the perimeter walls of the building. The wall which aligns between the main building and the adjacent buildings is constructed with the gas-concrete bricks. The rest of the perimeter walls and the ceiling are covered with self-supporting metal panels and building's floor is covered with normal weight concrete. The thermal properties and unit weights of these linings are given in Table 4.5.

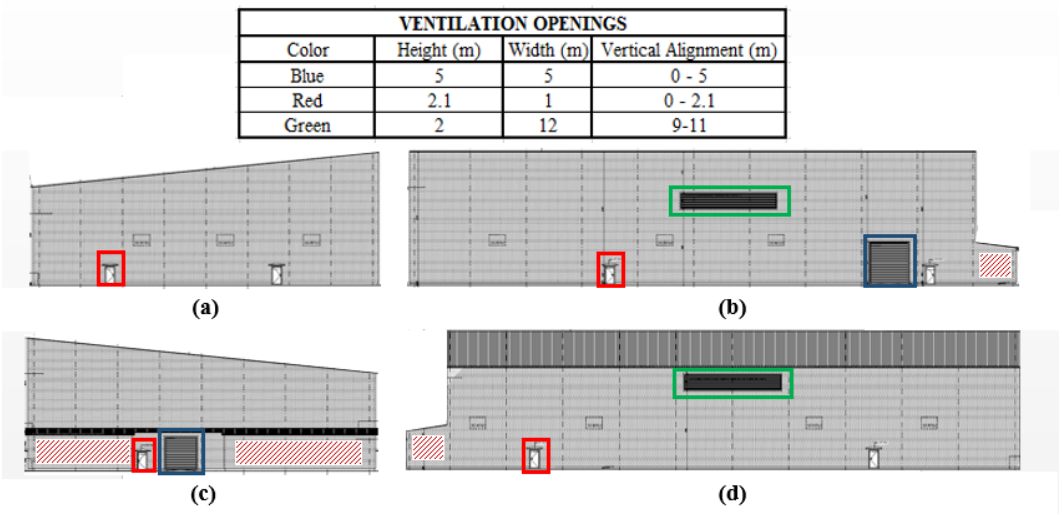

Figure 4.18. Architectural Drawings of the Building with the Highlighted Ventilation Openings, (a) A Axis View, (b) 1 Axis View, (c) K Axis View, (d) 9 Axis View.

Characteristic value of the snow load that is applied to the roof of the building is given in Table 4.2 and there is not any specified live load on the structure. The snow loads are multiplied by the design load coefficient that is described in Section 3.2 and applied to the respective structural members according to tributary area method. The weight of the perimeter walls and ceiling are also applied to the respective structural members according to the tributary area method, but they are not multiplied by any design load coefficients, similar to the weight of the steel sections.

Structurally critical region of the building is determined by a dynamic implicit structural analysis with the application of 10 times increased gravitational loads. Figure 4.19 shows the area of the building that corresponds to the structurally critical region of the building with the highlighted members.

Characteristic fire load density of the building is conservatively assumed as generic fire load for an office building according to Eurocode - 1 Part 1-2 Annex-E (CEN, 2002) due to lack of information about the fire load and it is given in Table 4.3. Design value of the fire load density for the floor surface of the building is given in Appendix-A.

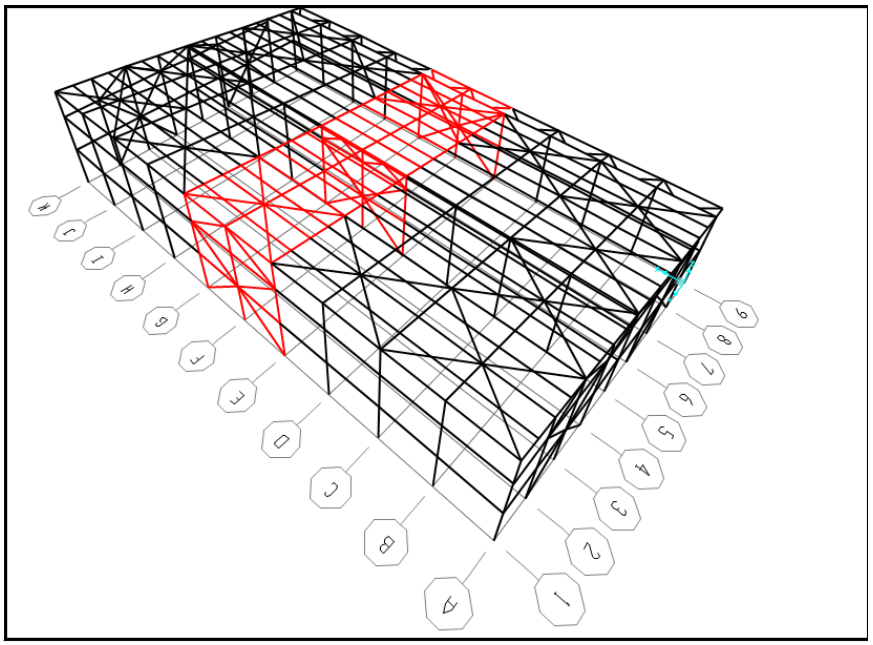

Figure 4.19. Structurally Critical Region.

4.3.2. Fire Simulation and Heat Transfer Analysis

The preliminary parameters to simulate the design fire for the building according to the methodologies explained in Section 3.5 are given in Appendix-A. The hot (gas/smoke) and cold zone temperatures, the heat release rate, the smoke elevation and the fire area for the entire duration of the fire are shown in Figure 4.20a, Figure 4.20b, Figure 4.20c and Figure 4.20d, respectively.

According to the results of the fire simulation of the building, the two-zone fire model switches to the one-zone fire model at the 35^{th} minute of the fire, because the upper layer (hot-zone) reaches to $< 20.0\%$ of the compartment and the maximum fire area reaches to 25% of the total floor area (2800.00 m^2). The fire has flashover (fully engulfed) at the 76^{th} minute of the simulation, because the hot-zone (gas/smoke) temperatures reach 500.0 ^oC. Due to the excessively large fire area, the fire is always fuel controlled and the heat release rate decreases very slowly. It is obvious from the sudden jump in the heat release rate and the fire area that the flashover occurs at the 76^{th} minute of the fire.

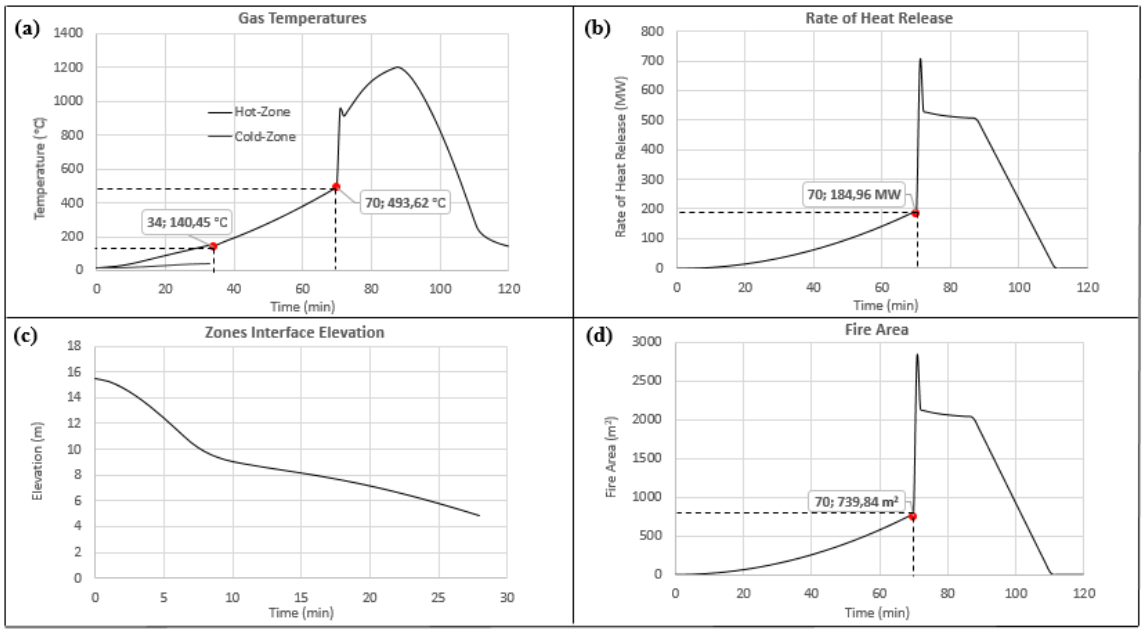

Figure 4.20. (a) Hot and Cold Zones Temperatures (Peak: 1208 °C at: 88 min), (b) RHR Computed (Peak: 700 MW at: 77 min, (c) Zones Interface Elevation (h = 3.1 m at: 35 min), (d) Fire Area (739.84 m^2 at: 70 min).

Pre-flashover localized fire is simulated with the methodologies explained in Section 3.5.2. Due to the flashover in relatively long duration (76^{th} minute of the fire), the localized fire area reaches to 924 m^2 and does not impact the ceiling (11.5 m). Moreover, spreading of the localized fire to large area results the flame height to be limited in 2 m above the ground level. However, effecting the localized fire simultaneously to 924 m^2 floor area is very conservative approach that's why the localized fire is only affected to the structurally critical region (576 m^2). Figure 4.21 shows the hot-zone gas time-temperature history, the localized fire time-temperature history for 1 m height of the flame and ISO834 standard fire curve (ISO, 1999). Until the flashover, to conduct the heat transfer analyses the first 2 m of the columns and cross diagonals that are located in the structurally critical region are exposed to the flame temperatures of the localized fire that are shown in Figure 4.21, and after the flashover these parts of the structural members are exposed to the hot-zone (gas/smoke) temperatures as explained in Section 3.6. Moreover, for the entire duration of the fire, structural members that are located in the structurally non-critical regions of the building and that align above 2 m height in the structurally critical region are simultaneously exposed to the

hot-zone (gas/smoke) temperatures for heat transfer analyses. The fire curves used for the heating of the structural members of Building - 2 are summarized in Table 4.9.

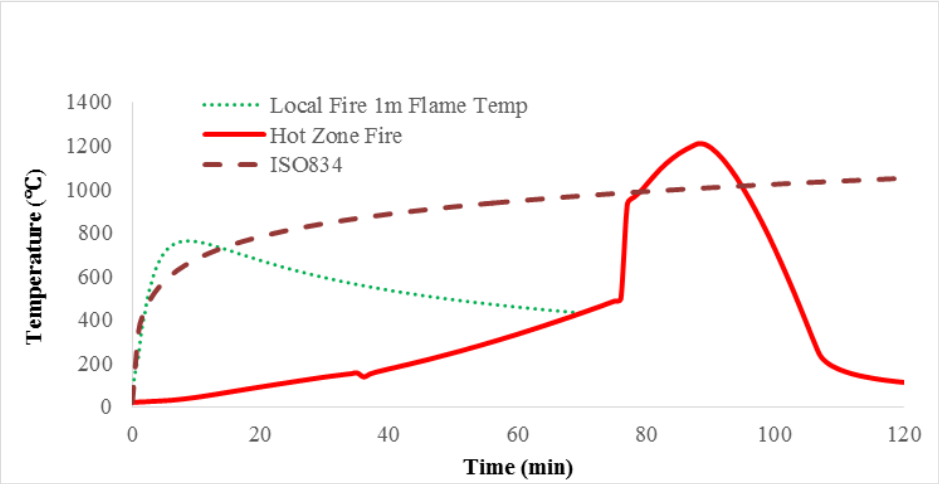

Figure 4.21. Hot-zone Gas Temperatures, Local Fire Flame Temperatures and ISO 834 Standard Fire Temperatures for 120 minutes.

Table 4.9. The Fire Curves Used for the Heating of the Structural Members of Building - 2.

CRITICAL REGION - (Refer to Figures 4.14 and 4.19)		
Columns		
Axis Coordinate	E1, F1, G1, E5, F5, G5, E9, F9, G9	
Vertical Alignment	0 - 2 m	2 m - Ceiling
Pre-flashover	1 m L.F.T.	H.Z.T
Post-flashover	H.Z.T	H.Z.T
Tie-Beams		
Axis Coordinate	E1 - F1, F1 - G1, E5 - F5, F5 - G5, E9 - F9, F9-G9	
Vertical Alignment	6 m, 11.5 m, 15 m	
Pre-flashover	H.Z.T	
Post-flashover	H.Z.T	
Cross Diagonals		
Axis Coordinate	E1 - F1, F1 - G1, E5 - F5, F5 - G5, E9 - F9, F9-G9	
Vertical Alignment	0 - 2 m	2 m - Ceiling
Pre-flashover	1 m L.F.T.	H.Z.T
Post-flashover	H.Z.T	H.Z.T
NON-CRITICAL REGIONS - (Refer to Figure 4.19)		
Pre-flashover	H.Z.T	
Post-flashover	H.Z.T	
L.F.T. = Local Fire Flame Temperatures, H.Z.T = Hot-zone Temperatures		

4.3.3. Structural Analysis

Implicit dynamic analysis method is utilized on the finite element model of the building with the predefined steel temperatures to determine fire induced structural performance of the building. Fire induced behaviors of one column and rafter in the structurally critical and non-critical regions are investigated to determine state of the building under the fire.

The perimeter columns of the portal frame that align on F axis (Figure 4.19) are the structural members in which the yielding occur firstly. Therefore, to determine the state of the structurally critical region under the fire detailed fire induced behaviors of the column that is located at F-1 axis coordinate (Figure 4.19) and the rafter that is located between F-1 and F-5 axes coordinates (Figure 4.19) are investigated

Structural instability for the columns that are located at B-5, C-5, I-5 and J-5 axis coordinates (Figure 4.19) develop in a short time difference due to the symmetry of the loading and the structural layout. Therefore, the column that is located at B-5 axis coordinate and the rafter that aligns between B-1 and B-5 axes coordinates are investigated to determine state of the structurally non-critical region.

Assessment of the investigated structural members are conducted with the allowable limits that are presented and formulated in Table 2.4. 50 mm/min mid-height vertical displacement rate (Gernay *et al.*, 2016) and the development of 15% equivalent plastic strain (CEN, 2005) along the investigated columns are used as the maximum allowable limits for the assessment of the columns. The maximum allowable mid-length vertical displacement and the rate of the vertical displacement for the rafters are 1005 mm (BS-476, 1976) and 50 mm/min (Gernay *et al.*, 2016), respectively. Moreover, development of 15% equivalent plastic strains (CEN, 2005) along the length of the investigated rafters is also used for the assessment of the rafters.

The first 2 m of the column that is located at F-1 axis coordinate is exposed to the 1 m flame temperatures until the flashover as explained in Section 4.3.2. Therefore,

column base is the critical part of the column and it yields at the 88.2^{nd} minute of the fire. Rate of the in-plane and out-of-plane displacements along the column height do not reach to 50 mm/min and the column does not buckle during the fire. Maximum out-of-plane displacements along the column height and the mid-height vertical displacements are shown in Figure 4.22a and Figure 4.22c for the entire duration of the fire. According to Figure 4.22c, mid-height vertical displacement rate of the column reaches 50.76 mm/min at the 91.8^{th} minute of the fire and column fails. Figure 4.22d (II) and (III) visualize the analysis times that correspond to the occurrence of the maximum allowable vertical displacement rate at the column mid-height and the maximum out-of-plane displacement rate along the column height.

Equivalent plastic strains that develop at the base of the column are shown in Figure 4.22b for the entire duration of the fire and the analysis time that corresponds to the yielding of the column base is visualized in Figure 4.22d (I). By the yielding of the column base, vertical displacements along the column increase immediately. It is clearly seen from Figure 4.22c that only after 3.6 minutes from the yielding of the column base, column fails due to initiation of the run away (50.76 mm/min) mid-height vertical displacements at the 91.8^{th} minute of the fire. The column located at F-9 axis coordinate (Figure 4.19) also shows similar structural behavior due to symmetry of the structure.

Failure of the columns that are located at F-1 and F-9 axis coordinates does not indicate collapse of the structurally critical region, due to load redistribution by the rafter to the columns that are located in the structurally non-critical regions of the building. Therefore, the rafter that is located between F-1 and F-5 axes coordinates is investigated to determine state of the structurally critical region as below.

Equivalent plastic strains at the knee point of the rafter that is located on F-5 axis coordinate is given in Figure 4.23b for the entire duration of the fire. According to the figure, the knee point yields at the 87.8^{th} minute of the fire, Figure 4.23d (I) visualize the analysis time that corresponds to the yielding of the knee point. Due to yielding, mid-length vertical displacements increase immediately, and at the 92^{nd}

minute of the fire mid-length vertical displacement rate reaches to 50 mm/min and the rafter fails.

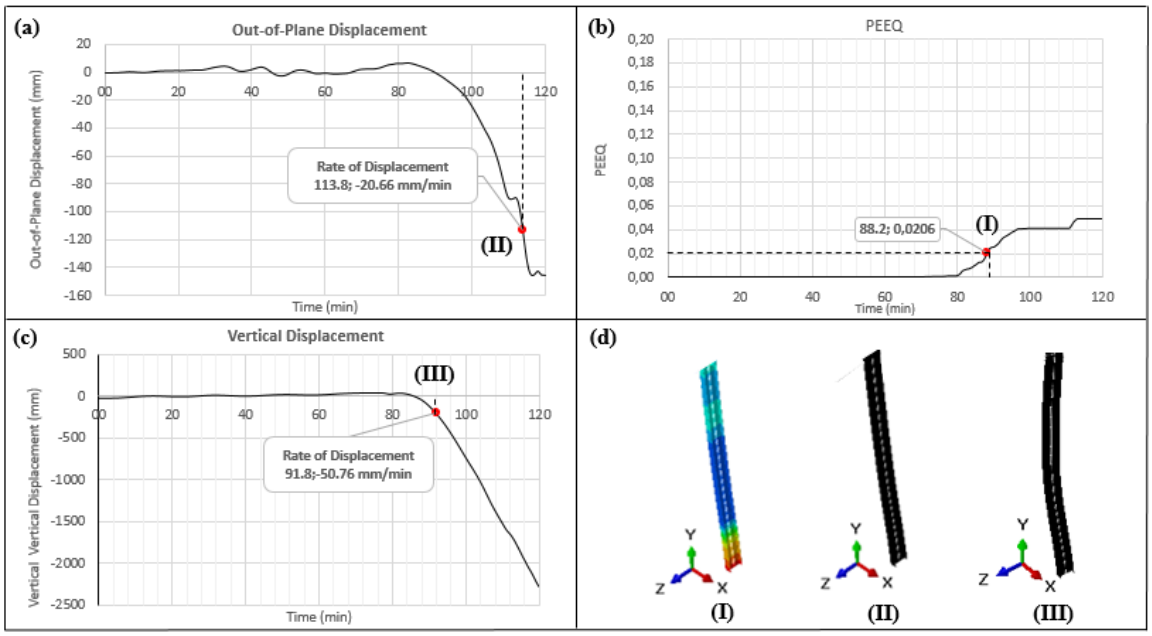

Figure 4.22. Fire Induced Behavior of the Column Located at F-1 Axis Coordinate, (a) Maximum Out-of-Plane Displacements, (b) Maximum PEEQ, (c) Mid-height Vertical Displacements, (d) Analysis Times - (I) Yielding - (II) Maximum Out-of-plane Displacement Rate - (III) Allowed Vertical Displacement Rate.

The mid-length vertical displacement rates of the rafter is shown in Figure 4.23c for the entire duration of the fire, with the highlighted failure time. Moreover, mid-length vertical displacements of the rafter reaches to the allowable limit at the 103.8^{th} minute of the fire as highlighted in Figure 4.23a. Due to excessive displacement along the rafter and steel stiffness decrease at high temperatures, the knee point of the rafter initiate to lose its strength by reaching 15% equivalent plastic strain at the 118^{th} minute of the fire. Figure 4.23d (II), (III) and (IV) visualize the analysis times that correspond to the initiation of the strength loss at the knee point, initiation of the run-away displacements and occurrence of the maximum allowable vertical displacement at the mid-length of the rafter, respectively.

Due to failure of the column that is located at F-1 axis coordinate at the 91.8^{th} minute of the fire and the failure of the rafter that is located between F-1 and F-5

axis coordinates at 92^{nd} minute of the fire, structurally critical region of the building collapses at the 92^{nd} minute of the fire.

Fire induced structural behaviors of the column that is located at B-5 axis coordinate and the rafter that is located between B-1 and B-5 axis coordinates are investigated to determine state of the structurally non-critical regions.

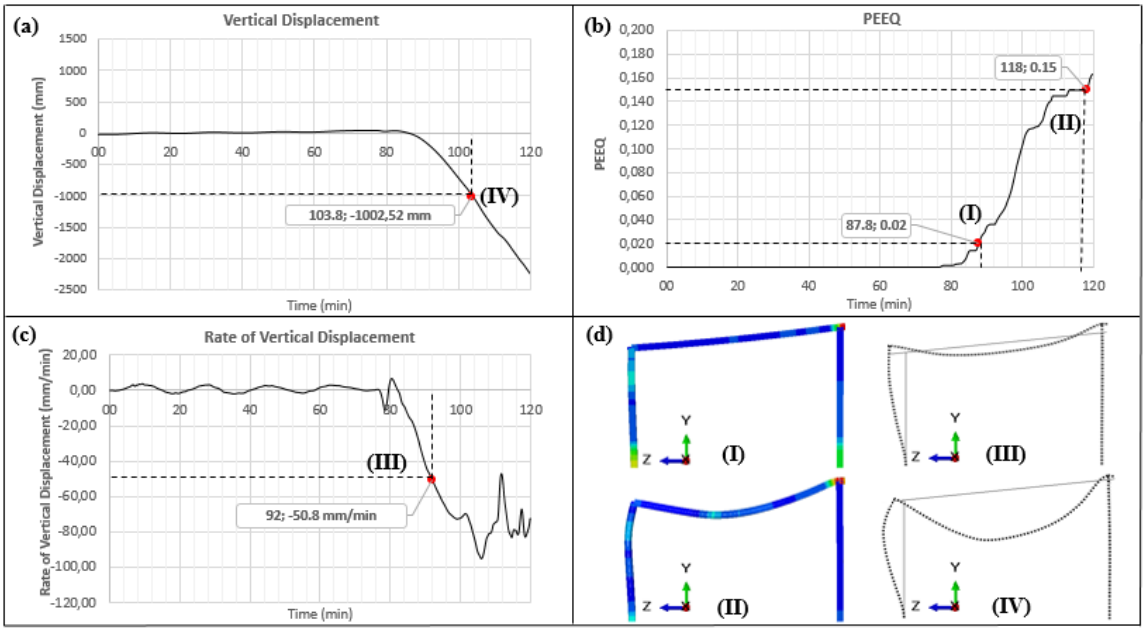

Figure 4.23. Rafter Located between F-1 and F-5 Axis Coordinates, (a) Mid-length Vertical Displacements, (b) Maximum PEEQ, (c) Mid-length Vertical Displacement Rates, (d) Analysis Times - (I) Yielding - (II) Strength Loss Initiation - (III) Allowed Vertical Displacement Rate (x5) - (IV) Allowed Vertical Displacement (x5).

Out-of-plane displacement rates along the column that is located at B-5 axis coordinate reaches to 50 mm/min at the 82.4^{th} minute of the fire, and the column buckles. Figure 4.24a shows the maximum out-of-plane displacements along the column height for the entire duration of the fire and the analysis time that corresponds to the buckling of the column is visualized in Figure 4.24d (III). Equivalent plastic strains along the height of the column reach to 2% at the 94.8^{th} minute of the fire and at this time column yields as visualized in Figure 4.24d (I). The column yields 12.4 minutes after from the buckling, this result indicates occurrence of the elastic column buckling due to loss of steel stiffness at high temperatures. However, due to post-buckling

strength of the column and load re-distribution by the rafter to the perimeter columns that are located at B-1 and B-9 axis coordinates (Figure 4.19) the buckling of the column does not indicate collapse of the structurally non-critical region. Moreover, mid-height vertical displacement rates of the column do not reach to 50 mm/min during the fire, thus the column hangs on its rafter after the buckling. Figure 4.24c shows the mid-height vertical displacements of the column for the entire duration of the fire with the highlighted maximum vertical displacement rate. Equivalent plastic strains along the height of the column reach to 15% at the 112.8^{th} minute of the fire and the column fails at this time due to initiation of the strength loss. Figure 4.24d (II) visualize the analysis time that corresponds to the failure of the column due to strength loss initiation.

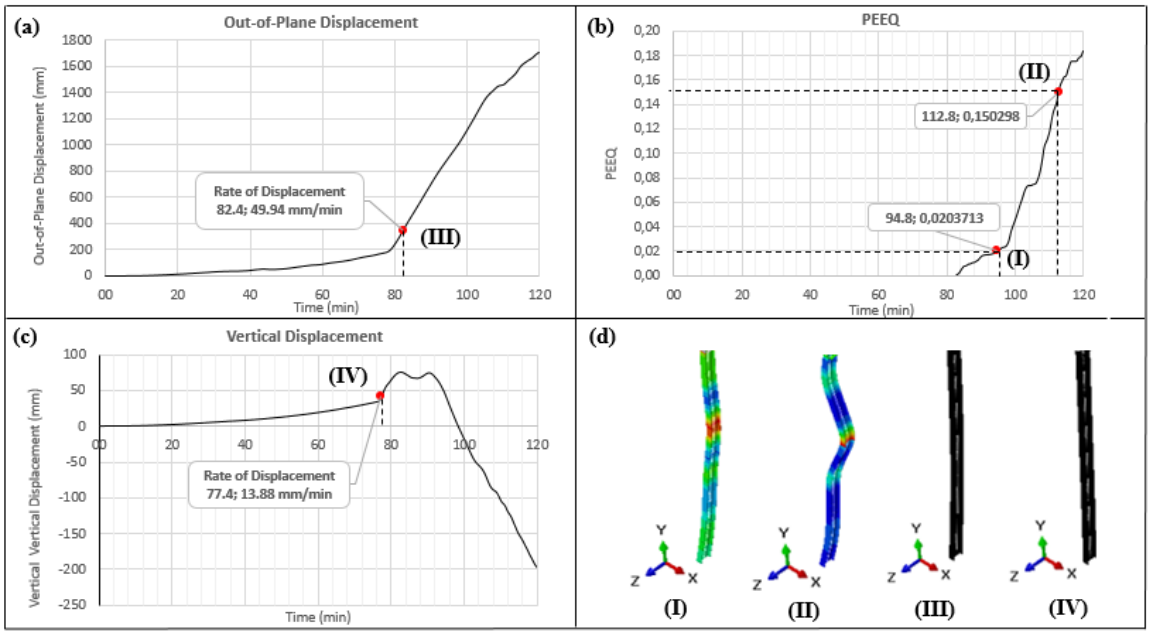

Figure 4.24. Fire Induced Behavior of the Column Located at B-5 Axis Coordinate (a) Maximum Out-of-plane Displacements, (b) Maximum PEEQ, (c) Mid-height Vertical Displacements, (d) Analysis Times - (I) Yielding - (II) Strength Loss Initiation - (III) Buckling - (IV) Maximum Vertical Displacement Rate.

The failure of the column that is located at B-5 axis coordinate does not indicate the failure of the portal frame, thus structurally non-critical regions. Therefore, state of the structurally non-critical regions are determined with detailed fire induced behavior

investigation of the rafter that aligns between B-1 and B-5 axis coordinate.

The knee point of the rafter that is located between B-1 and B-5 axis coordinates yields at the 87.2^{nd} minute of the fire as shown in Figure 4.25b (2% PEEQ). Figure 4.25c shows the mid-length vertical displacement rates of the rafter for the entire duration of the fire and as highlighted in the figure 50 mm/min mid-length vertical displacement rate which corresponds to the failure of the rafter occurs at the 91.4^{th} minute of the fire. Analysis times that correspond to the yielding of the knee point and the failure of the rafter due to initiation of the run-away vertical displacements at the mid-length of the rafter are visualized in Figure 4.25d (I) and Figure 4.25d (II), respectively. Although, the rafter fails due to initiation of the run-away vertical displacements at the 91.4^{th} minute of the fire, dynamic implicit analysis continues for the entire duration of the fire and this allows to understand post-failure behavior of the rafter. Figure 4.25a shows the mid-length vertical displacements of the rafter with the highlighted analysis time (102.6^{th} minute of the fire) that corresponds to the development of the allowable vertical displacement limit state, this analysis time is also visualized in Figure 4.25d (III).

Fire induced performances of the investigated structural members of Building - 2 are summarized in Table 4.10. According to the table, failure of the column that is located at B-5 axis coordinate and the rafter that is located between B-1 and B-5 axis coordinates indicate the collapse of the structurally non-critical regions, thus the building in the 91^{st} minute of the fire. Therefore, the building pass the 60 minutes fire resistance rate which is given in Table 4.3.

4.4. Building - 3

4.4.1. Building Description

Building - 3 is structurally the most complex building with various cross diagonals, crane beams, adjacent building, out-building platforms, in-building platforms and piping systems. The building is 60.5 m in length, 52 m in width and 13 m to 32.5 m in

height and utilized as pressure oxidation utility. Figure 4.26 represents general layout of the building with the distances the between portal frames, crane support columns, purlins, tie-beams, and the roof inclination angle.

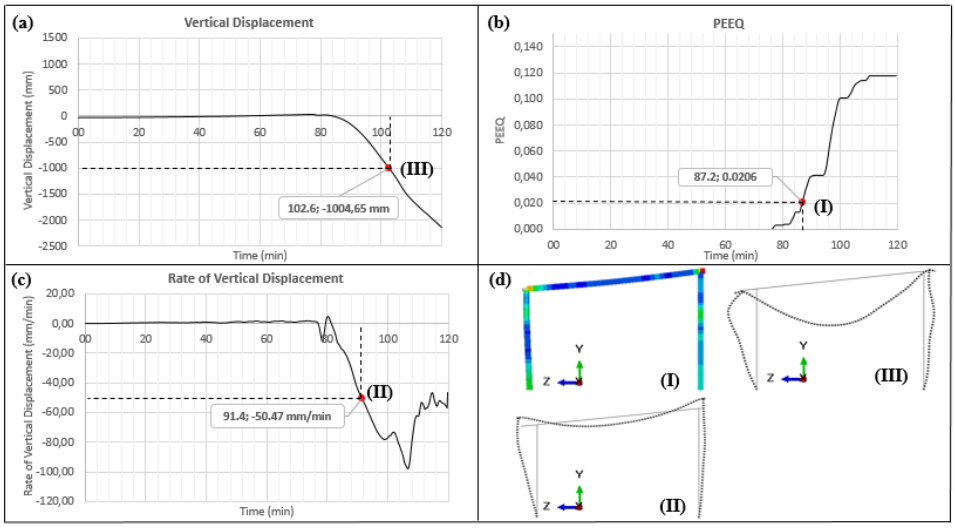

Figure 4.25. Fire Induced Behavior of the Rafter Located Between B-1 and B-5 Axis Coordinates, (a) Mid-length Vertical Displacements, (b) Maximum PEEQ, (c) Mid-length Vertical Displacement Rates, (d) Analysis Times - (I) Yielding - (II) Allowed Vertical Displacement Rate (x5) - (III) Allowed Vertical Displacement (x5).

Table 4.10. Fire Induced Performances of the Investigated Structural Members of Building - 2.

CRITICAL REGION (Refer to Figure 4.19)		
Refer to Figures Figure 4.22 and Figure 4.23	Columns	Rafters
Location	F1 Axis Coordinate	F1 - F5 Axis Coordinate
Yielding Time (min)	88.2	88.7
Buckling Time (min)	N/A	N/A
Failure Time (min)	91.8	92
Failure Criteria	Mid-height Vertical Displacement Rate (50mm/min)	Mid-length Vertical Displacement Rate (50mm/min)
NON-CRITICAL REGIONS (Refer to Figure 4.19)		
Refer to Figure 4.24 and Figure 4.25	Columns	Rafters
Location	B5 Axis Coordinate	B1 - B5 Axis Coordinate
Yielding Time (min)	94.8	87.2
Buckling Time (min)	82.4	N/A
Failure Time (min)	112.8	91.4
Failure Criteria	15% PEEQ	Mid-length Vertical Displacement Rate (50mm/min)
PEEQ = Plastic Equivalent Strain		

Two different steel portal frame types are utilized as the main load carrying mechanism of the building. The first type of the steel portal frames is a single bay portal frame with a single roof pitch and it aligns between axes 1 and 5 along axes A and I. The second type portal frame is a double bay portal frame with a flat roof and it aligns between axes A and I along axes 6 and 10. The height of the second type portal frames increase with roof inclination angle from axis 10 to axis 6. Moment resistance alignment of these portal frames are shown in Figure 4.27.

The general alignments of the two different out-building platform and the adjacent building are shown in Figure 4.28. The perimeter beams of the out-building platform and the adjacent building are connected to the columns of the main building, thus they transmit force to the columns of the main building. Therefore these structures are modelled in the finite element model of the building, but they are not modelled in the fire simulation of the building because compartment volume of the adjacent building is separated from the main building by gas-concrete brick walls that are constructed along axes I and 1 and the out-building platform does not form a compartment.

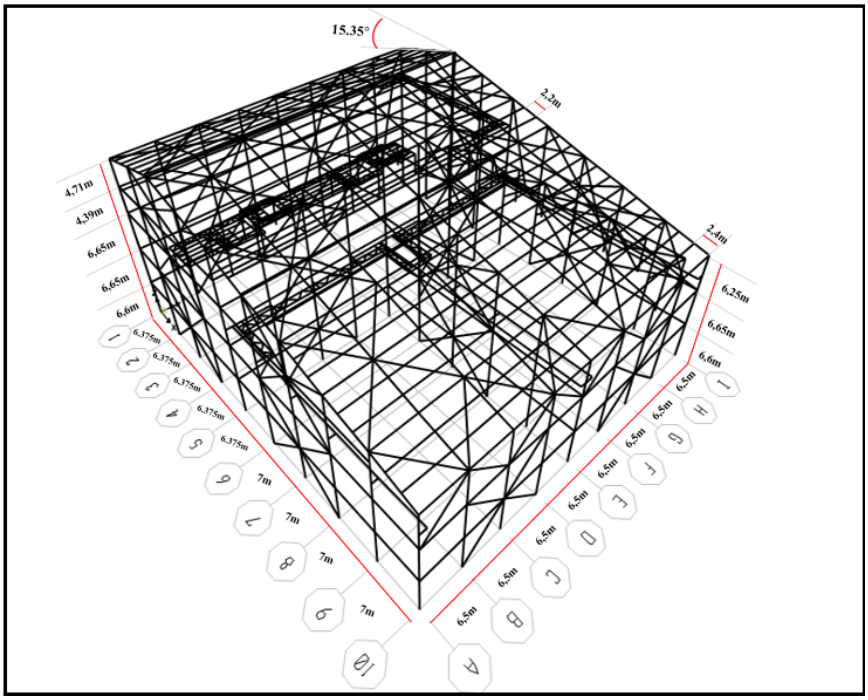

Figure 4.26. General Layout of Building - 3.

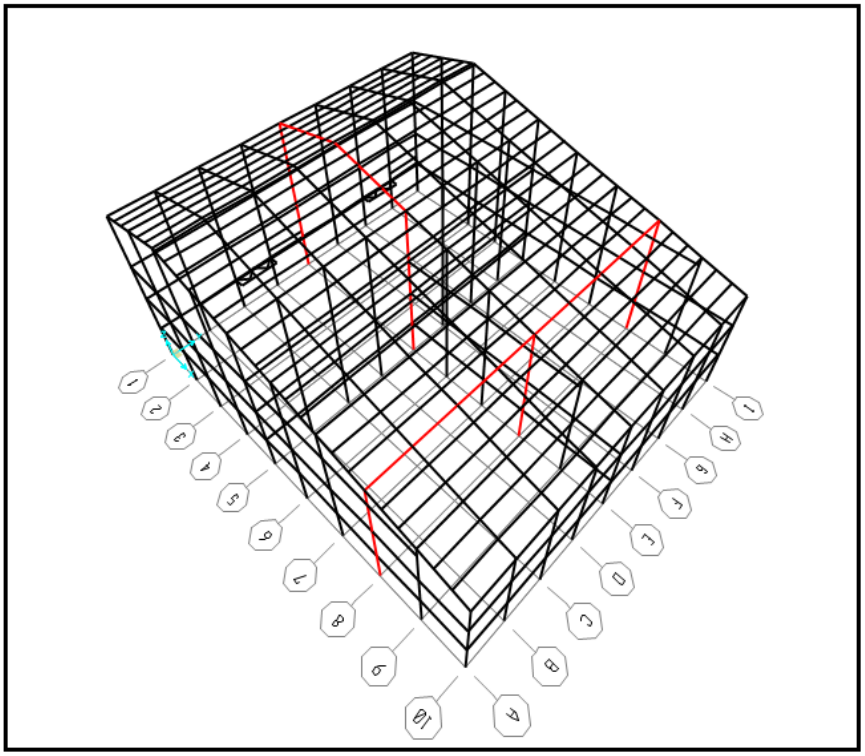

Figure 4.27. Moment Resistance Alignment of the Two Different Type Portal Frames.

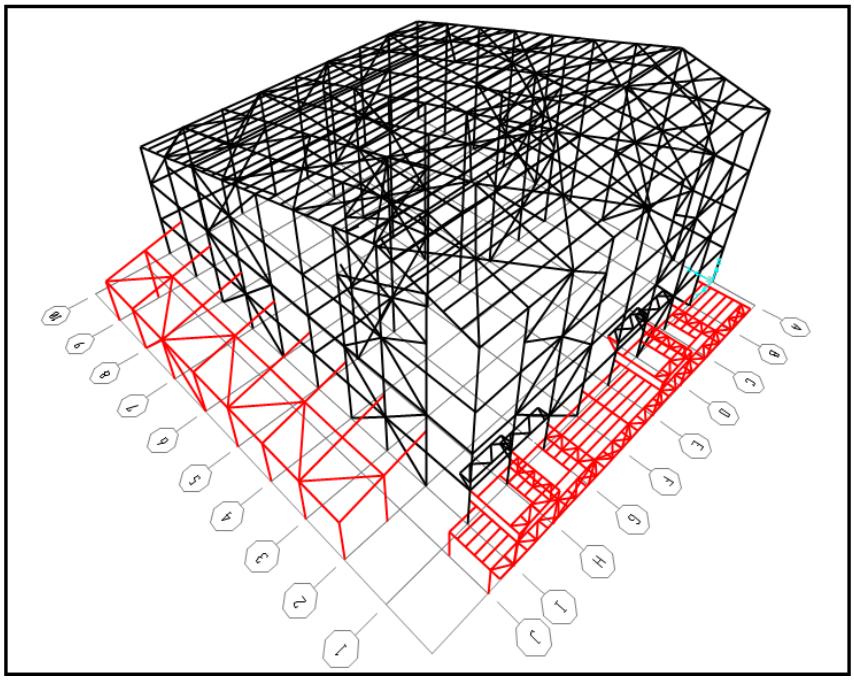

Figure 4.28. General Layout of the Adjacent Building and Out-building Platform.

The steel sections of the portal frames that align along axes A and I, and the steel sections of the in-plane diagonals and tie-beams that connect the crane support

columns to these portal frames are shown in Figure 4.29a. Steel sections of the portal frames that align along axes B and H are shown in Figure 4.29b, and the steel sections of the out-of-plane diagonals and tie-beams that connect parallel portal frames to each other are shown in Figure 4.29c.

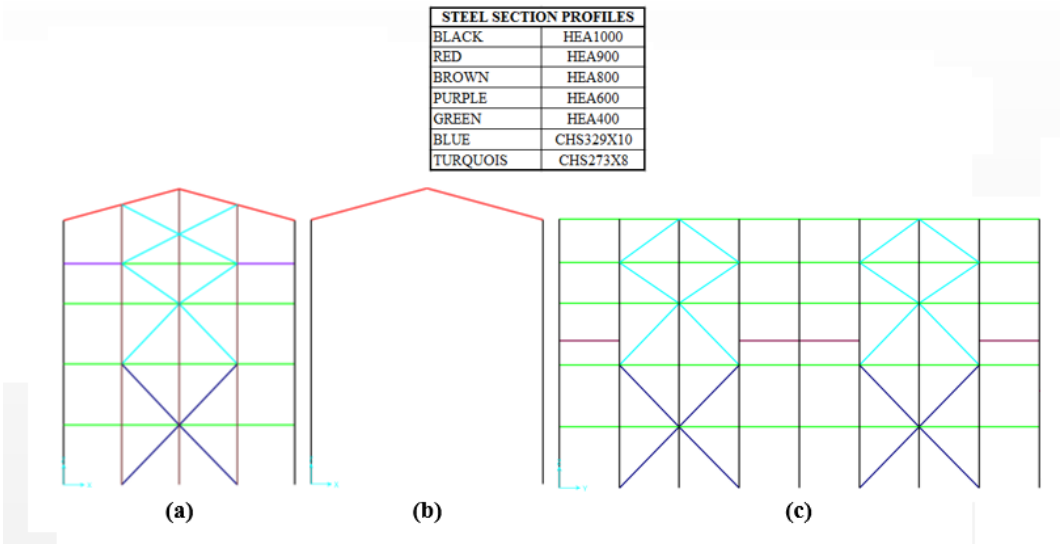

Figure 4.29. Steel Sections of the (a) Portal Frames, Diagonals and Tie-Beams along A and I Axes (b), Portal Frames along Axis B and H, (c) Diagonals and Tie Beams along Axes 1 and 5.

Steel sections of the double-bay portal frame, tie-beams, diagonals and wind columns that align along axis 10 are shown in Figure 4.30a. Steel sections of the parallel portal frames between axis 6 and 9 are identical. Therefore, the steel sections of typical portal frame that align along axis 8 is shown in Figure 4.30b to illustrates the steel sections of the portal frames that align between axis 6 and 9.

The rafter of the second type portal frame is specially produced for the large span opening of the portal frame. The dimensions of the built-up section is given in Figure 4.31.

Steel sections of the diagonals and tie-beams that connect second type portal frames to crane support columns along E, A and I axes are shown in Figure 4.32a and Figure 4.32b.

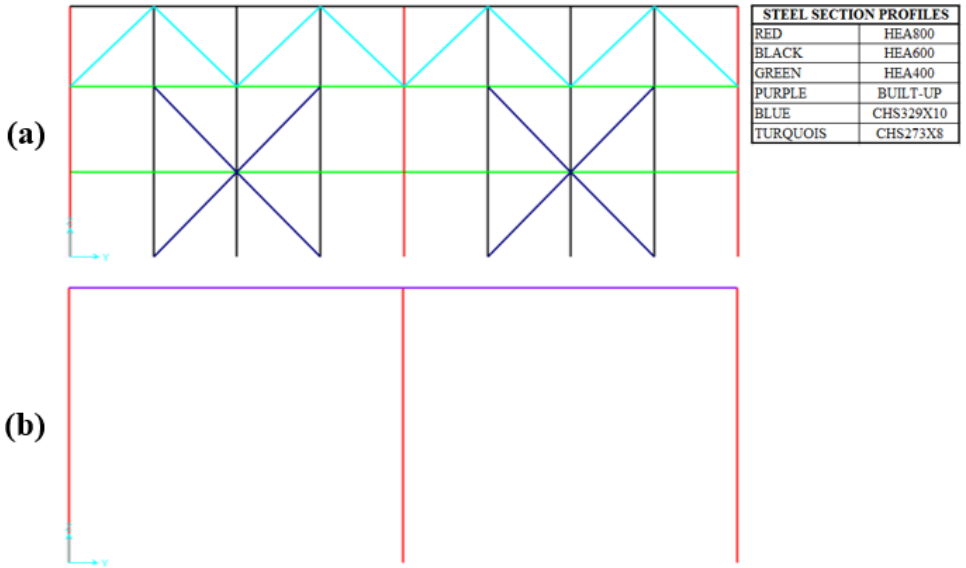

Figure 4.30. Steel Sections of the (a) Portal Frame, Diagonals and Tie-beams located along Axis 10 (b) Portal Frame located along Axis 8.

The general roof layout is shown in Figure 4.33 with the steel sections of the purlins, roof diagonals and the rafters.

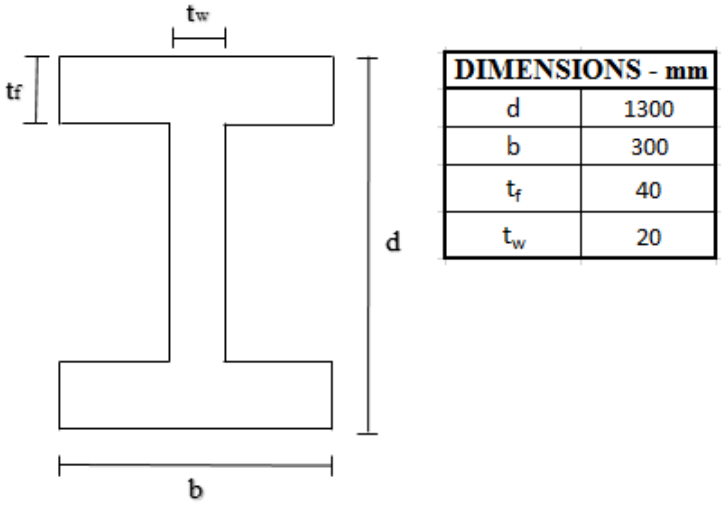

Figure 4.31. Dimensions of the Built - up Section.

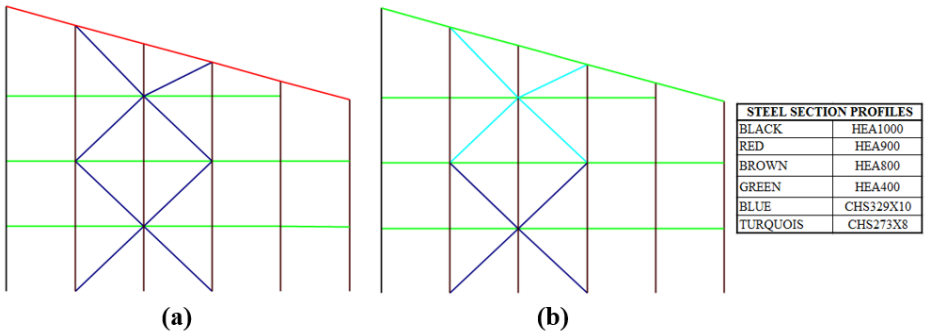

Figure 4.32. Steel Sections of the Tie-beams, Diagonals and Crane Support Columns (a) along E Axis, (b) Along A and I Axes.

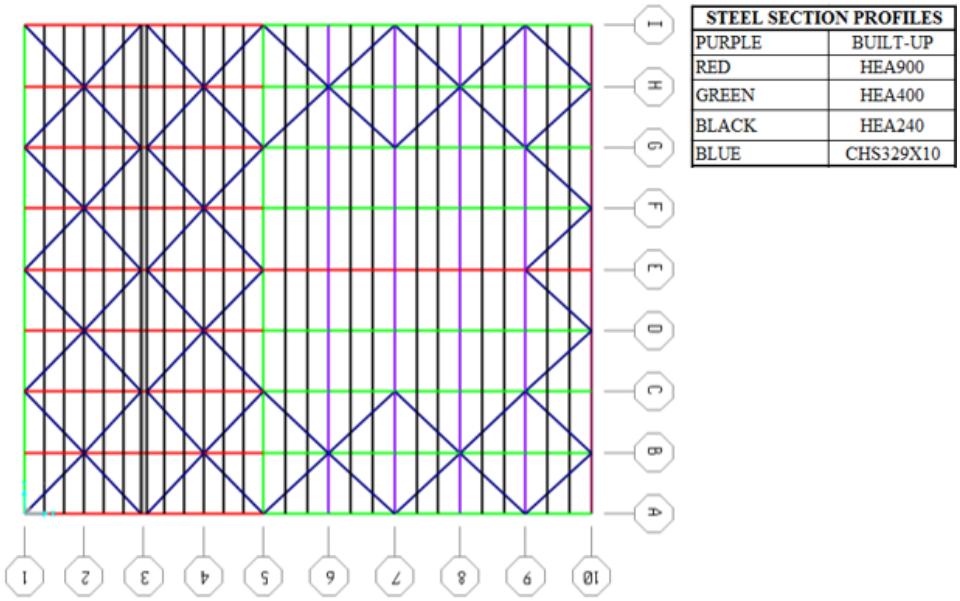

Figure 4.33. General Layout and Steel Sections at Roof of the Building.

There are three cranes in the building. Two of them are identical and they align at the 15.9 m height of the building, and the other one aligns at the 24.29 m height of the building. The cranes that are located at 15.9 m height move between axes 5 and 10, and the span length of these cranes equals to distance between axes A and E. The crane that is located at 24.9 m height moves between axes A and I and its' span length equals to the distance between axes 1 and 5. General layout of the crane beams and the stability bracings, and steel sections of these structural members located at 15.9 m and 24.29 m heights of the building are shown in Figure 4.34a and Figure 4.34b.

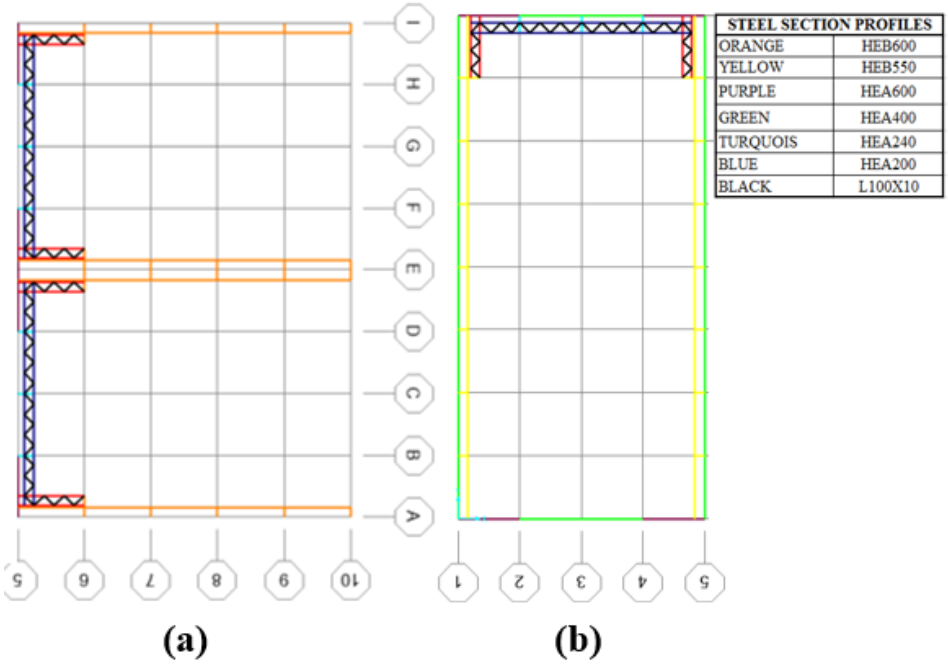

Figure 4.34. General Layout and the Steel Section Profiles at Crane Levels (a) 15.9 m (b) 24.29 m.

5 different ventilation opening types exist on the perimeter walls of the building, 3 of them are identical with respect to their dimensions, but they differentiate with respect to their vertical alignments. Figure 4.35 shows general layout, dimensions and vertical alignment of these ventilation openings and the identical opening types are only highlighted once in the figure. Roll-up doors shown with the blue rectangles in Figure 4.35a, Figure 4.35b and Figure 4.35d are assumed to be open in case of fire. The hatched area shown in Figure 4.35c represents the openings of the adjacent building, thus they are not modelled in the fire simulation of the building because compartment volume of this adjacent building is separated from the main building with gas-concrete brick wall that is constructed along the I axis.

The perimeter walls and ceiling of the building are covered with the self-supporting metal panels and the floor of the building is covered with normal-weight concrete. Thermal properties and unit weights of these materials are given in Table 4.5.

VENTILATION OPENINGS			
Color	Height (m)	Width (m)	Vertical Alignment (m)
Red	2.1	2	0-2.1
Blue	5	5	0 - 5
Green	1	2	7-8
Yellow	1	2	19-20
Purple	1	2	27-28

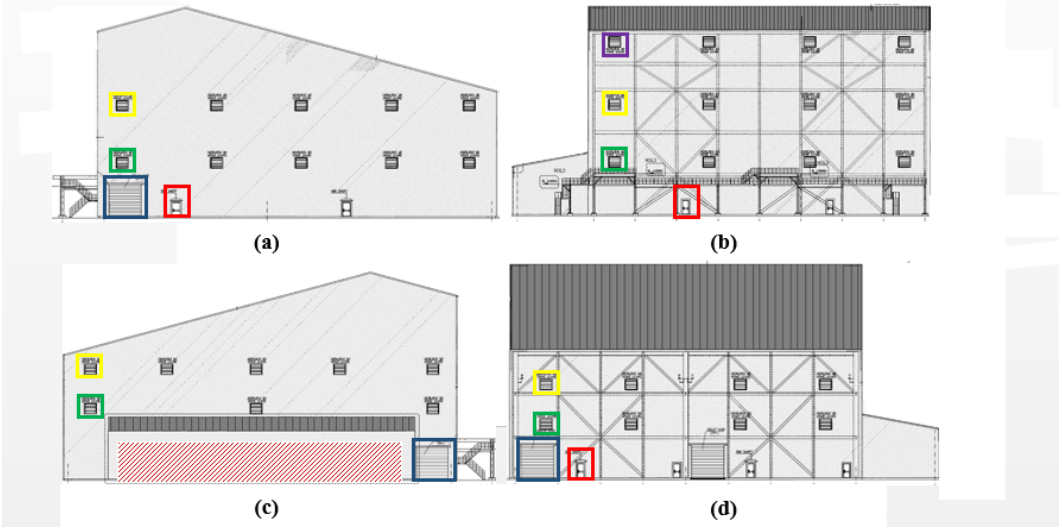

Figure 4.35. Architectural Drawings of the Building with the Highlighted Ventilation Openings (a) A Axis View (b) 1 Axis View (c) J Axis View (d) 10 Axis View.

Characteristic value of the snow loads that is applied to the roof of the building is given in Table 4.2. The live loads on the building arise from the piping systems, in-building platforms and the technical equipment that are located on the crane platforms and adjacent building. The surfaces highlighted with the grey color in Figure 4.36 represent crane platforms. The live loads on these platforms equal to 5kN/m^2. Moreover, the red and yellow circles shown in Figure 4.36a represent application points of 30kN equipment self-weights at the 5 m and the 6,6 m heights, respectively. The weights of the cranes are determined according to the Stahl Crane Systems technical manual (Stahl, 2008) and applied to the highlighted points in Figure 4.36b and Figure 4.36c.

Moreover, there are also thermal friction forces on the columns that align along axis 5 due to large piping systems attached to the these columns. Points of application, direction and magnitude of these forces are shown in Figure 4.37. These forces are assumed as to be as one of the primary variable action on the building to consider the

worst case fire scenario.

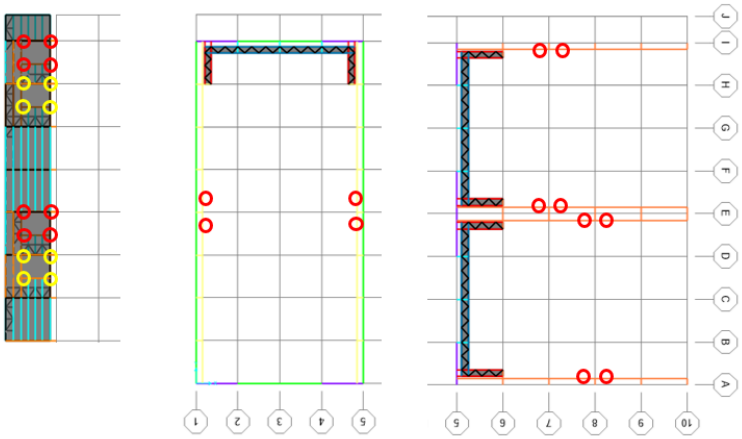

Figure 4.36. Live Load Application Areas (Grey Surfaces) and Application Points of the Crane and Equipment Self-Weights (Hollow Circles) (a) Out-building Platform, (b) 24.29 m Crane Level, (c) 15.9 m Cranes Level.

The platforms, the equipment on these platforms and the piping systems located in the main building are attached to the columns that are located along axes 5 and 10. These facilities are not modelled in the finite element model of the building, but the live loads on these facilities and the weights of these facilities are included in the structural analysis. Application points of these forces are highlighted in Figure 4.38 and magnitudes of these forces are given in Table 4.11.

The snow load, the distributed live loads and the self-weight of the wall and ceiling linings are applied to the respective structural members according to tributary area method. All of the loadings, except self-weights, explained in this section are multiplied by the design load coefficients that are described in Section 3.2 for the performance-based structural analysis of the building.

Structurally critical region of the building is determined by a dynamic implicit structural analysis with the application of 10 times increased gravitational loads. Figure 4.39 shows the area of the structurally critical of the building with the highlighted members. The crane beams, the stability bracings, and some of the roof purlins are

not shown in Figure 4.38 for clarity of the figure.

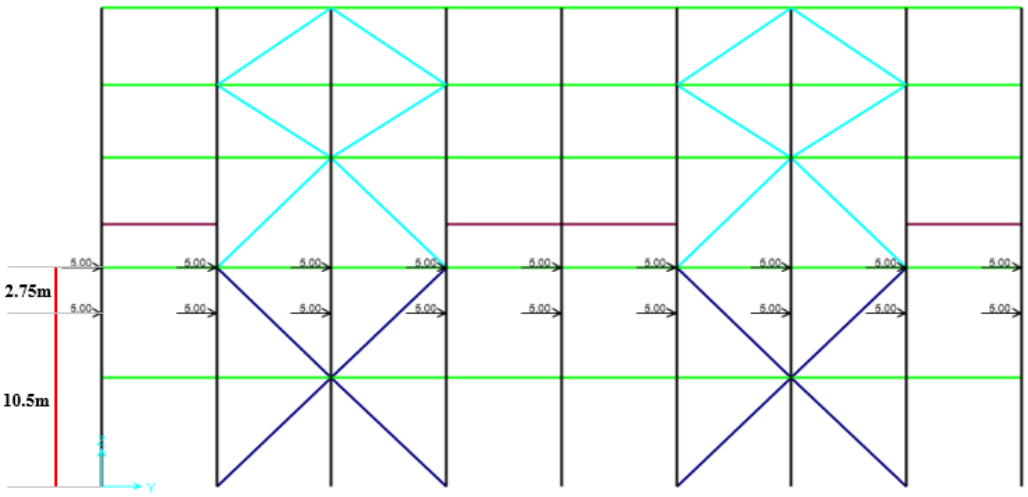

Figure 4.37. The Point of Application, Magnitude and Direction of Thermal Friction Forces along Axis 5.

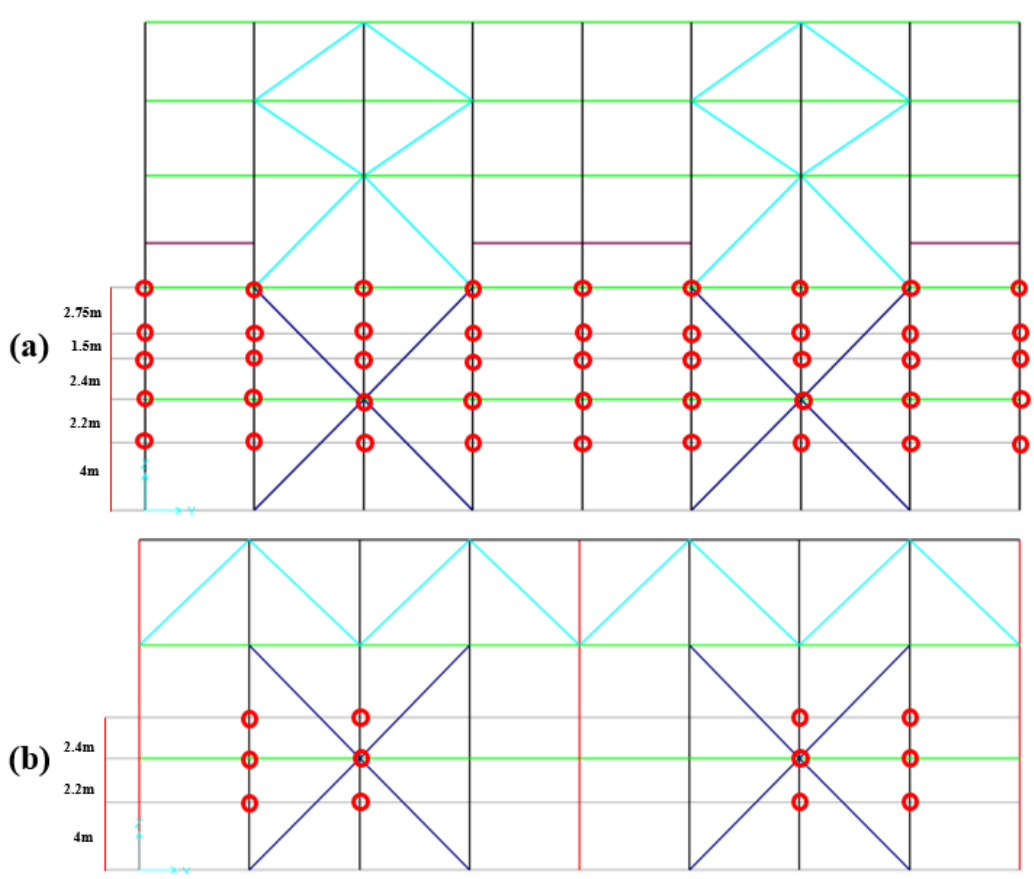

Figure 4.38. The Point of Application of Indoor Platform and Equipment Self weights and Live Loads (a) Along Axis 5 (b) Along Axis 10.

Fire load survey of the building is carried out by the operator of the building, and the total amount of the combustible materials (lubricants and diesel) located in the building are listed in Table 4.12.

Table 4.11. The Equipment and Piping Systems Self-Weights, Live Loads and the Equipment Loads Applied to the Columns that Align on the Axes 5 and 10 (Refer to Figure 4.28 for Axes).

POINT OF APPLICATION	Self - Weight (kN)		Live Loads (kN)		Equipment Loads (kN)	
	Axis 5	Axis 10	Axis 5	Axis 10	Axis 5	Axis 10
4.0 m	33	33	115	115	-	-
6.2 m	33	33	115	115	-	-
8.6 m	33	33	115	115	-	-
10.10 m	16	-	-	-	50	-
12.85 m	16	-	-	-	50	-

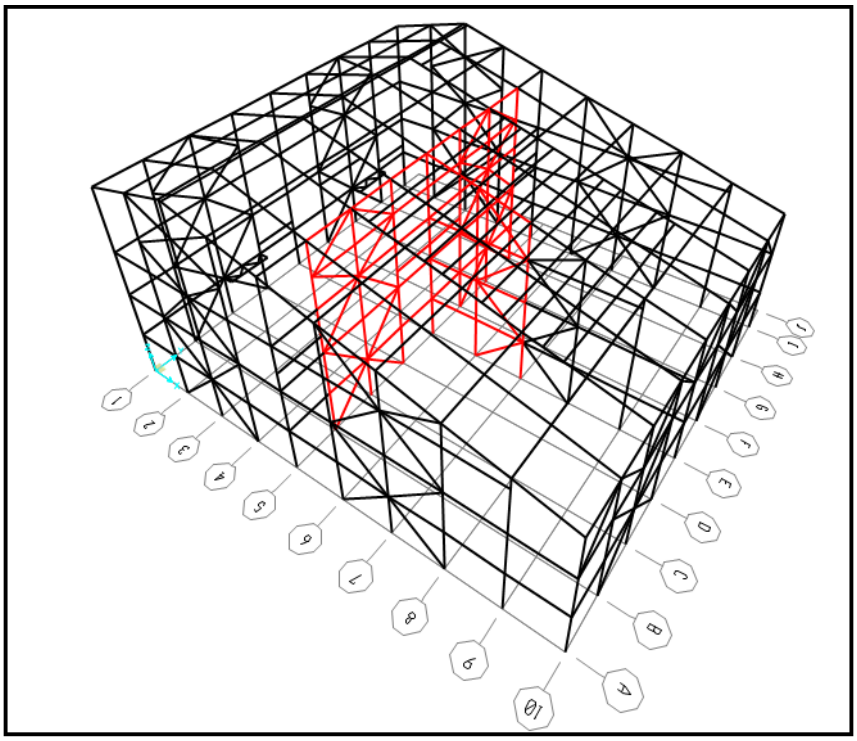

Figure 4.39. Structurally Critical Region.

Table 4.12. Type and Amount of the Combustible Materials that exist in Building - 3.

Lubricants	6383 Liter
Diesel	10 m^3
Estimated Fire Load Density for the Building : 210 MJ/m^2	
Yellow Book (ASFP, 2004) Suggested Fire Load Density for the Building : 246 MJ/m^2	

The characteristic value of the total fire load density is estimated as 210 MJ/m^2 for the floor surface of the building according to the calorific values of the combustible materials listed in the Table 4.12. But, Structural Fire Protection Yellow Handbook (ASFP, 2014) suggests 246 MJ/m^2 (mean) fire load for industrial buildings that are used as production facilities. Therefore, 246 MJ/m^2 is taken as the characteristic fire load density for the building. Design value of the fire load density is given in Appendix - A.

4.4.2. Fire Simulation and Heat Transfer Analysis

The preliminary parameters to simulate the design fire for the building according to the methodologies explained in Section 3.5 are given in Appendix-A. The hot (gas/smoke) and cold zone temperatures, the heat release rate, the smoke elevation level and the fire area for the entire duration of the fire are shown in Figure 4.40a, Figure 4.40b, Figure 4.40c and Figure 4.40d, respectively.

According to results of the fire simulation of the building, the two-zone fire model switches to the one-zone fire model at the 32^{nd} minute of the fire because the upper layer (hot-zone) reaches $< 20.0\%$ of the compartment and maximum fire area reaches to 25% of the total floor area (3146.00 m^2). The fire has flashover (fully engulfed) at the 53^{rd} minute of the fire because the hot-zone (gas/smoke) temperatures reach above 500.0 ^{o}C. Occurrence of the flashover is obvious from the sudden jump in the fire area at the 53^{rd} minute of the fire. At the analysis time that corresponds to the flashover the heat release rate becomes 0 and remains in this state until the 62^{nd} minutes of the fire, this is due to lack of oxygen mass in the building volume.

Pre-flashover localized fire is simulated with the methodologies explained in Section 3.5.2. The local fire does not impact the ceiling (19 m) and height of the flames reaches up to 9 m above the floor surface. The maximum local fire area is 899 m^2, which is larger than the area of the structurally critical region, but effecting the local fire simultaneously to 899 m^2 floor area is very conservative approach that's why local fire is only affected to the structurally critical region (546 m^2). According to the alignment

of the tie-beams and maximum flame height three different local fire time-temperature histories are used for the heat transfer analyses of the structural members that are located in the structurally critical region. Figure 4.41 shows the hot-zone (gas/smoke) time-temperature history, time-temperature histories of the varying flame heights and ISO834 standard fire curve (ISO, 1999).

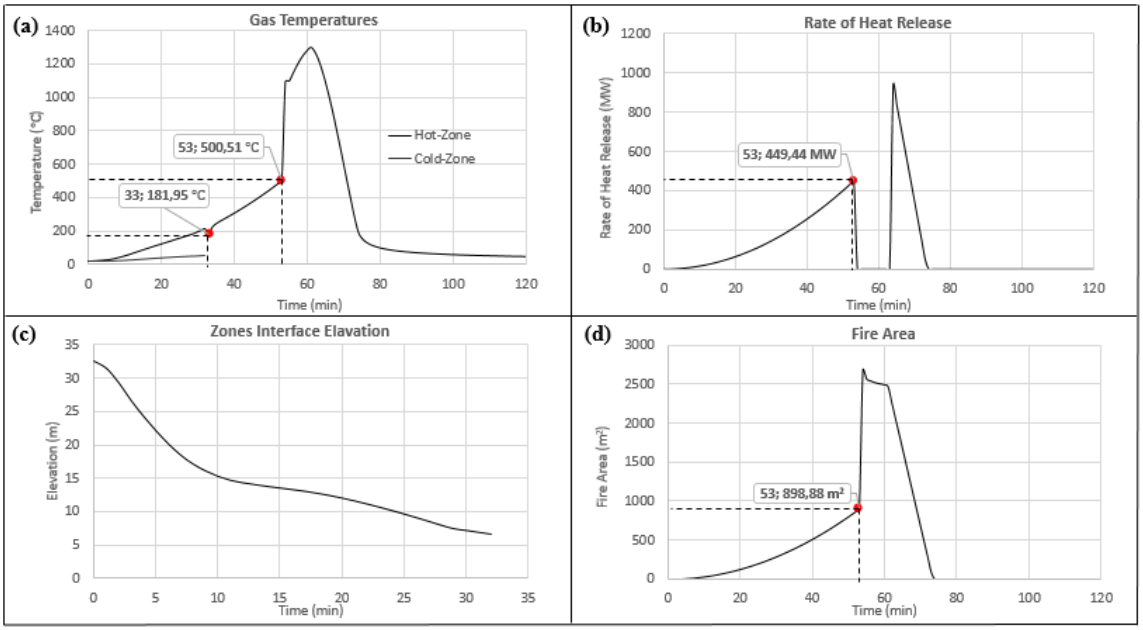

Figure 4.40. (a) Hot and Cold Zone Temperatures (Peak: 1300 °C at: 61 min) (b) RHR Computed (Peak: 935 MW at: 65 min), (c) Zones Interface Elevation (h = 6.71 m at: 32 min), (d) Fire Area (2678.12 m^2 at 54 min).

To conduct heat transfer analyses, until the flashover, the 0-6 m and 6.6 - 9 m heights of the columns and diagonals that align in the structurally critical region are exposed to the 3.3 m and 7.8 m flame temperatures, respectively and the tie-beams that are located at 6.6 m height of the structurally critical region are exposed to the 6.6 m flame temperatures as explained in Section 3.6. After the flashover, due to respectively high hot-zone (gas/smoke) temperatures, these parts of the columns and diagonals, and the tie beams are exposed to the hot-zone (gas/smoke) temperatures as explained in Section 3.6. Moreover, for the entire duration of the fire, structural members that are located in the structurally non-critical regions of the building and that align above the 9 m height in the structurally critical region are simultaneously

exposed to the hot-zone (gas/smoke) temperatures for heat transfer analyses. The fire curves used for the heating of the structural members of Building - 3 are summarized in Table 4.13.

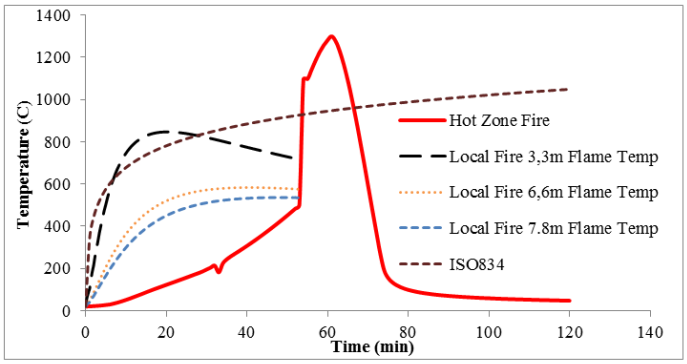

Figure 4.41. Hot-zone Gas Temperatures, Local Fire Flame Temperatures and ISO 834 Standard Fire Temperatures for 120 minutes.

Table 4.13. The Fire Curves Used for the Heating of the Structural Members of Building - 3.

CRITICAL REGION - (Refer to Figures 4.26 and 4.39)			
Columns			
Axis Coordinate	B5, C5, D5, E5, E6, E7, F5, G5, H5		
Vertical Alignment	0 - 6.6 m	6.6 m - 9 m	9 m - Ceiling
Pre-flashover	3.3 m L.F.T.	7.8 m L.F.T.	H.Z.T
Post-flashover	H.Z.T	H.Z.T	H.Z.T
Tie-Beams & Crane Beams			
Axis Coordinate	B5 - C5, C5 - D5, D5 - E5, E5 - E6, E6 - E7, F5 - G5, G5- H5		
Vertical Alignment	6.6 m	13.25 m, 15.9 m,19.9 m, 24.29 m, 29 m	
Pre-flashover	6.6 m L.F.T.	H.Z.T	
Post-flashover	H.Z.T	H.Z.T	
Cross Diagonals			
Axis Coordinate	B5 - C5, C5 - D5, E6 - E7, F5 - G5, G5 - H7		
Vertical Alignment	0 - 6.6 m	6.6 m - 9 m	9 m - Ceiling
Pre-flashover	3.3 m F.T.	7.8 m	H.Z.T
Post-flashover	H.Z.T	H.Z.T	H.Z.T
NON-CRITICAL REGIONS - (Refer to Figure 4.39)			
Pre-flashover	H.Z.T		
Post-flashover	H.Z.T		
L.F.T. = Local Fire Flame Temperatures, H.Z.T = Hot-zone Temperatures			

4.4.3. Structural Analysis

Implicit dynamic analysis method is utilized in the finite element model of the building with the predefined steel temperatures to determine fire induced structural performance of the building. Fire induced behaviors of two columns and two rafters that

align in the structurally critical region, and one rafter that align in the structurally non-critical regions of the building are investigated to determine the state of the building under fire. Moreover, total kinetic energy of the entire structure is investigated to understand and verify estimated collapse mechanism of the building due to termination of the structural analysis at the 69.5^{th} minute of the fire.

The columns that are located at D - 5 and E - 7 axis coordinates (Figure 4.26) are the structural members in which the yielding and structural instabilities firstly occur. These columns align in the structurally critical region of the building, and located at the region where the excessive crane self-weights are applied (Figure 4.36). Moreover, the other columns that are located in the structural critical region of the building show similar fire induced behavior with these columns with short time difference. Therefore, fire induced behavior of these columns are investigated in details. However, due to post-buckling column strength and load re-distribution phenomenon, fire induced behavior of the rafters that align between A - 7 and E - 7, and E - 1 and E - 5 axis coordinates determine state of the structurally critical region.

The rafter that align between B - 1 and B - 5 axis coordinates (Figure 4.26) is the structural member in which the structural instabilities and yielding occur firstly in the structurally non-critical regions of the building. Therefore, state of the structurally non-critical regions of the building is determined with the detailed fire induced behavior investigation of this rafter.

Assessment of the investigated structural members are conducted with the allowable limits that are presented and formulated in Figure 2.4 50 mm/min mid-height vertical displacement rate (Gernay *et al.*, 2016) and the development of 15% equivalent plastic strains (CEN, 2005) along the height of the columns are used as the maximum allowable limits for the assessment of the columns. For the rafters that align between axes 1 and 5 the maximum allowable mid-length vertical displacement and rate of the vertical displacement are 1332 mm (BS-476, 1976) and 50 mm/min (Gernay et al., 2016), respectively. For the rafters that align between axes A and E, and E and I the maximum allowable mid-length vertical displacement and rate of the vertical displace-

ment are 1330 mm (BS-476, 1976) and 50 mm/min (Gernay *et al.*, 2016), respectively. Moreover, the development of 15% equivalent plastic strains (CEN, 2005) along the rafters is also used for the assessment of the rafters.

The first 6.6 m of the column that is located at D - 5 axis coordinate is exposed to the 3.3 m flame temperatures until the flashover as explained in Section 4.4.2. Therefore, first 6.6 m of the column is critical and yielding occurs along this length of the column at the 15.4^{th} minute of the fire. Figure 4.42b shows the maximum equivalent plastic strains that develop along the critical length of the column for the entire duration of the fire. The analysis time that corresponds to the yielding of the columns is visualized in Figure 4.42d (I). Due to yielding of the column and steel stiffness decrease at elevated temperatures, out-of-plane displacements along the critical column length increase immediately and at the 54.9^{th} minute of the fire, the rate of out-of-plane displacements reaches to 49.98 mm/min and the column buckles. Moreover, almost in the same analysis time (54.7^{th} minute of the fire) maximum equivalent plastic strains along the critical column length reach to 15% and column fails due to initiation of the load carrying capacity loss. Figure 4.42a shows the maximum out-of-plane displacement along the critical column length for the entire duration of the fire with the buckling time. Figure 4.42d (II) and (III) visualize the analysis time that correspond to the 15% equivalent plastic strain along the critical column length and the buckling of the column, respectively. Figure 4.42c shows the mid-height vertical displacements of the column during the fire, according to the figure by the buckling of the column the mid-height vertical displacements increase immediately and vertical displacement rate reaches to 50 mm/min rate at the 69.5th minute of the fire. The analysis time that corresponds to occurrence of the maximum allowed mid-height vertical displacement rate is visualized in Figure 4.42d (IV).

As a summary, the column yields at the 15.4^{th} minute of the fire and fails at the 54.7^{th} minute of the fire due to initiation of the load carrying capacity loss, and it buckles at the 54.9^{th} minute of the fire. The first 6.6 m of the column that is located at the E - 5 axis coordinate is exposed to the 3.3 m flame temperatures until the flashover as explained in Section 4.4.2. Therefore, first 6.6 m of the column is critical

and yielding occurs along this part of the column at the 16.9^{th} minute of the fire. Figure 4.43b shows the maximum equivalent plastic strains along the critical length of the column for the entire duration of the fire. The analysis time that corresponds to the yielding of the column is visualized in Figure 4.43d (I).

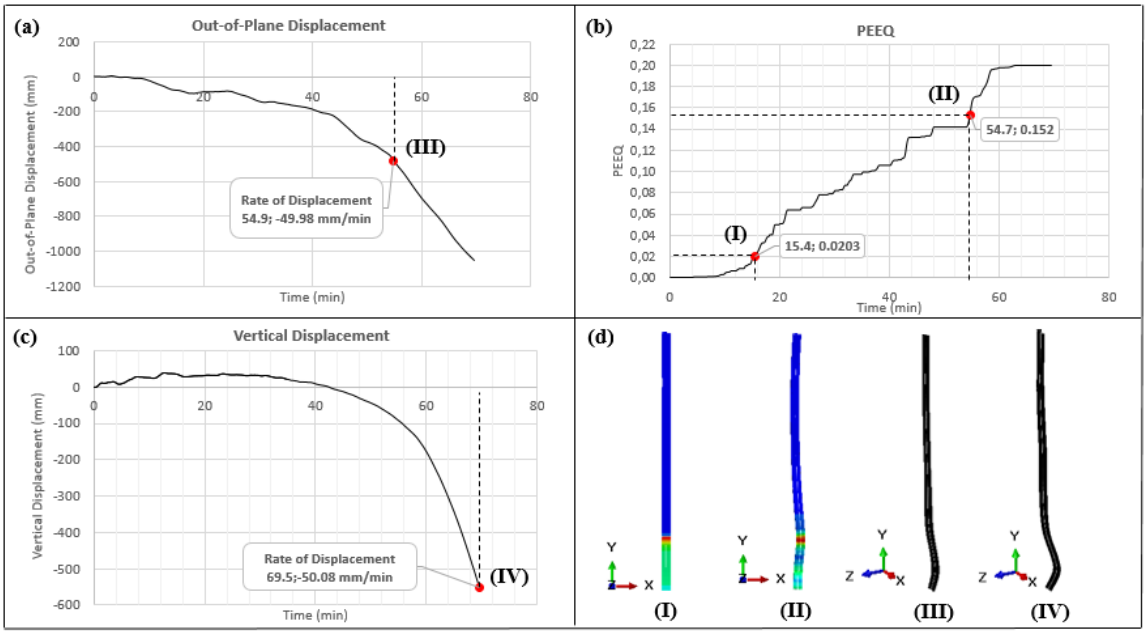

Figure 4.42. Fire Induced Behavior of the Column that is Located at D - 5 Axis Coordinate, (a) Maximum Out-of-Plane Displacements, (b) Maximum PEEQ, (c) Mid-height Vertical Displacements, (d) Analysis Times - (I) Yielding - (II) Strength Loss Initiation - (III) Buckling - (IV) Allowed Vertical Displacement Rate.

On the other hand, according to Figure 4.43a which shows the maximum out-of-plane displacements along the critical column length, 50 mm/min out-of-plane displacement rate which corresponds to the buckling of the column occurs at the 15.7^{th} minute of the fire. These results indicate the occurrence of the elastic column buckling. Figure 4.43d (II) visualize the analysis time that corresponds to the buckling of the column and it is clearly seen that there is not excessive deformation along the column at the buckling instant. Moreover, although the fire temperatures increase and steel stiffness decreases after the buckling time, out-of-plane displacements along the critical column length almost remain constant between the 19.2^{nd} and 46^{th} minutes of the fire. Figure 4.43c shows the mid-height vertical displacements of the column

during the fire, according to the figure the column does not vertically displace in the downward direction for the first 46 minutes of the fire. Moreover, mid-height vertical displacement rates do not reach to 50 mm/min during the fire. Figure 4.43d (III) visualize the analysis time that correspond to occurrence of the maximum mid-height vertical displacement rate. These results indicate that column hangs on its rafter after the buckling and the loads carried by the column are redistributed to the columns that are located in the structurally non-critical regions of the building.

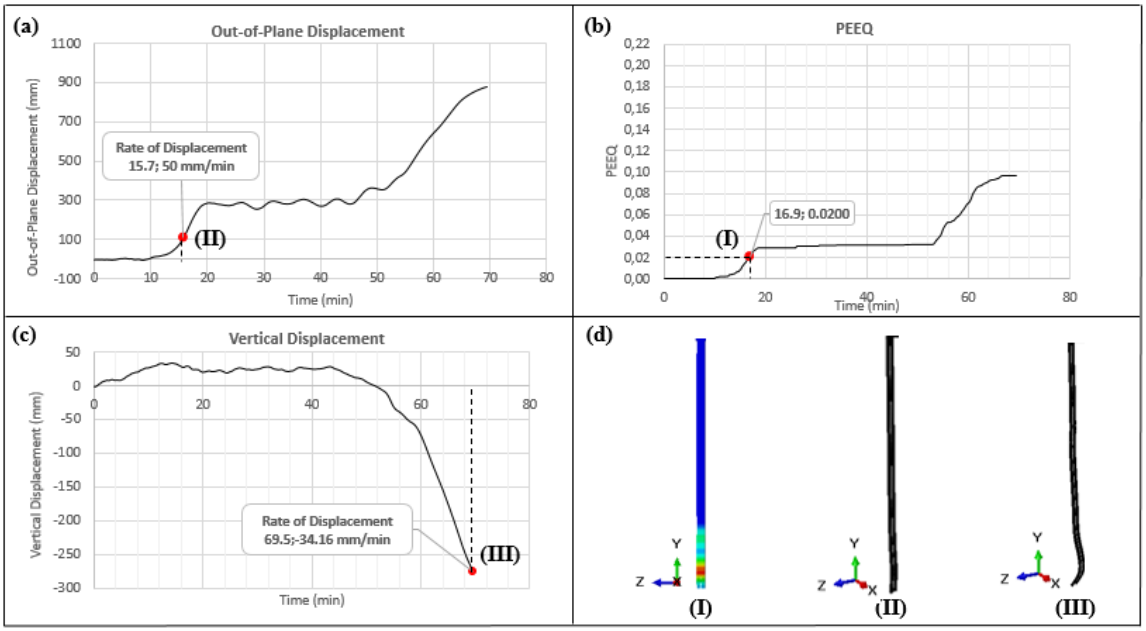

Figure 4.43. Fire Induced Behavior of the Column Located at E - 5 Axis Coordinate, (a) Maximum Out-of-Plane Displacements, (b) Maximum PEEQ (c) Mid-height Vertical Displacements, (d) Analysis Times - (I) Yielding - (II) Buckling - (III) Maximum Vertical Displacement Rate.

As a summary, the column buckles and yields at the 15.7^{th} and 16.9^{th} minutes of the fire, respectively. But it does not fail for the entire duration of the fire due to load re-distribution phenomenon and post-buckling strength.

The failure of the investigated columns does not indicate collapse of the structurally critical region of the building due to column post buckling strength and load re-distribution. Moreover, the column that is located at E-5 axis coordinate does not

fail during the fire. Therefore, fire induced performance of the structurally critical region of the building is determined with the detailed fire induced behavior investigations of the rafters that are located between A - 7 and E - 7, and E - 1 and E - 5 axis coordinates.

Maximum equivalent plastic strains along the rafter that is located between A - 7 and E - 7 axis coordinates are shown in Figure 4.44b during the fire. The critical part of the rafter yields at the 52.5^{th} minutes of the fire, and Figure 4.44d (I) visualize the analysis time that corresponds to the yielding of the critical rafter part. Figure 4.44a and Figure 4.44c show the mid-length vertical displacements and rate of the displacements during the fire. According to the figures, the mid-length vertical displacements increase immediately by the yielding of the rafter and at the 68.3^{rd} minute of the fire the mid-length vertical displacement rate reaches to 50.5 mm/min, thus the rafter fails due to the run-away vertical displacement initiation. Figure 4.44d (II) visualize the analysis time that corresponds to the initiation of the run-away vertical displacement at the mid-length. Moreover, maximum mid-length vertical displacements reach to 837 mm at the 69.5^{th} minutes of the fire and at this instant analysis terminates, the state of the rafter at the termination of the analysis is visualized in Figure 4.44d (III).

As a summary, the rafter yields at the 52.5^{th} minute of the fire and due to the yielding and stiffness decrease in the steel it fails at the 68.3^{rd} minute of the fire by the initiation of the run-away vertical displacements at the mid-length.

Maximum equivalent plastic strains at the critical part of the rafter that is located between E-1 and E-5 axis coordinates are shown in Figure 4.45b during the fire. According to the figure, the critical part of the rafter yields at the 56.3^{rd} minute of the fire. The analysis time that corresponds to the yielding of the critical rafter part is visualized in Figure 4.45d (I). Figure 4.45a shows the mid-length vertical displacements of the rafter for the entire duration of the fire. According to the figure by the yielding of the rafter the mid-length vertical displacements increase immediately. However, mid-length of the rafter displaces in the upward direction for 3.8 minutes after the yielding as a result of lateral torsional buckling with in the rafter.

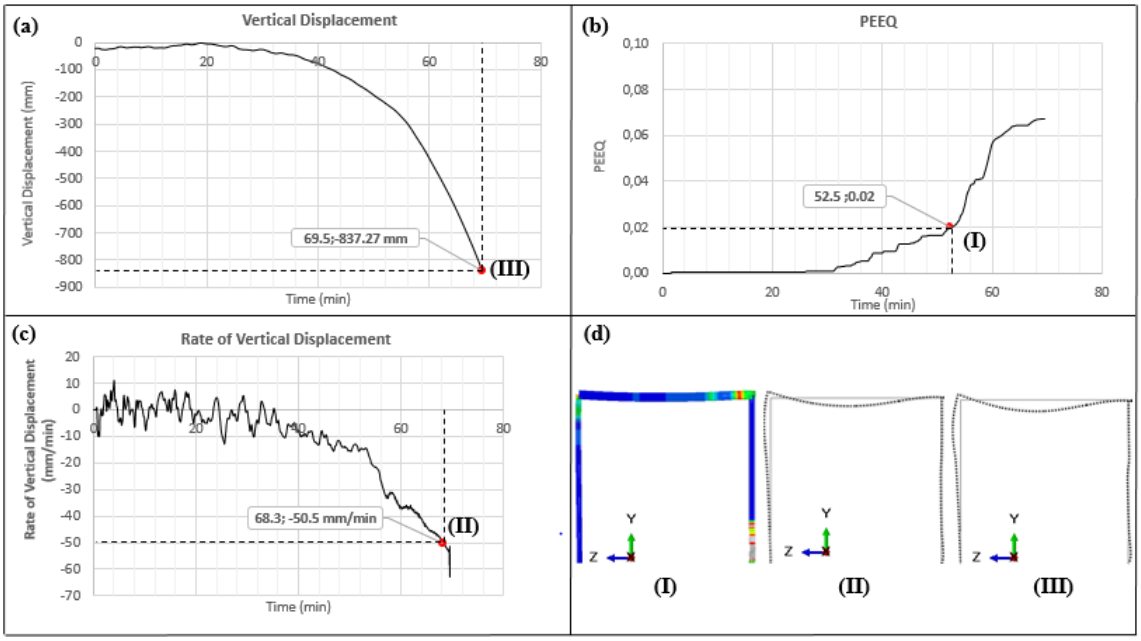

Figure 4.44. Fire Induced Behavior of the Rafter Located Between A - 7 and E - 7 Axis Coordinates, (a) Mid-length Vertical Displacements, (b) Maximum PEEQ, (c) Mid-length Vertical Displacement Rates, (d) Analysis Times - (I) Yielding - (II) Allowed Vertical Displacement Rate (x2) - (III) Allowed Vertical Displacement (x2).

After the lateral torsional buckling (56.7^{th} minute of the fire) due to the excessive torsional deformation along the rafter run-away vertical displacements in the downward direction take place at the 60.5^{th} minute of the fire and rafter fails at the 66.4^{th} minute of the fire by the occurrence of 50.75 mm/min mid-length vertical displacement rate in the downward direction. Figure 4.45c shows the mid-length vertical displacement rates during the fire and the analysis time that corresponds to the failure of the rafter due to the initiation of the run-away mid-length vertical displacement in the downward direction is visualized in Figure 4.45d (II). In addition, Figure 4.45d (III) visualizes the analysis time that corresponds to the maximum vertical displacement of the mid-length in the downward direction.

As a summary, the rafter yields at the 56.3^{rd} minute of the fire and it buckles due to the excessive torsional deformations. Due to the lateral torsional buckling and steel temperature increase after the buckling stiffness of the rafter decreases immediately

and it fails as a result of excessive displacements at the 66.4^{th} minute of the fire.

Structurally critical region of the building collapse at the 66.4^{th} minute of the fire due to the failure of the rafter that is located between E-1 and E-5 axis coordinates.

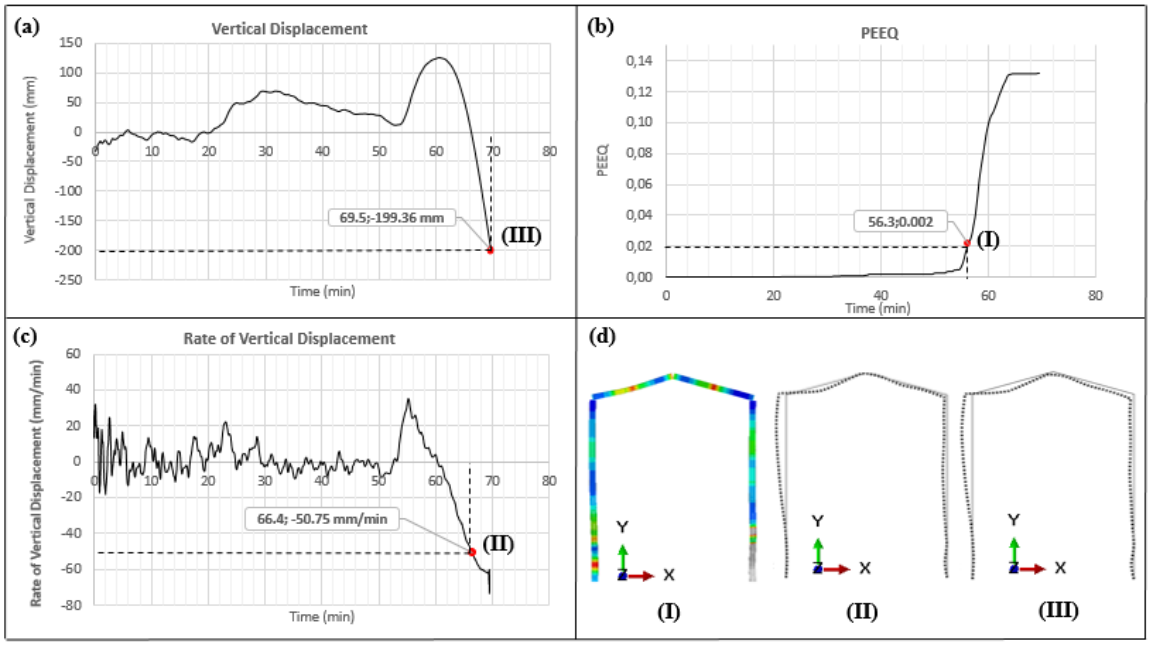

Figure 4.45. Fire Induced Behavior of the Rafter Located Between E-1 and E-5 Axis Coordinates, (a) Mid-length Vertical Displacements, (b) Maximum PEEQ, (c) Mid-length Vertical Displacement Rates, (d) Analysis Times - (I) Yielding - (II) Allowed Vertical Displacement Rate (x2) - (III) Maximum Vertical Displacement (x2).

Fire induced performance of the structurally non-critical regions of the building is determined with the detailed fire induced behavior investigation of the rafter that is located between B - 1 and B - 5 axis coordinates.

Maximum equivalent plastic strains at the critical part of the rafter that is located between B - 1 and B - 5 axis coordinates are shown in Figure 4.46b during the fire. The critical part of the rafter yields at the 55.6^{th} minute of the fire and initiate to loss its load carrying capacity at the 61.8^{th} minute of the fire due to 15% equivalent plastic strains. Therefore, the rafter fails at the 61.8^{th} minute of the fire. Figure 4.46d (I) and Figure 4.46d (II) visualize the analysis times that correspond to the yielding and the failure

of the rafter. Figure 4.46a shows the mid-length vertical displacements for the entire duration of the fire. According to the figure, by the yielding of the rafter, mid-length vertical displacements increase immediately. But, mid-length of the rafter displaces in the upward direction for 7.8 minutes after the yielding. This is due to the occurrence of the lateral torsional buckling with in the rafter at the 56.2^{th} minute of the fire. As a result of the lateral torsional buckling excessive torsional deformations develops along the rafter and run-away vertical displacements in the downward direction initiate at the 64^{th} minute of the fire. Figure 4.46c shows the mid-length vertical displacement rates for the entire duration of the analysis and the rate of vertical displacements reach to 50.65 mm/min in the downward direction at the 67.3^{rd} minute of the fire. The analysis time that corresponds to the occurrence of the maximum allowable mid-length displacement rate in the downward direction is visualized in Figure 4.46d (III).

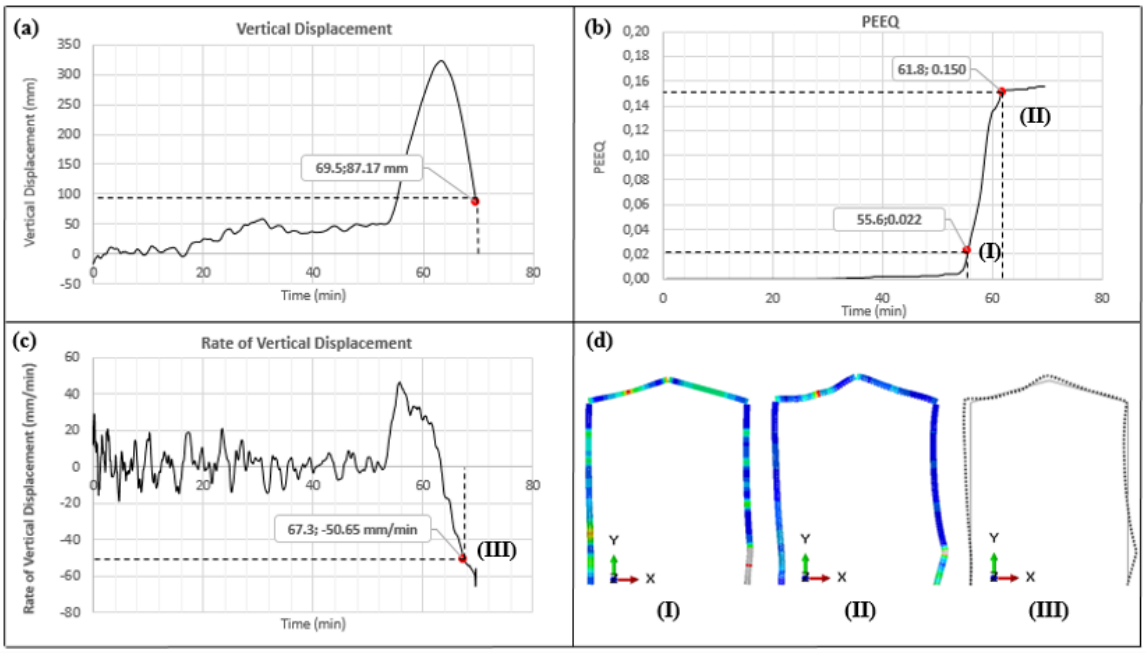

Figure 4.46. Fire Induced Behavior of the Rafter Located Between B - 1 and B - 5 Axis Coordinates, (a) Mid-length Vertical Displacements, (b) Maximum PEEQ (c) Mid-length Vertical Displacement Rates, (d) Analysis Times - (I) Yielding - (II) Strength Loss Initiation- (III) Allowed Vertical Displacement Rate (x2).

As a summary, the rafter yields at the 55.6^{th} minute of the fire and initiate to lose its load carrying capacity at the 61.8^{th} minute of the fire due to the development of 15%

equivalent plastic strains at the critical rafter part. The development of 15% equivalent plastic strains along the rafter cause the rafter to fail and to laterally buckle. After the buckling, rafter initiate to displace in the downward direction and at the 67.3^{rd} minute of the fire the mid-length vertical displacement rate of the rafter reaches to maximum allowable limit (50 mm/min). Therefore, structurally non-critical regions of the building collapse at this time.

To conclude, the columns that align along D axis in the structurally critical region of the building fail between the 50^{th} and 60^{th} minutes of the fire and this propagate the failure of all the rafters between the 60^{th} and 69.5^{th} minutes of the fire. Therefore, the building collapses and the analysis terminates at the 69.5^{th} minutes of the fire due to development of the excessive displacements along the structural members. Figure 4.47 shows the total kinetic energy of the entire model during the analysis and according to the figure at the 69.5^{th} minute of the fire there is a sudden increase in the kinetic energy. This result verify the collapse time of the building estimated with investigation of the structural members.

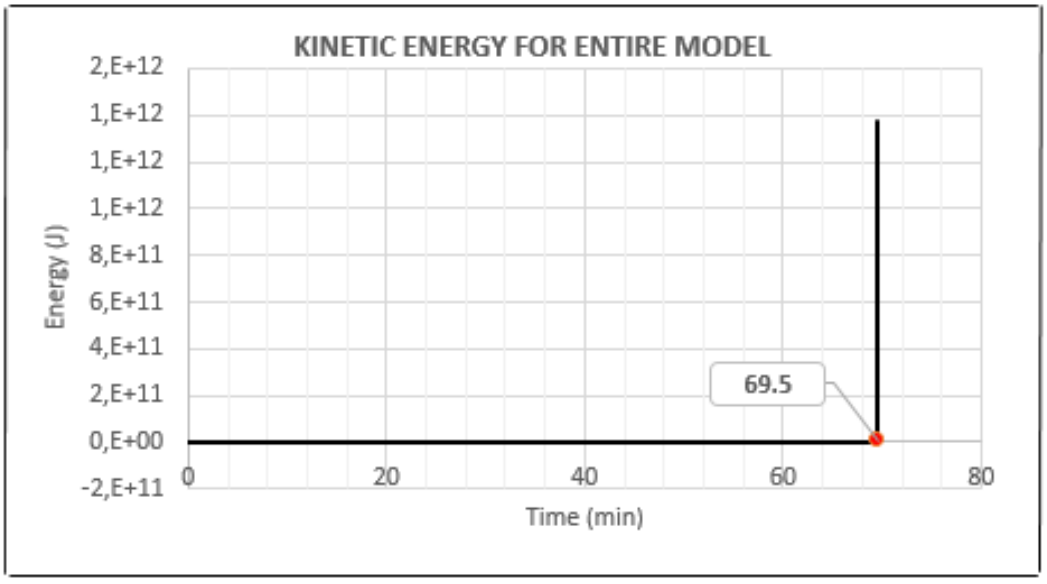

Figure 4.47. Entire Model Kinetic Energy.

Fire induced performances of the investigated structural members of Building - 3 are summarized in Table 4.14.

Table 4.14. Fire Induced Performances of the Investigated Structural Members of Building - 3.

CRITICAL REGION (Refer to Figure 4.39)				
Refer to Figures 4.42, 4.43, 4.44, 4.45	Columns		Rafters	
Location	D5 Axis Coordinate	E5 Axis Coordinate	A7 - E7 Axis Coordinate	E1 - E5 Axis Coordinate
Yielding Time (min)	15.4	16.9	52.5	56.3
Buckling Time (min)	54.9	15.7	N/A	56.7 (LTB*)
Failure Time (min)	54.7	N/A	63.3	66.4
Failure Criteria	15% PEEQ	N/A	Mid-length Vertical Displacement Rate (50mm/min)	Mid-length Vertical Displacement Rate (50mm/min)
NON-CRITICAL REGIONS (Refer to Figure 4.39)				
Refer to Figure 4.46	Columns		Rafters	
Location	-		B1 - B5 Axis Coordinate	
Yielding Time (min)	-		55.6	
Buckling Time (min)	-		56.2 (LTB*)	
Failure Time (min)	-		61.8	
Failure Criteria	-		15% PEEQ	
LTB = Lateral Torsional Buckling, PEEQ = Plastic Equivalent Strain				

4.5. Building - 4

4.5.1. Building Description

The building is 30 m in length, 7 m in width and 11.75 m to 12.65 m in height. Figure 4.48 shows general layout of the building with distances between the portal frames, floors and the roof, purlins, and the roof inclination angle. Single pitch steel portal frames with composite floor systems are utilized as the main load carrying mechanism for the building.

The building consist of a steel-framed reinforced-concrete-slab composite floors between each story. The perimeter and the secondary beams of the composite floors are included in the finite element model of the building, but the reinforced-concrete-slab of the composite floors are not included in the finite element model of the building as explained in Section 3.4. Thermo mechanical analysis of the composite floors of the fire compartment is conducted by simplified methodologies that are described in Chapter - 5.

Each of the portal frames are identical and the steel sections of the portal frames are shown in Figure 4.49a, and Figure 4.49b shows steel sections of the diagonals that are located along axes 1 and 2.

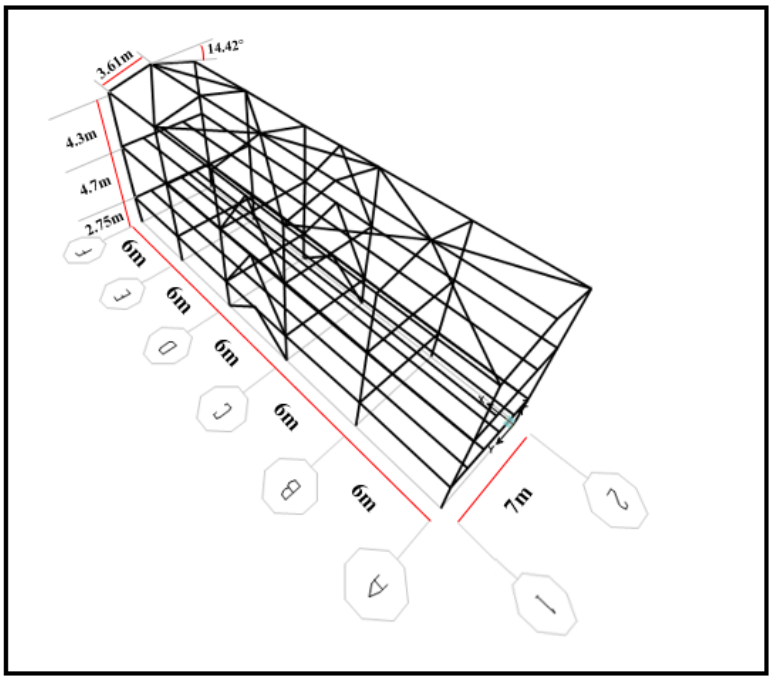

Figure 4.48. General Layout of Building - 4.

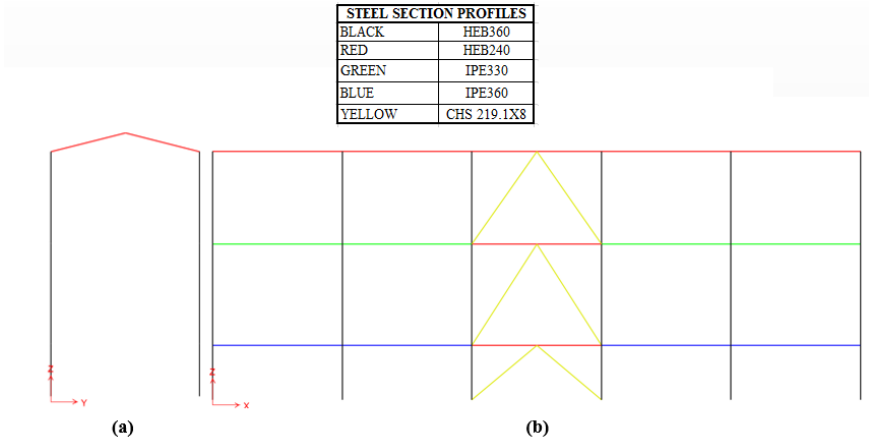

Figure 4.49. Steel Sections of the (a) Portal Frames (b) Cross Diagonals along Axes 1 and 2.

The Steel sections of the perimeter and secondary composite floor beams that are located at 2.75 m and 7.45 m heights of the building, and steel sections of the structural members at the roof level of the building are shown in Figure 4.50a, Figure

4.50b and Figure 4.50c, respectively.

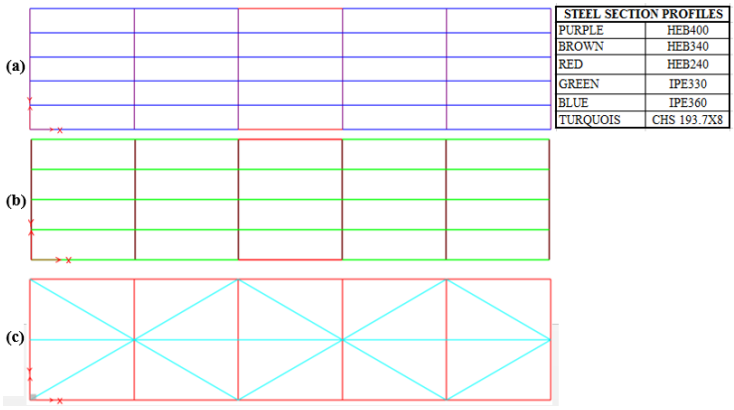

Figure 4.50. Steel Sections of the (a) Perimeter and Secondary Beams at 2.75 m Height (b) Perimeter and Secondary Beams at 7.45 m Height, (c) Structural Members at the Roof Level.

The building is compartmentalized in two regions (210 m^2 2^{nd} floor office area and 84 m^2 DCS room 1^{st} floor). However, structural fire performance analysis of the building is conducted for DCS room fire scenario only. Moreover, the other compartment volume of the first floor is separated from DCS room with non-combustible gas-concrete brick wall along D axis and does not contain any fire load. The building volume that correspond to the fire compartment of the first floor is shown in Figure 4.51. Some of the cross diagonals are not shown in Figure 4.51 for the clarity of the figure.

Three different ventilation openings exist on the perimeter walls of the building. Two of them open to the out of the building and one of them opens in to the building compartment that is located between D-1, A-1 and D-2, A-2 axis coordinates. The ventilation opening that connects two different compartments of the first story is included in the fire simulation of the building, due to the fact that there is an oxygen feed from the other compartment to the fire compartment via this opening in case of a fire. Figure 4.52 shows general layout, dimensions and vertical alignments of these openings. The plan view of the fire compartment is shown in Figure 4.52c to identify the location of the ventilation opening that opens to the other compartment of the first story. Moreover, the location of the openings that are highlighted in Figure 4.52a and Figure 4.52b are also shown in Figure 4.52c.

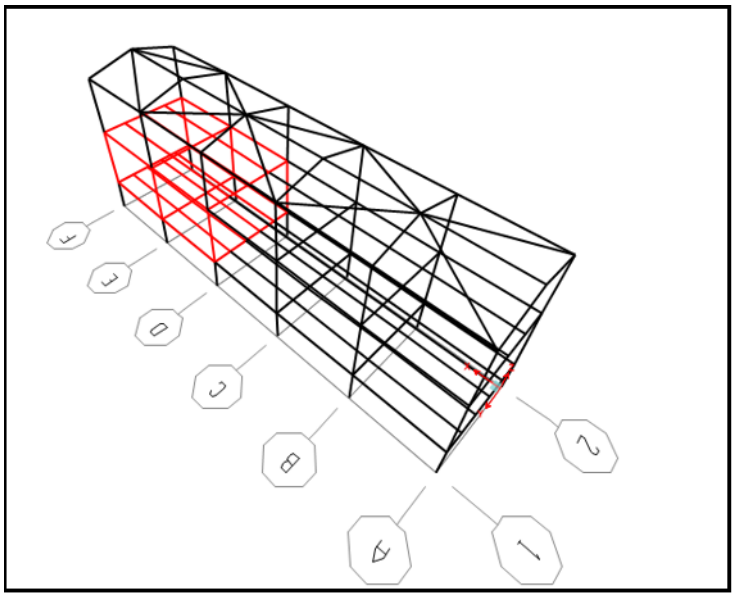

Figure 4.51. Fire Compartment of Building - 4.

VENTILATION OPENINGS			
Color	Height (m)	Width (m)	Vertical Alignment (m)
Blue	3	2.4	0 - 3
Red	2.1	1	0 - 2.1
Green	2.1	1	0 - 2.1

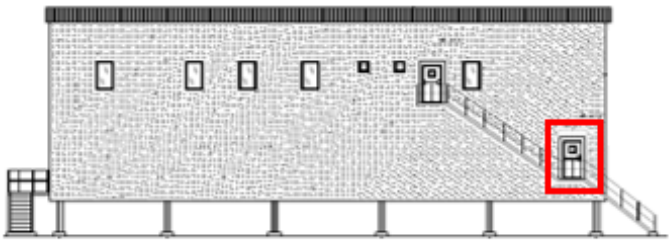

(a)

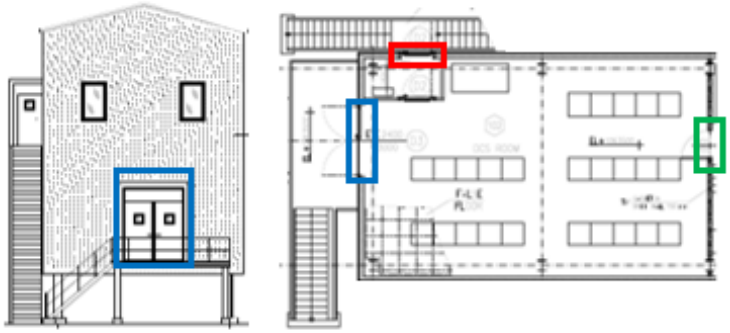

(b) (c)

Figure 4.52. Architectural Drawings of the Building with Highlighted Ventilation Openings (a) 1 Axis View (b) F Axis View (c) Fire Compartment Plan View.

The perimeter walls and ceiling of the building is covered with self-supporting metal panels according to the information collected by the building operator. 20 cm normal weight concrete slab covers the floor of the each story and the fire compartment of the building is separated from the other volumes of the first floor by the gas-concrete brick wall that is constructed along D axis. The thermal properties and unit weights of these materials are given in Table 4.5.

Characteristic value of the snow load applied to the roof of the building is given in the Table 4.2. Characteristic value of the live loads applied on the floor surface of the each story are calculated according to the Turkish Standard of Design Loads for Buildings - TS498 (Turkish Standard Institution, 1997) and equal to 10 kN/m^2.

Snow load and live loads are multiplied by the design load coefficients that are described in Section 3.2 and applied to the respective structural members according to tributary area method. The weight of the perimeter and inner walls, ceiling and floor slab are also applied to the respective structural members according to the tributary are method, but they are not multiplied by any design load coefficients, similar to the weight of the steel sections.

Fire load survey is carried out by the building operator and fire load in the DCS room is reported to have a total volume of 4.2 m^3 of wood due to wooden false floor. (1 m^2 false floor panel is taken as 33.5 kg and calorific value of the 1 kg wood is taken as 20 MJ conservatively). Characteristic value of the fire load density for the floor surface is given in Table 4.3. Design value of the fire load density for the floor surface of the building is given in Appendix-A.

4.5.2. Fire Simulation and Heat Transfer Analysis

The preliminary parameters to simulate the design fire for the building according to the methodologies explained in Section 3.5 are given in Appendix-A. The hot (gas/smoke) and cold temperatures, the heat release rate, the smoke elevation level and the fire area for the entire duration of the fire are shown in Figure 4.53a, Figure

4.53b, Figure 4.53c and Figure 4.53d, respectively.

According to results of the fire simulation of the building, the two-zone fire model switches to the one-zone fire model at the 10^{th} minute of the fire, because the upper layer (hot-zone) reaches to $< 20.0\%$ of the compartment and maximum fire area reaches to 25% of the total floor area (84.00 m^2). The fire has flashover (fully engulfed) at the 16^{th} minute of the fire because the hot-zone (gas/smoke) temperatures reach 500.0 ^oC. It is obvious from the sudden jump in the heat release rate and the fire area the flashover occurs at the 16^{th} minute of the fire.

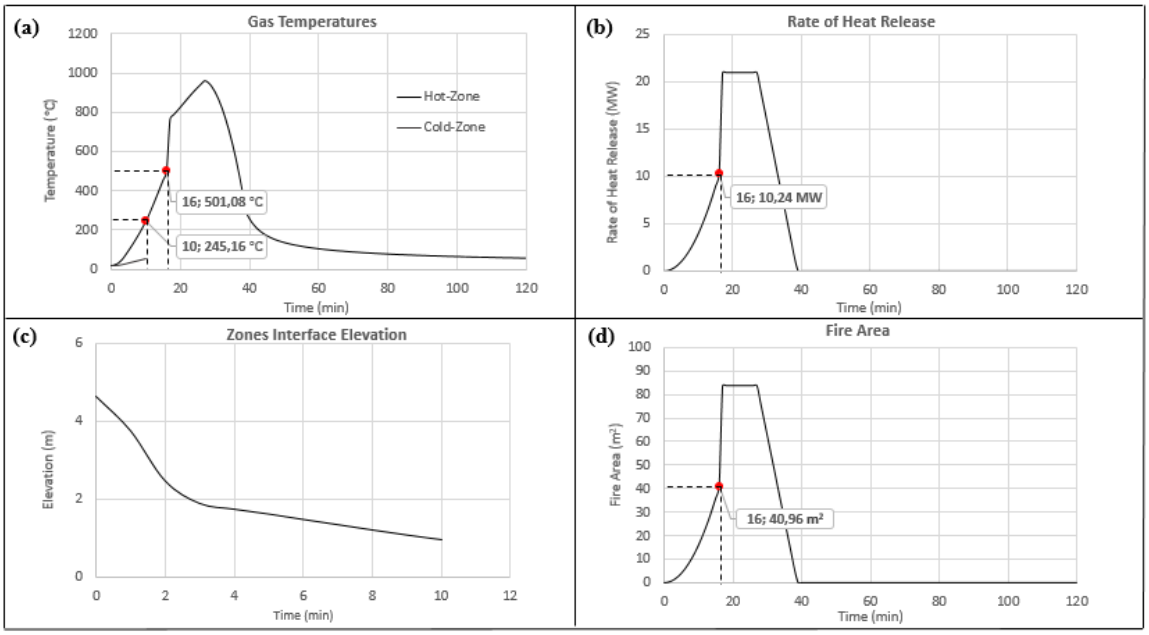

Figure 4.53. (a) Hot and Cold Zones Temperatures (Peak: 962 ^oC at: 27 min) (b) RHR Computed (Peak: 21 MW at: 17 min), (c) Zones Interface Elevation (h = 0.96 m at: 10.00 min), (d) Fire Area (84 m^2 at 17 min).

Due to the small floor area (84 m^2) and low height (4.3 m) of the fire compartment, the two-zone fire model of the building switches to the one-zone fire model in the relatively short duration (10^{th} minute of the fire). Moreover, the flashover also occurs in very short duration (16^{th} minute of the fire). Therefore, localized fire scenario is not considered for the fire simulation of the building and all of the structural members located in the fire compartment are simultaneously exposed to the hot-zone (gas-smokes) temperatures to conduct heat transfer analyses.

4.5.3. Structural Analysis

The entire structure is analyzed but fire is applied to 84 m^2 floor area of the DCS room only as explained in Section 4.5.1. The structural analysis is uncoupled from the thermal analysis and the temperature input for structural members is applied as a predefined field into the structural analysis program. An implicit dynamic analysis method is utilized in order to determine instabilities in the structure. Fire induced behaviors of the composite floor systems that are located at the 7.45 m height of the DCS room are analyzed with the developed simplified methodologies in Chapter - 5. But state of the building is determined with fire induced performances of one column, one composite floor perimeter beam and one composite floor secondary beam that are located in DCS room.

According to the tributary area concept maximum gravitational loads are applied to the perimeter beam that is located between E - 1 and E - 2 axis coordinates (Figure 4.51). Moreover, the secondary beams that are located between E and F axes (Figure 4.51) are critical structural members located in DCS room. Therefore, these beams and the column that is connected to the perimeter beam on E-1 axis coordinate are investigated in details to determine state of the building under fire.

Assessment of the investigated structural members are conducted with the allowable limits that are presented and formulated in Table 2.4. 50 mm/min mid-height vertical displacement rate (Gernay *et al.*, 2016) and the development of 15% equivalent plastic strains (CEN, 2005) along the height of the column are used as the maximum allowable limits for the assessment of the column. The maximum allowable mid-length vertical displacement and rate of vertical displacement for the perimeter beam are 350 mm (BS-476, 1976) and 16.01 mm/min (BS-476, 1976), respectively. The maximum allowable mid-length vertical displacement and rate of vertical displacement for the secondary beam are 300 mm (BS-476, 1976) and 12.12 mm/min (BS-476, 1976), respectively. Moreover, the development of 15% equivalent plastic strains (CEN, 2005) along the perimeter and the secondary beams are also used as assessment criteria for the beams.

Maximum equivalent plastic strains along the column that is located at E - 1 axis coordinate develop at the joint where the perimeter beam and the column connect each other. Figure 4.54b shows the equivalent plastic strains at this joint for entire duration of the fire. According to Figure 4.54b, this joint yields at the 39.5^{th} minute of the fire but does not lose its load carrying capacity during the fire. Figure 4.54d (I) visualize the analysis time that corresponds to the yielding of the connection joint. Moreover, the rate of in-plane and out-of-plane displacements along the column height do not reach to 50 mm/min for the entire duration of the fire. Therefore, the column does not buckle during the fire. Maximum in-plane displacements along the column are shown in Figure 4.54a for the entire duration of the fire with the highlighted maximum rate of the displacement. Figure 4.54d (II) visualize the analysis time that corresponds to the maximum in-plane displacement rate along the column height. Moreover, column mid-height vertical displacement rate also does not reach to 50 mm/min during the fire.Figure 4.54c shows mid-height vertical displacements of the column for the entire duration of the fire with the highlighted maximum vertical displacement rate. In addition, Figure 4.54d (III) visualize the analysis time that corresponds to the maximum mid-height vertical displacement rate. According to these results the column does not fail during the fire.

Although the column that is located at E - 1 axis coordinate does not fail, this does not indicate the non-failure of the composite floor systems that are located at the ceiling of the fire compartment, because fire induced behavior of composite floor systems are mainly depend on the fire induced performances of the perimeter beams and the secondary beams. Therefore, the perimeter beam that is located along E axis and one of the secondary beams that are located between E and F axes are investigated to determine state of the structure under the fire. The mid-length vertical displacement rate of the perimeter beam that is located along E axis reaches to 16.03 mm/min at the 28.3^{rd} minute of the fire, and the perimeter beam fails due to initiation of the run-away vertical displacements. Figure 4.55c shows the mid-length vertical displacement rates of the perimeter beam for the entire duration of the fire, with the highlighted failure time. This analysis time also visualized in Figure 4.55d (III). As a result of the run-away vertical displacement initiation at the mid-length, the joints where the

columns and the perimeter beam connect yield at the 31.3^{rd} minute of the fire and these joints lose their load carrying capacity due to the development of 15% equivalent plastic strains at the 34^{th} minute of the fire.

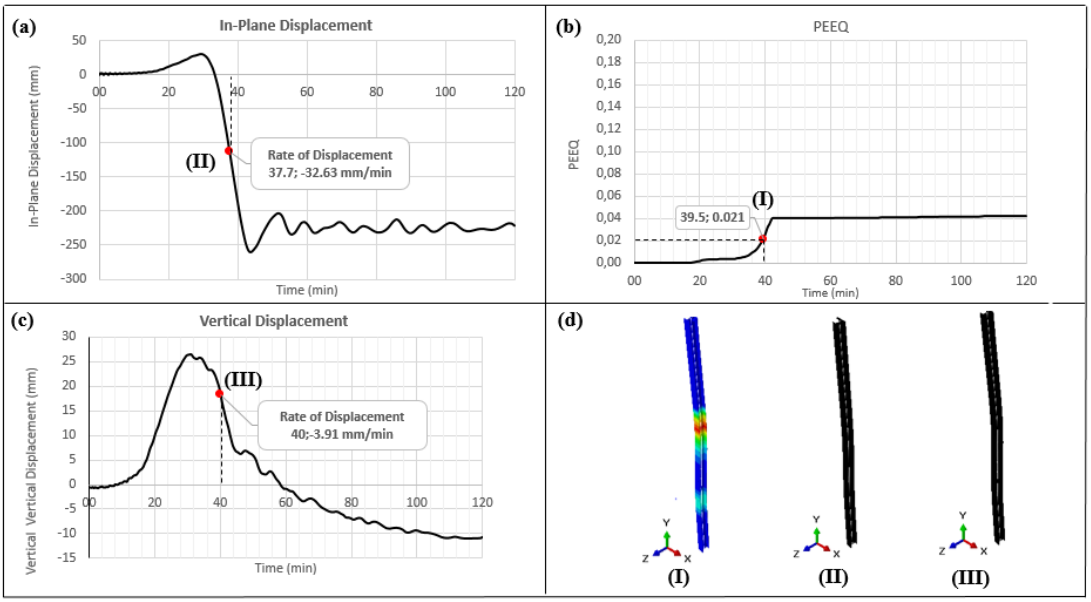

Figure 4.54. Fire Induced Behavior of the Column Located at E-1 Axis Coordinate (a) Maximum In-plane Displacements, (b) Maximum PEEQ, (c) Mid-height Vertical Displacements, (d) Analysis Times - (I) Yielding - (II) Maximum In-plane Displacement Rate - (III) Maximum Vertical Displacement Rate.

Figure 4.55b shows the equivalent plastic strains that develop at the one of these joints during the fire with the analysis times that correspond to the yielding and the strength loss initiation. Figure 4.55d (I) and (II) also visualize these analysis times. Moreover, according to Figure 4.55a which shows the mid-length vertical displacements during the fire, the allowable mid-length vertical displacement is exceed at the 34.2^{nd} minute of the fire.

As a summary the critical perimeter beam of the composite floor systems fails at the 28.3^{rd} minute of the fire due to initiation of the mid-length run-away vertical displacements. Moreover the fire induced structural behaviors of the joints where the columns and the perimeter beam connect each other also indicate similar duration for the failure time of the perimeter beam.

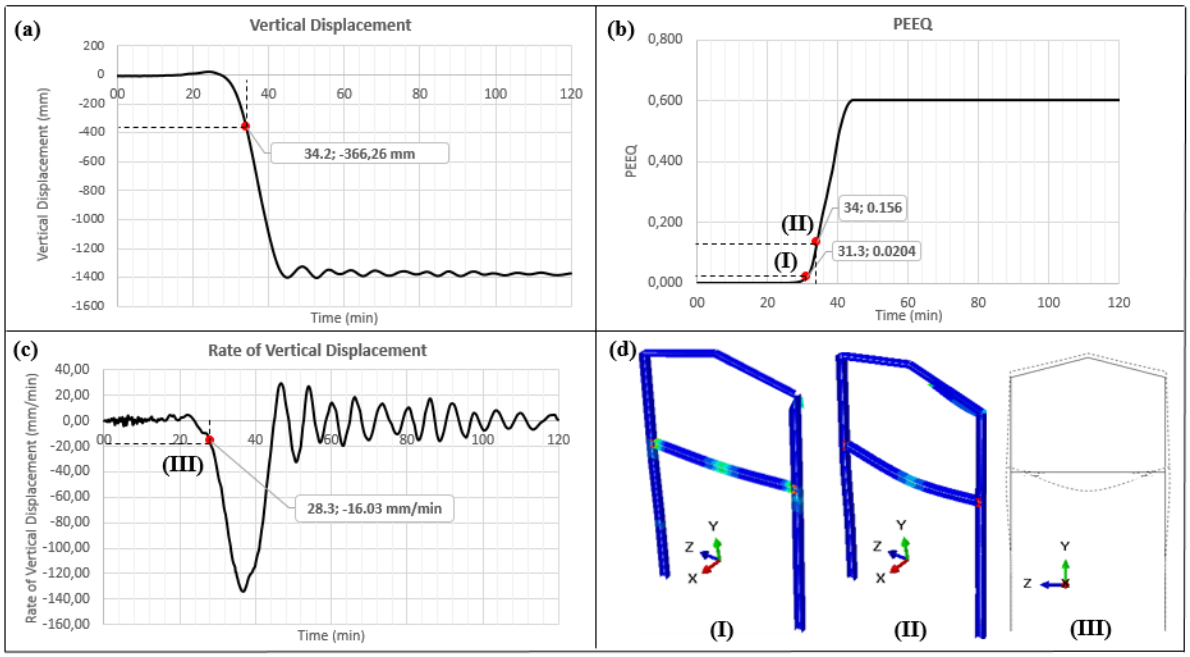

Figure 4.55. Fire Induced Behavior of the Perimeter Beam Located along E Axis, (a) Mid-length Vertical Displacements, (b) Maximum PEEQ (c) Mid-length Vertical Displacement Rates, (d) Analysis Times - (I) Yielding - (II) Strength Loss Initiation - (III) Allowed Vertical Displacement Rate (x5).

The secondary beams that align between E and F axes are identical with respect to the applied loading, the steel section and the heating. Therefore, only the secondary beam that is located at the middle of the floor area is investigated.

Figure 4.56c shows the mid-length vertical displacement rates of the secondary beam during the fire. According to the figure, the mid-length vertical displacement rate reaches to 12.87 mm/min at the 20.3^{rd} minute of the fire, and the beam fails due to initiation of the run-away vertical displacements. The analysis time that corresponds to the failure of the beam is visualized in Figure 4.56d (II). Figure 4.56a shows the mid-length vertical displacements for the entire duration of the fire, and according to the figure, 5.7 minutes after from the initiation of the run-away vertical displacements at beam mid-length, maximum allowable limit for the vertical displacement is exceeded. The maximum equivalent plastic strains along the beam also develop at the mid-length of the beam. Figure 4.56b shows the equivalent plastic strains at the mid-length of

the beam during the fire, and according to the figure the mid-length yields at the 28.3^{rd} minute of the fire due to excessive vertical displacements, but does not lose load carrying capacity during the fire. Figure 4.56d (I) visualizes the analysis time that correspond to the yielding at the beam mid-length.

As a summary, the secondary beam fails at the 20.3^{rd} minute of the fire due to initiation of the run-away vertical displacements at the mid-length. Moreover, the post-failure fire induced behavior of the secondary beam also supports the failure time of the beam.

To conclude, the columns of the fire compartment do not fail during the fire, but due to failure of the perimeter and the secondary beams of the composite floor systems that are located at the ceiling of the fire compartment, the building collapses at the 28.3^{rd} minute of the fire. Fire induced performances of the investigated structural members of Building - 4 are summarized in Table 4.15. According to the table, the building does not pass the 60 minutes fire resistance rate which is given in Table 4.3.

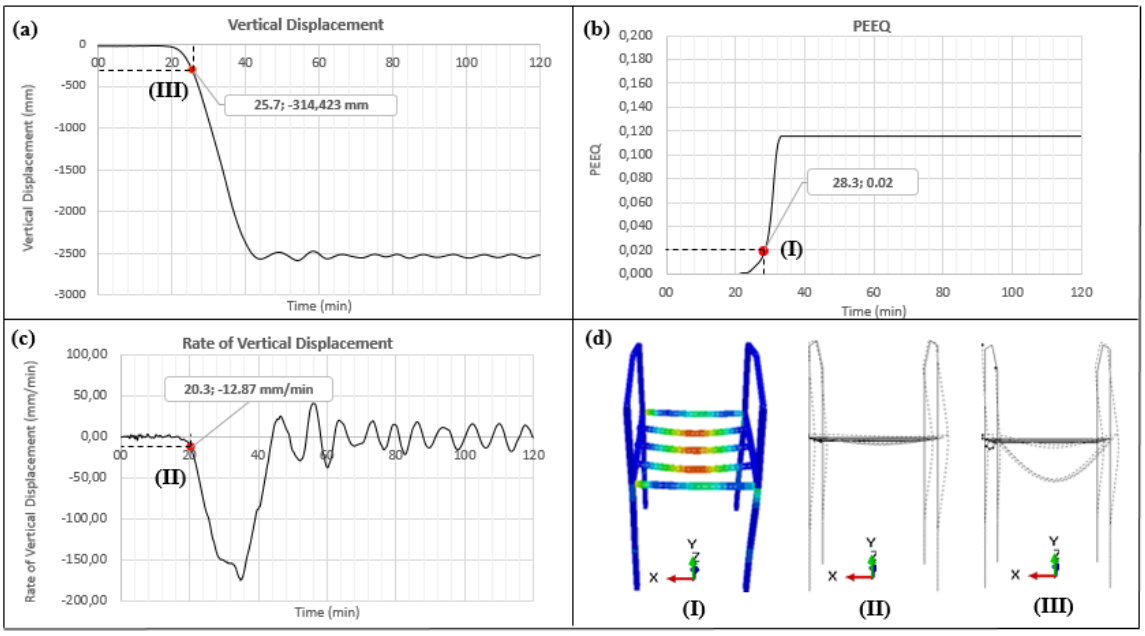

Figure 4.56. Fire Induced Behavior of the Secondary Beam Located between E and F Axes, (a) Mid-length Vertical Displacements, (b) Maximum PEEQ, (c) Mid-length Vertical Displacement Rates, (d) Analysis Times - (I) Yielding - (II) Allowed Vertical Displacement Rate (x5) - (III) Allowed Vertical Displacement (x5).

Table 4.15. Fire Induced Performances of the Investigated Structural Members of Building - 4.

FIRE COMPARTMENT (Figure 4.51)			
Refer to Figures 4.54, 4.55 and 4.56	Columns	Perimeter Beams	Secondary Beams
Location	E1 Axis Coordinate	E1 - E2 Axis Coordinate	E1 - E5 Axis Coordinate
Yielding Time (min)	N/A	31.3	28.3
Buckling Time (min)	N/A	N/A	N/A
Failure Time (min)	N/A	28.3	20.3
Failure Criteria	N/A	Mid-length Vertical Displacement Rate (16.03 mm/min)	Mid-length Vertical Displacement Rate (12.87 mm/min)

4.6. Building - 5

4.6.1. Building Description

The building is 18 m in length, 13 m in width and 11.7 m to 13.45 m in height. Figure 4.57 shows the general layout of the building with distances between the portal frames, the floors and the roof, the roof purlins, and the roof inclination angle. As the main load carrying mechanism of the building, double-bay single pitch steel portal frames are utilized.

The building consist of a steel-framed reinforced-concrete-slab composite floors between each story. The perimeter and the secondary beams of the composite floors are included in the finite element model of the building, but the reinforced-concrete-slabs of the composite floors are not included in the finite element model of the building as explained in the Section 3.4. Moreover, thermo mechanical behavior of these composite floor have not been analyzed, due to non-existence of the fire load in the first floor and the basement of the building.

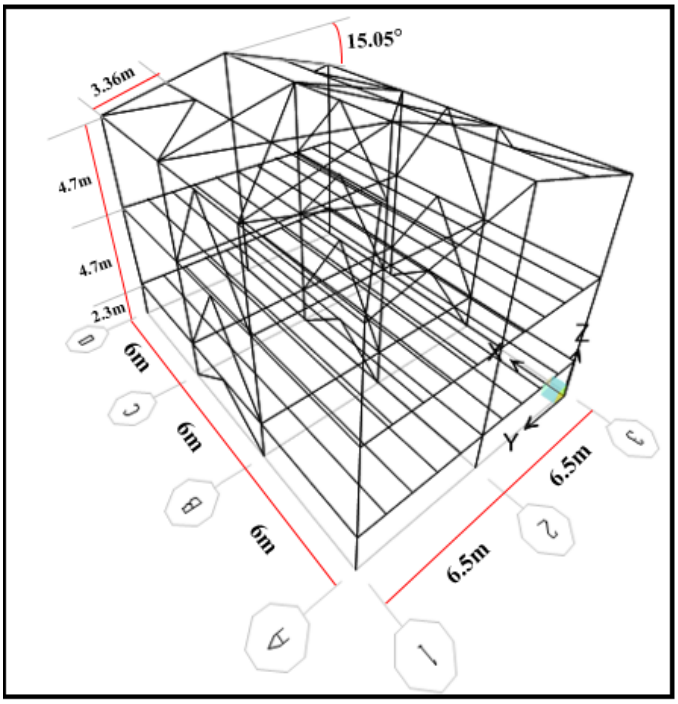

Figure 4.57. General Layout of Building - 5.

Each of the portal frames are identical and the steel sections of the portal frames are shown in Figure 4.58a, and Figure 4.58b shows steel sections of the diagonals that are located along axes 1, 2 and 3.

The Steel sections of the perimeter and the secondary composite floor beams that are located at 2.3 m and 7 m heights of the building are identical and shown in Figure 4.59a, and the steel sections of the structural members at the roof level of the building are shown in Figure 4.59b.

The building is compartmentalized in one region 117 m^2 (2^{nd} floor DCS room), and the other compartment volumes of the second floor is separated from the DCS room with non-combustible gas-concrete brick wall that is constructed along axis 2. Therefore, structural fire performance analysis of the building is conducted for DCS room fire scenario only. The building volume that corresponds to the fire compartment is shown in Figure 4.60. The cross-diagonals and the purlins are not shown in Figure 4.60 for the clarity of the figure.

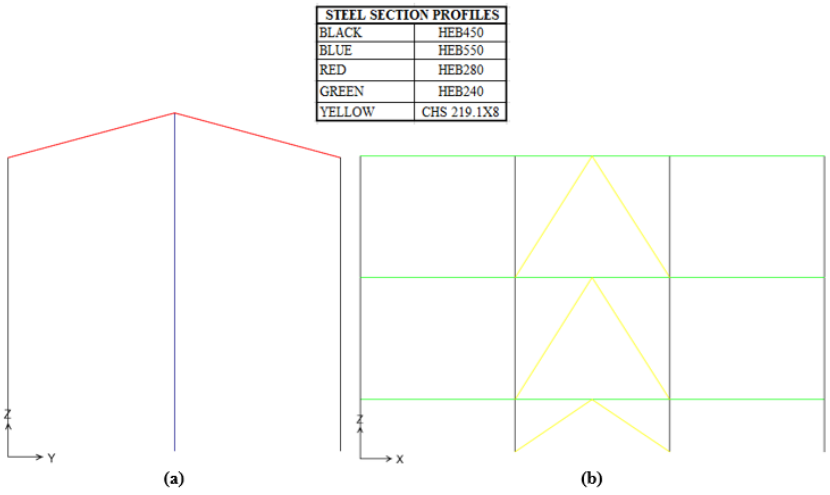

Figure 4.58. Steel Sections of the (a) Portal Frames, (b) Cross Diagonals along Axes 1, 2 and 3.

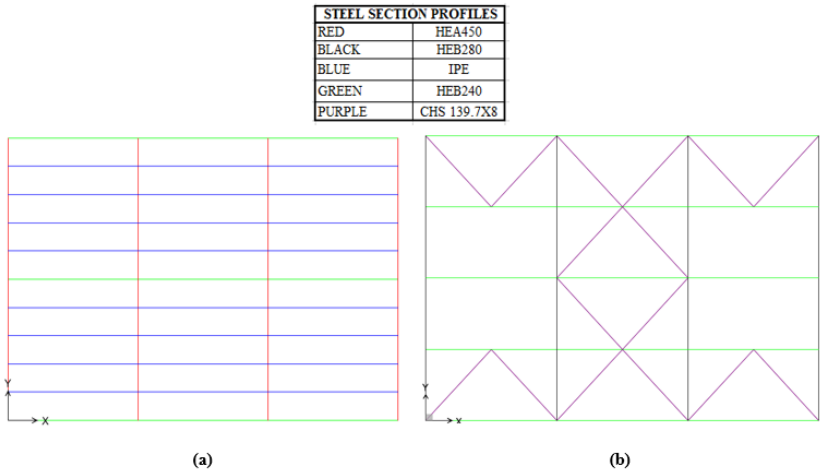

Figure 4.59. Steel Sections of the (a) Perimeter and Secondary Composite Floor Beams at 2.3 m and 7 m Heights, (b) Structural Members at the Roof Level.

Two different ventilation openings exist on the perimeter walls of the building. One of them opens to the out of the building and the other one opens to the building compartment that aligns between axes 1 and 2 . The ventilation opening that connect two different compartment of the second story is included in the fire simulation of the building, due to the fact that there is an oxygen feed from the other compartment to the fire compartment via this opening in case of a fire. Figure 4.61 shows the general layout, dimensions and the vertical alignments of these openings.

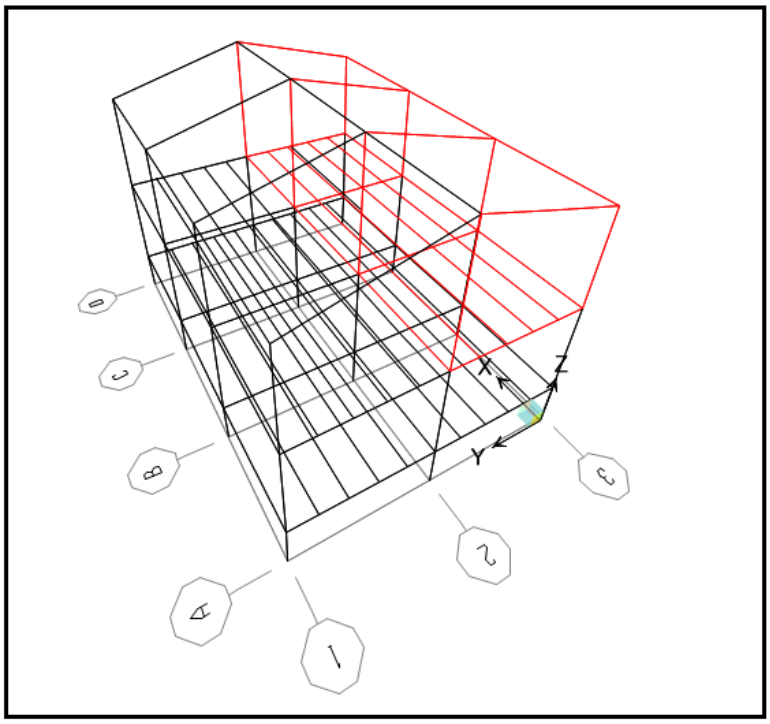

Figure 4.60. Fire Compartment of Building - 5.

The plan view of the fire compartment is shown in Figure 4.61a to identify the location of the ventilation opening that opens to the other compartment of the second story. Moreover, the location of the opening that is highlighted in Figure 4.61b is also shown in Figure 4.61a.

The perimeter walls and ceiling of the building is covered with self-supporting metal panels according to the information collected by the building operator. The 20 cm normal weight concrete slabs cover the floors of the each story and the fire compartment of the building is separated from the other volumes of the second floor with non-combustible gas-concrete brick wall that is constructed along 2 Axis. The thermal properties and unit weights of these materials are given in Table 4.5.

Characteristic value of the snow load applied to the roof of the building is given in Table 4.2. Characteristic value of the live loads applied on the floor of the each story are calculated according to the Turkish Standard of Design Loads for Buildings - TS498 (Turkish Standard Institution, 1997) and equal to 10 kN/m^2.

VENTILATION OPENINGS			
Color	Height (m)	Width (m)	Vertical Alignment (m)
Red	2.5	2.4	0 - 2.5
Green	2.1	1	0 - 2.1

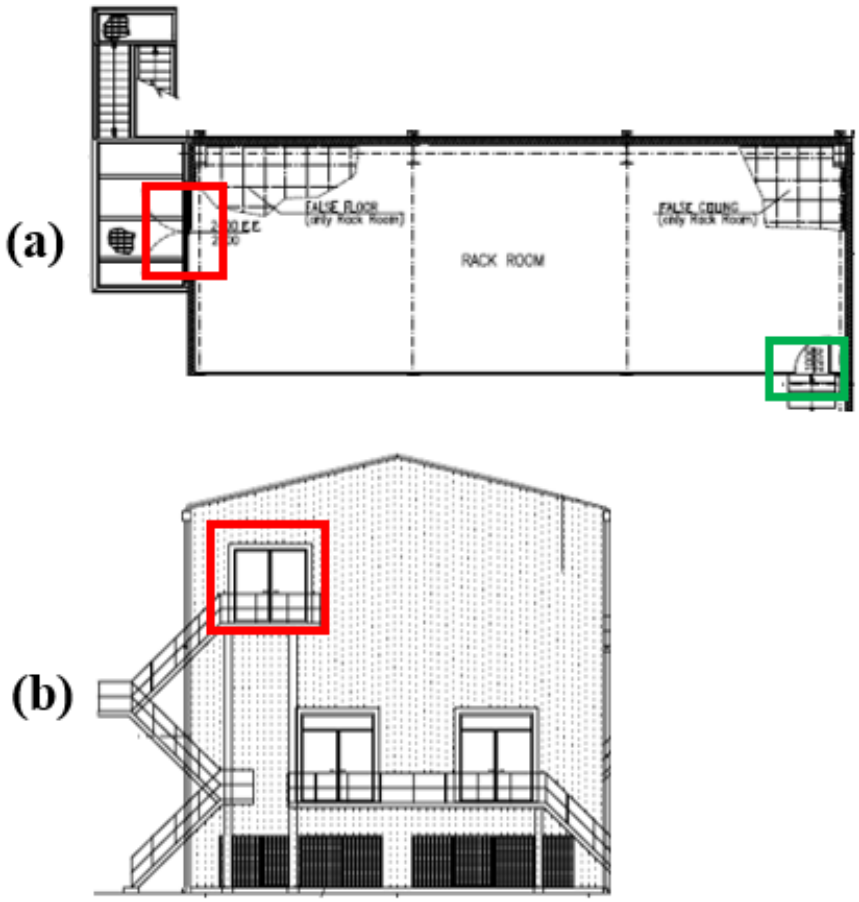

Figure 4.61. Architectural Drawings of the Building with the Highlighted Ventilation Openings (a) Fire Compartment Plan View (b) D Axis View.

Snow loads and live loads are multiplied by the design load coefficients that are described in Section 3.2 and applied to the respective structural members according to tributary area method. The weights of the perimeter and inner walls, the ceiling and the floor slab are also applied to the relevant structural members according to the tributary are method, but they are not multiplied by any design load coefficients, similar to the weight of the steel sections.

Fire load survey is carried out by the building operator and fire load in the DCS room is reported to have a total volume of 5.85 m^3 of wood due to wooden false floor.

(1 m^2 false floor panel is taken as 33.5 kg and 1 kg wood calorific value is taken as 20 MJ conservatively). Characteristic value of the fire load density for the floor surface is given in Table 4.3. Design value of the fire load density for the floor surface of the building is given in Appendix-A.

4.6.2. Fire Simulation and Heat Transfer Analysis

The preliminary parameters to simulate the design fire for the building according to the methodologies explained in Section 3.5 are given in Appendix-A. The hot (gas/smoke) and cold zone temperatures, the heat release rate, the smoke elevation level and the fire area for the entire duration of the fire are shown in Figure 4.62a, Figure 4.62b, Figure 4.62c and Figure 4.62d, respectively.

According to results of the fire simulation of the building, the two-zone fire model switches to the one-zone fire model at the 4^{th} minute of the fire, because the upper layer (hot-zone) reaches to $< 20.0\%$ of the compartment height and maximum fire area reaches to 25% of the total floor area (117.00 m^2). The fire has flashover (fully engulfed) at the 13^{th} minute of the fire, because the hot-zone (gas/smoke) temperatures reach 500.0 ^oC. It is obvious from the sudden jump in the heat release rate and the fire area the flashover occurs at the 13^{th} minute of the fire.

Due to the small floor (117 m^2) area and low height (4.7 m) of the fire compartment, the two-zone fire model switches to the one-zone fire model in relatively short duration (4^{th} minute of the fire). Moreover, the flashover also occurs in very short duration (13^{th} minute of the fire). Therefore, localized fire scenario is not considered for the fire simulation of the building and all of the structural members located in the fire compartment are simultaneously exposed to the hot-zone (gas-smokes) temperatures to conduct heat transfer analyses.

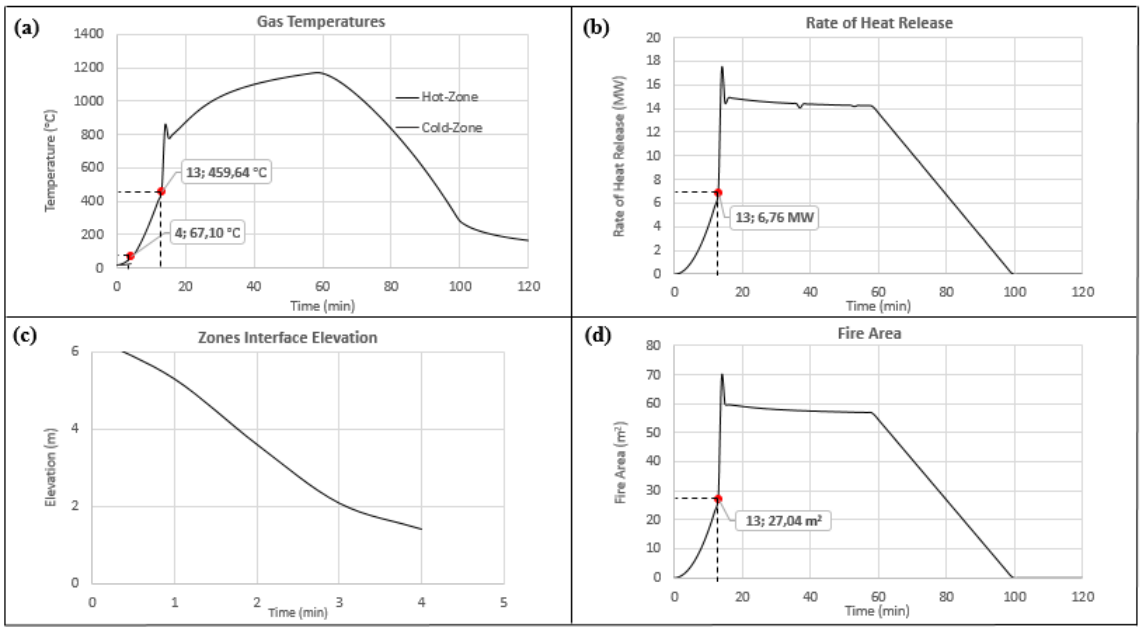

Figure 4.62. (a) Hot and Cold Zones Temperatures (Peak: 1172 ^{o}C at: 58 min) (b) RHR Computed (Peak: 17.29 MW at: 14 min), (c) Zones Interface Elevation (h = 1.43 m at: 4 min), (d) Fire Area (69.17 m^2 at 14 min).

4.6.3. Structural Analysis

The entire structure is analyzed but fire is applied to 117 m^2 floor area of the DCS room only as explained in Section 4.5.1. The structural analysis is uncoupled from the thermal analysis and the temperature input for structural members is applied as a predefined field into the structural analysis program. An implicit dynamic analysis method is utilized in order to determine instabilities in the structure.

The internal columns that align along axis 2 are isolated from the fire with non-combustible gas-concrete brick wall that is constructed along axis 2 to separate the fire compartment and other building volumes. Therefore, fire induced behaviors of the rafters that are located between axis 2 and 3, and the columns that are located along axis 3 determine the state of the building under fire. Moreover due to non-existence of the localized fire scenario for the fire compartment, and symmetry in the structural layout and the loading, fire induced performances of all the columns and the rafters located in the fire compartment of the building are similar to each other in themselves.

Therefore, the column that is located at B-3 axis coordinate (Figure 4.60) and the rafter that is located between B-2 and B-3 axis coordinates (Figure 4.60) are investigated in detail to determine state of the building under the fire.

Assessment of the investigated structural members are conducted with the allowable limits that are presented and formulated in Table 2.4. 50 mm/min mid-height vertical displacement rate (Gernay *et al.*, 2016) and the development of 15% equivalent plastic strains (CEN, 2005) along the column height are used as the maximum allowable limits for the assessment of the column. The maximum allowable mid-length vertical displacement and mid-length vertical displacement rate for the rafter are 325 mm (BS-476, 1976) and 16.77 mm/min (BS-476, 1976), respectively. Moreover, the development of 15% equivalent plastic strains (CEN, 2005) along the rafter is also used for the assessment of the rafter.

Maximum equivalent plastic strains along the column that is located at B-3 axis coordinate is shown in Figure 4.63b, and according to the figure the part of the column in which the maximum equivalent plastic strains develop yields at the 49.7^{th} minute of the fire. But the column does not lose its load carrying capacity during the fire. Figure 4.63d (I) visualize the analysis time that corresponds to the yielding of the column part. Moreover, the mid-height vertical displacement rates do not reach to 50 mm/min during the fire. Figure 4.63c shows the mid-height vertical displacements during the fire and the maximum rate of displacements is highlighted in the figure. Moreover, Figure 4.63d (II) visualize the analysis time that corresponds to occurrence of the maximum mid-height vertical displacement rate. These results indicate non-failure of the column according to the assessment criteria. On the other hand, according to Figure 4.63a which shows the maximum in-plane displacements along the column during the fire, 50 mm/min in-plane displacement rate develops along the column at the 74.5^{th} minute of the fire. Development of the run-away in-plane or out-of-plane displacements normally indicate buckling of the column. However, for this specific case, the run-away in-plane displacements along the column is the result of the rafter collapse because of the fully compatibility between the column and the rafter at the knee point as explained in Section 3.4.

As a summary, the failure of the rafter cause the column to collapse inside the fire compartment at the 74.5^{th} minute of the fire.

Since the structural performances of the columns that are located along E axis are mainly depend to the structural performances of the rafters that are located between axes 2 and 3, to determine state of the building the rafter that is located between B - 2 and B - 3 axis coordinates is investigated in details.

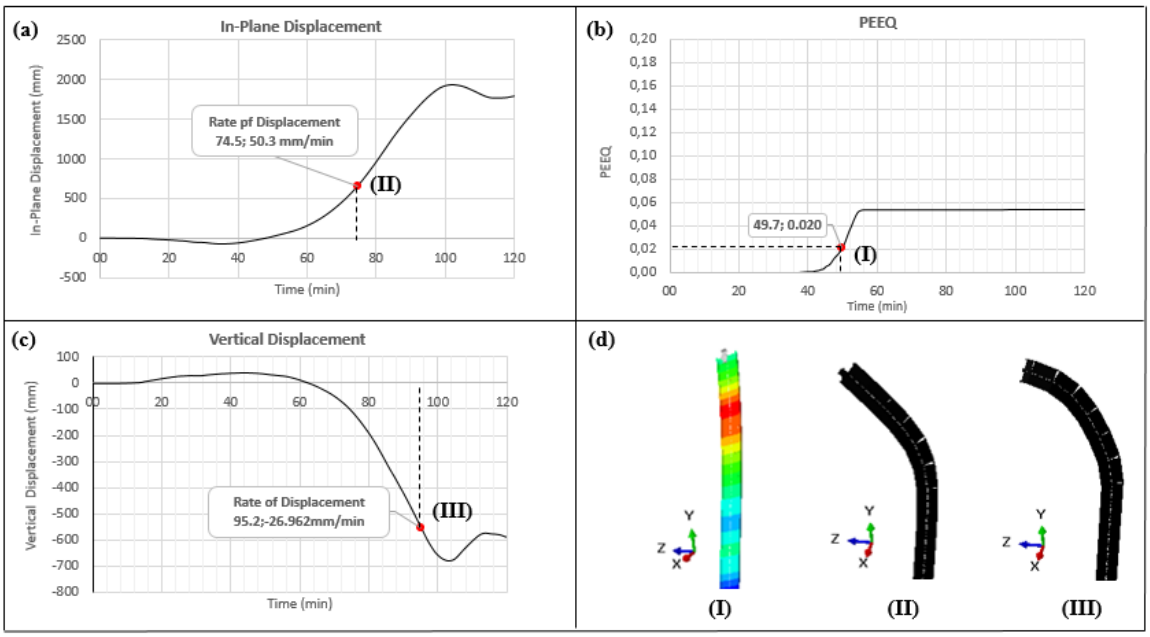

Figure 4.63. Fire Induced Behavior of the Column Located at the B-3 Axis Coordinate (a) Maximum In -Plane Displacements, (b) Maximum PEEQ, (c) Mid-height Vertical Displacements, (d) Analysis Times - (I) Yielding - (II) Maximum In-plane Displacement Rate - (III) Maximum Vertical Displacement.

Knee point of the rafter yields at the 23.8^{th} minute of the fire, Figure 4.64b shows the equivalent plastic strains at the knee point of the rafter during the fire. Due to yielding around the knee points and loss of steel stiffness at elevated temperatures, mid-length vertical displacement rate of the rafter reaches to 16.71 mm/min at the 27.9^{th} minute of the fire and the rafter fails. Figure 4.64c shows the rate of vertical displacements at the mid-length during the fire with the highlighted failure time. Figure 4.64d (I) and Figure 4.64d (III) visualize the analysis time that correspond to the

yielding of the knee point and the failure of the rafter due to initiation of the run-away mid-length displacement. Figure 4.64a shows the mid-length vertical displacement of the rafter for the entire duration of the fire and Figure 4.64d (IV) visualize the analysis time that correspond to occurrence of the maximum allowed vertical displacement at the mid-length of the rafter.

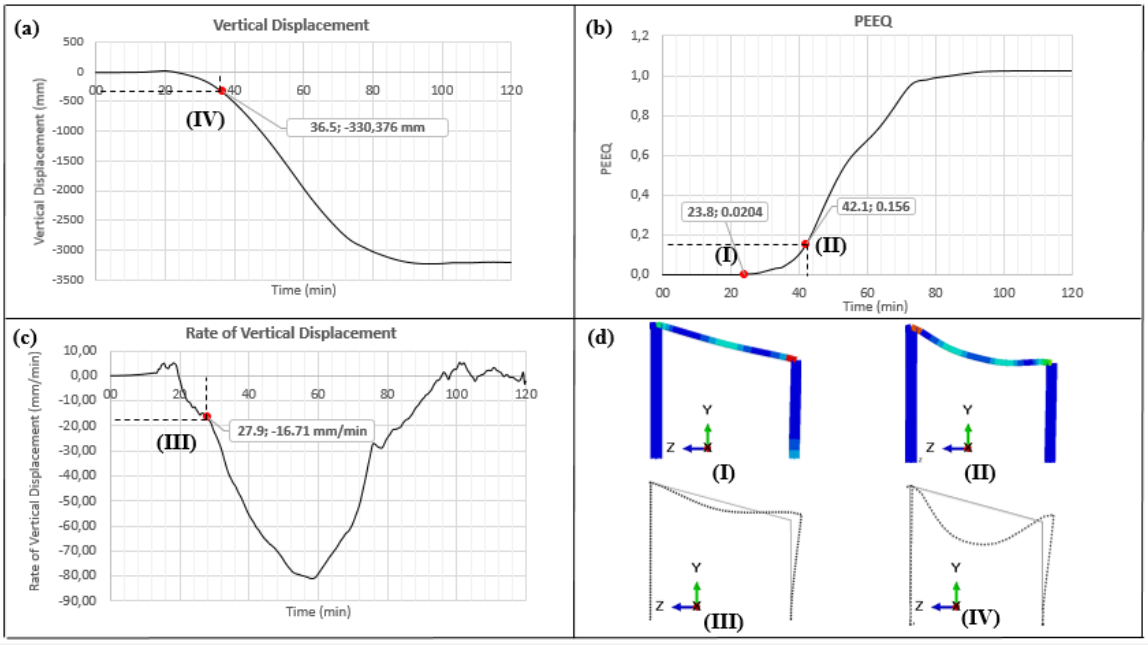

Figure 4.64. Rafter Located between B-2 and B-3 Axis Coordinates, (a) Mid-length Vertical Displacements, (b) Maximum PEEQ, (c) Mid-length Vertical Displacement Rates, (d) Analysis Times - (I) Yielding - (II) Strength Loss Initiation (III) Allowed Vertical Displacement Rate - (IV) Allowed Vertical Displacement.

As a summary, the rafter fails at the 27.9^{th} minute of the fire due to initiation of the run-away displacement at the mid-length. Moreover, according to Figure 4.64a the mid-length vertical displacements reach excessive values and continuously increase even in the cooling phase of the fire. These results validate the failure of the investigated rafter.

To conclude, the rafters that are located in the fire compartment of the building fail in the first 30 minutes of the fire due to run-away vertical displacement initiation and the excessive vertical displacements along the rafters cause failure of the columns

that are located along axis 3 (Figure 4.60) due to fully compatibility between the rafters and the columns. Fire induced performances of the investigated structural members of Building - 5 are summarized in Table 4.16. The fire compartment of the building collapses at the 74.5^{th} minute of the fire and the building does not pass 90 minutes fire resistance rating which is shown in Table 4.3.

Table 4.16. Fire Induced Performances of the Investigated Structural Members of Building - 5.

FIRE COMPARTMENT (Figure 4.60)		
Refer to Figures 4.63 and 4.64	Columns	Rafters
Location	B3 Axis Coordinate	B2 - B3 Axis Coordinate
Yielding Time (min)	49.7	22.3
Buckling Time (min)	N/A	N/A
Failure Time (min)	74.5	27.9
Failure Criteria	Mid-height Vertical Displacement Rate (50mm/min)	Mid-length Vertical Displacement Rate (16.77 mm/min)

5. THERMO-MECHANICAL BEHAVIOR OF STEEL FRAMED CONCRETE SLAB COMPOSITE FLOOR SYSTEMS

5.1. General

Steel framed reinforced concrete slab composite floor systems are commonly used in steel constructions, especially in high-rise buildings. An accurate fire performance estimation of composite floor systems is therefore critical. Although, finite element method has been widely used to determine thermo-mechanical behavior of composite floors (Huang *et al.*, 2000), constitution of these models is computationally expensive, time consuming and it is tedious to conduct parametric studies. Due to these limitations, a simplified semi-analytical method is developed with an iterative algorithm and implemented in Matlab to estimate thermo-mechanical behavior of composite floors systems.

In this study, an efficient and simplified algorithm is developed to calculate composite floor deflections under fire conditions by considering in-plane normal forces that result from mean temperature increase and large deflections due to thermal gradient. It is possible to estimate moments and tensile membrane forces across the composite floor section by knowing the deflections of the composite floor system. Moreover, stresses developed along the composite floor system can be calculated with force resultants and it becomes possible to properly design these floor systems for fire action.

Current closed form equations that are developed to determine thermo-mechanical behavior of plates do not include in-plane normal forces that result from large deflections. These forces are also known as tensile membrane forces (Ugural, 1981). However, large deflections develop due to thermal gradient along the composite floor system during fire and the tensile membrane forces become crucial to determine thermo-mechanical behavior of composite floor systems (Usmani *et al.*, 2001).

5.2. Thermo-Mechanical Behaviors of Beams and Plates

5.2.1. Deflections of a Beam Subjected to Membrane Force, Thermal Gradient and Transvers Loading

In this section, the governing differential equation to calculate beam deflections under transverse loading, membrane (axial) force and temperature gradient is derived. Classical beam theory assumes that straight lines normal to the middle surface of the beam remain straight, normal to the middle surface of the beam and unchanged in length after the deformations. However, when beam boundaries are restrained, in plane normal forces may arise as a result of temperature change or large deflections due to thermal gradient or large transverse loading and the assumption becomes invalid. Therefore, Equation 5.1 which represents governing differential equation for beam deflection under transverse loading must be revised to consider the in-plane normal forces.

$$EI\frac{\partial^4 w}{\partial x^4} = p \tag{5.1}$$

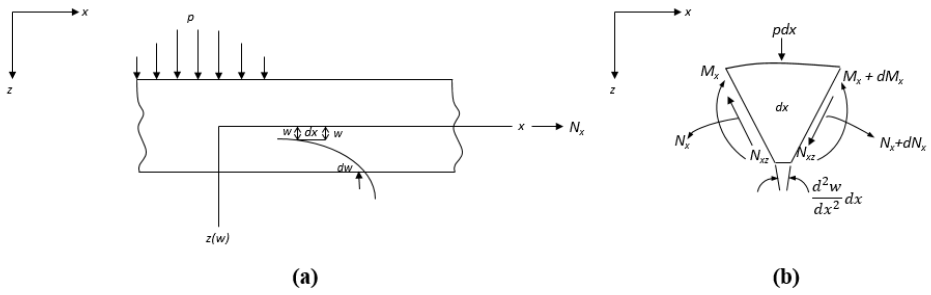

Figure 5.1. (a) Beam Element Subjected to Transverse Loading (b) Internal Forces Acting on the Infinitesimal Beam Length (Ugural, 1981).

Figure 5.1 represents the beam element that is subjected to transverse loading and in-plane normal force. The internal forces acting on the infinitesimal length of the beam element is shown in Figure 5.1b. Considering the equilibrium of the moments acting on infinitesimal length of the beam element and also knowing that as the limit

d_x tends to zero and neglecting the shear force dN_{xz} the equilibrium of the moments leads to Equation 5.2 and Equation 5.3.

$$N_{xz}dx - (M_x + dM_x) + M_x = 0 \tag{5.2}$$

$$N_{xz} = \frac{dM_x}{dx} \tag{5.3}$$

By considering Equation 5.2 and Equation 5.3 it is possible to write force equilibrium in z direction, $\sum F_z = 0$, as Equation 5.4.

$$dN_{xz} + pdx + N_x \frac{\partial^2 w}{\partial x^2} dx = 0 \tag{5.4}$$

Dividing Equation 5.4 with dx and substituting Equation 5.5 which corresponds to moment resultant that also includes thermally induced moment (M*) to Equation 5.4, the governing differential equation that represents beam deflection under transverse loading, normal force and thermal gradient is obtained as Equation 5.7.

$$M_x = EI \frac{\partial^2 w}{\partial x^2} - M^* \tag{5.5}$$

n which M* is the thermal stress resultant and is found with Equation 5.6.

$$\mathrm{M}^* = E\alpha \int_{-t/2}^{t/2} \Delta T\,(z)\, z dz \tag{5.6}$$

$$EI \frac{\partial^4 w}{\partial x^4} = p + \frac{\partial^2 M^*}{\partial x^2} + N_x \frac{\partial^2 w}{\partial x^2} \tag{5.7}$$

5.2.2. Deflections of a Simply Supported Beam Subjected to Uniform Transverse Loading and Thermal Gradient

In this section, the governing beam deflection equation represented with Equation 5.7 is solved for simply supported boundary conditions. The boundary conditions of a simply supported beam with length equals to L is shown with Equation 5.8.

$$w = 0, u = 0, M_x = 0 at x = 0, L \tag{5.8}$$

For the boundary conditions shown with Equation 5.8, solution of Equation 5.7 under uniform transverse loading of po is found as Equation 5.9.

$$w\left(x\right) = \frac{p_o x}{24EI}(L^3 - 2Lx^2 + x^3) \tag{5.9}$$

For elastic material behavior, it is possible to superpose the deflections that result from varying temperature over the beam thickness and transverse loading. Therefore, Equation 5.7 reduces to Equation 5.10 for the simply supported beam subjected to varying temperature over the beam thickness.

$$EI\frac{\partial^4 w}{\partial x^4} = \frac{\partial^2 M^*}{\partial x^2} + N_x\frac{\partial^2 w}{\partial x^2} \tag{5.10}$$

$$w\left(x\right) = w_T \sin\frac{\pi x}{L} \tag{5.11}$$

$$M^*\left(x\right) = M_1^* \sin\frac{\pi x}{L} \tag{5.12}$$

where the Fourier coefficient wT represents mid-length deflection of the beam.

In addition, as shown with Equation 5.15 in-plane normal force (N_x) that develop in the beam due to thermal gradient can be defined as sum of the thermally induced in-plane normal force (N*) and deflection resulted tensile membrane force (N_{xm}) (Donnell, 1976). The formulation of the thermally induced in-plane normal force and the tensile membrane force due to beam mid-length displacement are represented formulated with Equation 5.13,Equation 5.14 for the simply supported beam.

$$N^* = E\alpha \int_{-t/2}^{t/2} \Delta T\,(z)\,dz \tag{5.13}$$

$$\tilde{N}_{xm} = EA\frac{\pi^2 w_T^2}{4L^2} \tag{5.14}$$

$$N_x = \mathrm{N}^* + N_{xm} \tag{5.15}$$

For Equation 5.15 the in-plane normal force must be defined as negative if it is compression and as positive if it is tension.

By substituting Equation 5.11, Equation 5.12 and Equation 5.15 into Equation 5.10, a cubic equation for mid-length deflection of simply supported beam subjected to temperature gradient across the beam depth is obtained as Equation 5.16 (Khazaeinejad *et al.*, 2015).

$$w_T^3 + \left(\frac{4A}{I} - \frac{4N^*L^2}{\pi^2 EA}\right) w_T + \frac{16M^*L^2}{\pi^3 EA} = 0 \tag{5.16}$$

Finally, having the mid-length deflection of the simply supported beam, it is possible to calculate deflection of any point along the beam length with Equation 5.11.

5.2.3. Deflections of a Plate Subjected to Membrane Forces, Transverse Loading and Temperature Gradient

According to fundamental assumption of small deflection theory of bending for isotropic, homogeneous, elastic, thin plates the mid-plane of thin plates does not stretch under small deformations. However, when the mid-plane is strained by in-plane normal forces, the fundamental assumption is no longer valid and if plate boundaries are restrained to lateral movement, these in-plane normal forces may arise from temperature change, thermal gradient and large transverse loading. Therefore, Equation 5.17 which represents governing differential equation for plate deflections under transverse loading should be revised to consider in plane normal forces.

$$\frac{\partial^4 w}{\partial x^4} + 2\frac{\partial^4 w}{\partial x^2 \partial y^2} + \frac{\partial^4 w}{\partial y^4} = \frac{p}{D} \tag{5.17}$$

Consider a plate element of sides dx and dy, under the action of normal forces N_x, N_y and shear forces $N_{xy} = N_{yx}$ which are functions of x and y only. Assume the body forces to be negligible. The top and front views of such an element, and other resultants affecting to the plate due to lateral forces simultaneously acting on the element are shown in Figure 5.2.

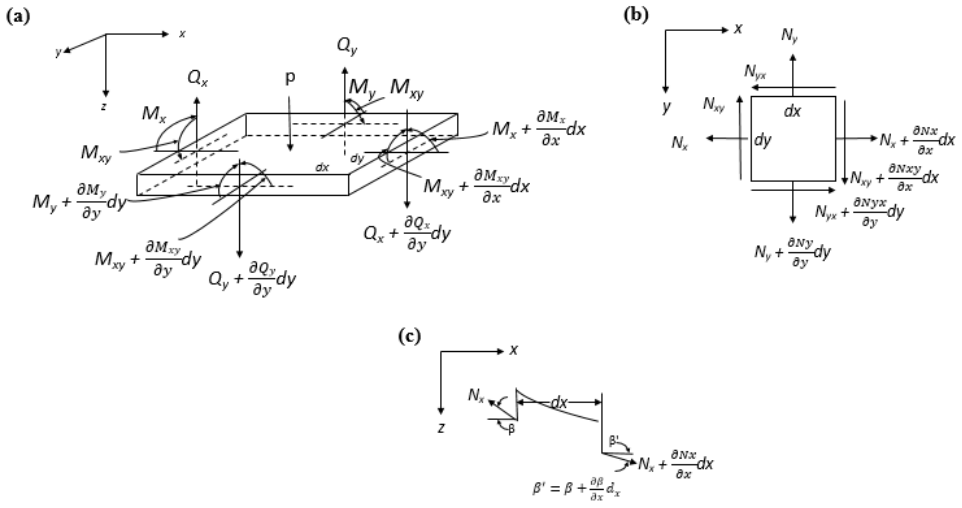

Figure 5.2. (a)Stress resultants on a plate subjected to transverse loading and in-plane normal forces (b) Top view (c) Front view (Ugural, 1981).

According to Figure 5.2b and Figure 5.2c, sum of the normal forces acting along the x direction can be written as Equation 5.18.

$$(N_x + \frac{\partial N_x}{\partial x}dx)dy\cos\beta' - N_x dy\cos\beta \tag{5.18}$$

For small β, Equation 5.18 reduces to $\frac{\partial N_x}{\partial_x}dxdy$ and if sum of the shear forces $Nxydx$ is treated in similar way, force equilibriums along the x and y axis, $\sum^{F_x} = 0$ and $\sum^{F_y} = 0$, can be written as Equation 5.19 and Equation 5.20.

$$\frac{\partial N_x}{\partial x} + \frac{\partial N_{yx}}{\partial y} = 0 \tag{5.19}$$

$$\frac{\partial N_{xy}}{\partial x} + \frac{\partial N_y}{\partial y} = 0 \tag{5.20}$$

To describe equilibrium in the z direction, it is necessary to consider the z components of the normal forces acting at each of the edges of the plate shown in Figure 5.2a. The z components of the forces acting on the x edges is represented with Equation 5.21 and reduced to Equation 5.22 for small deflection (small β).

$$-N_x dy\sin\beta + \left(N_x + \frac{\partial N_x}{\partial x}dx\right)dy\sin B' \tag{5.21}$$

$$N_x\frac{\partial^2 w}{\partial x^2}dxdy + \frac{\partial N_x}{\partial x}\frac{\partial w}{\partial x}dxdy \tag{5.22}$$

The slope of the deflection in the y direction on the x edges equals to $\frac{\partial w}{\partial y}$ and $\left(\frac{\partial w}{\partial y} + \left(\frac{\partial^2 w}{\partial x \partial y}\right)dx\right)$. Therefore, z components of the shear forces N_{xy} and N_{yx} can be written as Equation 5.23 and Equation 5.24.

$$N_{xy}\left(\frac{\partial^2 w}{\partial x \partial y}\right)dxdy + \frac{\partial N_{xy}}{\partial x}\frac{\partial w}{\partial x}dxdy \tag{5.23}$$

$$N_{yx}\left(\frac{\partial^2 w}{\partial x \partial y}\right)dxdy + \frac{\partial N_{yx}}{\partial y}\frac{\partial w}{\partial x}dxd \tag{5.24}$$

For the forces shown in Figure 5.2a, force equilibrium along the z axis, $\sum F_z)0$, leads to Equation 5.25.

$$\begin{aligned}&\tfrac{\partial Q_x}{\partial x} + \tfrac{\partial Q_y}{\partial y} + p + N_x\tfrac{\partial^2 w}{\partial x^2} + N_y\tfrac{\partial^2 w}{\partial y^2} + 2N_{xy}\tfrac{\partial^2 w}{\partial x \partial y}\\ &+\left(\tfrac{\partial N_x}{\partial x} + \tfrac{\partial N_{yx}}{\partial y}\right)\tfrac{\partial w}{\partial x} + \left(\tfrac{\partial N_{xy}}{\partial x} + \tfrac{\partial N_y}{\partial y}\right)\tfrac{\partial w}{\partial x} = 0\end{aligned} \tag{5.25}$$

Last 2 terms of Equation 5.25 vanish according to Equation 5.26 and Equation 5.27. Moreover, according to Figure 5.2, equilibrium of the moments with respect to x and y axes can be written as Equation 5.26 and Equation 5.27.

$$Q_x = \frac{\partial M_x}{\partial x} + \frac{\partial M_{xy}}{\partial y} \tag{5.26}$$

$$Q_y = \frac{\partial M_y}{\partial y} + \frac{\partial M_{xy}}{\partial x} \tag{5.27}$$

Moment resultants that include thermally induced stress resultant are given with Equation 5.28, Equation 5.29, Equation 5.30 (Ugural, 1981). Substituting these equations to Equation 5.26 and Equation 5.27, it is possible to write the vertical shear forces, Q_x and Q_y, shown in Figure 5.2a as Equation 5.31 and Equation 5.32.

$$M_x = -D\left(\frac{\partial^2 w}{\partial x^2} + \frac{v\partial^2 w}{\partial y^2}\right) - \frac{M^*}{(1-v)} \tag{5.28}$$

$$M_y = -D\left(\frac{\partial^2 w}{\partial x^2} + \frac{v\partial^2 w}{\partial y^2}\right) - \frac{M^*}{(1-v)} \tag{5.29}$$

$$M_{xy} = -(1-v)\,D\left(\frac{\partial^2 w}{\partial x \partial y}\right) \tag{5.30}$$

$$Q_x = -D\left(\frac{\partial}{\partial x}\right)\nabla^2 \tag{5.31}$$

$$Q_y = -D\left(\frac{\partial}{\partial y}\right)\nabla^2 \tag{5.32}$$

Finally, substituting Equation 5.31 and Equation 5.32 into Equation 5.25, governing differential equation to determine thin plate deflections under combined transverse loading, normal forces and thermal gradient is obtained as Equation 5.33.

$$\begin{aligned} &\tfrac{\partial^4 w}{\partial x^4} + 2\tfrac{\partial^4 w}{\partial x^2 \partial y^2} + \tfrac{\partial^4 w}{\partial y^4} \\ &= \tfrac{1}{D}(p + N_x \tfrac{\partial^2 w}{\partial x^2} + N_y \tfrac{\partial^2 w}{\partial y^2} + 2N_{xy}\tfrac{\partial^2 w}{\partial x \partial y} - \tfrac{1}{(1-v)}\nabla^2 M^*) \end{aligned} \tag{5.33}$$

5.2.4. Deflections of a Simply Supported Plate Subjected to Uniform Transverse Loading and Thermal Gradient

The boundary conditions of simply supported plate with an edges length equal to a and b are shown with Equation 5.34 and Equation 5.35.

$$w = 0, u = 0, M_x = 0 \quad at \quad x = 0, a \tag{5.34}$$

$$w = 0, v = 0, M_y = 0 \quad at \quad y = 0, b \tag{5.35}$$

As explained in Section 5.2.2, it is possible to superpose the deflections that result from varying temperature over plate thickness and transverse loading, and the

developed simplified method does not take account effect of shear forces N_{xy} and N_{yx}. Therefore, the solution of the governing differential equation for simply supported thin plate deflections under the uniform transverse loading of p_o is found as below.

$$w = \frac{16p_o}{\pi^6 D} \sum_{m=1}^{\infty} \sum_{n=1}^{\infty} \frac{\sin\frac{m\pi x}{a} \sin\frac{n\pi x}{b}}{mn\left[\left[\left(\frac{m}{a}\right)^2+\left(\frac{n}{b}\right)^2\right]^2+\frac{N_x}{D}\left(\frac{m}{a\pi}\right)^2+\frac{N_y}{D}\left(\frac{n}{b\pi}\right)^2\right]} \quad for \quad m,n = 1,3,5... \tag{5.36}$$

As explained in Section 5.2.2, for elastic material behavior it is possible to superpose the deflections that result from thermal gradient and transverse loading. Therefore, by ignoring the shear forces Equation 5.33 reduces to Equation 5.37 for the simply supported plate subjected to thermal gradient.

$$\begin{aligned} &\frac{\partial^4 w}{\partial x^4} + 2\frac{\partial^4 w}{\partial x^2 \partial y^2} + \frac{\partial^4 w}{\partial y^4} \\ &= \frac{1}{D}\left(N_x \frac{\partial^2 w}{\partial x^2} + N_y \frac{\partial^2 w}{\partial y^2} - \frac{1}{(1-v)}\nabla^2 M^*\right) \end{aligned} \tag{5.37}$$

Solution of Equation 5.37 is obtained by defining thermal moment (M*) and plate deflections (w) by Fourier sine series as shown with Equation 5.38 and Equation 5.39, respectively. Equation 5.38 and Equation 5.39 satisfy the boundary conditions that are given with Equation 5.34 and Equation 5.35. Moreover, the condition shown with Equation 5.40 which is derived from Equation 5.28 and Equation 5.29 is satisfied at the boundaries.

$$\mathrm{w} = \sum_{\mathrm{m}=1}^{\infty} \sum_{\mathrm{n}=1}^{\infty} \mathrm{a_{mn}} \sin\frac{\mathrm{m}\pi\mathrm{x}}{\mathrm{a}} \sin\frac{\mathrm{n}\pi\mathrm{y}}{\mathrm{b}} \tag{5.38}$$

$$M^* = \sum_{m=1}^{\infty} \sum_{n=1}^{\infty} p_{mn} \sin\frac{m\pi x}{a} \sin\frac{n\pi y}{b} \tag{5.39}$$

$$D\nabla^2 w = -\frac{M^x}{(1-v)} \tag{5.40}$$

Substituting Equation 5.38 and Equation 5.39 into Equation 5.37, the Fourier series equation is obtained to determine deflections of the simply supported plate subjected to thermal gradient as represented with Equation 5.41:

$$w = \frac{16M^*}{\pi^4 D(1-v)} \sum_{m=1}^{\infty} \sum_{n=1}^{\infty} \frac{\sin\frac{m\pi x}{a} \sin\frac{n\pi x}{b} \left[\left(\frac{m}{a}\right)^2 + \left(\frac{n}{b}\right)^2\right]}{mn\left[\left[\left(\frac{m}{a}\right)^2 + \left(\frac{n}{b}\right)^2\right]^2 + \frac{N_x}{D}\left(\frac{m}{a\pi}\right)^2 + \frac{N_y}{D}\left(\frac{n}{b\pi}\right)^2\right]} \qquad (5.41)$$

$$for \quad m, n = 1, 3, 5...$$

where the normal forces are found with Equation 5.42 and Equation 5.43

$$N_x = \frac{N^*}{(1-v)} + N_{xm} \qquad (5.42)$$

$$N_y = \frac{\mathrm{N}^*}{(1-v)} + N_{ym} \qquad (5.43)$$

5.3. Validation of the Governing Beam and Plate Deflection Equations

To validate the solutions of equations derived under Sections 5.2.2 and 5.2.4, a series of finite element analyses are carried out.

The beam that is used to validate Equation 5.16 is 5 m in length, 300 mm in width and 300 mm in depth. C20 calcareous aggregate elastic concrete material properties with ambient condition thermal expansion coefficient and modulus of elasticity is used for the investigated beam. The thermal gradient through the depth of the beam is considered as $T_z = 1$ ^{o}C/mm with the mean temperature increase varies between 0 ^{o}C to 300 ^{o}C with 50 ^{o}C increments.

Figure 5.3 shows that mid-length deflections of the investigated beam under the given thermal gradient and mean temperature increase. The mid-length deflections that are calculated with Equation 5.16 deviate at most 3.33% against the finite element analysis results.

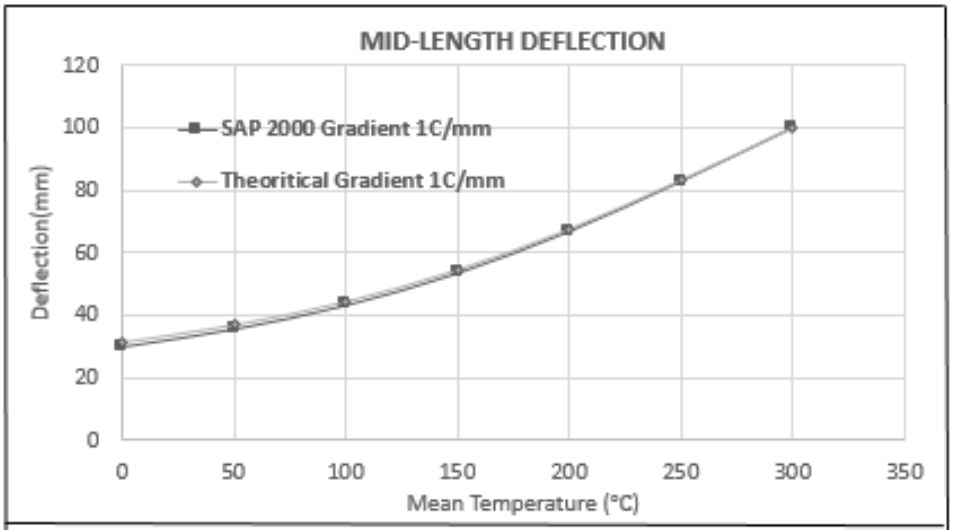

BEAM MID-LENGTH DEFLECTION for Tz=1C/mm			
Mean - Temperature (°C)	CODE (mm)	SAP2000 (mm)	Percentage of Accuracy
0.00	31.24	30.23	96.77
50.00	36.80	35.83	97.34
100.00	44.32	43.41	97.95
150.00	54.46	53.67	98.56
200.00	67.62	67.02	99.11
250.00	83.32	82.92	99.52
300.00	100.24	100.01	99.77

Figure 5.3. The Beam Mid-length Deflections under $T_z = 1\ ^oC/mm$.

The plate element that is used to validate Equation 5.41 is 5 m in length, 5 m in width and 200 mm in depth. C20 calcareous aggregate elastic concrete material properties with ambient condition thermal expansion coefficient and modulus of elasticity is used for the investigated plate. The thermal gradient through the depth of the plate is taken as $T_z = 1\ ^oC/mm$ with the mean temperature increase varies between 0 ^oC to 150 ^oC with 25 ^oC increments.

Figure 5.4 shows mid-point deflections of the investigated plate under the given thermal gradient and mean temperature increases. The mid-point deflections that are calculated with Equation 5.41 deviate at most 13.35% against the finite element analysis results. The reason of increasing deviation percentage with increasing deflection is due to assumption used in the developed simplified methodology. The simplified methodology assumes that the tensile membrane forces are uniformly distributed along

the plate edges, but in reality these forces increase from the edges of the plate to the mid-length of the edges. Moreover, because tensile membrane forces that are developed along the edges of the plate are related with square of the deflections as shown in Equation 5.14, once the deflections along the plate increase the deviation percentage between finite element analysis and Equation 5.41 results also increases.

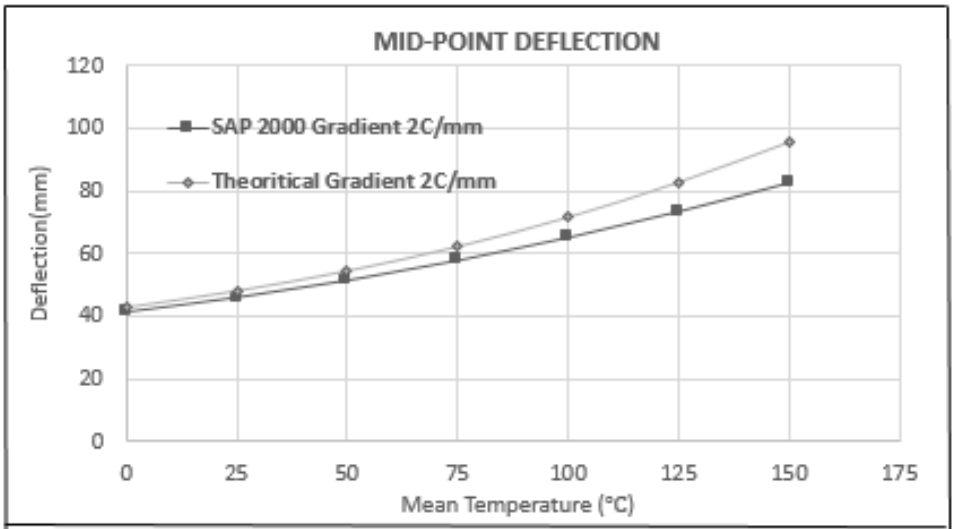

PLATE MID-POINT DEFLECTION for Tz=2C/mm			
Mean - Temperature (°C)	CODE (mm)	SAP2000 (mm)	Percentage of Accuracy
0.00	42.82	41.49	96.90
25.00	48.05	46.11	95.96
50.00	54.40	51.53	94.72
75.00	62.14	57.86	93.12
100.00	71.48	65.18	91.19
125.00	82.61	73.47	88.94
150.00	95.35	82.63	86.65

Figure 5.4. The Plate Mid-point Deflections under $T_z = 1\ ^oC/mm$.

5.4. Simplified Method to Calculate Interior Steel Beam Reinforced Concrete Slab Composite Floor System Deflections under Fire Conditions

The simplified method uses the equations that have been derived in Section 5.2.2 and 5.2.4 to calculate deflections of simply supported interior steel beam reinforced concrete slab composite floor system under fire and it assumes elastic mechanical material behaviors for structural steel, steel reinforcement and concrete materials under

elevated temperatures. In case of a fire, the temperature distribution along the depth of the composite floor differs. Therefore, in the simplified method the concrete slab is layered as equal length elements and the steel beam is layered as bottom flange, top flange and web, and each layers' temperature dependent mechanical properties are calculated separately according to their temperatures. In the simplified method, transformed area method (Gere, 2004) is utilized to find equivalent mechanical properties of the layers for the entire duration of the fire so that by knowing the layers' temperatures it is possible to calculate thermally induced resultant forces and moments along the composite floor section can be calculated.

In the simplified method, the composite floor section is treated as beam section by utilizing transform area method until the interior steel beam average temperature reaches to 700 ^{o}C. Therefore until this analysis time, deflections along the composite floor system are calculated with the beam deflection equations that are represented in Section 5.2.2. When the average steel temperature reaches 700 ^{o}C, the steel beam losses 87% of its stiffness (CEN, 2005) and can therefore be neglected in the calculations. As a result, after that time deflections along the composite floor system are calculated with the plate deflection equations that are represented in Section 5.2.4. In short, at 700 ^{o}C composite beam deflection calculations switches to plate deflection calculation.

Until the average steel beam temperature reaches to 700 ^{o}C, Equation 5.9 and Equation 5.16 separately used and their results are superposed to find mid-length deflection of the transformed beam of the composite floor. Having the mid-length deflection of the transformed beam, it is possible to find deflections for each point of the composite floor by using Equation 5.11 for the both direction of the composite floor edges. When the average steel beam temperature reaches to 700 ^{o}C the deflections along the composite floor is determined by superposing results of Equation 5.36 and Equation 5.41. However, to use Equation 5.36 and Equation 5.41, uniformly distributed in-plane normal forces along the composite floor edges must be known, but realistically the tensile membrane forces are not uniformly distributed along the composite floor edges and they increase from the corners of the composite floor to the mid-length of the edges. Therefore, the assumption described in the following paragraphs and the

iterative solution algorithm that is shown in Figure 5.6 are adopted.

The reinforcements of the concrete slab can be thought as comprised of finite strips as shown in Figure 5.5. As explained before, at the analysis time that corresponds to 700 ^{o}C average steel temperature, mid-length deflections of each of these strips can be determined by using Equation 5.11 for both direction of the composite floor. Having each finite strip mid-length deflections, the tensile membrane force that develop in each of the finite strips (reinforcements) can be calculated with Equation 5.14. Then in the simplified method, the calculated tensile membrane force in each of the finite strips is assumed to be uniformly distributed along the composite floor edges. Summing these uniformly distributed tensile membrane forces with the thermally induced in-plane normal forces makes possible to start using Equation 5.36 and Equation 5.41 for the first analysis time that corresponds to average steel temperature higher than 700 ^{o}C.

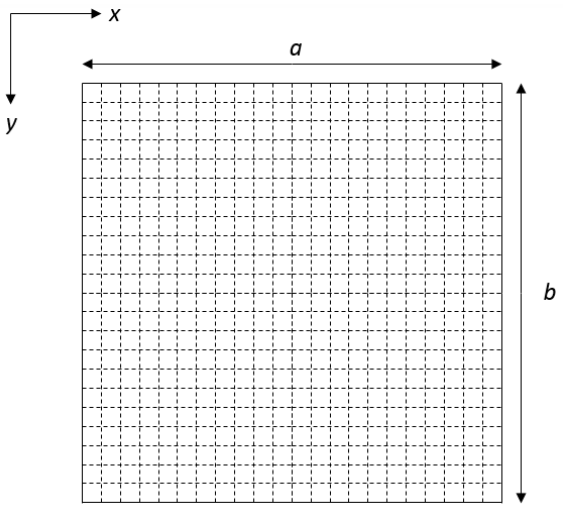

Figure 5.5. Finite Strips Demonstration of Rectangular Plate.

The previous paragraph indicates that calculating composite floor deflections with Equation 5.36 and Equation 5.41 for current analysis time it is required to use the tensile membrane forces that are calculated at the previous analysis time. However, when the deflections along the composite floor are calculated with superposing Equation 5.36 and Equation 5.41 results, the tensile membrane forces will be updated in the current analysis time due to updated deflections. Therefore to properly calculate composite floor deflections after the analysis time that corresponds to 700 ^{o}C average steel temper-

ature, it is required to follow iterative solution method. The adopted iterative solution method for the simplified methodology is shown in Figure 5.6. Moreover, solutions of Equation 5.36 and Equation 5.41 results with composite floor deflections without considering deflections of the composite floor until the average steel beam temperature reaches to 700 ^{o}C. Therefore results of Equation 5.36 and Equation 5.41 must be summed with the deflections at the analysis time that corresponds to 700 ^{o}C average steel temperature.

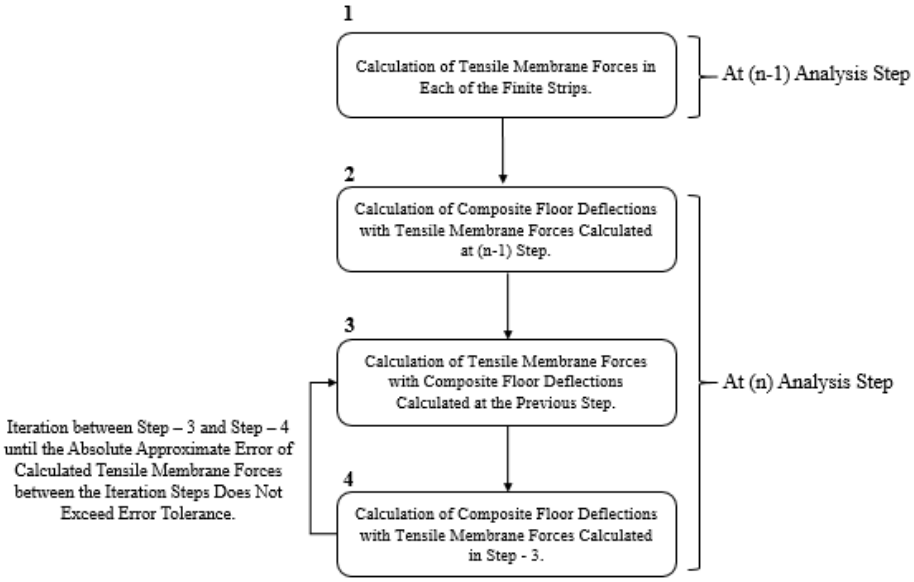

Figure 5.6. Iterative Solution Method to Calculate Composite Floor Deflections with Closed form Plate Deflection Equations.

The entire algorithm that describes the developed simplified methodology to determine thermo-mechanical behavior of steel beam reinforced concrete slab composite floor system under fire conditions is shown in Figure 5.7.

5.5. Validation of the Simplified Method

The developed simplified algorithm shown in Figure 5.7 is implemented into Matlab to calculate composite floor deflections under fire and a finite element analysis is conducted to validate developed algorithm. In this section, details of the finite element model and comparison of the finite element analysis and developed algorithm

results for a specific composite floor system are given. Moreover, assumptions that are adopted for the developed simplified algorithm are summarized, and the capabilities of the Matlab code are represented.

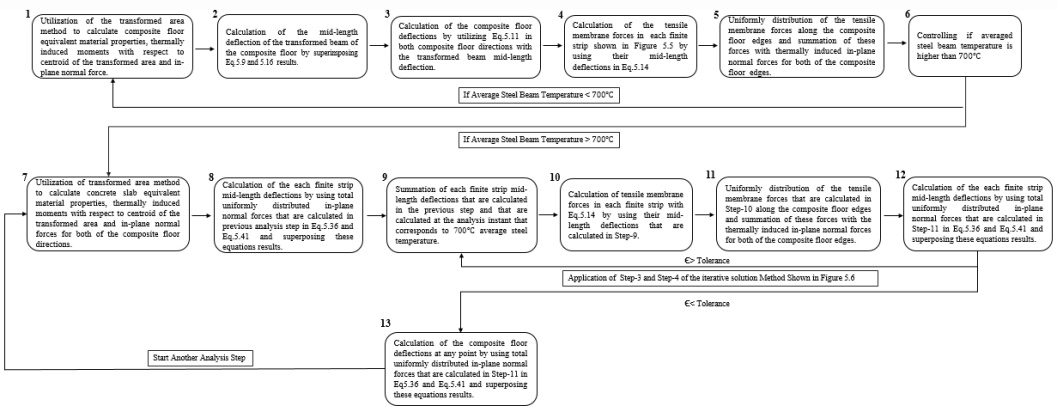

Figure 5.7. Entire Algorithm that for the Developed Simplified Methodology.

5.5.1. Summary of the Assumptions Adopted in the Simplified Method and Capabilities of the Matlab Code

Following assumptions are adopted in the developed simplified algorithm and they are implemented into the Matlab code.

- Stress-strain relationships of the structural steel, steel reinforcement and concrete are assumed to have temperature dependent linear elastic behavior for entire duration of the heating, and material softening and damage are not included in the stress-strain relationships of the materials.
- Temperature dependent linear material properties and thermal properties of structural steel and steel reinforcement, and concrete are taken from Eurocode - 3 Part 1-2 and Eurocode - 4 Part 1-2 (CEN 2005, 2004), respectively.
- Cooling period of composite floor members are not included in the Matlab Code. Therefore, if the interior steel beam or any part of the concrete slab pass to the cooling period, they are assumed to have no load-bearing capacity.
- The concrete material is assumed to have no tensile strength and it is assumed that all the tensile membrane forces are carried by the steel reinforcements.

- Membrane forces in the concrete slab are uniformly distributed along the composite floor edges for the utilization of Equation 5.36 and Equation 5.41.
- The Matlab Code is only capable to calculate composite floor deflections for simply supported boundary conditions with an interior beam located at the one of the edges mid-length.
- Behavior of the concrete slab perimeter beam connection and perimeter beam interior beam connection are not in the scope of this study. Therefore, these connections are assumed to survive for the entire duration of the fire and not included in the Matlab code.
- Full composite action (perfect bonding) between the interior steel beam and the concrete slab is assumed.
- When the averaged steel temperature of the web and the flanges becomes 700^{o}C, the interior beam is assumed to have no load-bearing capacity and to contribute only as a dead load on the concrete slab.
- The Matlab Code is capable to calculate composite floor vertical deflections, the membrane forces developed in the interior beam, steel reinforcement and concrete slab.

In future studies, it is expected to implement stress and strain control algorithm in to the Matlab code to investigate effects of non-linear material behaviors to the composite floor deflections and the tensile membrane action.

5.5.2. Description of the Finite Element Model

Abaqus (DS Simulia, 2012), finite element software, is used to conduct finite element analysis of a composite floor system. The analyzed composite floor consist of 5 m by 5 m concrete slab and IPE330 interior beam that is located along the mid-length of one of the concrete slab edges as shown in Figure 5.8. The slab is discretized using 10 mm x 10 mm finite elements of 4-node doubly curved thick shells with reduced integration (S4R), large strain formulation and enhanced hourglass control to eliminate distortion. The slab is modelled with thickness of 200 mm as illustrated in Figure 5.9a. The concrete slab is reinforced by S500 strength 100 mm spaced 16

mm diameter longitudinal and transverse steel rebars. The reinforcement is modeled using the *Rebar Layer command, and the reinforcement is placed at 100 mm below the concrete top surface. Interior beam (IPE330), are discretized using reduced integration continuum elements (C3D8R) with enhanced hourglass stiffness to eliminate distortion. Interior beam ends are restrained with kinematic coupling constraint and concrete slab edges are restrained with edge boundaries. Both the concrete slab edges and interior beam ends are pin connected. The model assumes full composite action (perfect bonding) between the interior steel beam and the concrete slab by using the *Surface Tie command.

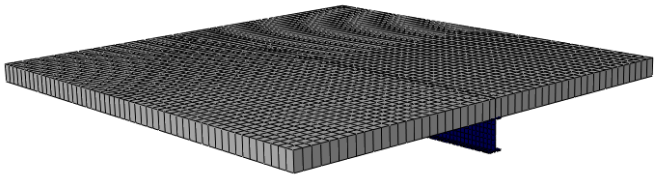

Figure 5.8. Composite Floor Assembly.

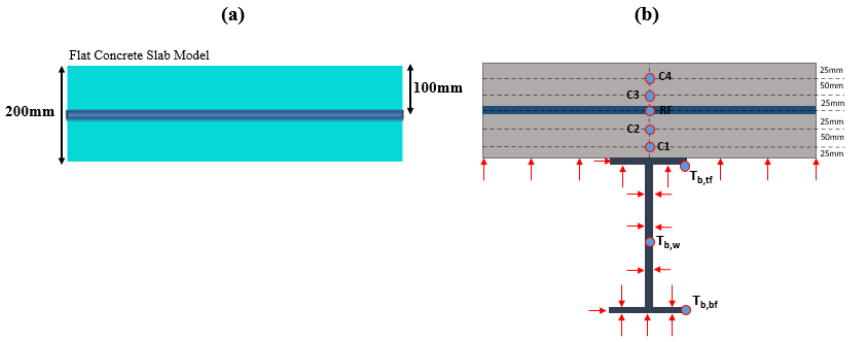

Figure 5.9. (a) Flat Concrete Slab Model (b) Fire Boundary and Temperature Points of the Composite Floor.

The fire is applied to the concrete bottom surface and three sides of the steel interior beam as illustrated in Figure 5.9b. The concrete slab and interior steel beam are heated with radiative and convection boundary conditions (on three-sides) using ISO834 fire for 120 minutes. The temperature distribution across the interior beam

section and the concrete slab is shown in Figure 5.10a and Figure 5.10b, respectively. The legend labels are illustrated in Figure 5.9b.

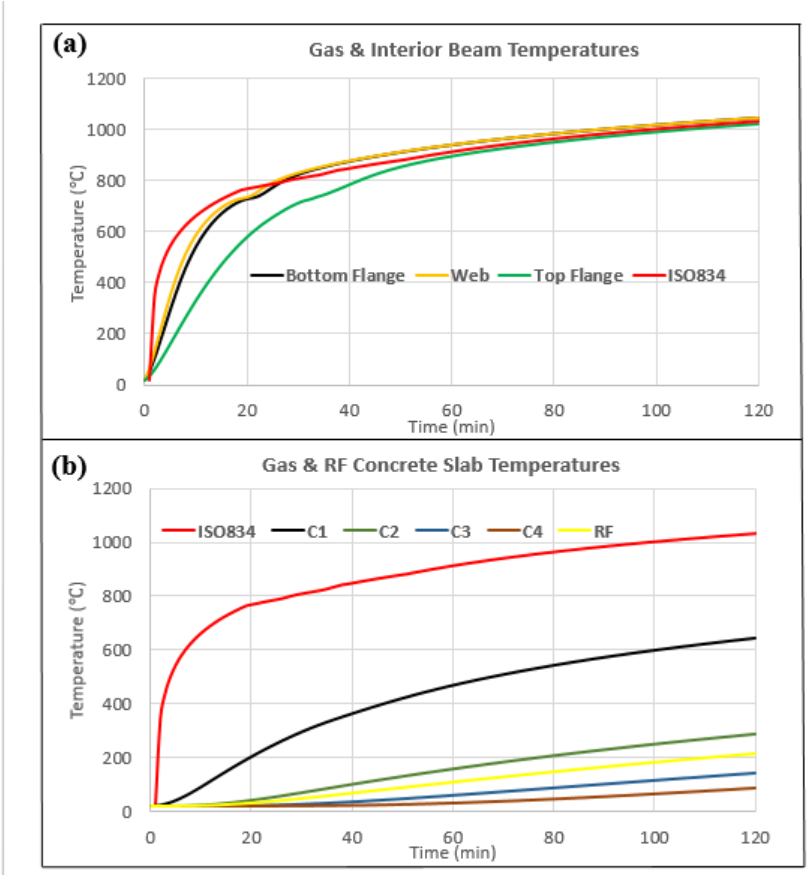

Figure 5.10. 120 minutes ISO834 Fire with the Temperature Distributions (a) Interior Beam (b) Concrete Slab.

Elastic mechanical and thermal material properties of the structural steel, steel reinforcement and concrete used in the finite element analysis are shown in Table 3.2 and Table 3.3. Moreover, structural steel material used in the finite element analysis are assigned plasticity according to Eurocode 1994-1-2 provisions (CEN, 2004) and the concrete material is assigned damaged plasticity criteria to model tensile failure of the concrete material. The structural steel plasticity and the concrete damaged plasticity and tensile behavior are shown in Table 5.1 and Table 5.2, respectively.

Table 5.1. S275 Structural Steel Plasticity.

T (°C)	20	100	200	300	400	500	600	700	800	900	1000	1100
σ_y (MPa)	275	275	275	275	275	214.5	129.3	63.25	30.25	16.5	11	5.5

Table 5.2. C20 Concrete Damaged Plasticity Coefficients Behavior.

φ	ε	f_{b0}/f_{c0}	K	μ
25	0.1	1.16	0.667	0
T (^{o}C)	ε_{cr}	ε_{cr}	f_t (MPa)	f_t (MPa)
0-1200	0	0.0002	1.564	1.095

The finite element model is quasi-statically loaded with a 10 kN/m^2 uniformly distributed load, and the concrete slab and interior beam self-weights. The solution method is an uncoupled thermal-stress analysis, for which the nodal temperatures calculated from the heat transfer analysis are directly transferred to the structural analysis. The analysis method is dynamic-implicit with quasi-static time integration.

5.5.3. Comparison of the FE Analysis and Simplified Method

The composite floor geometry and the loading conditions described in Section 5.5.2, elastic mechanical and thermal material properties listed in Table 3.2 and Table 3.3, and the heat transfer analysis results shown in Figure 5.10a and Figure 5.10b are applied into the Matlab code to compare thermo-mechanical behaviors of the composite floor system obtained from the finite element analysis and the simplified algorithm.

Results of the finite element analysis and the simplified algorithm are compared against the concrete slab mid-point deflections and the membrane forces developed in the steel reinforcements.

Figure 5.11a shows the concrete slab mid-point deflections obtained from the finite element analysis and the simplified algorithm. According to the figure the analysis time that correspond to development of the tensile membrane action nearly the same for the finite element model and simplified algorithm. This analysis time corresponds to the 12^{th} minute of the fire and highlighted in Figure 5.11a at the simplified algorithm mid-point deflection curve. Moreover, at the 12^{th} minute of the fire the membrane forces developed in the steel reinforcement along the X axis are shown in Figure 5.11b and

Figure 5.11c for finite element analysis and simplified algorithm results, respectively. According to Figure 5.11b and 5.11c the membrane forces are relatively close for the finite element analysis and simplified algorithm.

According to Figure 5.11a, at the 22^{nd} minute of the fire the interior steel beam average temperature reaches to 700 ^{o}C and the simplified algorithm switches to plate deflection equation as explained in Section 5.4. Therefore, there is an immediate increase in the mid-point deflections that are obtained from the simplified algorithm in this analysis time. On the other hand, for the finite element analysis due to the existence of the interior steel beam during the entire duration of the fire and the definition of the structural steel plasticity, the rate of deflections does not immediately increase at the 22^{nd} minute of the fire and cause to result large divergence between the simplified algorithm and the finite element analysis results. However, by the initiation of the yielding of the entire interior steel beam section in the finite element analysis, the divergence between the finite element analysis and simplified algorithm decreases and becomes 5.15% at the end of the analyses.

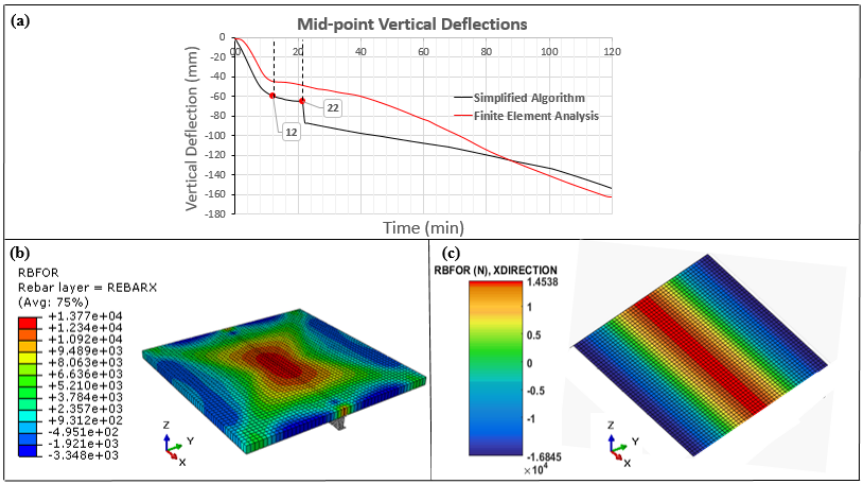

Figure 5.11. (a) Composite Floor Mid-point Deflections for FE Analysis and Simplified Algorithm, Membrane Forces (N) in the Reinforcements along X Axis at the 12^{th} Minute of the Fire (b) FE Analysis (c) Simplified Algorithm.

Figure 5.12a and Figure 5.12b shows the composite floor deflections obtained from the finite element analysis and the simplified algorithm, respectively at the end

of the analyses.

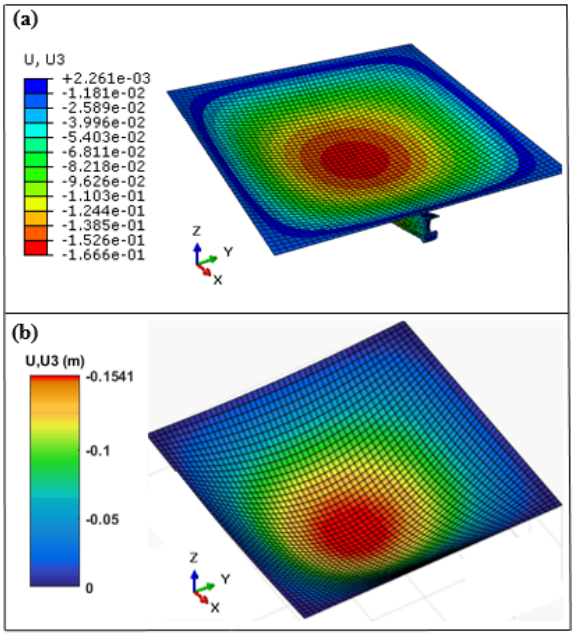

Figure 5.12. Deflections (m) along the Composite Floor at the end of the analysis (120^{th} minute of the Fire) (a) Finite Element Analysis (b) Simplified Algorithm.

In this section, the simplified methodology that is developed to determine thermo-mechanical behavior of composite floor systems is verified against the finite element analysis results with the composite floor mid-point deflections and the membrane forces developed along the steel reinforcements.

5.6. Thermo-Mechanical Behavior of the Composite Floor Systems Located in Building - 4

The verified simplified methodology is utilized to determine thermo-mechanical behavior of the composite floor systems located at the fire compartment ceiling of Building - 4. The geometric properties of the fire compartment are described in Section 4.5.1 and the temperature dependent material properties of the structural steel, steel reinforcement and the concrete are explained in Section 3.3, summarized in Section 5.5.1 and listed in Table 3.2 and Table 3.3. According to Figure 4.50 and Figure 4.51, composite floor assemblies located at the ceiling of the fire compartment are identical

with respect to their geometry, interior steel beams (secondary beams) and concrete slab sections. Moreover, as explained in Section 4.5.2 these composite floor assemblies are subjected to identical fire (Hot-zone Temperatures). On the other hand, these composite floor assemblies are not identical with respect to their boundary conditions. The composite floor assembly that is located between F and E axes does not continue along the E axis, but the composite floor assembly located between D and F axes is continuous along both of D and F axes. Therefore, thermally induced compression forces in the concrete slab will be higher for the composite floor assembly located between D and F axes that's why this composite floor assembly is more critical for fire. Moreover, as described in Section 5.5.1 the Matlab code of the developed simplified methodology is only capable to analyze thermo-mechanical behavior of simply supported composite floor systems. Therefore, thermo-mechanical behavior of the composite floor assembly that is located between D and F axes can be more accurately calculated with the developed simplified methodology.

The analyzed composite floor consist of 7 m by 6 m concrete slab and 3 IPE330 interior beams that are located between D and F axes. Interior beams are located with equal distances between each other as shown in Figure 4.50b. The concrete slab is 200 mm thick and reinforced by S500 strength 100 mm spaced 16 mm diameter longitudinal and transverse steel rebars. The reinforcement is placed at 100 mm below the concrete top surface.

2D heat transfer analysis is conducted in Abaqus for the composite section of the floor assembly. The fire is applied to the concrete bottom surface and three sides of the steel interior beams as illustrated in Figure 5.9b. Temperatures of the layers whose legend labels are shown in Figure 5.9b are given into the Matlab Code as temperature input. Results of the heat transfer analyses across the composite floor depth is shown in Figure 5.13 for the legends labels highlighted in Figure 5.9b.

There is 10 kN/m^2 uniformly distributed live load on the analyzed composite floor assembly as described in Section 4.5.1. Characteristic value of the live load is multiplied by the design load coefficient that is described in Section 3.2 and it is defined in the

Matlab code. Moreover, self-weights of the concrete slab and the interior beams are also defined in the Matlab code. As explained in Section 5.5.1, the Matlab code is only capable to analyze thermo-mechanical behavior of composite floor systems with a single interior steel beam that is located at the one of the mid-length of the concrete slab edges. On the other hand, the investigated composite floor system has 3 interior beams as shown in Figure 4.50b, that's why the interior beams located at the right and left side of the mid-length are not considered in the analysis. Moreover, material cooling phase are not included in the simplified algorithm. Therefore, the analysis is continued until the maximum fire temperature of the first concrete slab layer (C1 Legend Label), this time is highlighted in the Figure 5.13b as 41.29th minute of the fire. In addition, the interior beam is assumed not to re-gain its load carrying capacity even its average temperature becomes lower than 700 ^{o}C. Figure 5.14a shows the mid-point vertical deflections of the composite floor system. According to the figure, tensile membrane action fully develops along the composite floor system at the 18^{th} minute of the fire and rate of vertical deflections decreases immediately. Figure 5.14b and Figure 5.14c show the membrane forces in the steel reinforcements located along X and Y axis, respectively. Due to composite floor geometry (7 m x 6 m) membrane forces in the steel reinforcements are not identical along the X and Y axis. Moreover, as highlighted in the Figure 5.14a, the interior steel beam average temperature reaches to 700 ^{o}C at the 22^{nd} minute of the fire and at this time the interior steel beam is assumed to be failed and taken out from the analysis as explained in Section 5.4.

Therefore, immediate increase in mid-point deflection occurs in this time. The failure time of the interior steel beams matches with the finite element analysis results of the entire structure that is described in Section 4.5.3. After the failure of the interior steel beam, tensile membrane action continues to govern deflection behavior of the composite floor system and rate of deflections does not increase and becomes 0.38 mm/min at the end of the analysis.

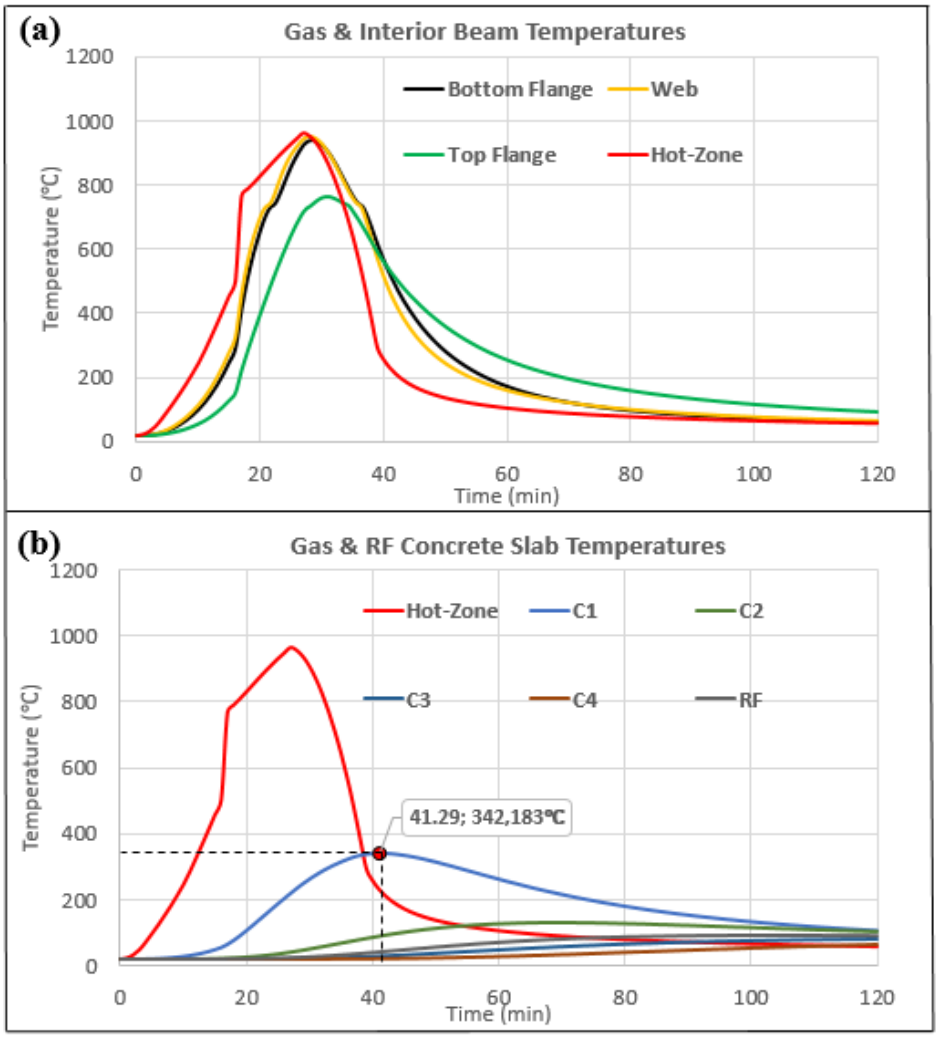

Figure 5.13. Hot-Zone Temperatures of Building - 4 with the Temperature Distribution Across the (a) Interior Beams (b) Concrete Slab.

According to results of Cardington Fire Tests (Vassart and Zhao, 2011) and the studies conducted by Lin and Wade (2002), development of tensile membrane action along reinforced concrete slab increases structural performance of composite floor systems under fire conditions and these floor assemblies can maintain large deflections. As a result, the analysis of the investigated composite floor system does not terminate and converge in all iteration steps of the analysis. Therefore, the composite floor systems located at the ceiling of the fire compartment of Building - 4 would not have collapsed if the perimeter beams survive during the fire. However, as explained in Section 4.5.3 perimeter beams of the composite floor system collapse due to initiation

of the runaway vertical displacements at mid-length of the beams, thus the composite floor system located at the ceiling of the fire would have assumed to collapse as well.

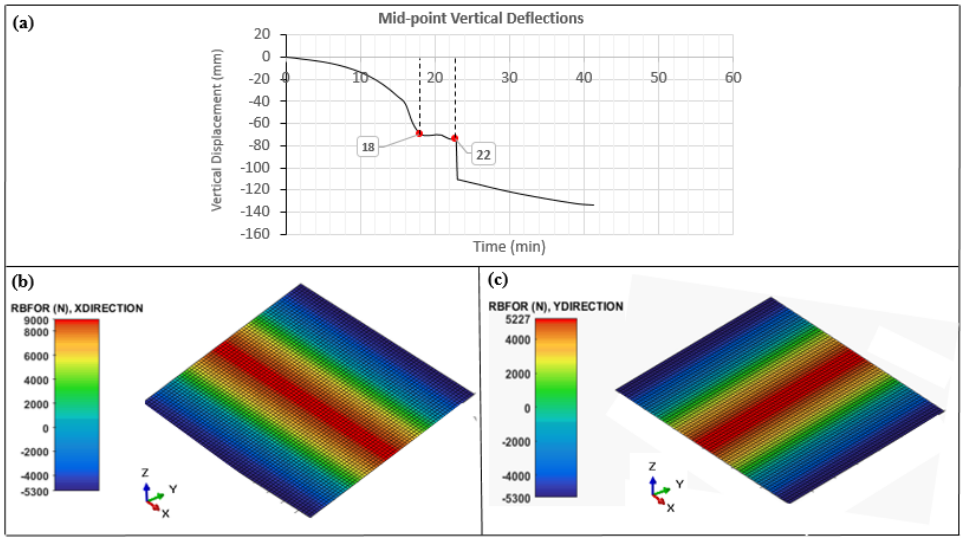

Figure 5.14. (a) Composite Floor Mid-point Deflections (b) Membrane Forces (N) in the Steel Reinforcement along X Axis at the 18^{th} Minute of the Fire (c) Membrane Forces (N) in the Steel Reinforcement Located along Y Axis at the 18^{th} Minute of the Fire.

Figure 5.15 shows the composite floor deflections at the end of the analysis. The maximum deflection (134.06 mm) occurs at the mid-point of the composite floor system.

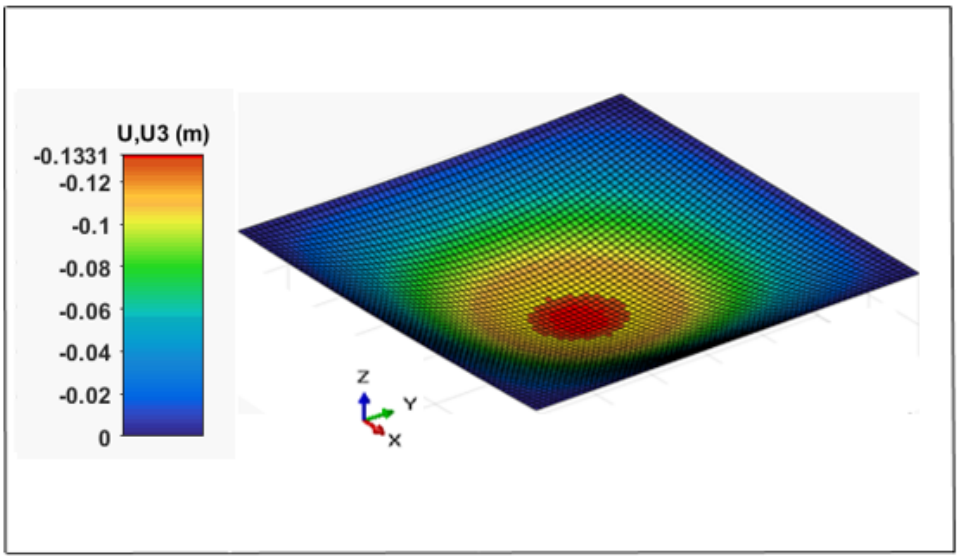

Figure 5.15. Deflections (m) Along the Composite Floor at the end of the Analysis (41.29^{th} Minute of the Fire).

6. SUMMARY AND CONCLUSIONS

6.1. Summary

The aim of this study is to investigate the structural performance of large scale industrial buildings under fire conditions. However, according to the literature, simulating large scale industrial building fires is not possible with the prescribed methods and it is too complex with the advanced computational fire dynamic methods. Moreover, advanced fire simulation methods must be verified with experimental research or real fire event data before they are used for design purposes. Therefore a new fire simulation approach is developed with consideration of local fire and global fire scenarios together for large scale industrial buildings.

Detailed performance-based structural fire safety concept is adopted to investigate fire performance of 5 different industrial buildings. Selection of these buildings are made with respect to their specific structural and fire characteristics to reflect suitability of the application of the developed simplified methodologies for performance-based structural fire safety concept of industrial buildings.

Zone modelling fire simulation technique is numerically studied by Pettersson (1976) firstly. Usage of the zone modelling technique to create fire simulations of the industrial buildings which is the one of the base line of this study, is described in detail. In addition, due to highly non-linear material and geometric behavior under fire conditions, it is required to conduct performance-based dynamic structural analysis for entire structure. Therefore, detailed finite element modelling techniques are adopted to model entire structure and capture realistic performance of the buildings. Fire simulation results are used to conduct heat transfer analyses which are incorporated with finite element analyses of the buildings.

Current closed form equations to calculate plate deflection under thermal gradient are improved to consider uniformly distributed membrane forces along the plate edges

and incorporated with the transformed area method (Gere, 2004) and implemented to a new simplified methodology that is developed to determine thermo-mechanical behavior of steel-framed reinforced concrete slab composite floor systems. Moreover, one of the building's composite floor system fire performance is investigated with the developed simplified algorithm.

Table 6.1. Summary of the Fire Simulations and Finite Element Analyses.

FIRE SIMULATION RESULTS					
Assessments	Building -1	Building -2	Building -3	Building -4	Building -5
Switching from Two-zone fire model to One-zone fire model (min.)	28	34	33	10	4
Local Fire Scenario	YES	YES	YES	NO	NO
Maximum Local Fire Temperature (^oC)	900	758	900	-	-
Time of the Maximum Local Fire Temperature (min.)	12.4	7.6	16.2	-	-
Local Fire Maximum Flame Length (m)	8	2	9	-	-
Time of the Flashover (min.)	32	70	53	16	13
Maximum Hot-zone Temperature (^oC)	979	1208	1300	962	1172
Time of the Maximum Hot-zone Temperature (min.)	37	89	61	27	58
Maximum Fire Area (m^2)	1105	2800	2678	84	69.17
Maximum Rate of Heat Release (MW)	552.5	700	935	21	17.29
Initiation of the Cooling Phase (min.)	38	90	62	28	59
FINITE ELEMENT ANALYSIS RESULTS					
Assessments	Building -1	Building -2	Building -3	Building -4	Building -5
Column Failure in the Structurally Critical Region (min.)	44.7	91.8	54.7	-	-
Rafter Failure in the Structurally Critical Region (min.)	N/A	92	66.4 - 68.3	-	-
Collapse of the Structurally Critical Region (min.)	N/A	92	63.3 - 66.4	-	-
Column Failure in the Structurally Column Failure in the Structurally	N/A	112.8	67.3	N/A	74.5
Rafter Failure in the Structurally Non-critical Regions (min.)	N/A	91.4	61.8	-	-
Perimeter Beam Failure in the Fire Compartment (min.)	-	-	-	28.3	27.9
Secondary Beam Failure in the Fire Compartment (min.)	-	-	-	20.4	N/A
Collapse of the Structure (min)	N/A	91.4	69.5	28.3	27.9

6.2. Conclusions

The following conclusions can be drawn on the basis of the fire simulations, finite element analyses results and the results obtained from the developed simplified methodology.

- The fire simulation results of the investigated buildings showed that there might be slightly different fire behavior for large scale industrial buildings depending on their geometry, and fire characteristics.
- It is demonstrated that, prescribed fire simulations methods do not reflect realistic large scale building fires due to non-consideration of pre-flashover fire phase and local fire scenarios.
- It is obtained that the fire induced performance of the structural members that are located around the localized fire region mostly determine the structural performance of the entire building. Therefore, it is important to distribute fire load uniformly and avoid to store large amounts of localized fire loads inside industrial buildings.
- It is demonstrated that single structural member failure does not cause collapse of the entire structure due to load-redistribution phenomenon and post-failure strength of the structural member.
- Finite element analyses results showed that there is a close relationship between failure criteria determined by the studies of Gernay *et al.* (2016), Eurocode (CEN, 2005) and British Standard Institute (BS-476, 1976). Once the structural members fail against one of these criteria they also fail against the other ones with a short time interval.
- According to the finite element analyses of the buildings, only two of the five building satisfy the prescribed fire resistance rating and the other three of the buildings are collapsed before satisfying their required fire resistance rating.
- Thermo-mechanical behavior of composite floor systems are accurately estimated with the developed simplified methodology and results obtained from the simplified algorithm are verified against finite element model.
- Comparing the results obtained from the simplified algorithm and the finite element analysis, it is observed that mid-span deflections of the composite floor system that exists in Building - 4 reduced 64% with the consideration of the reinforced concrete slab. However, while the simplified algorithm indicates non-failure of the composite floor systems, the failure of the perimeter beams in the finite element model results the collapse of the composite floor systems located in Building - 4.

- Another important result obtained from this study is related with the activation of tensile membrane forces with in the composite floor systems due to large deflections under fire. The verified simplified algorithm shows that increasing tensile load capacity of the reinforced concrete slab can increase the fire performance of the composite floor systems.

6.3. Recommended Future Studies

The following recommendations can be made for future studies related with the scope of this thesis:

- The simplified fire simulation method that includes pre-flashover fire phase and localized fire scenario can be validated with advanced computational fire dynamic simulations and structural performance of the industrial buildings can be re-investigated with results of the advanced fire simulations.
- Thermo-mechanical behavior of composite floor systems for different boundary conditions other than simply supported boundary condition can be added to the developed simplified algorithm.
- Determination of thermo-mechanical behavior of composite floor systems with more than one interior beam can be added to the developed simplified algorithm.
- Material plasticity and damage criteria, and stress-strain control algorithm can be implemented into the developed simplified methodology to understand effects of plastic material behavior to fire induced performance of composite floor systems.
- Future studies can also include effects of stress resultant that arise from fire induced behaviors of composite floor to entire structure performance.

REFERENCES

American Institute of Steel Construction, 2005, *Specifications for Steel Buildings American Institute of Steel Construction 360-05*, American Institute of Steel Construction, Reston, Virginia.

American Society for Testing and Materials, 2016, *Standard Test Method for Fire Tests of Building Construction and Material American Society for Testing and Materials E-119*, American Society for Testing and Materials, United States of America.

American Society of Civil Engineers, 1992, *Structural Fire Protection - Manual of Practice*, American Society of Civil Engineers, Reston, Virginia.

American Society of Civil Engineers, 2007, *Seismic Rehabilitation of Existing Buildings American Society of Civil Engineers, Stockholm Environment Institute-41/06*, American Society of Civil Engineers, Reston, Virginia.

Association of Specialist Fire Protection, 2014, *Yellow Book: Fire Protection for Structural Steel in Buildings, 5^{th} Edition*, Association of Specialist Fire Protection, Hampshire, United Kingdom.

Babrauskas V, R.B. Willamson, 1978, "The Historical Basis of Fire Resistance Testing - Part I and II", *Fire Technology*, Vol. 14, No. 3, pp. 184-194 and Vol. 14, No. 4, pp. 314-316.

Badger, S.G., 2015, "Large Loss Fire in the United States 2014", *National Fire Protection Association*, United States of America.

Bailey, C., 2004, "Structural Fire Design: Core of Specialist Subject?", *The Structural Engineer*, Vol. 82, pp. 32-38.

Barnett C.R., G.C. Clifton, 2004, "Examples of Fire Engineering Design for Steel Mem-

bers Using Standard Curve versus A New Parametric Curve", *Fire and Materials*, Vol.28, No. 24, pp. 309-322.

Barnett, C.R., 2002, "A New Empirical Model for Fire Compartment Temperatures", *Fire Safety Journal*, Vol. 37, No. 5, pp. 437-463.

Barnett, C.R., 2007, "Replacing International Temperature-Time Curves with BFD Curve", *Fire Safety Journal*, Vol. 42, No.4, pp. 321-327.

Behnam B., F.H. Rezvani, 2014, "Evaluation of Tall Steel Moment-Resisting Structures in Simulated Horizontally Traveling Postearthquake Fire", *Journal of Performance of Constructed Facilities*, Vol. 30, No. 2, pp. 04014207.

Boring, D.E., J.C. Spence, W.G. Wells, 1981, *Fire Protection through Modern Building Codes*, 5^{th} Edition, American Iron and Steel Institute, Washington, District of Columbia.

British Standards Institution, 1987, *Fire Test on Building Materials and Structures. Method for Determination of Elements of Construction (General Principles), 476-20.*

Cadorin J.F., J.M. Franssen, D. Pintea, 2001, *The Design Fire Tool Ozone V2.0 - Theoretical Description and Validation On Experimental Fire Test*, University of Liege, Liege.

Campbell, R., 2016, *Fire in Industrial or Manufacturing Properties*, National Fire Protection Association, United States of America.

Canadian Wood Council 1996, *Fire Safety Design in Buildings*, Canadian Wood Council, Ottawa.

Deutsches Institut für Normung, 1998, *Fire Behaviour of Building Materials and Building Components - Part 1: Building Materials; Concepts, Requirements and Tests - Deutsches Institut für Normung 4102-1*, Deutsches Institut für Normung, Ger-

many.

Donnell, L.H., 1976, *Beams, Plates and Shells*, 6^{th} Edition, McGraw-Hill, New York.

Drysdale, D., 1985, *An Introduction to Fire Dynamics*, John Wiley & Sons Inc, United Kingdom.

DS-Simulia, 2012, *ABAQUS Version 6.12 Documentation*, Providence, Rhode Island.

European Committe for Standardization, 2002, *Eurocode 1: Actions on Structures - Part 1-1: General Actions - Densities, Self-weight, Imposed Loads for Buildings EN 1992-1-1*, Brussels, Belgium.

European Committee for Standardization, 2002, *Eurocode 1: Basis of Design and Actions on Structures: Part 1-2 Actions on Structures Exposed to Fire ENV 1991-1-2*, Brussels, Belgium.

European Committee for Standardization, 2005, *Eurocode 3: Design of Steel Structures - Part 1-2 General Rules - Structural Fire Design - EN 1993-1-2*, European Committee for Standardization, Brussels, Belgium.

European Committee for Standardization, 2005, *Eurocode 3: Design of Steel Structures - Part 1-1: General Rules and Rules for Buildings - EN 1993-1-1*, European Committee for Standardization, Brussels, Belgium.

European Committee for Standardization, 2005, *Eurocode 4: Design of Composite Steel and Concrete Structures - Part 1-2: General Rules - Structural Fire Design - EN 1994-1-2*, CEN, Brussels, Belgium.

European Committee for Standardization and British Standards Institution, 1996, *Eurocode 1: Basis of Design and Actions on Structures: Part 2.2 Actions of Structures Exposed to Fire - ENV 1991-2-2*, European Committee for Standardization, Brussels, Belgium.

European Convention for Constructional Steelwork Technical Committee 3, 2001, *Model Code on Fire Engineering*, No.111, European Convention for Constructional Steelwork, Brussels, Belgium.

Fransen, J.M., 2000, "Failure Temperature of a System Comprising a Restrained Column Submitted to Fire", *Fire Safety Journal*, Vol. 34, pp. 191-207.

Franssen, J.M, P.V. Real, 2015, *Fire Design of Steel Structures*, European Convention for Constructional Steelwork and Ernst & Sohn, Second Edition, Oxford, United Kingdom.

Franssen, J.-M., 2015, "SAFIR: A Thermal/Sturctural Program for Modeling Structures Under Fire", *Engineering Journal*, Vol. 42, No. 3, pp. 143-158.

Franssen, J.M., V. Kodur, R. Zaharia, 2009, *Designing Steel Structures for Fire Safety*, Committee on the Rights of the Child Press/Balkema.

Gere, J.M., 2004, *Mechanics of Materials*, 6^{th} Edition, Thomson Learning, Belmont.

Gernay, T., N.E Khorasani, M. Garlock, 2016, "Fire Fragility Curves for a Steel Buildings in a Community Context: A Methodology", *Engineering Structures*,Vol. 113, pp. 259-276.

Gilvery, K., R. Dexter,1997, "Evaluation of Alternative Methods for Fire Rating Structural Members, Building and Fire Research Laboratory", *National Institute of Standards and Technology.*

Guo-wei, Z., Z. Guo-qing, W. Xiao-Ian, W. Wei-hua, 2011,"The Comparison of Fire Numerical Simulations based on the Large Space Factory Fire Experiment", Yao H.-W. editions, *The 5^{th} Conference on Performace-based Fire and Fire Protection Engineering*, Guangzhou, China, December 2010, Elsevier Procedia Engineering.

Hailemichael, K., B. Liivo, 2014, *Stability of Slender Columns*, M.Sc. Thesis, Lund University.

Huang, Z., I.W. Burgess, R.J. Plank, 2000, "Three Dimensional Analysis of Composite Steel Framed Building in Fire", *Journal of Structural Engineers*, Vol. 126, No. 3, pp. 389-397.

Ingberg, S.H., 1928, "Tests of the Severity of Building Fires", *National Fire Protection Association Quarterly*, Vol, 22, No. 1, pp. 43-61.

International Code Council, 2001, *Performance Code for Buildings and Facilities*, International Code Council, Falls Church, Veterans Affairs.

International Organization for Standardization, 1999, *Fire resistance tests - Elements of Building Construction - Part 1: General Requirements International Organization for Standardization 834-1:1999*, International Organization for Standardization, Geneva, Switzerland.

Jarmai, K., 2010, "Design Softwares of Steel Structure for Fire Safety", International Institute of Welding, Vol. 1, pp. 87-10.

Jiang, J., Li, G.Q., A. Usmani, 2014,"Progressive Collapse Resistance Braced Steel Frames Exposed to Fire", X. Liu and A.H.S Ang editions, *Sustainable Development of Critical Infrastructure*, Shanghai, May 2014, American Society of Civil Engineers, United States of America.

Johann, M.A., L. Albano, R. Fitzgerald, and B. Meacham, 2006, "Performance-Based Structural Fire Safety", *Journal of Performance of Constructed Facilities*, Vol. 20, No. 1, pp. 45-53.

Johann, M.A., 2002, *Fire-Robust Structural Engineering: A framework Approach to Structural Design for Fire Conditions*, M.Sc. Thesis, Worcester Polytechnic Institute.

Khazaeinejad P., X. Dai, A.S. Usmani, 2015, "Analysis of Heated Beams: Modelling Benchmark", *The First International Conference on Structural Safety under Fire*

& Blast, Glasgow, Vol. 1, pp. 469-473.

Kılınc, S., S. Selamet, 2013, "Symmetric and Asymmetric Collapse Mechanism of a Multi-Story Steel Structure Subjected to Gravity and Fire", Brian, J.L., Jonathan, M. editions, *Structures Congress 2013: Bridging Your Passion with Your Profession*, Pittsburgh, May 2013, American Society of Civil Engineers, United States of America.

Law, M., 1983, "A Basis for the Design of Fire Protection of Building Structures", *The Structural Engineer*, Vol. 61, No. A, pp. 25-33.

Lennon, T., D. Moore, 2003, "Natural Fire Safety Concept - Full-scale Tests at Cardington", *Fire Safety Journal*, Vol. 38, pp. 623-643.

Lie, T.T., 1974, "Characteristics Temperature Curves for Various Fire Severities", *Fire Technology*, Vol. 10, No. 4, pp. 315-326.

Lim, L., C. Wade, 2002, "Experimental Fire Tests of Two-Way Concrete Slabs", *Fire Engineering Research Report*, 02/12, University of Canterbury, New Zealand.

Lu, X., Y. Li, H. Guan, et al., 2016, "Progressive Collapse Analysis of a Typical Super-Tall Reinforced Concrete Frame-Core Tube Building Exposed to Extreme Fires", *Fire Technology*, Vol. 10694, pp. 1-27.

Magnusson, S.E., S. Thelandersson, 1970, "Temperature-time Curves of Complete Process of Fire Development", *Bulletin of Division of Structural Mechanics and Concrete Construction*, Vol. 16.

National Fire Protection Association, 2002, *Building Construction and Safety Code National Fire Protection Association 5000*, National Fire Protection Association, Quincy, Mass.

National Fire Protection Association, 2015, *Standard Methods of Test of Fire Resistance of Building Construction and Materials National Fire Protection Association*

251, National Fire Protection Association, United States of America.

National Research Council of Canada, 1995, *National Building Code of Canada*, Associate Committee on the National Building Code, Ottawa.

Neal, M., M. Garlock, S. Quiel, and S. Marjanishvili, 2012,"Effects of Fire on a Tall Steel Building Designed to Resist Progressive Collapse", Carroto, J., Burns, J. editions, *Structures Congress 2012*, Chicago, United States of America, March 2012, American Society of Civil Engineers, United States of America.

Parkinson, D.L, V. Kodur, 2006, "Performance Based Design of Structural Steel for Fire Conditions: A Calculation Methodology", *Structures Congress 2006: Structural Engineering and Public Safety*, Missouri, United States of America, May 2006, American Society of Civil Engineers, United States of America.

Parkinson, D.L., 2002, *Performance Based Design of Structural Steel for Fire Conditions*, M.Sc. Thesis, Worchester Polytechnic Institute.

Pettersson O., S.E. Magnusson, J. Thor, 1976, "Fire Engineering Design of Steel Structures", *Bulletin of Division of Structural Mechanics and Concrete Construction*, Vol. 52.

Pettersson, O., 1978, "Structural Fire Protection Report at Commercial International Bank W14 Meeting", International Council of Buildings, *Commercial International Bank W14*, Copenhagen, 1998, Lund University, Lund.

Portier R.W., P.A. Reneke, W.W. Jones, and R.D. Peacock, 1992,"User´s Guide for Cfast Version 1.6", NISTIR-4985, 1992.

Quiel, S., M. Garlock, 2008, "Modelling High Rise Steel Framed Buildings Under Fire", D. Anderson, C. Ventura, D. Harvey, M. Hoit, *Structures Congress 2008: Crossing Borders*, Vancouver, April 2008, American Society of Civil Engineers, United States of America.

Quiel, S.E, S.M. Marjanishvilli, S.M, 2012, "Fire Resistance of a Damaged Steel Building Frame Designed to Resist Progressive Collapse", *Journal of Performance of Constructed Facilities*, Vol. 26, No. 4, pp. 402-409.

Republic of Turkey Ministry of Environment and Urbanization, 2009, *Binaların Yangından Korunması Hakkında Yönetmelik*, Turkish Official Journal, 27344, 45, Turkey.

Rini, D. and Lamont, S., 2008, "Performance Based Structural Fire Engineering for Modern Building Design", Anderson, D., Ventura, C., Harvey, D., Hoit, M. editions, S*tructures Congress 2008: Crossing Borders*, Vancouver, April 2008, American Society of Civil Engineers, United States of America.

Rini, D., R. Gerard, I. Almufti, and G. Nielson, 2011, "Structural Fire Engineering for Modern Building Design-Case Study", *Building Integrated Solution*, Architectural Engineering Conference 2011, pp. 351-360.

Selamet, S., 2013, "Fire Performance of an Unprotected Composite Beam, Behavior with Finite Beam End Restraints, Rebar Size and Locations", Wald F., Burges I., Horova K., Jana T., Jirku T. editions, *Application of Structural Fire Engineering*, Prague, April 2013, Creative Talents Unleashed Publishing House, Czech Technical University in Prague.

Selamet, S., Garlock, M., 2011, "A Comparison between Single Plate and Angle Shear Connection Performance under Fire", D. Ames, T.L. Droessler, M. Hoit, editions, *Structures Congress*, Las Vegas, April 2011, American Society of Civil Engineers, United States of America.

Selamet, S., M. Garlock, 2014, "Fire Resistance of Steel Shear Connections", *Fire Safety Journal*, Vol. 68, pp. 52-60.

Shepherd, P.G., 1999, *The Performance in Fire of Restrained Columns in Steel-Framed Construction*, PhD Thesis, University of Sheffield.

Society of Fire Protection Engineers, 2002, Handbook of Fire Protection Engineering, 3^{rd} Edition, National Fire Protection Association.

Stahl CraneSystems, 2008, *Product Information Technical Manual*, STAHL CraneSystems GmbH, Germany.

Sultan, M.A., 1996, "Effect of Furnace Parameters on fire Everity in Standard fire Resistance Tests", *Fire Mater*, Vol. 20, No. 5, pp. 245-252.

Thomas, P.H., 1986, "Design Guide Structural Fire Safety - Commercial International Bank W14 Workshop Report", *Fire Safety Journal*, Vol. 10, pp. 77-137.

Thomson, G., R.B. Preston, 1996, "Towards Harmonized Standard fire Resistance Testing", *Fire Safety Journal*, Vol. 27, No. 2, pp. 91-112.

Turkish Standard Institution, 1997, Turkish Standard of Design Loads for Buildings - TS498, Turkish Standard Institution, Ankara.

Ugural, A.C., 1981, *Stresses in Plates and Shell*, McGraw-Hill, New York.

Usmani, A.S., J.M. Rotter, S. Lamont, A.M. Sanad, M. Gillie, 2001, "Fundamental Principle Structural Behavior under Thermal Effects", *Fire Safety Journal*, Vol. 36, pp. 721-744.

Vassart O., Z. Bin, 2013, *Membrane Action of Composite Structures in Case of Fire*, Emergency Core Cooling Systems, Brussels, Belgium.

Vassort, O., L.G. Cajot, M. O'Connor, Y. Shenkai, C. Fraud, Zhao, et al., "3D Simulation of Industrial Hall in case of Fire: Benchmark between ABAQUS, ANSYS and SAFIR", *10^{th} International Fire Science and Engineering (Interflam) Conference*, London, UK, July 2004, Interscience Communications Limited, UK, 2004.

Wang, Y.C., D.B. Moore, 1994, "Effect of Thermal Restraint on Column Behavior in a Frame", T. Kashiwagi, *Proc. 4^{th} International Symposium on fire Safety*

Science, Ottawa, June 1994, International Association for Fire Safety Science, United States of America, Maryland.

Wickstrom U, 1981, "Temperature Calculation of Insulated Steel Columns Exposed to Natural Fire", *Fire Safety Journal*, Vol. 4, pp. 219-25.

Zaforteza, I., and M. Garlock, 2012, "A Numerical Investigation on the Fire Response of a Steel Girder Bridge", *Journal of Constructional Steel Research*, Vol. 75, No. 08, pp. 93-103.

Zehfuss, J., D. Hosser, 2007, "A Parametric Natural Fire Model for the Structural Fire Design of Multi-storey Buildings", *Fire Safety Journal*, Vol. 42, pp. 115-126.

Zhou, Y., Z. Sun, Q. Gao, 2016,"Performance-based fire Protection Design of Ruins Pavilion Based on Air-supported Membrane Structure", J. Taler, A. Mohamad, A.C. Benim, editions, *7th International Conference on Performance-based Fire and Fire Protection Engineering 20015*, December 2015, Guangzhou, Elsevier Ltd., Procedia Engineering Vol. 157, pp. 486-494.

APPENDIX A: FIRE SIMULATION PARAMETERS OF THE BUILDINGS

PARAMETERS

Openings

Radiation Through Closed Openings:	0,8
Bernoulli Coefficient:	0,7

Physical Characteristics of Compartment

Initial Temperature:	293 K
Initial Pressure:	100000 Pa

Parameters of Wall Material

Convection Coefficient at the Hot Surface:	25 W/m²K
Convection Coefficient at the Cold Surface:	9 W/m²K

Calculation Parameters

End of Calculation:	7200 sec
Time Step for Printing Results:	60 sec
Maximum Time Step for Calculation:	10 sec

Air Entrained Model:	Heskestad

Temperature Dependent Openings

All openings activated at:	400 °C

Stepwise Variation

Temperature [°C]	% of Total Openings [%]
20	10
400	50
500	100

Linear Variation

Temperature [°C]	% of Total Openings [%]
20	10
400	50
500	100

Time Dependent Openings

Time [sec]	% of Total Openings [%]
0	5
1200	100

Figure A.1. General Fire Parameters of Building.

COMPARTMENT

Form of Compartment:	Rectangular Floor	
Height:	17	m
Depth:	26	m
Length:	42,5	m
Roof Type:	Double Pitch Roof	
Celling Height:	3,5	

DEFINITION OF ENCLOSURE BOUNDARIES

Floor

Material (from inside to outside)	Thickness [cm]	Unit Mass [kg/m³]	Conductivity [W/mK]	Specific Heat [J/kgK]
Normal weight Concrete [EN1994-1-2]	20	2300	1,6	1000

Ceiling

Material (from inside to outside)	Thickness [cm]	Unit Mass [kg/m³]	Conductivity [W/mK]	Specific Heat [J/kgK]
PUR	15	30	0,026	1470

Wall 1

Material (from inside to outside)	Thickness [cm]	Unit Mass [kg/m³]	Conductivity [W/mK]	Specific Heat [J/kgK]
PUR	15	30	0,026	1470

Openings

Sill Height [m]	Soffit Height [m]	Width [m]	Variation	Adiabatic
0	2,1	1	Constant	no

Wall 2

Material (from inside to outside)	Thickness [cm]	Unit Mass [kg/m³]	Conductivity [W/mK]	Specific Heat [J/kgK]
PUR	15	30	0,026	1470

Openings

Sill Height [m]	Soffit Height [m]	Width [m]	Variation	Adiabatic
0	5	20	Constant	no
0	2,1	1	Constant	no
11	13	4	Constant	no

Wall 3

Material (from inside to outside)	Thickness [cm]	Unit Mass [kg/m³]	Conductivity [W/mK]	Specific Heat [J/kgK]
PUR	15	30	0,026	1470

Openings

Sill Height [m]	Soffit Height [m]	Width [m]	Variation	Adiabatic
0	2,1	1	Constant	no
11	13	2	Constant	no
11	13	2	Constant	no

Wall 4

Material (from inside to outside)	Thickness [cm]	Unit Mass [kg/m³]	Conductivity [W/mK]	Specific Heat [J/kgK]
PUR	15	30	0,026	1470

Openings

Sill Height [m]	Soffit Height [m]	Width [m]	Variation	Adiabatic
0	5	20	Constant	no
11	13	5	Constant	no

Figure A.2. Compartment Details of Building.

FIRE

Fire Curve:	NFSC Design Fire			
Maximum Fire Area:	1105	m²		
Fire Elevation:	0	m		
Fuel Height:	0	m		
Occupancy	Fire Growth Rate	RHRf [kw/m²]	Fire Load qf,k [MJ/m²]	Danger of Fire Activation
User Defined	150	500	136,35	1

Active Measures Description	Active	Value
Automatic Water Extinguishing System	No	$\delta_{n,1} = 1$
Independent Water Supplies	No	$\delta_{n,2} = 1$
Automatic Fire Detection by Heat	Yes	$\delta_{n,3} = 0,87$
Automatic Fire Detection by Smoke	No	
Automatic Alarm Transmission to Fire Brigade	No	$\delta_{n,5} = 1$
Work Fire Brigade	No	$\delta_{n,6} = 1$
Off Site Fire Brigade	No	
Safe Access Routes	Yes	$\delta_{n,8} = 1$
Staircases Under Overpressure in Fire Alarm	No	
Fire Fighting Devices	Yes	$\delta_{n,9} = 1$
Smoke Exhaust System	No	$\delta_{n,10} = 1,5$

Fire Risk Area:	1105	m²	$\delta_{q,1} = 1,76$
Danger of Fire Activation:			$\delta_{q,2} = 1$
$q_{f,d}$=	250,5	MJ/m²	
Combustion Heat of Fuel:	17,5	MJ/kg	
Combustion Efficiency Factor:	0,8		
Combustion Model:	Extended fire duration		

Figure A.3. Detailed Fire Parameters of Building.

PARAMETERS

Openings

Radiation Through Closed Openings:	0,8
Bernoulli Coefficient:	0,7

Physical Characteristics of Compartment

Initial Temperature:	293 K
Initial Pressure:	100000 Pa

Parameters of Wall Material

Convection Coefficient at the Hot Surface:	25 W/m²K
Convection Coefficient at the Cold Surface:	9 W/m²K

Calculation Parameters

End of Calculation:	7200 sec
Time Step for Printing Results:	60 sec
Maximum Time Step for Calculation:	10 sec

Air Entrained Model:	Heskestad

Temperature Dependent Openings

All openings activated at:	400 °C

Stepwise Variation

Temperature [°C]	% of Total Openings [%]
20	10
400	50
500	100

Linear Variation

Temperature [°C]	% of Total Openings [%]
20	10
400	50
500	100

Time Dependent Openings

Time [sec]	% of Total Openings [%]
0	5
1200	100

Figure A.4. General Fire Parameters of Building.

COMPARTMENT

Form of Compartment:	Rectangular Floor	
Height:	15,5	m
Depth:	40	m
Length:	70	m
Roof Type:	Single Pitch Roof	
Ceiling Height:	4	

DEFINITION OF ENCLOSURE BOUNDARIES

Floor

Material (from inside to outside)	Thickness [cm]	Unit Mass [kg/m³]	Conductivity [W/mK]	Specific Heat [J/kgK]
Normal weight Concrete [EN1994-1-2]	20	2300	1,6	1000

Ceiling

Material (from inside to outside)	Thickness [cm]	Unit Mass [kg/m³]	Conductivity [W/mK]	Specific Heat [J/kgK]
PUR	15	30	0,026	1470

Wall 1

Material (from inside to outside)	Thickness [cm]	Unit Mass [kg/m³]	Conductivity [W/mK]	Specific Heat [J/kgK]
PUR	15	30	0,026	1470

Openings

Sill Height [m]	Soffit Height [m]	Width [m]	Variation	Adiabatic
0	2,1	2	Constant	no
5	6	6	Constant	no

Wall 2

Material (from inside to outside)	Thickness [cm]	Unit Mass [kg/m³]	Conductivity [W/mK]	Specific Heat [J/kgK]
PUR	15	30	0,026	1470

Openings

Sill Height [m]	Soffit Height [m]	Width [m]	Variation	Adiabatic
0	2,1	2	Constant	no
5	6	7	Constant	no
0	5	5	Constant	no
9	11	12	Constant	no

Wall 3

Material (from inside to outside)	Thickness [cm]	Unit Mass [kg/m³]	Conductivity [W/mK]	Specific Heat [J/kgK]
Gas-concrete Bricks	20	550	0,14	840

Openings

Sill Height [m]	Soffit Height [m]	Width [m]	Variation	Adiabatic
0	2,1	1	Constant	no
0	5	5	Constant	no
0,75	1,75	6	Constant	no

Wall 4

Material (from inside to outside)	Thickness [cm]	Unit Mass [kg/m³]	Conductivity [W/mK]	Specific Heat [J/kgK]
PUR	15	30	0,026	1470

Openings

Sill Height [m]	Soffit Height [m]	Width [m]	Variation	Adiabatic
0	2,1	2	Constant	no
5	6	8	Constant	no
9	11	12	Constant	no

Figure A.5. Compartment Details of Building.

FIRE

Fire Curve:	NFSC Design Fire		
Maximum Fire Area:	1105	m²	
Fire Elevation:	0	m	
Fuel Height:	0	m	

Occupancy	Fire Growth	RHRf	Fire Load qf,k	Danger of Fire
Rate [kw/m²]	[MJ/m²]	Activation		
User Defined	150	500	136.35	1

Active Measures

Description	Active	Value
Automatic Water Extinguishing System	No	$\delta_{n,1} = 1$
Independent Water Supplies	No	$\delta_{n,2} = 1$
Automatic Fire Detection by Heat	Yes	$\delta_{n,3} = 0.87$
Automatic Fire Detection by Smoke	No	
Automatic Alarm Transmission to Fire Brigade	No	$\delta_{n,5} = 1$
Work Fire Brigade	No	$\delta_{n,6} = 1$
Off Site Fire Brigade	No	
Safe Access Routes	Yes	$\delta_{n,8} = 1$
Staircases Under Overpressure in Fire Alarm	No	
Fire Fighting Devices	Yes	$\delta_{n,9} = 1$
Smoke Exhaust System	No	$\delta_{n,10} = 1.5$

Fire Risk Area:	1105	m²	$\delta_{q,1} = 1.76$
Danger of Fire Activation:			$\delta_{q,2} = 1$
$q_{f,d}$=	250.5	MJ/m²	

Combustion Heat of Fuel:	17.5	MJ/kg
Combustion Efficiency Factor:	0.8	
Combustion Model:	Extended fire duration	

Figure A.6. Detailed Fire Parameters of Building.

PARAMETERS

Openings

Radiation Through Closed Openings:	0.8
Bernoulli Coefficient:	0.7

Physical Characteristics of Compartment

Initial Temperature:	293 K
Initial Pressure:	100000 Pa

Parameters of Wall Material

Convection Coefficient at the Hot Surface:	25 W/m²K
Convection Coefficient at the Cold Surface:	9 W/m²K

Calculation Parameters

End of Calculation:	7200 sec
Time Step for Printing Results:	60 sec
Maximum Time Step for Calculation:	10 sec

Air Entrained Model:	Heskestad

Temperature Dependent Openings

All openings activated at:	400 °C

Stepwise Variation

Temperature [°C]	% of Total Openings [%]
20	10
400	50
500	100

Linear Variation

Temperature [°C]	% of Total Openings [%]
20	10
400	50
500	100

Time Dependent Openings

Time [sec]	% of Total Openings [%]
0	5
1200	100

Figure A.7. General Fire Parameters of Building.

COMPARTMENT

Form of Compartment:	Rectangular Floor	
Height:	32.5	m
Depth:	60.5	m
Length:	52	m
Roof Type:	Single Pitch Roof	
Ceilling Height:	13	

DEFINITION OF ENCLOSURE BOUNDARIES

Floor

Material (from inside to outside)	Thickness [cm]	Unit Mass [kg/m³]	Conductivity [W/mK]	Specific Heat [J/kgK]
Normal weight Concrete [EN1994-1-2]	20	2300	1.6	1000

Ceiling

Material (from inside to outside)	Thickness [cm]	Unit Mass [kg/m³]	Conductivity [W/mK]	Specific Heat [J/kgK]
PUR	15	30	0.026	1470

Wall 1

Material (from inside to outside)	Thickness [cm]	Unit Mass [kg/m³]	Conductivity [W/mK]	Specific Heat [J/kgK]
PUR	15	30	0.026	1470

Openings

Sill Height [m]	Soffit Height [m]	Width [m]	Variation	Adiabatic
0	5	5	Constant	no
14.25	15.25	10	Constant	no
25	27	10	Constant	no

Wall 2

Material (from inside to outside)	Thickness [cm]	Unit Mass [kg/m³]	Conductivity [W/mK]	Specific Heat [J/kgK]
PUR	15	30	0.026	1470

Openings

Sill Height [m]	Soffit Height [m]	Width [m]	Variation	Adiabatic
0	5	12	Constant	no
13	14	14	Constant	no
17	18	7	Constant	no

Wall 3

Material (from inside to outside)	Thickness [cm]	Unit Mass [kg/m³]	Conductivity [W/mK]	Specific Heat [J/kgK]
PUR	15	30	0.026	1470

Openings

Sill Height [m]	Soffit Height [m]	Width [m]	Variation	Adiabatic
0	5	6	Constant	no
14.25	15.25	10	Constant	no
25	27	10	Constant	no

Wall 4

Material (from inside to outside)	Thickness [cm]	Unit Mass [kg/m³]	Conductivity [W/mK]	Specific Heat [J/kgK]
PUR	15	30	0.026	1470

Openings

Sill Height [m]	Soffit Height [m]	Width [m]	Variation	Adiabatic
0	2.1	2	Constant	no
13	14	14	Constant	no

Figure A.8. Compartment Details of Building.

FIRE

Fire Curve:	NFSC Design Fire			
Maximum Fire Area:	3146	m²		
Fire Elevation:	0	m		
Fuel Height:	0	m		
Occupancy	Fire Growth Rate	RHRf [kw/m²]	Fire Load $q_{f,k}$ [MJ/m²]	Danger of Fire Activation
User Defined	150	500	246	1

Active Measures Description	Active	Value
Automatic Water Extinguishing System	No	$\delta_{n,1} = 1$
Independent Water Supplies	No	$\delta_{n,2} = 1$
Automatic Fire Detection by Heat	Yes	$\delta_{n,3} = 0.87$
Automatic Fire Detection by Smoke	No	
Automatic Alarm Transmission to Fire Brigade	No	$\delta_{n,5} = 1$
Work Fire Brigade	No	$\delta_{n,6} = 1$
Off Site Fire Brigade	No	
Safe Access Routes	Yes	$\delta_{n,8} = 1$
Staircases under Overpressure in Fire Alarm	No	
Fire Fighting Devices	Yes	$\delta_{n,9} = 1$
Smoke Exhaust System	No	$\delta_{n,10} = 1.5$

Fire Risk Area:	3146	m²	$\delta_{q,1} = 1.93$
Danger of Fire Activation:			$\delta_{q,2} = 1$
$q_{f,d}$=	495.7	MJ/m²	
Combustion Heat of Fuel:	17.5	MJ/kg	
Combustion Efficiency Factor:	0.8		
Combustion Model:	Extended fire duration		

Figure A.9. Detailed Fire Parameters of Building.

PARAMETERS

Openings

Radiation Through Closed Openings:	0,8
Bernoulli Coefficient:	0,7

Physical Characteristics of Compartment

Initial Temperature:	293 K
Initial Pressure:	100000 Pa

Parameters of Wall Material

Convection Coefficient at the Hot Surface:	25 W/m²K
Convection Coefficient at the Cold Surface:	9 W/m²K

Calculation Parameters

End of Calculation:	7200 sec
Time Step for Printing Results:	60 sec
Maximum Time Step for Calculation:	10 sec

Air Entrained Model:	Heskestad

Temperature Dependent Openings

All openings activated at:	400 °C

Stepwise Variation

Temperature [°C]	% of Total Openings [%]
20	10
400	50
500	100

Linear Variation

Temperature [°C]	% of Total Openings [%]
20	10
400	50
500	100

Time Dependent Openings

Time [sec]	% of Total Openings [%]
0	5
1200	100

Figure A.10. General Fire Parameters of Building.

COMPARTMENT

Form of Compartment:	Rectangular Floor	
Height:	4,7	m
Depth:	7	m
Length:	12	m
Roof Type:	Flat Roof	

DEFINITION OF ENCLOSURE BOUNDARIES

Floor

Material (from inside to outside)	Thickness [cm]	Unit Mass [kg/m³]	Conductivity [W/mK]	Specific Heat [J/kgK]
Normal weight Concrete [EN1994-1-2]	19	2300	1,6	1000

Ceiling

Material (from inside to outside)	Thickness [cm]	Unit Mass [kg/m³]	Conductivity [W/mK]	Specific Heat [J/kgK]
Normal weight Concrete [EN1994-1-2]	19	2300	1,6	1000

Wall 1

Material (from inside to outside)	Thickness [cm]	Unit Mass [kg/m³]	Conductivity [W/mK]	Specific Heat [J/kgK]
PUR	15	30	0,026	1470

Openings

Sill Height [m]	Soffit Height [m]	Width [m]	Variation	Adiabatic
0	3	2,4	Constant	no

Wall 2

Material (from inside to outside)	Thickness [cm]	Unit Mass [kg/m³]	Conductivity [W/mK]	Specific Heat [J/kgK]
PUR	15	30	0,026	1470

Wall 3

Material (from inside to outside)	Thickness [cm]	Unit Mass [kg/m³]	Conductivity [W/mK]	Specific Heat [J/kgK]
Gas-concrete Bricks	15	550	0,14	840

Openings

Sill Height [m]	Soffit Height [m]	Width [m]	Variation	Adiabatic
0	2,1	1	Constant	no

Wall 4

Material (from inside to outside)	Thickness [cm]	Unit Mass [kg/m³]	Conductivity [W/mK]	Specific Heat [J/kgK]
PUR	15	30	0,026	1470

Openings

Sill Height [m]	Soffit Height [m]	Width [m]	Variation	Adiabatic
0	2,1	1	Constant	no

Figure A.11. Compartment Details of Building.

FIRE

Fire Curve:	NFSC Design Fire	
Maximum Fire Area:	84	m²
Fire Elevation:	0	m
Fuel Height:	0	m

Occupancy	Fire Growth Rate	RHRf [kw/m²]	Fire Load qf,k [MJ/m²]	Danger of Fire Activation
User Defined	300	250	622	1

Active Measures Description	Active	Value
Automatic Water Extinguishing System	Yes	$\delta_{n,1}$ = 0,61
Independent Water Supplies	No	$\delta_{n,2}$ = 1
Automatic Fire Detection by Heat	No	
Automatic Fire Detection by Smoke	Yes	$\delta_{n,4}$ = 0,73
Automatic Alarm Transmission to Fire Brigade	No	$\delta_{n,5}$ = 1
Work Fire Brigade	No	$\delta_{n,6}$ = 1
Off Site Fire Brigade	No	
Safe Access Routes	Yes	$\delta_{n,8}$ = 1
Staircases Under Overpressure in Fire Alarm	No	
Fire Fighting Devices	Yes	$\delta_{n,9}$ = 1
Smoke Exhaust System	Yes	$\delta_{n,10}$ = 1

Fire Risk Area:	84	m²	$\delta_{q,1}$= 1,32
Danger of Fire Activation:			$\delta_{q,2}$= 1
$q_{f,d}$=	292,5	MJ/m²	

Combustion Heat of Fuel:	17,5	MJ/kg
Combustion Efficiency Factor:	0,8	
Combustion Model:	Extended fire duration	

Figure A.12. Detailed Fire Parameters of Building.

PARAMETERS

Openings

Radiation Through Closed Openings:	0,8
Bernoulli Coefficient:	0,7

Physical Characteristics of Compartment

Initial Temperature:	293 K
Initial Pressure:	100000 Pa

Parameters of Wall Material

Convection Coefficient at the Hot Surface:	25 W/m²K
Convection Coefficient at the Cold Surface:	9 W/m²K

Calculation Parameters

End of Calculation:	7200 sec
Time Step for Printing Results:	60 sec
Maximum Time Step for Calculation:	10 sec

Air Entrained Model:	Heskestad

Temperature Dependent Openings

All openings activated at:	400 °C

Stepwise Variation

Temperature [°C]	% of Total Openings [%]
20	10
400	50
500	100

Linear Variation

Temperature [°C]	% of Total Openings [%]
20	10
400	50
500	100

Time Dependent Openings

Time [sec]	% of Total Openings [%]
0	5
1200	100

Figure A.13. General Fire Parameters of Building.

COMPARTMENT

Form of Compartment:	Rectangular Floor	
Height:	6,45	m
Depth:	6,5	m
Length:	18	m
Roof Type:	Double Pitch Roof	
Ceilling Height:	1,75	

DEFINITION OF ENCLOSURE BOUNDARIES

Floor

Material (from inside to outside)	Thickness [cm]	Unit Mass [kg/m³]	Conductivity [W/mK]	Specific Heat [J/kgK]
Normal weight Concrete [EN1994-1-2]	20	2300	1,6	1000

Ceiling

Material (from inside to outside)	Thickness [cm]	Unit Mass [kg/m³]	Conductivity [W/mK]	Specific Heat [J/kgK]
PUR	15	30	0,026	1470

Wall 1

Material (from inside to outside)	Thickness [cm]	Unit Mass [kg/m³]	Conductivity [W/mK]	Specific Heat [J/kgK]
PUR	15	30	0,026	1470

Wall 2

Material (from inside to outside)	Thickness [cm]	Unit Mass [kg/m³]	Conductivity [W/mK]	Specific Heat [J/kgK]
PUR	15	30	0,026	1470

Wall 3

Material (from inside to outside)	Thickness [cm]	Unit Mass [kg/m³]	Conductivity [W/mK]	Specific Heat [J/kgK]
Gas-concrete Bricks	15	550	0,14	840

Openings

Sill Height [m]	Soffit Height [m]	Width [m]	Variation	Adiabatic
0	2,5	2,4	Constant	no

Wall 4

Material (from inside to outside)	Thickness [cm]	Unit Mass [kg/m³]	Conductivity [W/mK]	Specific Heat [J/kgK]
PUR	15	30	0,026	1470

Openings

Sill Height [m]	Soffit Height [m]	Width [m]	Variation	Adiabatic
0	2,1	1	Constant	no

Figure A.14. Compartment Details of Building.

FIRE

Fire Curve:	NFSC Design Fire			
Maximum Fire Area:	117	m²		
Fire Elevation:	0	m		
Fuel Height:	0	m		
Occupancy	Fire Growth Rate	RHRf [kw/m²]	Fire Load qf,k [MJ/m²]	Danger of Fire Activation
User Defined	300	250	622	1

Active Measures		
Description	Active	Value
Automatic Water Extinguishing System	No	$\delta_{n,1} = 1$
Independent Water Supplies	No	$\delta_{n,2} = 1$
Automatic Fire Detection by Heat	No	
Automatic Fire Detection by Smoke	Yes	$\delta_{n,4} = 0,73$
Automatic Alarm Transmission to Fire Brigade	No	$\delta_{n,5} = 1$
Work Fire Brigade	No	$\delta_{n,6} = 1$
Off Site Fire Brigade	No	
Safe Access Routes	Yes	$\delta_{n,8} = 1$
Staircases Under Overpressure in Fire Alarm	No	
Fire Fighting Devices	Yes	$\delta_{n,9} = 1$
Smoke Exhaust System	Yes	$\delta_{n,10} = 1$

Fire Risk Area:	117	m²	$\delta_{q,1} = 1,38$
Danger of Fire Activation:			$\delta_{q,2} = 1$
$q_{f,d} =$	501,3	MJ/m²	
Combustion Heat of Fuel:	17,5	MJ/kg	
Combustion Efficiency Factor:	0,8		
Combustion Model:	Extended fire duration		

Figure A.15. Detailed Fire Parameters of Building.